Influence of Seal Binders and Rheology on Aggregate Orientation and Embedment Leading to Texture Loss

by

Timon Christiaan von Benecke

Thesis presented in partial fulfilment of the requirements for the degree of Master of Engineering (Civil) in the Faculty of Engineering at Stellenbosch University

Supervisor: Prof. K.J. Jenkins
Co-supervisor: Mr G.D. van Zyl

December 2021

Declaration

By submitting this thesis electronically, I declare that the entirety of the work contained therein is my own, original work, that I am the sole author thereof (save to the extent explicitly otherwise stated), that reproduction and publication thereof by Stellenbosch University will not infringe any third party rights and that I have not previously in its entirety or in part submitted it for obtaining any qualification.

Date: ....December 2021..........

Abstract

There are important functions of road surfacing seals including the surface to act as a durable, waterproof, all-round weather, dust-free riding surface with sufficient skid resistance to ensure road safety and adequate road serviceability. Seal aggregate behavioural characteristics include both aggregate embedment and aggregate orientation under trafficking. The orientation of aggregate particles to average least dimension reduces the voids available for binder to occupy. Therefore, a reduction in macrotexture and an increase in bleeding is introduced, both resulting in a loss of skid resistance in the wet and dry conditions.

The primary goal of this research project was to investigate aggregate orientation, in single seals, for the S-E1, S-E2, S-R1 and S-R2 hot polymer modified binders. This was achieved by constructing a BSM-emulsion base with 1.5% cement, to minimise the effect of aggregate embedment, on which a shoulder-to-shoulder and an over application aggregate matrix, for each binder, was constructed. The testing matrix included the trafficking of the surfacing seals by means of the Model Mobile Load Simulator 3 (MMLS3), in interval sets up to 5000 load repetitions at the following temperatures:

- 10°C colder temperature boundary,
- 20°C intermediate temperature and
- 30°C elevated temperature boundary.

After each trafficking set, the Laser Profilometer was applied on the surface, enabling a laser scan to obtain the mean profile depth in the wheel path of the MMLS3.

Based on the analysis of the data, it was established that the reduction in mean profile depth (MPD), as measured by means of the LPM, occurs with an increase in MMLS3 load repetitions. The MPD reduction is both a function of aggregate embedment and aggregate orientation with contributing behaviour including the transverse movement of aggregate in the over application aggregate matrices. Aggregate orientation in the seal mat, was governed by the rubber or polymer modification at 30°C whilst embedment behaviour was more prominent at 10°C as a result of binder and aggregate dominating due to increased binder stiffness.

The results yielded that the shoulder-to-shoulder aggregate matrices experienced greater decreases in MPD with an increase in trafficking temperature, relating to more aggregate orientation occurring as a result of more voids available in the seal mat. A greater reduction in MPD was prominent within the first 500 MMLS3 load repetitions, for all binders, over all trafficking temperature ranges. The less stiff rubber binders, in comparison with the elastomers, experienced greater reductions in MPD whilst the S-E1 showed a greater reduction in MPD in comparison with the S-E2 binder. Between 500 - 2000 MMLS3 load repetitions, the shoulder-to-shoulder matrices provided a higher rate of reduction in MPD whilst the over application matrices yielded higher rates of reduction in MPD between 2000 - 5000 load repetitions.

The research findings revealed that binder type plays a significant role in the selection of binder conversion factors for seal design. Temperature, loading characteristics, aggregate properties, base layer properties, binder application rate and seal aggregate spread rate all influence seal aggregate orientation and as a result thereof, the overall performance of the seal.

Uittreksel

Daar is belangrike funksies van oppervalkseëls insluitend om te dien as ’n duursame, waterdigte, weerbestande, stofvrye ryoppervlak met voldoende glyweerstand om padveiligheid en voldoende paddiens te verseker. Gedragseienskappe van die seëlaggregaat sluit beide die inbedheid en oriëntasie van seëlaggregaat onder verkeerlaste in. Die oriëntasie van aggregaat partikels na die gemiddelde kleinste dimensie verminder die leemtes beskikbaar wat die seëlbindmiddel kan inneem. Daarom word ’n afname in makrotekstuur en ’n toename in bindmiddelbloeding aangebring, wat beide lei tot ’n verlies aan glipweerstand in nat en droë toestande.

Die hoofdoel van hierdie navorsingsprojek was om die aggregaatoriëntasie in enkelseëls te ondersoek vir die S-E1, S-E2, S-R1 en S-R2 warm polimeer gemodifiseerde bindmiddels. Dit is bereik deur ’n BSM-emulsiebasis met 1.5% sement te bou om die effek van aggregaatinbedheid, waarop ’n skouer-tot-skouer-matriks en ’n oor-aanwendingsmatriks vir elke bindmiddel gebou is, te verminder. Die toetsmatriks het die verkeer van die oppervlakseëls ingesluit deur middel van die Model Mobiele Las-Simulator 3 (MMLS3), in intervalle tot in met 5000 lasherhalings by die volgende temperature:

- 10°C kouer temperatuurgrens,
- 20°C intermediêre temperatuur en
- 30°C verhewe temperatuurgrens.

Na elke verkeersstel was die Laserprofielmeter op die oppervlak aangebring, wat ’n laserskandering voltooi het om die gemiddelde profieldiepte in die wielbaan van die MMLS3 te kry.

Op grond van die ontleding van die data is daar vasgestel dat die vermindering van die gemiddelde profieldiepte (MPD), soos gemeet duer die LPM, plaasvind met ’n toename in MMLS3 lasherhalings. Die MPD vermindering is beide ’n funksie van inbedheid en oriëntasie van seëlaggregaat met laterale beweging in die oor-aanwendingsmatrikse ’n bydraende gedrag. Die aggregaat oriëntasie in die oppervlakseëlmat word bepaal deur die rubber- of polimeer -modifikasie teen 30°C, terwyl die inbeddingsgedrag meer plaasgevind het teen 10°C as gevolg van bindmiddel- en aggregaatoorheersing deur verhoogde bindmiddelstyfheid.

Die resultate het opgelewer dat die skouer-tot-skouer aggregaatsmatrikse groter afnames in MPD ondervind het met ’n toename in die verkeerstemperatuur, wat verband hou met meer aggregaatoriëntasie as gevolg van meer leemtes in die oppervlakseëlmat. ’n Groter afname in MPD was prominent tydens die eerste 500 MMLS3 lasherhalings,

vir alle bindmiddels, oor alle verkeerstemperature. Die minder styf rubber-bindmiddels, in vergelyking met die elastomere, het ’n groter afname in MPD ondervind, terwyl die S-E1 ’n groter vermindering in MPD getoon het in vergelyking met die S-E2-bindmiddel. Tussen 500 - 2000 MMLS3 lasherhalings het die skouer-tot-skouer aggregaatsmatrikse ’n hoër verlies in die tempo van MPD opgelewer, terwyl die oor-aanwendingsmatrikse ’n hoër verlies in MPD tussen 2000 - 5000 lasherhalings opgelewer het.

Die navorsingsbevindinge het aan die lig gebring dat die tipe seëlbindmiddel ’n belangrike rol speel in die keuse van bindmiddel-omskakelingsfaktore vir seëlontwerp. Temperatuur, las-eienskappe, aggregaat-eienskappe, basislaag-eienskappe, bindmiddel-aanwendingskoers en seëlaggregaat-verspreidingsmatriks het ’n invloed op die aggregaat en die oriëntasie daarvan en as gevolg daarvan die gedrag van die oppervlakseël.

Acknowledgements

My sincerest gratitude and thanks go to the following people as my thesis would not have been without them.

Prof Kim Jenkins at Stellenbosch University for his overall guidance, project commitment and patience throughout.

Mr Gerrie van Zyl (MyCube), as co-supervisor, for his valuable seal performance input.

My fellow researcher, **Mr Daymen Gerber** (Stellenbosch University), for the two years of hard work in parallel.

Mr Guillaume Nel (Stellenbosch University) for his assistance and patience during the project and the laboratory technicians, **Mr Colin Isaacs, Gavin Williams and Eric** for their contribution during the physical demanding setup of the project.

Mr Justin Miller (CubeSpace), for his data reworking assistance.

My fellow researchers at Stellenbosch University for the unforgettable memories over the last few years.

My close friends and family, thank you for giving me a reason.

Earnestly, **God**, my rock.

Contents

List of Figures

List of Tables

List of Abbreviations

Symbols

G^*	Complex modulus (kPa)
ω	Frequency (rad/s)
ϵ_p	Plastic strain
N	Load cycles / load applications
ΔT	Critical low temperature difference (°C)
T_{ref}	Reference temperature (°C)
$T_{R\&B}$	Ring and Ball Softening Point (temperature) (°C)
δ	Phase angle (°)

Abbreviations

AAR	Aggregate application rate
ALD	Average least dimension (mm)
ALF	Accelerated Loading Facility
APT	Accelerated Pavement Testing
BP	Ball penetration test
CBP	Corrected ball penetration value
CPAF	Cumulative percentage of aggregate on flattest side
CT	Computed tomography
DD	Dry density (kg/m^3)
ELV	Equivalent light traffic
EVA	Ethylene-vinyl-acetate
E80	Equivalent 80 kN axle load
FEM	Finite element method
FT	Fischer-Tropsch synthesis process
G-R	Glover-Rowe parameter (Pa)
HVAC	Heating, ventilation and air conditioning

HVS Heavy Vehicle Simulator

LTM Laser texture meter
LPM Laser profilometer

MC Moisture content (%)
MDD Maximum dry density (kg/m^3)
MLS Model Load Simulator
MMLS Model Mobile Load Simulator
MMLS3 Model Mobile Load Simulator 3
MPD Mean profile depth (mm)
MTD Mean texture depth (mm)

NCCB Net cold conventional binder

OMC Optimum moisture content (%)

PSV Polished Stone Value
pen Penetration

SAMI Stress absorbing membrane interlayer
SIM Stress-in-Motion
Sh-Sh Shoulder-to-shoulder aggregate matrix
SP Softening point (°C)

TxMLS Texas Mobile Load Simulator

Chapter 1

Introduction

1.1 Research Background

According to Milne (2004), bitumen based surfacing seals have been utilized in industry to respond to the damage of the existing soil by the developing sector of auto mobiles with rubber wheels, since the 1900's. Throughout the years, ongoing research and experiments have been conducted and carried out, from materials used to construction and design methods. Although the constant research has provided profound information, there is still much about road surfacing seals to be understood, improved and refined. As a pavement wearing course, pavement engineers have the option of using either an asphalt (graded aggregate with pre-manufactured bitumen binders as a complete product) or a surfacing seal (which includes different types of bituminous binders which are sprayed onto the surface after which aggregate is applied in a single or double layer, depending on the need) as a wearing course.

The function of a road surfacing seals extends to act as a durable, waterproof, all-round weather and dust-free surfacing layer, with sufficient skid resistance to maximize safety and road serviceability. As a result of industry experience in the use of surfacing seals, the road industry has built up valuable knowledge on the design, construction and maintenance of the surfacings. South African researchers have carried out various road and laboratory experiments, in addition to the experience. As a result, guidelines have been established for the design, construction and maintenance of these bituminous seals for the use thereof under local conditions as per SABITA Manual 40 (2021).

Together with the uncertainties and the variability in the behaviour of seals, there are also a number of factors affecting the performance thereof. One of the major behavioural characteristics affecting seal performance, includes aggregate embedment and aggregate orientation during the construction period as well as the initial trafficking period. Aggregate orientation is of major importance, as it is desirable to orientate the aggregate particles so that their least dimension is perpendicular to the surfacing level.

Over the past twenty years, Mobile load simulation (MLS) has been effectively used to simulate road loading conditions. Unlike other structural layers in a pavement, it is difficult to construct and replicate a seal in a laboratory environment whilst producing a realistic loading system. In the early 1990's, Professor Fred Hugo, together with his team, developed the first Mobile Load Simulator after which a scaled down (1/3) version, of the full scale MLS, was proposed and designed. This version was known as the Model Mobile Load Simulator 3 (MMLS3) and it was found to be more practical and feasible than both the full scale MLS and the MLS1 (1/10 scale). MLS technology allows users to perform accelerated pavement testing (APT) on road pavements as various inputs are available. This resulted in many countries, around the world, acquiring their own MMLS machinery for the purpose of research (Kemp, 2006).

It can be of value to understand seal aggregate behaviour in terms of aggregate embedment and aggregate orientation by evaluating the decreases in both profile and texture depth. By making use of the MMLS3 machine, and a Laser Profilometer (LPM), realistic loads can be applied to a seal surfacing layer, to examine aggregate orientation and its effect on the void content, which relates to an additional amount of binder to be added without leading to adhesion, bleeding or flushing problems. Subsequently, aggregate behaviour during construction and during the in-service trafficking phase should be recorded. Relationships between the decrease in texture depth, void content and aggregate behaviour could result in a better understanding of seal performance as a result of different trafficking and environmental conditions, binder rheology, aggregate properties, such as flakiness and particle shape, and spread rate as well as the effect of the substrate in terms of embedment performance.

1.2 Need for Research

Aggregate orientation, onto average least dimension (ALD), ensures a greater bonding surface area between the tack coat and the aggregate particles, resulting in improved adhesion properties whilst lowering the risks of seal failure. However, stone orientation reduces the voids between the seal stones and thus the volume of the binder to occupy. This poses two risks, including a reduction in macro-texture, which reduces skid resistance in the wet, and increases the risk of bleeding, therefore reducing skid resistance in the dry and wet conditions. Furthermore, aggregate spread rate, affecting void content, influences the bituminous binder application rate. This is an important design aspect as failure to produce the optimum binder application rate can lead to seal failure, relating chip loss as a result of insufficient binder or bleeding as a result of excess binder relative to the voids in the seal mat, during initial trafficking. Seal failure mechanisms are texture loss, shelling, rutting, cracking and moisture damage.

1.3 Goal and Objectives

The primary goal of this research project is to investigate the aggregate orientation behaviour for different hot polymer modified binders as a result of different temperatures and aggregate spread rates. To achieve this, the study requires:

- the determination of mean profile depth and mean texture depth values over a trafficking period.

The goal, as mentioned, is achieved by executing the following objectives:

- Construct shoulder-to-shoulder and over application aggregate matrices for different hot polymer modified single binders.
- Make use of the Model Mobile Load Simulator 3 to implement pre-determined trafficking sets on all seals at different temperatures.
- Make use of the Laser Profilometer and the sand patch test, after each trafficking set, to evaluate both the mean profile depth and the mean texture depth.
- Identify and report on the aggregate orientation behaviour in the different seal binders for the different aggregate matrices at different temperatures.
- Comment on the appropriateness of current conversion factors from net cold conventional binders to hot modified binders based on the behaviour of seal aggregate.

1.4 Thesis Chapter Outline

The highlights of each chapter is indicated below:

1. Introduction: The research background, need fo research, goals and objectives are provided.
2. Literature Study: This chapter elaborates on pavements in general, together with the need thereof. Furthermore, the chapter investigates bitumen and its fundamental properties together with aggregates and the different types. An introduction to seals and the implementation thereof in South Africa is then further elaborated on, together with the functionality and performance thereof. Seal failure and seal behaviour is provided with a focus on both aggregate embedment and aggregate orientation. The MMLS3 is elaborated on together with the performance variables for implementing accelerated pavement testing (APT). Lastly, various surface texture measurements are given.
3. Experimental Design: This chapter provides the reasoning as to the design considerations. The experimental design outline is also provided.
4. Experimental Test Setup and Process: This chapter elaborates on the test setup and the testing process itself. Firstly, the pre-investigation and preparation phase is given after which the base construction and the seal construction phases are provided. The testing procedure is then described. Lastly, the process followed to obtain quality and representative data is mentioned.
5. Results: The test results, together with the trends observed are analysed. The mean texture depth and mean profile depth relationships for each binder type is investigated and shown. Furthermore, visual analyses are done to determine the movement of aggregate in the seal mat.
6. Interpretation and Discussion: This chapter discusses the data analysis results as provided in the previous chapter. Comments and observations are made regarding the different trafficking conditions, different binder types and different aggregate spread rates. Furthermore, a summary regarding the main findings are highlighted.

7. Conclusions and Recommendations: Findings regarding the objectives, as mentioned in this chapter, are discussed. Aggregate orientation and the correlation thereof to the texture and profile changes are mentioned. Further research is also recommended.

Chapter 2

Literature Study

2.1 Introduction

This chapter discusses various aspects relating to the research matter of this study. The literature in this chapter provides comprehensive insight to the current and past research on seals, in particular aggregate orientation and embedment and the influence thereof on seal performance. Firstly, a broad idea of different pavement structures is discussed and the need for pavements. Subsequently, different surfacings are discussed, with a focus on the material needed to construct these layers. Material behaviour is furthermore elaborated on. An overview of the history of seals, the functions and the uses thereof in South Africa is then discussed together with different seal failure mechanisms. Aggregate embedment and aggregate orientation, and its effect on seal performance is elaborated on with a focus on how aggregate orientation during construction and traffic influences the void content and binder application rate. Thereafter, rheology, Shakedown Theory and an overview of accelerated pavement testing is provided and discussed along with previous research and methodologies applicable to the devices. Current surface texture measurement procedures are also mentioned.

2.2 Pavements

2.2.1 The need for pavements

Pavements, as we know them today, are a big necessity in the modern world. Apart from social factors such as medical transportation, fire and emergency access and public visiting, a good road system is of utmost importance to ensure economic growth through the transportation of goods and services. Thus, for effective global competitiveness, good road infrastructure is required. This also includes the construction of rural roads as they play an important role in stimulating the economy by providing routes from farms to markets. Furthermore, roads are provided to serve communities, stakeholders, individuals and the government. As a result, roads generally serve two purposes namely providing mobility to facilitate quick and safe movement, and accessibility to facilitate users making use of the higher order mobility road network (SAPEM, 2014).

2.2.2 Pavement Structures

The structure as to which a pavement is constructed determines the performance of the pavement in correspondence with its design functionality. According to Wirtgen (2012), road pavements consist of three basic components.

- Surfacing: the physical visual riding surface.
- Layers: the layers in the pavement which act as load spreading mechanisms, while consisting of different materials.
- Subgrade: the natural ground upon which the pavement is built.

The components of a pavement structure can be seen in Figure 2.1, as adapted from Wirtgen (2012).

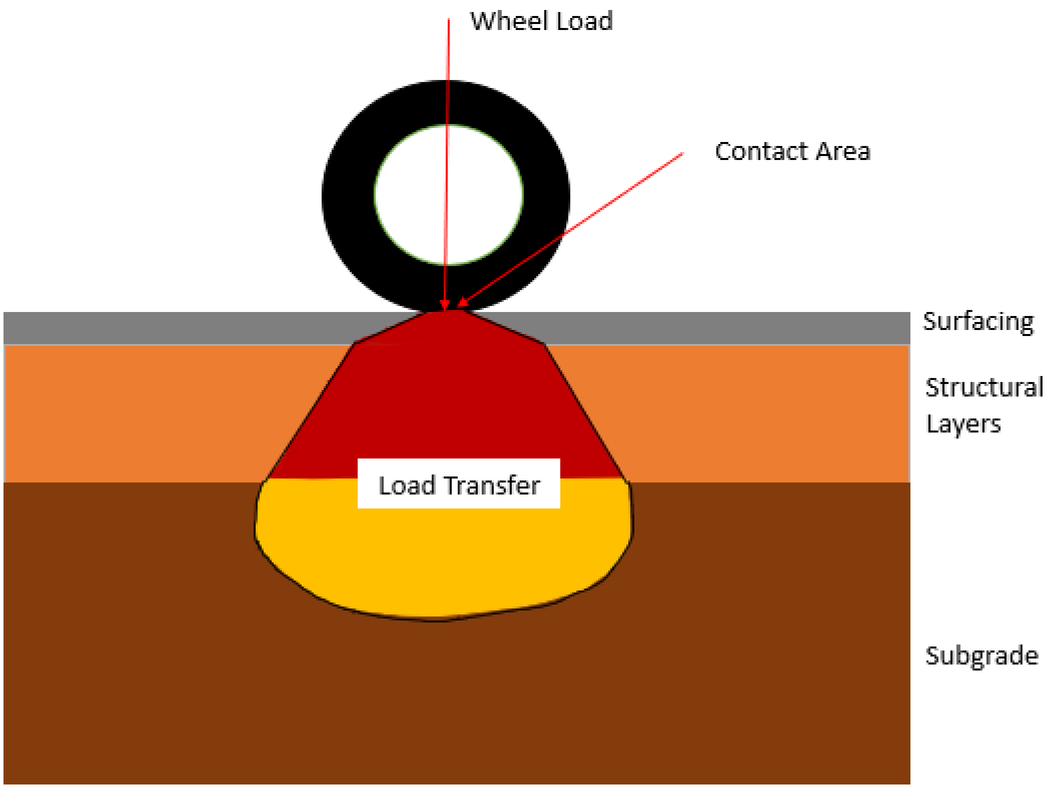

Figure 2.1: The spreading of load through the pavement as adapted from Wirtgen (2012)

There are two fundamental pavement structures that could be built (Wirtgen, 2012):

- Rigid pavements which consist of a high strength concrete layer overlaying a bound layer.
- Flexible pavements with full or partial bitumen or cement bound upper layers together with natural material used to construct the deeper layers.

2.2.3 Pavement Components

2.2.3.1 Surfacing

The surfacing layer of a pavement is the interface of the pavement with traffic and environmental conditions. The function of this layer is to protect the pavement structure from trafficking and environmental conditions whilst providing a durable and waterproof layer. Traffic affects the surfacing layer in two ways. The first way includes the stresses imparted by the wheel loads, predominantly in the vertical direction, whilst another includes the abrasion of the tyres on the surface. Abrasion causes a polishing result on the surface which reduces the skid resistance as well as the texture depth. These surfaces then become slippery and a safety hazard during wet conditions. Due to environmental conditions such as oxidation, thermal effects and ultraviolet radiation, a surfacing layer requires sufficient elasticity (for expansion properties) and durability to withstand forces and daily environmental bombardment (Wirtgen, 2012).

According to Wirtgen (2012), hot mixed asphalt (with a bitumen content of 5% by mass) is usually implemented as a surfacing premium for heavily loaded traffic while a surfacing seal is generally used for more low volume roads.

2.2.3.2 Structural Layers

As stated previously, the function of the structural layers, including both the base and the subbase, beneath the surfacing layer, is to transfer loads to the lower section of the pavement. The stress endured by traffic wheel loads are reduced within the pavement layers by allowing for a larger distribution area down to the subgrade. Each structural layer, such as the base and the subbase, generally consists of different material with varying strength and stiffness characteristics, all with the purpose of load distribution. The upper layers are generally constructed from stiffer and stronger material due to the higher stresses occurring in these layers. Layer response to an imposed load, such as a wheel load from traffic, is dependent on the material characteristics such as elasticity, viscosity and plasticity, as well as the load properties such as rate of loading and magnitude. According to Wirtgen (2012), flexible pavements are constructed from:

- Unbound material such as crushed stone and gravels.
- Bound materials such as cement stabilised and asphalt.
- Non-continuously bound materials such as bitumen stabilised materials (BSM).

2.2.3.3 Subgrade

Deeper pavement layers refer to subgrade layers. It can either be constructed from in-situ material or imported material, depending on the quality of the in-situ material. The ability of the subgrade layer to attain compaction, and therefore stiffness and strength, dictates the load distribution of the upper layers. Therefore, a high subgrade stiffness relates to higher stiffness parameters for the upper layers such as the base and subbase. In pavement design methods, the subgrade material is often an input parameter and thus, it is an important parameter as it sets the primary conditions and restrictions for the above-placed pavement layers.

2.3 Surfacing Seals

2.3.1 History of Seals

According to Milne (2004), bituminous seals are common in practice due to them being economically cheaper to construct, easy to maintain and durable if constructed for the correct conditions. From pre-1935, where traffic volumes were much lower than today, up until presently, where there was an increase in traffic, seal design was based on industry experience as there was no formal seal design method. Developing countries (then), such as South Africa, New Zealand and Australia, continued to implement a seal as surfacing layer while more economically developed countries, such as the USA, turned to asphalt surfacings due to increases in traffic. Hanson implemented the first viable seal design method in 1930, based on the Average Least Dimension (ALD) of the aggregate. This method related the smallest dimension of the surfacing stone to determine the volume of the aggregate mat together with the voids, and it was also relatable to the application rate of the binder. Due to an increase in traffic after World War II in 1945, surfacing seals were more common but failed due to a lack of adequate design methods.

The effect of traffic as well as the environment, played a role in the failure of the successful implementation of seals. According to Gransberg and James (2005), Hanson's method or sections thereof, can be found in chip (surfacing) seal methods presently. The Kearby and McLeod method can be found in the western areas of the world, especially in North America. The United Kingdom's Transport Research Laboratory (1996) has developed and published chip seal design methods called the Road Note 39. South Africa, Australia and New Zealand have also developed their principle-based methods for use in their respective countries. South Africa's method can currently be found in the Design and Construction of Surface Treatments: SABITA Manual 40. Milne (2004) also stated that several road authorities invented and implemented their own seal design methods due to there not being a general guideline.

2.3.2 Seals in South Africa and Globally

According to the SABITA Manual 40 (2021), 20% or 150 000 km of the total South African road network (750 000 km) is surfaced. The estimated total road pavement distance, which was either surfaced or resurfaced with a surfacing seal, corresponds to 120 000 km. Van Zyl and Jenkins (2015) stated that seals covered more than 80% of the roads in South Africa. The current road network in South Africa can be seen in Figure 2.2.

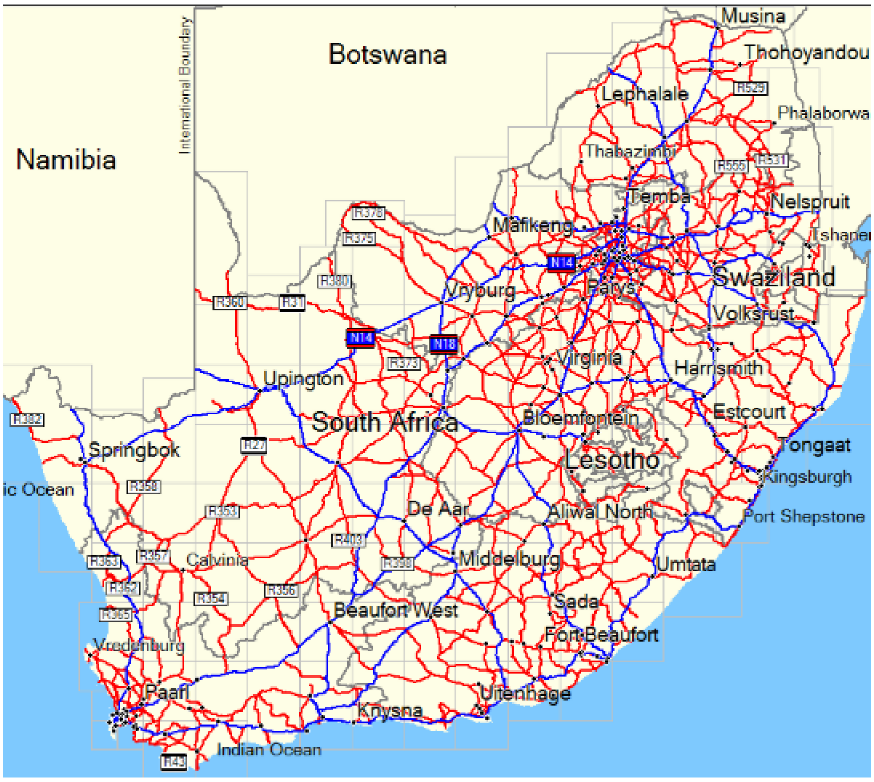

Figure 2.2: Current road network in South Africa

A large portion of the rural roads in South Africa, is surfaced with either double seals or Cape seals while, at a later stage during the seal's design life, a slurry or single seal is used to reseal (SABITA Manual 40, 2021). Countries such as Australia, South Africa, New Zealand and the United Kingdom have developed and implemented their chip seal practices according to the fundamental principles such as texture depth, hardness and aggregate size. These principles minimize the effect of binder application rate and aggregate application rate, due to a reduction in uncertainties. Countries such as Canada and the United States of America do not depend on these fundamental principles as they rather depend on empirical and industry experience. In the countries using these fundamental principles, the chip (surfacing) seal projects have transferred from rehabilitation and maintenance into the construction contract division (Gransberg and James, 2005).

2.3.3 Seals as a Wearing Course

A surfacing seal in simple form, consists of a quantity of bituminous binder which is sprayed onto a road surface, after which a layer of aggregate is applied to cover the surface. The aggregate can either be in the form of sand or stone, depending on the type of seal. To ensure adequate adhesion between the bituminous binder and the aggregate, the aggregate is placed immediately after the binder is applied. By making use of rollers, the aggregate particles are orientated into a mosaic matrix while the air voids, between the stones, are filled with binder. The initial traffic forms part of the orientation and void-filling process by means of further compaction. The construction and early traffic period ensures that an impermeable pavement structure is created which, if successful, should be durable with adequate skid resistance (SABITA Manual

40, 2021).

The SABITA Manual 40 (2021) states that it is expected of surfacing seals to carry between 125 to 20 000 light vehicles per lane per day. In contrast, there have been cases where surfacing seals have carried up to 60 000 equivalent light vehicles (ELV) and performed well. Generally, an asphalt surfacing layer is constructed when traffic volumes are higher than 20 000 ELV. Although chip seals (surfacing seals) could be implemented as a rehabilitation mechanism, it should be noted that chip seals are not intended to provide influential structural capacity. Thus, they should not be implemented on roads that provide evidence of major distress. With that being stated, it is common practice, according to Gransberg and James (2005), to apply chip seals as a stop-gap measure on roads that have structural distress.

The SABITA Manual 40 (2021) also states that seals are generally thin in comparison with the structural orientated layers of the pavement. Subsequently, and as stated previously, the seal layer should not perform as an effective structural bearing layer but it should withstand the vertical and horizontal stresses from traffic.

2.3.4 Functionality of Seals

According to the SABITA Manual 40 (2021), the main functions of a road surfacing seal are as follows:

- Provide an effective and durable waterproof cover to the structural layers beneath.
- Ensure an adequate clean and dust-free driving surface, with sufficient skid resistance during any weather conditions.
- Provide protection to the structural pavement layers from the stress and forces from the traffic and environment.
- Withstand horizontal and vertical stresses induced by traffic wheel loads.

2.3.5 Structures and Types

In industry, there are various types of seals used as a surfacing layer. The most commonly used and most simplistic surfacing seal, as described in the SABITA Manual 40 (2021), is illustrated in Figure 2.3. This type of seal is referred to as a single seal, due to it only having one layer of single sized aggregates on top of the existing substrate.

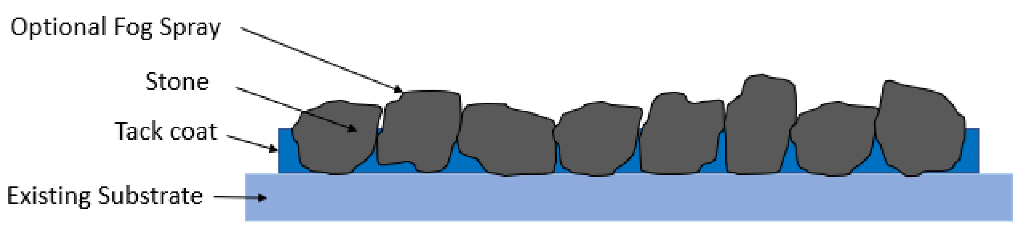

Figure 2.3: Single Seal Structure as adapted from SABITA Manual 40 (2021)

As seen in Figure 2.3, seals are constructed from three basic components: the aggregate stone, bituminous binder (tack coat and optional fog spray) and the existing soil on which the seal is being constructed. As explained in Section 2.5.3, the binder is firstly sprayed onto the existing subgrade, after which aggregate stones are applied. Rollers are then implemented to orientate the particles into a pattern whilst working the tack coat binder into the voids. A dense pavement surfacing is then completed by finishing the process by action of traffic (SABITA Manual 40, 2021).

Other commonly used seals, according to the SABITA Manual 40 (2021) and SAPEM (2014), include double seals, Cape seals, slurry and sand seals. The less commonly implemented seal types are geotextile, inverted double seals, choked seals, split seals and graded aggregate seals.

2.3.6 Seal Performance

2.3.6.1 Overview of Factors Influencing Performance

The performance of a surfacing seal is determined by the degree that it has fulfilled its function during the service life. A combination of factors and external influences affect the performance capability thereof. If a surfacing seal does not fulfil any of the following, as stated in the SABITA Manual 40 (2021), it can indicate the end of an effective service life:

- Pavement structure and substrate
- Traffic
- Geometry of the road
- Design methodology
- Bitumen and Aggregate materials
- Pre-construction processes
- Construction processes
- Maintenance and repairs
- Environmental Conditions

According to Transit New Zealand (2005), surfacing seal performance can be divided into two important distinct phases, namely the post-construction (setting down) phase and the in-service performance phase. During the post-construction phase, the performance of a seal is hugely affected by the conditions and methods used during construction. All the factors are listed in Table 2.1.

Table 2.1: Post-construction versus in-service factors (Transit New Zealand, 2005)

Post-Construction	In-Service
Binder application rate	Binder application rate
Aggregate application rate	Aggregate application rate
Environmental conditions	Construction inadequacies
Layer compaction	Substrate adequacy
	Ageing of materials
	Traffic conditions
	Environmental conditions
	Binder properties

The following sections will elaborate on the factors influencing the performance of surfacing seals. An introductory description is provided along with an explanation of the performance factor.

2.3.6.2 The condition and structure of the pavement

The SABITA Manual 40 (2021) states that the performance of a seal is largely governed by the structural capacity of the underlying structural layers. The response of the structural layers, beneath the seal, when exposed to the stress conditions induced by wheel loads, determines the performance of the seal layer.

The type of base that is constructed beneath the seal affects the performance thereof due to the degree to which the base resists aggregate to penetrate. Aggregate penetration is directly related to the base material, aggregate geometry and degree of compaction. When aggregate penetration occurs, there is a decrease in voids, which increases the probability to cause fattiness, bleeding and also a loss of texture depth, or skid resistance. According to Kashaya (2013) and the SABITA Manual 40 (2021), pavement structures should be able to withstand high loading stresses and resist high deflections to ensure no fatigue failing in the seal layer. If the seal binder cracks, water ingress occurs which could cause the whole deterioration process of the pavement to accelerate. Milne (2004) mentions that cracking of the surfacing layer is directly related to load repetitions, temperature changes and moisture changes. Therefore, it is of importance to select and design seals based on pavement suitability.

2.3.6.3 Substrate Layer

The layer condition of the existing surface will be used to determine what type of seal is to be constructed and the design thereof. According to the SABITA Manual 40 (2021), these factors should be taken into consideration due to them being the variables in determining the seal type, binder quality and quantity, nominal stone size and the necessary pre-treatment. It is of note that a uniform surface has to be developed to ensure a successful construction and performance of a uniform seal. Subsequently, the condition of the existing substrate is evaluated by means of visual inspection (e.g. cracking) whilst measurements of the texture depth, expected aggregate embedment and permeability are also completed. The SABITA Manual 40 (2021) specifies the following detail for each variable:

- Texture depth: These values give an indication of the possible need for pre-treatment. Generally, a texture slurry is applied prior to the construction of a seal.
- Permeability: Provides an indication as to the need to pre-treat the existing surface by introducing extra binder such as a fog spray or a rejuvenator.
- Stone embedment: The expected embedment relates to the hardness of the existing substrate. The ball penetration test is currently used to determine the condition and reaction of the substrate layer under loading and therefore provide an indication of expected embedment.
- Cracking: This provides an indication of crack reflection from the existing substrate to the surface. An indication of the brittleness and flexibility decreases of the existing surface, is also noted.

2.3.6.4 Traffic Loading

The performance of a seal is greatly influenced by traffic. According to the SABITA Manual 40 (2021), the following parameters, related to trafficking, is important:

- Traffic volumes (especially heavy vehicles)
- Heavy vehicle loading
- Tyre contact stress or tyre inflation pressure
- Vehicle type and movement
- Vehicle speed
- Trafficking patterns such as concentrated movement in the wheel path

Furthermore, and as documented in SABITA Manual 40 (2021), a heavy vehicle is equivalent to 40 light vehicles. Heavy vehicles influence the performance of a seal, especially embedment of aggregate, more so than lighter vehicles. Therefore, the equivalency relationship between light and heavy vehicles is important when designing seals. The current factor originated and increased due to the increases in tyre pressure and axle loads.

It is important for surfacing seals to be exposed to traffic to keep the bituminous binder working and flexible. Milne (2004) states that a minimum of 50 vehicles per day is required for the binder to remain flexible. It is believed that traffic plays a role in breaking down the chain of hydrocarbons that form due to oxidation, and the removal of heavily oxidised matter by traffic forces. But, traffic is also a downfall when it comes to the effect thereof on seals. Embedment, surface polishing and wearing of the stone, are all derived from the effects of heavy vehicles. The volume of traffic causes the above mentioned processes which could often lead to further problems such a reduction in skid resistance resulting in bleeding (SABITA Manual 40, 2021).

Furthermore, Milne (2004) states that heavy axle loads result in stone embedment while increases in tyre pressures result in bleeding of the binder. High shear loads, from tandem axles, damage the seal surfacing when turning while low speed traffic results in a longer loading time exposure while increasing the horizontal stresses due to traction. According to Transit New Zealand (2005), a seal will fail either during the early stages in its life (first days or months) or they will last many years. Due to this, Milne (2004) reported that high concentrated traffic stresses in the wheel paths affect the performance of seals tremendously when traffic is introduced too early before curing.

2.3.6.5 Geometry of the road

According to the SABITA Manual 40 (2021) and Milne (2004), steep gradients initiate slow moving traffic which results in an increase in traction. Subsequently, this causes the adhesion between the aggregate and the bituminous binder to break. Furthermore, the increase in traction also causes bleeding and slippage. Steep gradients also result in difficulties during construction with regards to the binder application rates and the non-uniform application thereof due to the gradient. Wet conditions and heavy rains lead to canalized water flow which result in the erosion of seal stones.

When roads include sharp curves, vehicles induce higher horizontal stresses when compared to a non-curved road. Slippage and ravelling are often surfacing problems that occur during these conditions. The outer parts of roads also become very brittle and dry due to vehicles cutting corners. This results in the outer sections losing stone. Fattiness is also another problem due to high stresses being transferred to the inside of the curves due to cambers existing (SABITA Manual 40, 2021).

Constant braking and acceleration at intersections, often including heavy vehicles, induces high horizontal stresses, which again are associated with slippage. Due to the deceleration of vehicles, there is an increase in fuel spillage which also softens up the binder, again leading to bleeding (Milne, 2004).

2.3.6.6 Design Process and Methodology

As with any design procedure, the pre-design process is of major importance. According to the SABITA Manual 40 (2021), this procedure relates directly to the performance and success of a seal during its service life. Care should be taken to account for varying conditions which might occur during the design process and adjustments should be made when new information arises during the construction process.

2.3.6.7 Materials

Both the aggregate and binder properties affect the performance of a seal. Table 2.2 mentions and describes the influencing properties of aggregate whilst the properties, linked to the mechanisms of seal failure, are further elaborated in Section 2.4.

Table 2.2: Aggregate influencing properties

Aggregate properties	Influence
Shape	The aggregate shape influences the interlocking compartment in the layer and plays a role in the overall stability of the seal. The shape also affects the void content and the movement of water by means of macro-texture. According to White *et al.* (2019), micro-texture and macro-texture influences the tyre wear and spray and splash during wet conditions. With an increase in angularity, there is also an increase in the interlocking ability of the stone, which is of an advantage.
Nominal Size	Small stones are more susceptible to bleeding due to the void content being lower than that of larger stones. Larger stones are also less susceptible to a non-uniform spread rate. Single sized aggregates are also desired as interlocking properties are improved while less polishing and abrasion occurs resulting in a higher skid resistance.
Spread Rate	A mosaic pattern of tightly knit aggregate, of single layer, is desired to create a uniform protective layer. According to the SABITA Manual 40 (2021), the aggregates should lie in a sh-sh pattern. The application rate should also be balanced as a too tightly knit application could result in crushing and stone loss while a too open matrix could leave the binder exposed to UV concentration from the sun.
Adhesion	Aggregates with the property to have good binder adhesion is desired. Dust, oil, mud and fuel reduce the ability of the binder to adhere to the stones effectively. According to the SABITA Manual 40 (2021), only 1% of dust is required on the aggregate to result in substantial stone loss. Water and the effect of moisture also negatively influence the ability of binder to adhere to aggregate, except when bitumen emulsions are used. To promote better adhesion characteristics, aggregates are often pre-coated as recommended for hot applied binders (SABITA TG 1, 2019).
Strength and durability	Aggregates with sufficient hardness characteristics are desired. Aggregate crushing value (ACV) and FACT tests should be compelled to not crush, break or chip away during construction and in-service traffic. The aggregate's resistance to weathering and erosion is determined by its mineral composition. Subsequently, mineral and weathering tests should also be done to determine whether or not the aggregate type is adequate.
Porosity and absorption	The lighter fractions of a bituminous binder are absorbed by porous aggregates. This results in a brittle and unstable seal. If the only aggregate type of availability is one of porous characteristics, a modified binder is recommended.

Binder properties affecting seal performance are listed and shown in Table 2.3.

Table 2.3: Binder influencing properties

Binder properties	Influence
Binder Type	Different types of binders are used in industry, such as penetration grade, cut-back, modified binders and emulsion binders. The ageing of binders as a result of ultraviolet exposure and temperature difference variations lead to increases in stiffness and decreases in elasticity. Furthermore, as per the SABITA TG 1 (2019), the polymer modification of binders are done to improve seal performance by altering the visco-elastic properties thereof whilst also extending the deformation phase.
Grade	Selection of a suitable binder grade is determined by the climatic conditions expected during the construction period and the in-service period's ambient temperatures. Expected traffic conditions during the in-service lifetime of the seal also play a significant role in the choice of binder grade to be used (SABITA Manual 40, 2021).
Application rate	The application rate of binders is limited by a minimum amount of binder needed to hold the aggregate in place and bind it to the existing substrate. A maximum amount is specified and when exceeded, overfilling of the voids would occur resulting in bleeding and a decrease in skid resistance during all conditions. The optimum application rate is determined as per the seal design method in the SABITA Manual 40 (2021).
Viscosity	A uniform application of the bituminous binder is governed by the viscosity of the binder, which varies with changes in temperature. Each binder grade has a temperature-viscosity relationship which indicates the optimum viscosity to obtain a uniform application.

Roque *et al.* (1991) mentions that additional binders, such as emulsion grade, reduced the macro-texture on worn-out surfaces. For levelled surfaces, the amount of aggregate that was retained was directly related to the application rate of the binder used. Thus, for example, stone retention on the lower emulsion application was not sufficient due to the binder being absorbed into the levelling course. The minimum binder amount, on worn surfaces, still proved to be sufficient to retain the aggregate while an increase in binder only resulted in a decrease in skid resistance and macro-texture.

2.3.6.8 Pre-construction preparation and pre-treatment

According to the SABITA Manual 40 (2021), it is necessary to prepare a clean and dense surface to optimise the adhesion properties between the surface and the seal, as well as between the aggregate and the bituminous binder. Pre-treatment should also be implemented if there are any signs of unevenness, dryness, porosity or varying surface textures. Pre-treatment is applied to ensure a uniform texture and smooth driving surface. This process can be seen in Figure 2.4.

Figure 2.4: Pre-treatment done on a pavement surfacing (Van Zyl, 2000)

Repairs should also be implemented to pavement failures (e.g. potholing) or pavement defects to prevent these defects to reflect through to the surface. Embedment can also be minimized by applying pre-treatment mechanisms or by implementing repairs. These procedures are required well before surfacing takes place to allow for effective evaporation of fluxing agents (Milne, 2004).

2.3.6.9 Construction process

According to industry experts, poor seal performance is often related to inadequate supervision on site. The correct uniform application of the binder and aggregate is required, as well as correct compaction techniques such as rolling and brooming. According to the SABITA Manual 40 (2021), it is of note that the machinery and equipment is to be correctly calibrated for the job. The roller compaction can be seen in Figure 2.5.

Traffic speeds should also be limited to 60 km/h to allow for adequate adhesion development between the existing base and the aggregate, as well as the aggregate and binder. Roque *et al.* (1991) reported that there was no relationship found between the number of roller passes and the MTD (mean texture depth) on both a new surfacing or worn out surface.

Figure 2.5: Roller compaction (Van Zyl, 2015)

2.3.6.10 Maintenance

Generally, to extend the life of a surfacing seal, diluted emulsion can be sprayed to increase or rejuvenate the bituminous binder before aggregate loss occurs as a result of traffic. The patching of small areas, where there are signs of de-bonding, and the application of fine slurry, to areas where ravelling has occurred, are also general maintenance solutions available to extend the performance of a seal (SABITA Manual 40, 2021).

2.3.6.11 Environmental and Social Conditions

Factors affecting seal performance through the physical conditions of the environment, are:

- **Climatic Conditions**
  The climate should be evaluated to accommodate the correct binder grade and type. This is done to account for the following:
  - Hot conditions where a reduction in cohesion occurs.
  - Cold conditions where adhesion is reduced and brittle and hard binders will lead to a loss of aggregate.
  - Weather uncertainties where varying temperature conditions occur.
  - Radiation where the binder ages faster when exposed to the UV radiation of the sun.
  - Humidity where volatiles evaporate and ageing increases.

  According to the SABITA Manual 40 (2021), hot modified bitumen is recommended for both wet and dry summers and winters, especially when trafficking conditions reach levels of more than 20 000 elv/lane/day. The South African climate produces average annual air temperatures varying from less then 13°C in central mountainous regions to temperatures of 17°C in the broader central and south coastal areas. The western, northern and eastern parts of the country produce warmer conditions averaging annual temperatures of 22°C. Although the South African climate produces such a variety of conditions, the maximum temperature in all of these areas may exceed 35°C and in the Highveld and the mountainous regions, minimum temperatures between -8°C and -10°C have been recorded during the winter months. Regions with an average rainfall of more than 150 mm during the winter and autumn months are considered critical areas and care should be taken when constructing seals (Van Zyl *et al.*, 2015).

- **Drainage systems**
  In urban areas where roads are often used to carry storm water, high volume and fast flowing water leads to erosion of the seal. Soil particles or detergents, which are in suspension, only accelerate the erosion process. According to the SABITA Manual 40 (2021), single seals, sand seals and slurry seals are more susceptible to erosion and should generally be avoided in urban areas where water flow occurs or where steep gradients are common.

- **Mechanical Damage**
  Any damage caused by traffic or by any of the construction machinery should

be repaired as soon as possible. This is of importance to prevent the ingress of water, potholing and other problems which indicate pavement distress (SABITA Manual 40, 2021).

- **Fine particles**
  Wind-blown sands and fine dust particles lead to poor adhesion between the binder and aggregate if these particles are present on freshly applied binders.

- **Animal droppings and fuel spillage**
  At intersections, where hard breaking and stationary vehicles are present, fuel spillage occurs. Access roads to fuel depots are also vulnerable to the spillage or leakage of fuel often leading to the softening up of bituminous binders and could lead to aggregate loss due to less adhesion being present. Research, according to the SABITA Manual 40 (2021), also shows that animal droppings, salt water, sugar cane and the presence of detergents also affect the performance of seals throughout their service lifetime.

- **Areas under development**
  Areas which are under development, with access roads often leading to the construction site, are also prone to a reduction in seal performance and a reduced lifetime. This is due to the construction materials potentially damaging the surfacing seal when falling off construction vehicles (SABITA Manual 40, 2021).

2.3.7 Economical Value of Seals

According to the Organisation for Economic Co-operation and Development (2005), many nations, with mature road networks, account for 50% of the road budget to be spent on new road construction. The goal of the Organisation for Economic Co-operation and Development was to determine if the costs of future maintenance and repaving are economically justified. From the results, maintenance costs in the future were seen as preferable to a new pavement. The SABITA Manual 40 (2021) also states that surfacing seals are preferred over typical asphalt surfacings due to them being cheaper. Thus, seals, from an economical perspective, are valuable as they provide the same service as asphalt surfacings whilst being more economical.

2.4 Mechanisms of Seal Failure

The binder composition greatly affects the performance of a seal, especially at molecular level. According to the research done by Robertson (1991) and Hunter *et al.* (2015), bitumen is built up of an internal multi-molecular matrix. This bituminous matrix consists of polar molecules that are dispersed in a phase, which is either less polar or non-polar at all. The polar molecule produces a material with elastic properties. The viscous behaviour of the binder is due to the matrix being able to flow under loading or prolonged loading. The visco-elastic properties of the binder affect seal performance. Furthermore, and continuing from the factors influencing seal performance, as stated in Section 2.3.6, the mechanisms of seal failure, referring to the mode and process in which surfacing seals fail, are investigated and elaborated on next.

2.4.1 Skid or Texture Loss

The texture on a road is governed by the skid resistance between tyres and the road surface. The safety of a road is primarily dominated and determined by the amount of skid resistance a road surface provides. Therefore, adequate skid resistance is required to ensure vehicle stability by ensuring sufficient frictional resistance to vehicle sliding (Fawzy *et al.*, 2021). Road user safety is also ensured as adequate skid resistance lowers the risk of increased breaking distance. Texture depth, an important design variable, is used to calculate the application rate of a bituminous binder. The aggregate geometry and texture depth relates to the amount of voids between the aggregate particles which the binder must fill to provide sufficient adhesion.

According to the design principles, as documented in the SABITA Manual 40 (2021), the minimum amount of voids to be filled with bituminous binder, to prevent aggregate loss, when no embedment is present, is 42% for single seals and 55% for double seals. As seen in Figure 2.6, 30% of the aggregate height is to be wetted as this corresponds to 42% of voids to be filled.

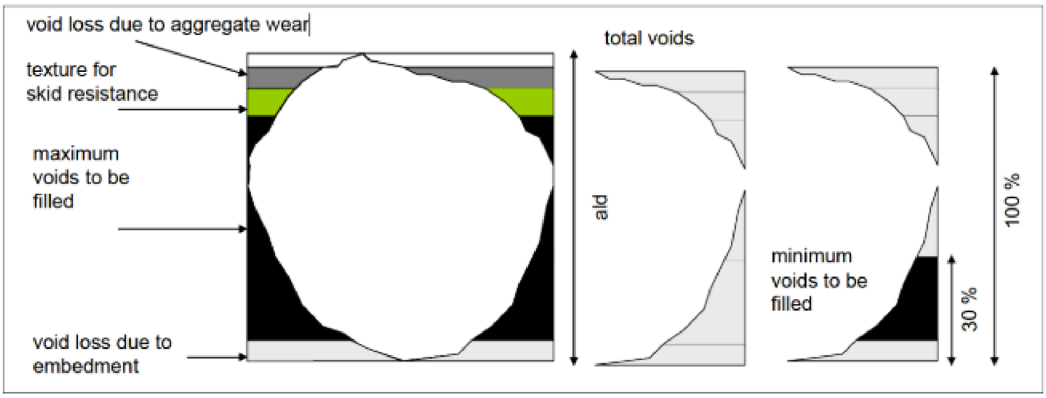

Figure 2.6: Void filling principles for determining the binder rate (SABITA Manual 40, 2021)

As seen in Figure 2.6, the amount of voids to be filled with the binder, determines the void loss due to aggregate wear and the texture for skid resistance. The filling of voids is also of importance as it can affect the binder application rate and indirectly, the performance of the seal if bleeding occurs. Another influencing factor, leading to texture loss by means of bleeding, is the influence of binder run-off during construction periods, especially in the case of emulsions. An inconsistent binder film thickness is produced in the up-or-downstream regions due to texture depth influences, steep gradients or binder application rates.

According to the results of Kashaya (2013), a 13.2 mm seal experiences more binder run-off than a 9.5 mm seal due to the binder flowing through the larger aggregate particle channels. It is observed that the binder does not flow over the aggregate particles unless embedment occurred with respect to the height of the surrounding aggregate particles. Evaluating the binder application rate, it was reported that an increase in spray rate results in an increase in binder run-off. Excess flow also occurred above an application rate of 1.9 l/m^2 for the 13.2 mm seal (Kashaya, 2013). Due to binder run-off, the binder application rate, as per the seal design, is not necessarily valid for all seal surfacing areas due to the binder flowing and possibly collecting in a certain area.

Thus, the amount of available voids is affected by the binder movement.

Furthermore texture loss is dependent on the rate of void loss during either or both the construction period or the in-service period. There are a number of different factors and mechanisms which contribute to void loss. They are explained in detail in Section 2.4.1.1 and Section 2.4.1.2

2.4.1.1 Aggregate Embedment

Embedment can be seen as the loss of voids in the seal due to surfacing aggregate being pushed, punched or forced into the existing substrate, such as a base. The concept of embedment can be seen in Figure 2.7.

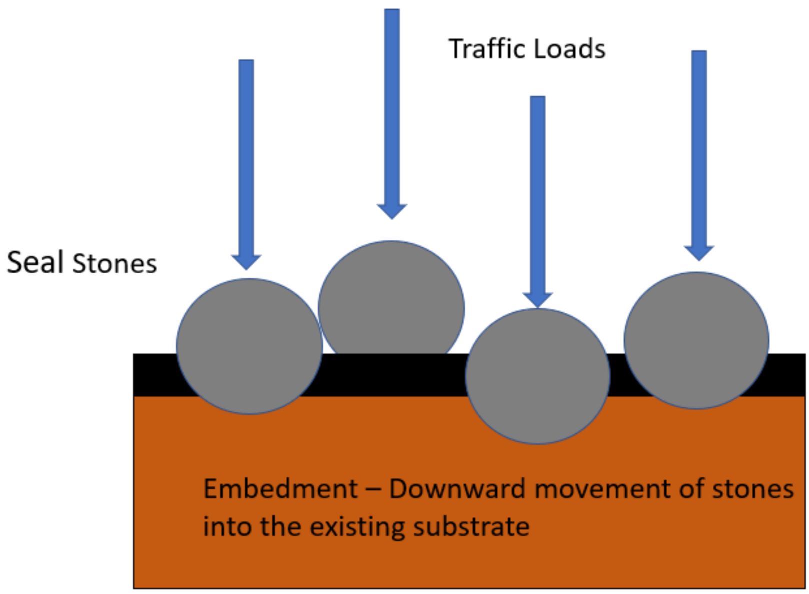

Figure 2.7: The concept of embedment as adapted from Abrahams (2015)

According to Woodward *et al.* (2000), a certain amount of embedment is required to ensure seal durability and performance. Milne (2004) states that the amount of embedment, which is required initially, cannot be predicted accurately. The following factors influence embedment during the construction phase.

- Hardness and condition of the existing substrate: The hardness of the surface affects the depth to which the particles become embedded in the surface. The aggregate size is directly related to the hardness of the surface. When using small aggregate chippings, there is a risk of early embedment which could result in a rapid loss of texture depth and even flushing of the binder. When using too large aggregate stones, there is a risk of immediate failure of the treatment due to stripping during construction. The hardness of the surface also affects the binder application rate. For soft surfaces, the application rate needs to be reduced to account for greater embedment (Hunter *et al.*, 2015). Milne (2004) describes that the ball penetration test is done to quantify the hardness of the existing surface. The results can then be reworked to estimate potential or expected embedment.

Although the test provides an idea as to the hardness of the surface, it does not take aggregate shape, flakiness, orientation and spread rate into account.

- Construction compaction: According to the SABITA Manual 40 (2021), half of the embedment, as determined by performing the ball penetration test, can be expected to occur during the construction period. Thus, during the rolling stage of construction, the aggregate chips would embed into the existing substrate to an approximate depth equal to half of the total expected embedment.

The following aspects address the embedment and void loss during the in-service lifetime of the seal.

- Traffic volumes and speed: The extent of embedment is a function of the quantity of vehicles, especially heavy vehicles, using the designed road (Milne, 2004).

- Aggregate composition: The composition or mineralogy which an aggregate consists of, influences the aggregate's ability to resist polishing when experiencing traffic forces. According to Kane *et al.* (2013), there are two types of polishing. The first is called general polishing which tends to chip away or smooth off the rough stone edges. Single mineral aggregates, such as limestone, are of relatively low hardness and thus, a low resistance to polishing exists. The second process relates to differential polishing which tends to create new rough textures. It is of note that differential polishing is only possible on aggregates which consist of multi-minerals. Examples of these aggregates include sandstone. The Polished Stone Value (PSV) test was developed to estimate the resistance to polishing of an aggregate for the first time. The test cannot be used in asphalt mixes due to the curved shape of the stone specimens. Subsequently, the PSV test is just used as a ranking tool for certain laboratory conditions (Kane *et al.*, 2013).

- Aggregate geometry: Embedment is also influenced by the geometric properties of aggregate, as elaborated on and continued from Table 2.2 in Section 2.3.6. Van Niekerk (2002) highlight that these properties include aggregate shape, angularity and Flakiness Index. Flakiness, as an aggregate property, provides a relative indication as to the shape of the aggregate particle. Figure 2.8 shows the difference between flaky aggregates and non-flaky particles. It should be noted that flakiness does not account for the shape as it does not differentiate between round, spherical or angular shapes. When performing the flakiness calculations, as per the TMH 1 (1986), a higher value would indicate that a large portion of the particles are flaky, whilst a lower value indicates that a small portion of the particles are flaky. Another aggregate property which could present a better indication as to the shape thereof, is the average least dimension (ALD). According to the TMH 1 (1986), the ALD of surfacing aggregates is determined by the gradation and Flakiness Index. The ALD can be described as the smallest perpendicular distance between two parallel plates through which the aggregate particle passes. Another definition describes the ALD as the overall average of the smallest dimension for a number of aggregate particles. Both the flakiness and ALD of aggregate particles affect the void content as they determine the thickness of the seal surfacing layer whilst establishing a pre-determined void content, which in result, affects the binder application rate. Under traffic loading, the void content decreases as the aggregates embed into the existing substrate based on their geometric properties. The effect of the ALD and flakiness of aggregate can be seen in Figure 2.9.

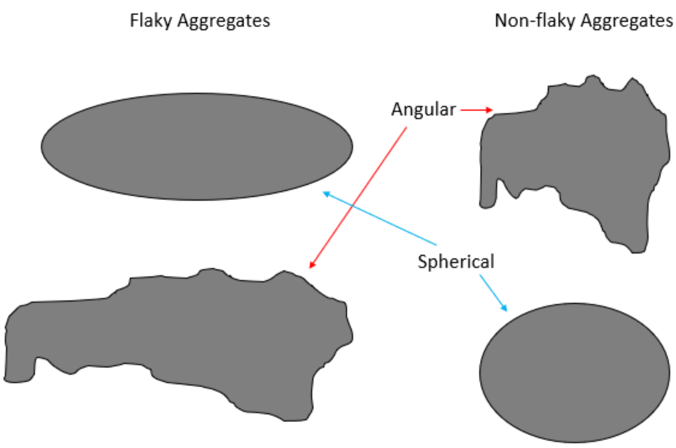

Figure 2.8: Flaky vs non-flaky aggregates as adapted from Abrahams (2015)

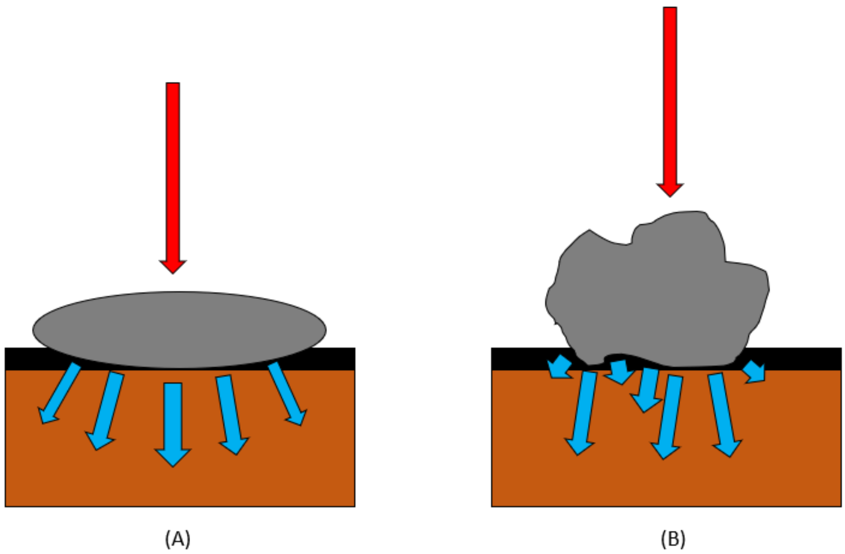

Figure 2.9: Aggregate shape influence on embedment where a) is a flaky aggregate and b) is a rounded angular aggregate as adapted from Abrahams (2015)

As seen in Figure 2.9 (a) and (b), the stress distributions differ for both a flaky (flat) particle and an angular (cubical) particle. The stresses transferred through a flaky particle, as shown in Figure 2.9 (a), is more equal whilst the stresses transferred through a non-flaky particle, as shown by (b), results in a larger amount of stress concentrations. Thus, the angular particle would have a higher chance of shearing the substrate surface below while the flaky aggregate distributes the loads onto a larger area, decreasing critical stress points. It can be expected that the angular particle embeds easier into the surface below when compared to the flaky aggregate.

- Binders: Hoffmann and Potgieter (2007) report that modified binders, with a focus on non-homogeneous bitumen rubber binders, are stiffer than traditional binders. A stiffer binder will bind the individual aggregate particles more together, resulting in a seal with a better load distribution. This will ensure that the surfacing seal will act as a rigid and uniformly distributed load on top of the existing substrate, such as a base. This, in effect, will lead to less embedment issues.

2.4.1.2 Aggregate Orientation

According to Van Zyl and Jenkins (2015), good adhesion is achieved between the bituminous binder and the aggregate by making use of steel wheel or pneumatic tyre rollers. The aggregate particles then orientate themselves to different degrees during construction and initial trafficking, based on the following factors:

- Aggregate spread rate.
- Aggregate characteristics such as shape, flakiness and ALD.
- Binder type.
- Binder application rate.
- Binder temperature/viscosity relationship.
- Type of compaction.
- Number of compaction blows or roller passes during construction.

Aggregate and binder application rate
Van Zyl (2000) mentions two different aggregate spread rates which correspond to the spread rates as per the SABITA Manual 40 (2021). The first spread matrix corresponds to a shoulder-to-shoulder (sh-sh) matrix, as seen in Figure 2.10 (a). The second application matrix, corresponds to an open spread matrix as seen in Figure 2.10 (b).

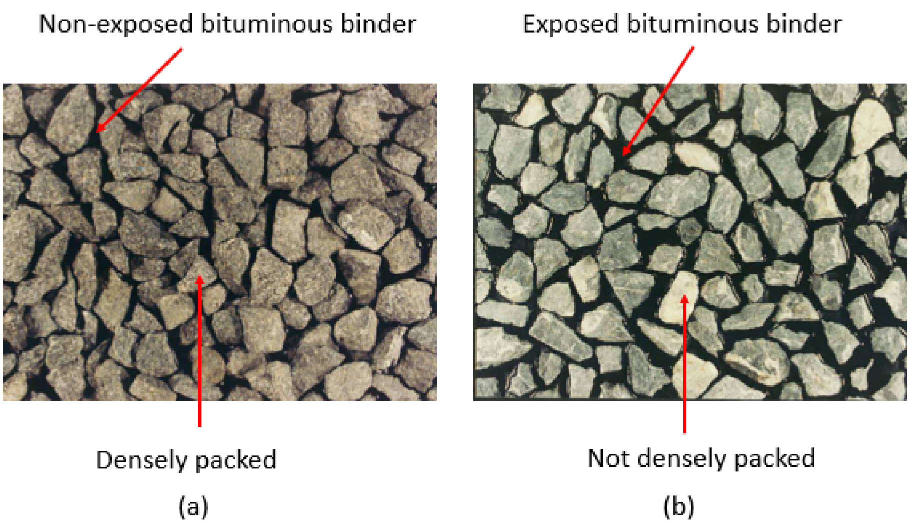

Figure 2.10: Aggregate Spread Matrix (Van Zyl, 2000)

A densely packed matrix results in a loss of voids in the mat. The bituminous binder will then have the ability to rise above the stone level when expanding during hot conditions. The balance between an aggregate packed matrix is of importance as noted by Lawson *et al.* (2007) reporting that aggregate particles should be placed so that they do not touch each other, but are close enough so that another particle will not be able to fit into the space between particles. It is generally required that a 15 - 20% void quantity is seen between the stone. Initially, once the aggregate has been spread, the matrix or mat typically looks very light. After construction compaction, such as rolling, and initial traffic, the particles begin to re-orientate themselves to go into their final position.

The SABITA Manual 40 (2021) states that over chipping or even dense chipping, prevents aggregate orientation. This results in the aggregates not orientating onto their respective ALD. Due to the matrix being overly chipped, more additional binder would be required than a dense shoulder-to-shoulder matrix after rolling. A more open spread rate can accommodate up to 30% more binder in a single seal than a dense matrix. Kumbargeri *et al.* (2019) states that it is of importance that all or most of the aggregates re-orientate themselves to lie on their flattest side. This process is required to form a one-stone thickness after rolling, in order to achieve desired performance. The cumulative percentage of aggregates lying on their flattest side (CPAF), is dependent on the following according to the results of Kumbargeri *et al.* (2019):

- The binder application rate (BAR): For the binder application rate, the CPAF results increased up until the BAR reached a rate of 0.35 Gal/yd^2 or 1.58 l/m^2. Thereafter, the CPAF drops down and decreases. Figure 2.11 shows this trend.

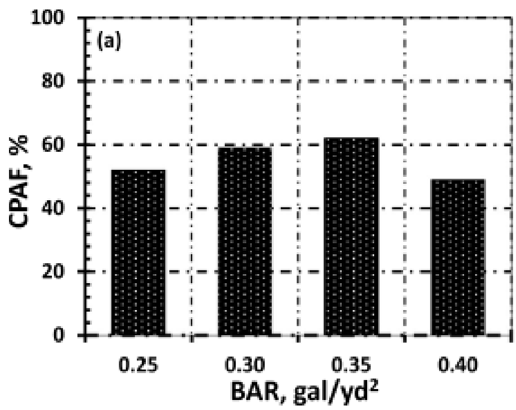

Figure 2.11: CPAF vs BAR (Kumbargeri *et al.*, 2019)

This trend is logical since the aggregate particles can rotate, translate and compact easier when there is more binder available as it acts as a lubricating fluid. The CPAF decreases when the BAR = 0.4 Gal/yd^2 or BAR = 1.81 l/m^2 due to there being too much binder present and it moving out and onto the surface during compaction. Again, when the binder moves out over surface during compaction, the uplifting forces rotate the aggregate particles vertically again. This process is schematically shown in Figure 2.12.

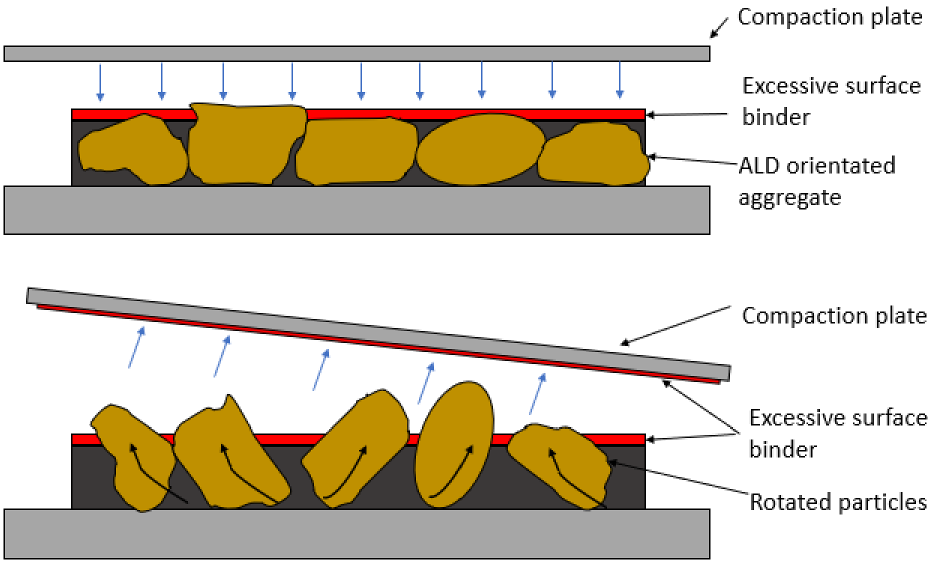

Figure 2.12: Particle rotation due to binder oozing out on the surface as adapted from Kumbargeri *et al.* (2019)

- The aggregate application rate (AAR): As seen in Figure 2.13, the CPAF value increases up until AAR = 18 lb/yd^2, after which it decreases again. After the AAR = 18 lb/yd^2, which is the optimum aggregate application rate, the particles begin to disorient in a perfect 2-D environment. The disorientation can be described by making use of *the wedge and lever* principle.

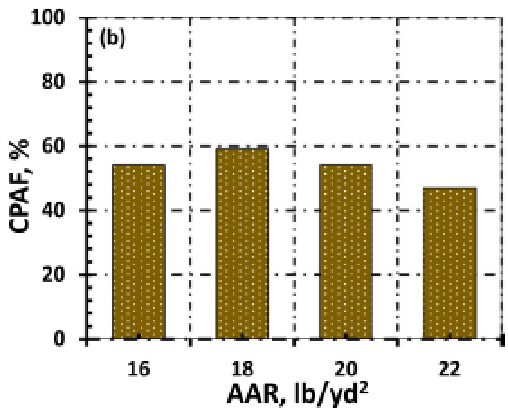

Figure 2.13: CPAF vs AAR (Kumbargeri *et al.*, 2019)

If the contact area between the aggregate and a single wheel is of such that in an ideal 2-D mosaic matrix, the aggregate amount reaches a high enough value, the particles begin to re-orientate themselves due to the pressing down of certain particles causing the uplift and rotation of neighbouring particles. The process can also be explained by noting that where the excessive aggregates bridge over the single layer aggregates, a pushing force causes them to disorient from their flattest side. This process can be seen in Figure 2.14.

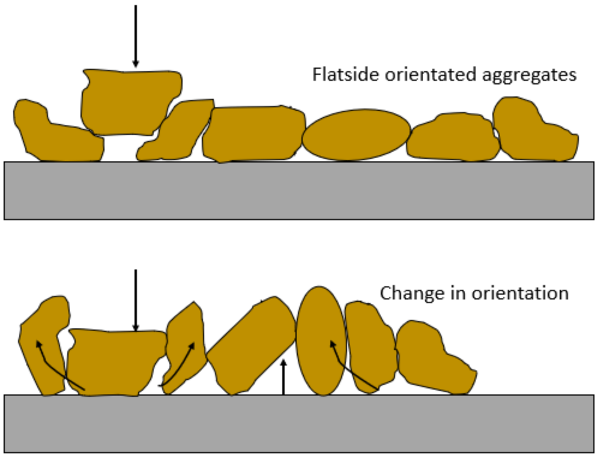

Figure 2.14: Wedge and Lever effect due to a high AAR (Kumbargeri *et al.*, 2019)

Although the over application principle, according to Kumbargeri *et al.* (2019), states that a high AAR results in the uplifting and rotating movement of aggregate under trafficking, it is of importance to analyse the aggregate movement as a function of wheel contact footprint and wheel contact stress. De Beer and Fisher (1999) mention that the introduction of non-uniform tyre-pavement contact stresses in pavement design and analysis, results in a more coherent understanding of the surface contact reaction. Furthermore, Hernandez *et al.* (2013) shows that there is a correlation between the applied load and tyre pressure on the contact length of a tyre. By means of Stress-in-Motion (SIM) simulations, variation of vertical, longitudinal and transverse stresses are observed. A typical vertical contact stress perspective, with variation in tyre inflation pressure, is seen in Figure 2.15.

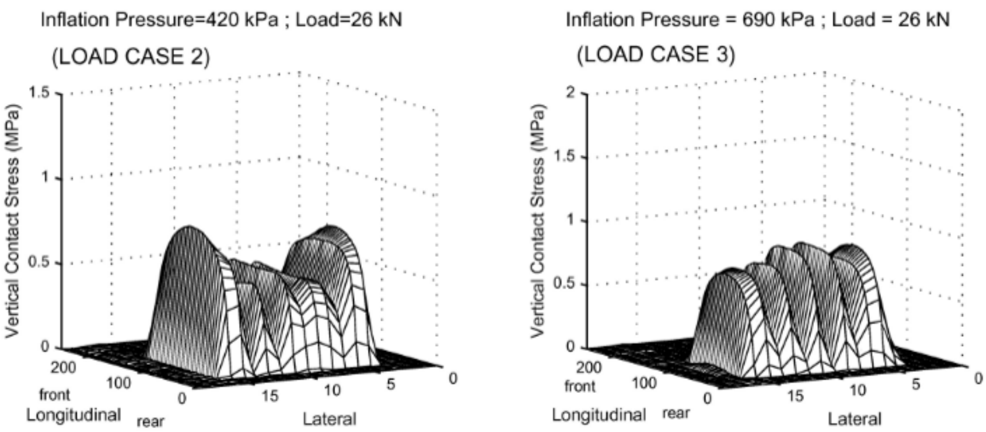

Figure 2.15: Vertical contact stress for an under inflated and overloaded tyre (De Beer and Fisher, 1999)

From Figure 2.15, it is seen that tyre inflation pressure, with either an increase or decrease, affects contact stress. A similar change in stress is observed with a change in load. Subsequently, from the results of De Beer and Fisher (1999) and Hernandez *et al.* (2013), in practice, a tyre footprint enables a contact pressure on a number of aggregate particles simultaneously. The movement of aggregate is thus dependent on the tyre footprint on a number of aggregate particles and not solely in an ideal 2-D environment as described by Kumbargeri *et al.* (2019). Therefore, the variation in vertical, longitudinal and transverse stresses differentiate per wheel load. As a result of stress variation, the behaviour of seal aggregate in terms of orientation differs. The movement of aggregate on the edge of the wheel path is influenced differently under an inflated and over loaded wheel when compared to an over inflated wheel. Subsequently, from the studies from De Beer and Fisher (1999) and Hernandez *et al.* (2013), it is apparent that the behaviour of aggregate in an over application matrix does not necessarily relate to the *wedge and lever* principle, but it is as a result of tyre footprint relating to tyre-pavement contact stresses.

Aggregate properties

As mentioned in Table 2.2, aggregate shape, as described by means of the flakiness and angularity, and nominal size influence orientation. With an increase in angularity, aggregate interlocking is improved, restricting the orientation movement thereof under trafficking onto ALD. With an increase in flakiness, aggregates are either prone to orientate onto ALD faster when upright whilst already ALD-placed particles restrict orientation movement.

Hot polymer modified binder behaviour

The main difference, in terms of aggregate orientation, with regards to S-E1 and S-E2 modified bitumen, is the amount of polymer added to the binder. Van Zyl (2018) reported that unmodified bitumen and modified bitumen behave very similarly during cold/low temperatures as both will have a high complex modulus (G*), which indicates the resistance of the binder to deformation. This can be seen in Figure 2.16 at the upper left top section. At these colder or lower temperatures, the bitumen dominates the behaviour as cold bitumen is very stiff. As the temperature increases from left to right, the complex modulus of the unmodified binder decreases, whilst the phase angle (which indicates the time lag between a load and the response of the binder) increases. Thus, the unmodified binder becomes less stiff and more viscous at higher temperatures.

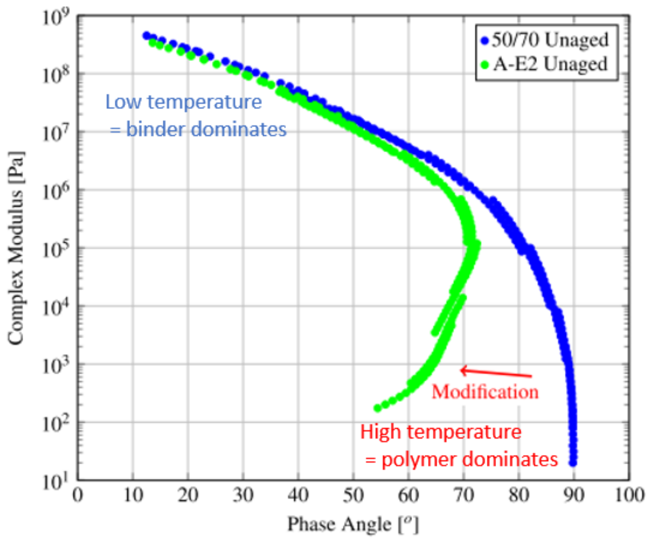

Figure 2.16: Black space diagram of SBS modified and Unmodified binder as adapted from Van Zyl (2018)

As the modified binder's (as indicated by the A-E2 line) temperature increases, the complex modulus decreases whilst the phase angle increases. This occurs until the phase angle reaches a range between 60 and 70 degrees, which is where the bitumen becomes very soft, loses stiffness and the polymer starts to dominate. Subsequently, the curve back-tracks and the elastic properties (due to the polymer) increase as seen in Figure 2.16. Thus, for the compaction of seals, the binder is at a high temperature and the polymer is dominating.

An S-E2 binder contains more elastic polymer, when compared to an S-E1 binder, which theoretically would cause the aggregate particles to bounce back and not orientate as much. The S-E1 binder, consisting of a lower elastomer modification, may experience less bounce-back and more orientation in comparison with the S-E2 binder.

According to personal communication from Van Zyl (2021), when hot modified bitumen rubber S-R1 is constructed, it is expected of the aggregate particles to only orientate between 5 - 10 years after construction. This is mainly due to the significant adhesion qualities between the aggregate particles and the binder, as well as the high stiffness and re-healing properties and the improved elasticity and flexibility characteristics. The later properties result in all aggregate particles that start to orientate under trafficking to just revert back to their original position (which is not always the ALD). This process can schematically be seen in Figure 2.17. The aggregate particles orientate themselves more onto their respective ALD's, but due to the stiffness, elastic and flexibility properties of the S-R1, the particles move back to their original positions (Van Zyl, 2021).

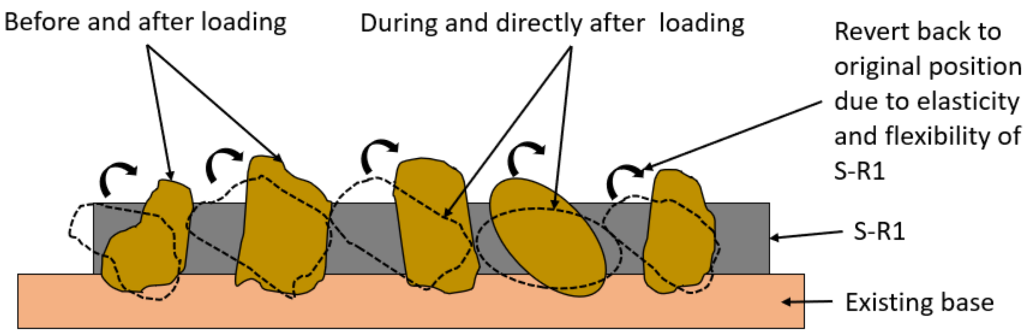

Figure 2.17: Influence of S-R1 on aggregate orientation

Due to this reason, the aggregate particles do not orientate much during the construction process. After initial trafficking has occurred, the bounce back effect could be problematic as a uniform aggregate mat is not formed which influences the voids between the aggregates and could later lead to chip loss, texture reductions and bleeding or flushing.

S-R2 modified binders are generally co-modified with Fischer Tropsch wax to reduce the viscosity of the binder during construction and increase it (which increases the stiffness) during the in-service period. The reduced viscosity is advantageous as the binder can be applied at very low temperatures during construction. Van Zyl (2021) mentions that the aggregate particles orientate too easily during the construction period due to the binder having such a low viscosity and it being very soft. The aggregate particles continue to orientate and do no necessarily end up on their flattest side which is the desired position. This orientation process can be seen in Figure 2.18. The dashed outlined stones display the constant orientation movement of the particles during construction compaction.

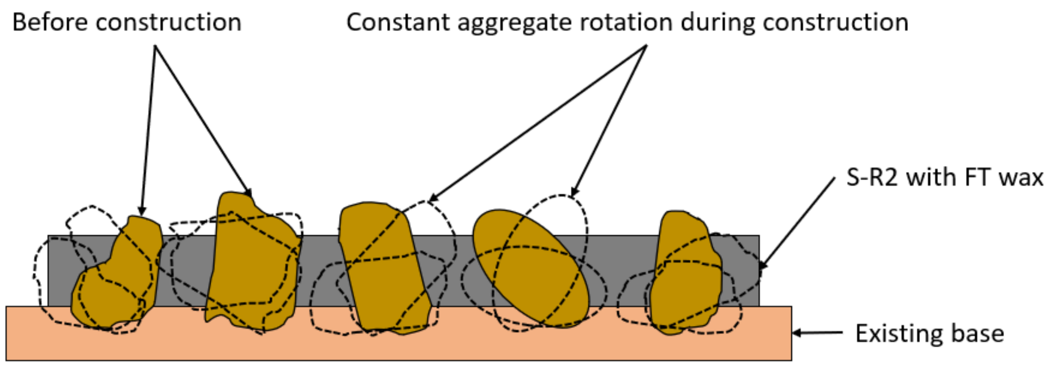

Figure 2.18: Influence of S-R2 co-modified with FT wax on aggregate orientation

Stone orientation plays an important role in the void content and effectively, the binder application rate. The SABITA Manual 40 (2021) states that ideal aggregate spread rates are based on the purpose of the seal and the shape and flakiness of the aggregate. The results from Kumbargeri *et al.* (2019) show that low binder application rates or excessive aggregate application rates can lead to aggregate particles disorienting themselves from their average least dimension. The influence of hot modified bitumen is also of note and it is clear that binder application adjustments are required to account for the aggregate particles orientating too easily or (due to elasticity and flexibility) too late during the in-service trafficking period. Subsequently, this study will investigate what effect the different types of modified binders and aggregate application rates have on aggregate orientation. As seen, the rheological properties of the polymer hot modified binders contribute directly towards the elasticity and flexibility properties and thus, a correlation between the rheological properties and the stone orientation is required.

2.4.2 Rutting and Permanent Deformation

According to Robertson (1991), bituminous binders in the dispersing phase are not generally very elastic. Although it is expected to be compatible, the binder is not at all sensitive to oxidation. The binder does not harden as well which leaves it vulnerable and exposed to rutting and deformation. This generally occurs at high temperatures. Due to this binder being in the dispersed phase, there are not a lot of large molecules available to provide sufficient elasticity. It is of note that the dispersing phase consists of non-associated material, which characteristically would harden at low temperatures. At these low temperatures, the bitumen would become very stiff and more susceptible to cracking, rather than rutting. Bituminous binders with a sufficient amount of associated material would produce a higher elastic modulus at a high temperature and as a result, deformation would reduce. With an increase in elasticity, the bitumen would also contain a higher proportion of large molecules and thus, it would not be as susceptible to failure at lower temperatures. According to Robertson (1991) and Milne (2004), the deformation of the seal is related to the rotation of the seal stone which affects the void content for the binder and the texture matrix , further leading to problems such as bleeding.

2.4.3 Shelling/Rock Loss

Hunter *et al.* (2015) report that there are five categories into which rock loss, or chip loss could be divided, namely: chip loss immediately after application, chip loss during the first winter, chip loss during the in-service period, bleeding during the first hot summer and fatting up during the in-service period.

Chip loss can explained by investigating Figure 2.19. The adhesion bond would increase from point 1 to point 4. According to Abrahams (2015), this is mostly due to cutbacks which evaporate quicker when there is a more direct path to the surface. When a road is opened too early and traffic loads are applied while cold temperatures dominate, it could be that surface 2 has fully bonded but surface 3 has not established a sufficient bond yet. As traffic hits the surfacing seal, the friction of the wheels and the load causes the partially unbound particles to dislodge from the binder. This process is known as rock loss, shelling or chip loss.

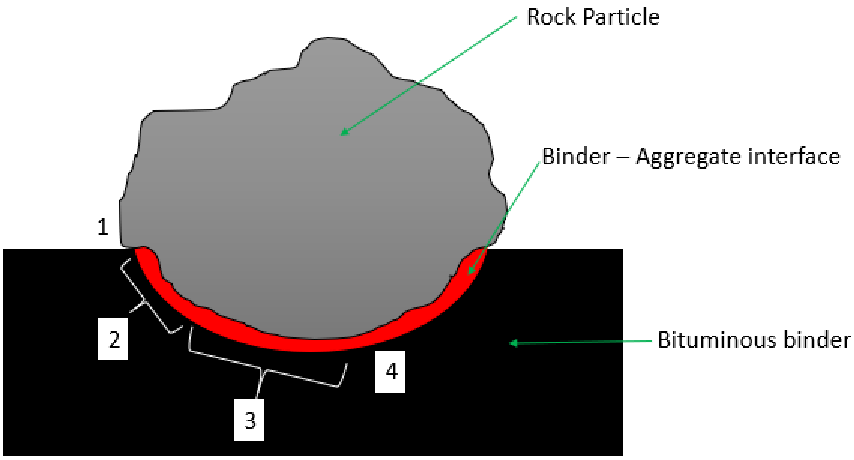

Figure 2.19: Aggregate and Binder interface as adapted from Abrahams (2015)

According to Lawson *et al.* (2007), both bleeding and flushing have to do with an excess amount of binder filling the voids in between the aggregate particles. Subsequently, when a chip seal loses aggregate, both bleeding and flushing will occur. In addition, excessive embedment will also contribute to bleeding and flushing.

When bleeding occurs, the binder at the top of the surface adheres to tyres and results in tracking which refers to the seal surfacing or seal aggregate rolling over and being picked up. Thus, bleeding can lead to chip loss as both the aggregate and the binder are effectively picked up from the pavement. A flushed pavement is very similar to bleeding, but it differs in the sense that flushing is not an immediate maintenance problem. The bituminous binder still fills the void and moves up to the top of the particles, but the binder is in either solid or semi-solid form. Herrington *et al.* (2012) also state that flushing occurs when the available void volume is insufficient to accommodate the volume of bitumen and the aggregate fines and any other detritus that is present. It is also concluded that the generation of fines from abrasive traffic action and the breakdown of aggregate during construction and in-service resulted in seal flushing. Secondary causes, such as the over application of binder or the build-up of detritus, such as tyre rubber and break linings, also contributed to flushed seals. Over time, flushing leads to bleeding. Chip loss can then occur with repeated traffic loading (Lawson *et al.*, 2007).

Lawson *et al.* (2007) report that chip loss problems occur when a seal is applied outside of the regional construction season. Chip loss problems tend to occur when abnormally cool or cold temperatures and conditions are present during or after the placement of a seal coat, before adhesion has fully developed between aggregate and bituminous binder. Aggregate loss problems could also potentially occur when:

- a too stiff binder is used for the environmental conditions.
- application rate of the bituminous binder is too light.
- the aggregate was not applied directly after the application of the binder.

A very sudden drop in temperature or the occurrence of rain during the night after construction also resulted in aggregate loss soon after construction. Areas in which winter rainfall occurs are particularly exposed and vulnerable to aggregate loss as well as areas exposed to short spells of cold temperatures together with wind or high humidity. In the case of hot polymer modified binders and 70/100 penetration grade bitumen, a minimum road surface temperature of 25°C is necessary to ensure adequate adhesion between the binder and the aggregate (Van Zyl *et al.*, 2015).

Hunter *et al.* (2015) report that early chip loss may be due to slow breaking when emulsions are present or poor surface wetting when cutback bitumen is used. This problem can be avoided by using cationic rapid setting emulsions with binder contents of > 70%. Poor wetting can be addressed by making use of adhesion agents or pre-coating methods. Subsequently, another problem is that the best aggregate for skid resistance often exhibits the lowest resistance to crushing.

2.4.4 Thermal and Fatigue Cracking

Cracking is often reflected from the structural layers through to the surface. Generally cracking failures can be associated with fatigue cracking, thermal cracking and cracking associated with their compound effect (Abrahams, 2015).

According to Robertson (1991), cracking can again be related to binder composition. If the molecular structure/matrix becomes too rigid over time, the layer loses its elastic ability. Due to a decrease in elasticity, fractures are more likely to occur to a point where healing cannot rectify the situation. The repetition of re-working the rigid matrix will eventually lead to fatigue and cracking. Cracking can also be related to another feature, namely temperature. At lower temperatures, neutral materials rearrange themselves into a structured matrix. This causes the binder to become more brittle and vulnerable to cracking under applied stresses. Due to the organisation of low polarity as well as non-polar components, materials could shrink at low temperatures. This process speeds up cracking. The performance between little association and highly associated pavements can be seen in Figure 2.20.

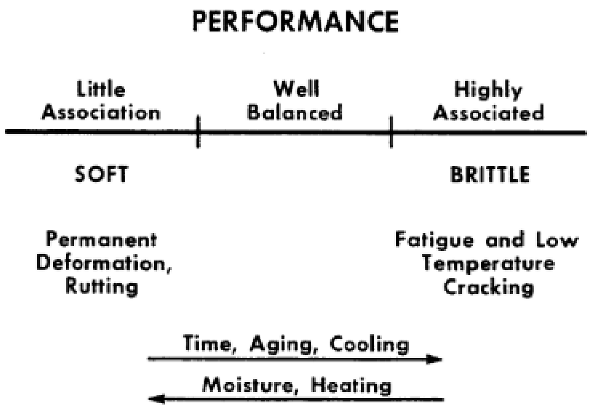

Figure 2.20: Performance of pavement with regards to association (Robertson, 1991)

2.4.5 Moisture and Adhesion Damage

According to Robertson (1991), adhesion and moisture damage go together, but only up until a certain point. Adhesion, as per definition, relates to the involvement of both the binder and aggregate. It appears to be governed by the molecular and intermolecular level. Polarity plays an important role as it promotes the attraction of polar binder contents to the also polar surface of the aggregate stones. Aggregates differ in polarity with variation in environmental changes. Adhesion exists through the connection of the polarity of bitumen and aggregate. Robertson (1991) mentions that polarity alone is not necessarily sufficient to achieve a good quality adhesion connection between the binders, layers and aggregates due to external factors, which are influenced by the environmental conditions.

The capacity to absorb water varies with the composition of bitumen. Apart from the damage that water has on the bitumen, seal and pavement, water has the potential to affect the bituminous binder due to its polarity. Water generally affects the bitumen characteristics and softens it up. Rutting and permanent deformation could occur due to a reduction in strength. Aged bitumen or oxidised bitumen has the potential to absorb more water due to polarity characteristics. They are also harder than newly constructed bitumen and thus, the effect of oxidation and moisture work against one another. It should again be noted, that behaviour is dependent on composition (Milne, 2004).

2.5 Bitumen

2.5.1 Introduction

According to Hunter *et al.* (2015), bitumen often refers to refined bitumen, which corresponds to a hydrocarbon product along with its derivatives. During the refining process, the lighter fractions including gas (petroleum), liquid and petrol and diesel are removed from crude oil. In some areas, bitumen is also found as a natural deposit. The physical appearance of bitumen corresponds to a viscous black or dark brown liquid, which could also be in a solid form, depending on the temperature thereof. This corresponds to a state when heated, dissolved in petroleum or when emulsified in water. As the temperature of the bitumen increases above its specified softening point (SP), the bitumen gradually softens, moving into a liquid state, whilst hardening as the temperature decreases below the SP, defining the solid state. Important attributes of bitumen include its solubility in trichloroethylene and its non-volatile characteristic (SABITA Manual 2, 2012).

2.5.2 Bitumen Properties

To fully understand bitumen and its behaviour, an understanding of its visco-elastic properties is required. Due to bitumen being a semi-solid, its behaviour cannot be defined by either a solid or fluid theory. Subsequently, the science of deformation and flow, also known as rheology, is used to defined these type of materials. Bitumen, with its visco-elastic properties, is thus dependent on temperature and loading time, making it a non-Newtonian fluid, as it does not correspond to Newton's law of viscosity (Hunter *et al.*, 2015). Due to bitumen's visco-elastic properties, it acts as an elastic solid at low temperatures, causing it to return to its position after a load is applied. Subsequently, bitumen can fail by cracking or by means of brittleness when exposed to excessive low temperatures. At elevated temperatures and extended loading, bitumen acts as a viscous fluid and thus, plastic strain occurs that is unrecoverable. During intermediate temperature conditions, bitumen displays both viscous and elastic behaviour as described by Burger's Model. Burger's model shows that after an immediate elastic response, an increase in strain occurs with time until the load is removed. The viscous behaviour of bitumen causes a change in strain whilst the elastic strain is recovered instantaneously with some additional recovery when the load is removed. This process is known as delayed elasticity. Due to the visco-elastic properties of bitumen, a permanent strain remains, also known as rutting (SABITA Manual 2, 2012).

The first uses of bitumen can be traced back to ancient times, where bitumen was often referred to as 'pitch' in the sacred language of Hindus in India. The Latin equivalent corresponded to the terms 'pertaining to pitch' which was shortened to bitumen. The uses of bitumen continued in the inhabited parts of the world, where natural bitumen deposits were readily available. These ancient techniques and practices are still used today (Hunter *et al.*, 2015).

According to SABITA Manual 2 (2012), bitumen is a readily adhesive, waterproof, strong and highly durable binder. Bitumen is referred to as a binder due to it providing adhesion between the stone (aggregate) and the road surface. Flexibility is also provided to mixtures containing mineral aggregates. The construction industry uses a large portion of bitumen in paving and roofing. 85% of all produced bitumen is used in road construction, while 10% is used in roofing applications and the remaining 5% corresponds to usages in sealants such as pipes and joints (Hunter *et al.*, 2015).

2.5.3 Origin

Small deposits of naturally occurring bitumen can be found in certain areas including, but not limited to West India, Mexico, USA and Germany. Natural deposits of bitumen refer to bitumen in a pure state whilst less pure bitumen deposits refer to high fractions of bitumen along with high proportions of mineral matter. Therefore, the composition of bitumen varies in that there are differences in purity. As described by Kim (2014), Gilsonite, found in the Uinta Basin outside the town of Bonanza Utah, is the largest bitumen deposit in a pure state.

Crude oil originates from the deposition of marine organisms and vegetable matter on the bottom of the ocean along with oceanic fractured material such as rock and mud. With deposits occurring over thousand of years, the pressure of the weight of the organic material compresses the lower sections into sedimentary rocks. Crude oil is then formed when the organic material (organisms and vegetable matter) converts to hydrocarbon. Areas where crude oil depositions have been found include Asia, the Atlantic Ocean, areas in the Americas as well as the Middle East and the North Sea (Hunter et al., 2015). In South Africa, bitumen is processed at various oil refineries in Durban, Cape Town and Sasolburg (SABITA Manual 2, 2012)

During the refining process of crude oil, to produce petroleum, one of the derivatives include bitumen. Bitumen, as a primary product, is not often produced and it is usually simply a secondary product of the process. The chemical composition of crude oil differs from region to region and is dependent on the organic matter from which it originates, as well as the environmental conditions under which it was produced naturally. Subsequently, bitumen can present varying chemical compositions and properties based on the refining process and the specific crude oil. Milne (2004) describes that of the 1500 types of crude oil known, only 250 are suited for the production of bitumen. Ideally, crude oils with a high proportion of residue, asphaltene and sulphur display high contents of aromatics, also known as hydrocarbons, and thus, they are most suited for the production of bitumen.

It should be noted that bitumen is not the same as tar or coal tar pitches. They are solely derived from coal products. Petroleum pitches, which correspond to hydrocarbon residue, are produced by temperature cracking, coking or the oxidation process of different petroleum proportions and should not be confused with bitumen. Also, natural asphalt, such as Trinidad Lake Asphalt, also differs from refined bitumen and it often contains high fractions of mineral matter leading to a mass loss during temperature increases (Hunter *et al.*, 2015).

2.5.4 Composition

Bitumen, consisting of hydrocarbons, is still dependent on the environment in which it is produced as well as the organic matter from which it originates. A few primary hydrocarbons, in small quantities, are always present. These include oxygen, sulphur, nitrogen and trace metals including vanadium and nickel. It is a difficult task to obtain the precise composition of bitumen due to it being dependent on its origin, and each bitumen being different than any other. Most of the crude oils contain the composition as described by Table 2.4.

Table 2.4: Composition of Crude Oil (SABITA Manual 2, 2012)

Carbon	82% - 88%
Hydrogen	8% - 11%
Sulphur	<6%
Oxygen	<1.5%
Nitrogen	<1%

The constituents of bitumen can be defined by making use of chromatographic techniques. These techniques are based on the initial precipitation of asphaltenes using n-heptane and subsequently, separating the remaining proportions (Hunter *et al.*, 2015). Thus, bitumen can be divided into two main chemical groups, namely asphaltenes and maltenes. The composition of crude oil is schematically displayed in Figure 2.21.

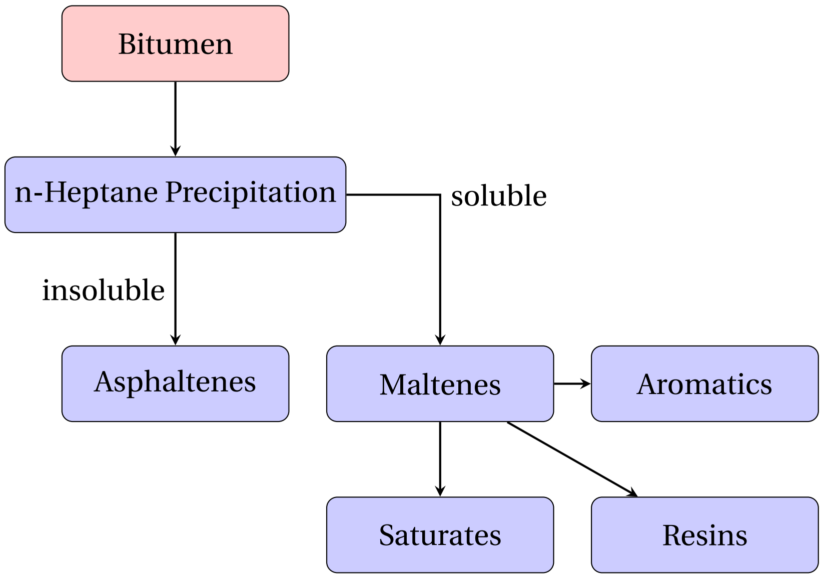

Figure 2.21: Approximate Bitumen Composition (SABITA Manual 2, 2012)

2.5.4.1 Asphaltenes

Asphaltenes, by appearance, are dark black and glossy in colour. These n-heptane insoluble solids, as seen in Figure 2.21, make up 5 - 25% of bitumen. They contain a relatively high molecular weight and influence the rheology of the bitumen tremendously. A harder (or more solid) bitumen product can be produced by increasing the asphaltene content thereof (SABITA Manual 2, 2012). The particle sizes of asphaltenes range between 2 - 5 nm and thus, corresponding to a result in a harder bitumen, the softening point increases together with a lower penetration (Hunter *et al.*, 2015).

2.5.4.2 Maltenes

Hunter *et al.* (2015) and SABITA Manual 40 (2021) describe the soluble n-heptane phase of bitumen in detail as per the following summary:

Maltenes correspond to the soluble phase of bitumen and by means of silica gel or alumina chromatography, they are subdivided into aromatics, resins and saturates.

Saturates contribute 5 - 20% of bitumen while being defined by a straight and branched aliphatic hydrocarbonous structure. Saturates correspond to a colourless, non-polar viscous type of oil. By increasing the saturates content of a mix, whilst keeping the ratio of aromatics and resins constant, the bitumen softens up.

Aromatics contribute to a large portion of bitumen (40 - 65%) although compromising of the lowest molecular weight. The structure corresponds to a non-polar chain consisting of carbon and unsaturated ring matrix's. The increase of aromatic content, in bitumen, has no effect on the rheology if the resins to saturates ratio is kept constant.

Resins act as dispersing or peptisers for asphaltenes. They consist largely of quantities of hydrogen and carbon whilst containing oxygen, sulphur and nitrogen atoms. Resins, being soluble in n-heptane, is a dark brown colour, polar orientated, containing adhesive properties and can be either in solid or semi-solid state. The addition of resin hardens up the bitumen and promotes a more solid state as the viscosity increases as well.

2.5.5 Types and Grades

In industry, various types of bitumen are used, depending on the environmental conditions of the project. Different types and grades of bitumen have been developed over the years based on the experience of industry experts together with research and new advances in bitumen technology. Subsequently, the use of modifiers in base bitumen produces a bituminous binder with various properties, resulting in the binder behaving different under specific environmental and trafficking conditions. The following subsections describe the major grades and types of bitumen used in industry.

2.5.5.1 Penetration Grade Bitumen

Penetration grade bitumen is one of the most widely and commonly used bitumen types in industry. According to SABITA Manual 2 (2012), penetration grade bitumen can either be produced by straight-run distillation or by blending two base components. This blending process can be described by mixing a hard penetration grade, such as 35/50 pen. and a softer grade, such as 150/200 pen. Penetration grade bitumens are specified by respective penetration and softening point tests.

It should be noted that soft bitumen cannot be tested by means of the penetration and softening point tests as the viscosity tests are measured at 135°C. The assumption made, when investigating the grading of penetration grade bitumen, is that the penetration depth is directly correlated to the binder performance. This, in simple terms, means that binders with high penetration values (soft) are used in cold environments while hard bitumen (low penetration depth) are used in warm climates (Hunter *et al.*, 2015). The requirements, according to SANS 4001-BT1 (2016), for penetration grade bitumen are presented in Table 2.5.

Table 2.5: Penetration Grade Bitumen requirements (SANS 4001-BT1, 2016)

1	2	3	4	5	6	7
Property	**Penetration Grade**					
	10/20	**15/25**	**35/50**	**50/70**	**70/100**	**150/200**
	Requirements					
Penetration at 25°C /100g/5 s, 1/10 mm	10-20	15-25	35-50	50-70	70-100	150-200
Softening point (ring and ball) °C	58-78	55-71	49-59	46-56	42-51	36-43
Min. viscosity at 60°C, Pa.s	700	550	220	120	75	30
Viscosity at 135°C, mPa.s	≥ 750	≥ 650	270-700	220-500	150-400	120-300
Flash point, °C minimum	245	235	240	230	230	220
Performance when subjected to rolling thin film oven test:						
a) mass change, % (by mass) fraction, max	-	0.5	0.3	0.3	0.3	0.3
(b) viscosity at 60°C, % of original, max.	-	-	300	300	300	300
(c) Softening point (ring and ball), °C, min	-	57	52	48	44	37
(d) increase in softening point, °C, max	10	8	7	7	7	7
(e) retained penetration, % of original, min	-	55	60	55	50	50
Spot test, % xylene, max	-	-	30	30	30	30

2.5.5.2 Cutback Bitumen

The process behind cutback bitumen is based on the idea that the bitumen is cured at a certain predetermined rate when exposed to air. Cutback bitumen is a mixture of penetration grade bitumen and petroleum solvents. The SABITA Manual 40 (2021) explicitly states that only petroleum-based cutters should be used. The main focus point of cutback bitumen is that it returns to a penetration grade bitumen when the solvent has evaporated. The viscosity is indirectly proportional to the amount of solvent added. Thus, to decrease the viscosity, more solvent is added. Cutback bitumen is of importance as it can be applied at much lower temperatures (due to a lower viscosity) whilst one disadvantage might include the fact that energy resources, which are not renewable, are lost in the process. In many cases, due to the advantage of cutback bitumen, it is only used as a patching material in very cold climatic conditions (SABITA Manual 2, 2012). Furthermore, cutback bitumen can be classified as rapid-curing (RC), medium-curing (MC) and even slow-curing (SC), depending on the solvent used. Wood *et al.* (2006) indicates that they are also classified according to their kinematic viscosity, where a low number indicates a lower viscosity.

2.5.5.3 Polymer Modified Bitumen

There is a definite need in industry to improve the characteristics of bitumen to improve the performance of the pavement system. According to the SABITA Manual 40 (2021) and the SABITA TG 1 (2019), improvements are needed to withstand:

- traffic volume increases,
- tyre pressure increases,
- wheel geometry adjustments,
- rising road temperatures and
- steep gradients.

Due to the above mentioned increases and the durability issues which can occur when bitumen is used, there is a need to improve the rheological properties thereof. According to the SABITA TG 1 (2019), modified binders are also controlled by the temperature, viscosity and transition phase characteristics. The purpose of implementing a modifier is to extend the deformation (plastic) phase and alter the visco-elastic range of the binder. Thus, in summary, a modified binder produces a bitumen binder with improved visco-elastic properties over a wider range of conditions including temperature and loading.

For a satisfactory performance of a bituminous binder, the following properties are essentially controlled, according to Hunter *et al.* (2015):

- Rheology of the bitumen
- Adhesion
- Cohesion
- Durability

Along with the improved properties, there is also an improvement in durability, stone retention, permanent deformation and fatigue cracking resistance and increases in cohesion and elasticity. To obtain a modified binder, various polymers, such as crumb rubbers, aliphatic wax or hydrocarbons, which occur naturally, are introduced. As seen in Figure 2.22, polymers can be either classified as elastomers or plastomers. Elastomers are needed to improve the elasticity of the binder whilst improving the strength and plastomers are used to improve viscosity-orientated properties (SABITA Manual 2, 2012).

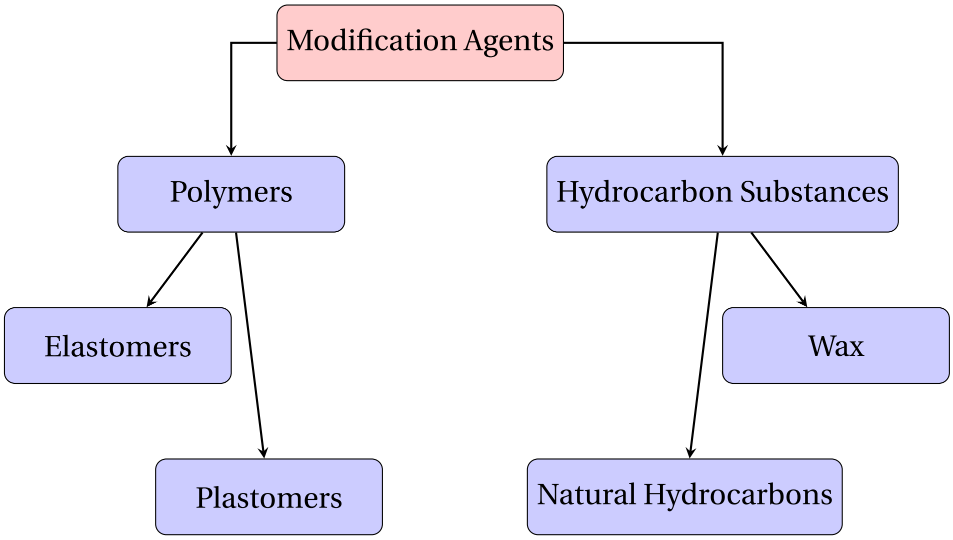

Figure 2.22: Modifying Agents (SABITA Manual 2, 2012)

Bitumen modifiers are also classified into two broad compositional groups namely either homogeneous binders or non-homogeneous binders according to the SABITA TG 1 (2019):

- Homogeneous binders are classified as modified bitumen, consisting of two undistinguished phases where the material acts single-phased as a result of the two phases being woven into one another. Homogeneous polymer modifiers generally used in bitumen modification include the following thermoplastic polymers:
  - Styrene-butadiene-rubber (SBR) latex (Elastomer).
  - Styrene-butadiene-styrene (SBS) (Elastomer).
  - Natural rubber latex (Elastomer).
  - Ethylene-vinyl-acetate (EVA) (Plastomer)
  - RET (Reactive Elastomeric Terpolymer)
- Non-homogeneous binders where there is clear distinction between the two phases. Non-homogenous bitumen rubber includes the usage of crumbed rubber particles from recycled vehicle tyres.

SBR latex and SBS, as homogeneous binders, together with bitumen rubber as a non-homogeneous binder, are explained below in detail. Aliphatic synthetic wax is also elaborated on as a copolymer.

SBR latex: Styrene-butadiene polymer is emulsified with solids, generally at a content greater than 50%. The butadiene content contributes towards the elasticity characteristic of SBR latex whilst the styrene contributes towards the stiffness and strength of the material. During the manufacturing of SBR latex, the hard styrene monomer and the soft butadiene monomer is copolomerised to form long, multiple units of monomers. The SABITA TG 1 (2019) states that the amount of SBR latex that can be added during the modification of bitumen is limited by the rapid increase in binder viscosity and the evaporation of the water content of the latex when mixed with hot bitumen. SBR polymers improve the elastic and flexibility properties of the binder whilst providing improved sealing and water ingress resistance. Better adhesion between the binder and the aggregate is also promoted, resulting in improved chip retention (SABITA TG 1, 2019).

SBS: Classified as a block copolymer and can either be classified as radial or linear, where a radial blocked copolymer results in an increase in viscosity and softening point, whilst increasing the difficulty of mixing with bitumen when in comparison to linear block copolymers. SBS is also considered as a thermoplastic rubber which is classified according to its glass transition point (Tg), which results in a high stiffness above the Tg. With styrene and butadiene being mutually incompatible and tend to separate in the modified binder mixture, it is important for copolymers to chemically link resulting in styrene end blocks agglomerating to form three dimensional cross-linked polystyrene domains. These domains provide mechanical properties to the polymer which can be compared to cross-linked rubber. The maltenes in the bitumen are absorbed by the SBS which results in swelling, whilst at high maltene dosages, a continuous molecular network phase is formed which make up the majority fraction by volume in the bitumen. The SABITA TG 1 (2019) states that the SBS will only form partial, fragmented molecular networks when 3 - 4% concentrations are absorbed. Concentrations between 4 - 6% enable the SBS to form a continuous network which results in a higher softening point. Molecular networks increase the elasticity characteristic of the bitumen which results in the recovery process after deformation. An increase in SBS content also increases the elastic property of the bitumen. SBS hot modified binders are often preferred to SBR latex due to a definite higher softening point as well as improved elastic recovery properties. Due to the lower relative viscosities, SBS modified binders can also be applied at lower temperatures (SABITA TG 1, 2019).

Bitumen-rubber: A non-homogeneous binder which compromises of hot bitumen modified by the addition of regular tyre rubber or rubber compounds with a specific grading, morphology and composition. Recently, product ranges have developed with regards to containing different levels of additives and modifiers to improve the ease of handling through lower application and handling temperatures and to extend the storage life thereof. The source and the type of rubber are influencing factors and thus, consistency is not always achieved from product to product. The natural rubber and the synthetic rubber content also varies and is dependent on the source. Rubber particle morphology influences the crumbed rubber's composition after mechanical grading. After application, when the bitumen rubber has cooled down, a rubber network, which is filled with bitumen, is formed from the larger rubber particles. This rubber network improves cohesion, elasticity, flexibility re-healing properties and strength of the material. Bitumen rubber can also somewhat act as a stress absorbing membrane interlayer (SAMI) and has been successfully implemented in the seal construction industry due to its significant improved elasticity and stiffness characteristics (SABITA TG 1, 2019).

Fischer-Tropsch wax: A specific type of hydrocarbon relates to aliphatic synthetic wax which is a long chain of hydrocarbons produced by the synthesis process called the Fischer-Tropsch (FT). These long chains extend the plasticity range of bitumen. Bitumen modified with FT wax, if implemented as a modifier, has a lower viscosity during the application range than conventional bitumen (above 100°C) but during the in-service range, the viscosity is higher than conventional bitumen. This enables bitumen modified with FT wax to be applied at lower temperatures than mixes with conventional bitumen. Another advantage of using FT wax is that it can be used as a co-modifier with polymer modified bitumen to produce hybrid substances to fulfill specific requirements (SABITA TG 1, 2019). Natural occurring hydrocarbons are generally used to stiffen up bitumen when implemented. Mixes with hydrocarbons display higher stiffness values than mixes with polymer modifications. Thus, these high stiffness values are of importance to resist permanent deformation and enable load-spreading abilities of the layers (SABITA Manual 2, 2012).

According to the SABITA TG 1 (2019), the following codes are used to classify and designate between the different modified binders:

- **Type of application**
  - Seal - S
  - Asphalt - A
  - Crack sealant - C
- **Type of modifier used**
  - Elastomer - E
  - Plastomer - P
  - Rubber - R
  - Hydrocarbon - H
- **Type of binder**
  - Emulsion (cold applied) - The letter C would appear directly after the letter corresponding to the type of application is the product if an emulsion
  - No letter is used to indicate a hot applied binder
- **Modification**
  - The higher the number following, the higher the softening point. It should be noted that this modification number does not necessarily indicate improved performance.
- **Fluxing agent or cutter**
  - A letter "t" should be shown if the binder application does not require the use of a cutter or flux.

The classification of seals, based on the modifiers applied, as listed in the SABITA TG 1 (2019), can be seen in Table 2.6.

Table 2.6: Classification of seals based on modification agents

Modification Agents	Modifier	Classification Terms
Elastomers	SBS	S-E2, A-E2
Elastomers	SBR latex	S-E1, A-E1, C-E1
Elastomers	Rubber crumb	S-R1, A-R1, C-R1
Plastomers	Ethylene vinyl acetate (EVA)	A-P1
Hydrocarbons	Natural hydrocarbons	A-H1
Hydrocarbons	Aliphatic wax	A-H2

2.5.5.4 Emulsions

For practical applications of bitumen, as a binder, it is required that bitumen behaves in a liquid phase during transportation and application. This makes the transportation process easier while ensuring that the phase of the bitumen is sufficient as an application binder.

To reduce the viscosity of bitumen, it can either be heated, dissolved in specific solvents or in the case of bitumen emulsions, it can be dispersed and exposed to an emulsifier (Hunter *et al.*, 2015). According to the SABITA Manual 2 (2012), bitumen emulsions consist of a two-phase systematic process. The first phase consists of bitumen being dispersed in an aqueous medium, such as water. An emulsifier, in the water, is then used to stabilise the bitumen-water mixture. It should be noted that the bitumen is not just mixed into the water, but it is held in suspension, and thus, the bitumen and water mixture contribute in the emulsion to maintain a homogeneous condition of each material. The emulsification process enables a reduction in the viscosity of the bituminous binder, permitting the transportation, handling and application thereof at lower (cold) temperatures. Emulsions generally consist of a net binder (bitumen) content ranging between 60% and 70%.

According to Hunter *et al.* (2015), there are four classes of emulsions namely:

- cationic
- anionic
- non-ionic
- clay-stabilised

The cationic and anionic emulsions are the most widely used emulsion types. As their names indicate, they originated from the positive and negative charges on the bitumen globules. Fundamentally, opposite charges attract one another and like charges repel. In the case that an anionic emulsion is charged, they would adhere to the anode and if a cationic emulsion is positively charged, the particles would adhere to the cathode. Due to the charges present in different types of emulsions, the adhesive forces between the binder and aggregate are greatly affected because of the polarity of the aggregate due to the mineralogy of the parent material (acidic or basic parent rock). Thus, to ensure adequate adhesion between binder and aggregate, it is required to decide on specific types that would compliment one another in terms of charges (Hunter *et al.*, 2015).

Cationic emulsions are generally used in South Africa when the aggregates granite and quartzite are present. This is due to these aggregates being negatively charged acidic aggregates. Subsequently, anionic emulsions would adhere better to positively charged aggregates such as dolomite and limestone. This principal does not necessarily indicate that effective adhesion would not develop when using a cationic emulsion with, for instance, positively charged limestone. A delay in the adhesion development would occur. Milne (2004) reports that due to the delay, only when the water has evaporated and the emulsion has returned to its base bitumen, then adequate adhesion properties would have been developed. In many cases, time is of the essence, and it would only be problematic to deal with a cause in the delay of the adhesion development. According to Wood *et al.* (2006), cationic emulsions perform more reliably in the field and revert back to their base bitumen faster than anionic emulsions. This is based on the electrochemical process required to break the cationic emulsion and therefore, weather conditions contribute to a lesser degree although still required to allow for full curing by means of evaporation. In contrast, anionic emulsions are dependent on the evaporation of water to break and cure and consequently, they are reliant on prevailing weather conditions. According to Ignatavicius *et al.* (2021), anionic emulsion are used for higher dust content aggregate due to a slower break. Therefore, to allow for both coarse and fine aggregate particles to be coated and bonded to the the residual binder before breaking, a slower breaking anionic emulsion is used. Furthermore, emulsions are classified according to the rate at which they revert back to their base bitumen. The terms RS (rapid-setting), MS (medium-setting) and SS (slow-setting) have been adopted to standardize this classification (Wood *et al.*, 2006).

Under certain conditions, emulsions have an advantage over hot modified binders. These instances, according to the SABITA Manual 2 (2012), include:

- Damp and dusty aggregate in chip seals.
- During chip sealing, when uncoated stones are present, adhesion of the aggregate to the cationic emulsion is improved.
- When application at lower (colder) temperatures is needed, to enhance worker safety, improve pollution and prolong construction periods.
- Lower application rates are required due to water dilution.

According to the SABITA TG 1 (2019), emulsions are classified as either SC-E1 or SC-E2 when indicating that their application is for a surfacing seal. Emulsions, in industry are used widely in fog sprays, slurries, stabilising conditions, chip seals, tack coats, crack sealants and cold mix asphalt (SABITA Manual 2, 2012).

2.5.5.5 Primes

As a preliminary treatment prior to the application of a bituminous surface dressing (base), a prime is applied. It consists of a bituminous binder which is applied to a non-bitumen surface. For a prime to act sufficiently and perform to its intended purpose, it needs to work in or penetrate the layer to which it has been applied, whilst leaving a residual amount of binder on the surface. According to SAPEM (2014), this is done to:

- improve quality adhesion between the base and the surface,
- block the movement of water into the base,
- absorb limiting binders and
- provide a binding source for fine particles to withstand light traffic before the new surfacing is applied.

Primes are generally applied when road pavements, with granular material in the base, are constructed.

2.5.5.6 Aggregate Pre-coating

Pre-coating of aggregate is done during construction to minimise the risk of poor adhesion and early chip loss. These pre-coating fluids adhere to a low viscosity bitumen property made out of products containing petroleum cutters and chemical adhesion agents. These fluids also act as a surface tension reducing agent between the cold aggregate surface and the hot binder during the construction of a seal. Pre-coating is generally applied in a manner such that the fluid should:

- coat dusty and damp stones,
- dry within an adequate time period and
- not leave a tacky film on the surface of the particles.

Pre-coating is usually applied when a single seal is constructed without the use of bitumen emulsion as a tack coat. When the binder type applied is a penetration grade binder, hot polymer modified binder or a bitumen rubber, pre-coating is also required. Quartzite, granite, porous, hydrophilic and aggregates with a dust content of more than 2% also require pre-coating (SAPEM, 2014).

2.5.5.7 Tack Coats

According to SAPEM (2014), tack coats are generally applied on top of a primed granular base or between asphalt layers to improve adhesion properties. The prime does not effectively provide good adhesion between the base and the asphalt layer on top, it only binds the surface of the granular base and protects it against water. This is where tack coats are needed. They serve the purpose to bind the layers.

Tack coats are generally applied to the following materials or conditions according to SAPEM (2014):

- granular bases which are primed.
- asphalt layers when another asphalt layer is to be paved on top and
- joints in asphalt layers.

2.5.6 Rheology

2.5.6.1 Ageing

Typically, the average performance life of a surfacing seal before resealing is ten years, with cracking being the leading distress influence (Van Zyl and Jenkins, 2015). During this stage, the structural layers are still protected and still serve their purpose but more failures start to appear. If resealing is not an option and no maintenance is incorporated, the failures increase in terms of degree, leading to further pavement damage including the possibility of partial structural failure together with the complete failure of the surface. A more costly rehabilitation is then expected to produce a pavement structure capable of functioning as initially designed for.

Integral characteristics of the seal binder that are directly related to the performance of the surfacing seal, include the seal type, the binder grade, viscosity, binder application rate and the quality of the application rate. The last two are directly related to the seal design process. Furthermore, the binder type and the grade thereof govern the inherent properties of the bituminous binder which include the elasticity, stiffness, temperature susceptibility and adhesion and cohesion (SABITA Manual 40, 2021).

Binder ageing, as such, occurs as a result of temperature difference variations and the effect of ultraviolet radiation and oxygen levels. Hunter *et al.* (2015) report that the factors contributing to binder ageing lead to an increase in binder stiffness and load spreading abilities whilst there is a decrease in the elasticity of the binder. As reported by Goosen and Jenkins (2019), when a binder is very stiff and is lacking sufficient elastic properties, then it will be more susceptible to cracking at lower temperature ranges under the effect of traffic loading. When a too soft binder lacks elasticity, it will become more susceptible to bleeding failure, especially at higher temperature ranges. Low ductility and aggregate loss is a result of cohesion and adhesion related problems. A general identified trend includes the deterioration of these properties with binder ageing. Subsequently, premature cracking can be resulted from the decrease in durability due to the effect of binder ageing (Goosen and Jenkins, 2019). Furthermore, Glover *et al.* (2005) report that modified binders have a significant lower rate of hardening when compared to their base bitumen. Lower oxidation levels are also reported. Therefore, modified binders are generally less susceptible to binder hardening. The ageing process of modified binders include the increase in asphaltene content in the binder whilst the modifier degrades (Glover *et al.*, 2005).

Durability parameters, including the Glover-Rowe (G-R) parameter, the critical low temperature difference (ΔT) and the ageing ratios are used to evaluate the change in rheological properties over time for certain seal in-service conditions. The research done focusses on the development of an extraction and recovery process for chip seals. The extracting and recovering procedure is implemented on samples from existing roads after which the results are evaluated by comparing the performance properties of the binders to the field ageing thereof.

From the extraction results obtained, as reported by Goosen and Jenkins (2019), modified binders age at higher rates when compared to unmodified binders. The visual evaluation shows that the surfaced modified binder displayed a larger extent of cracking, even though the unmodified binder surfaces are younger in age. Figure 2.23 shows an increase in the G-R parameter with an increase in age. A similar trend is followed for the (ΔT) plot as seen in Figure 2.24. The difference between the rate of ageing can be seen in Figure 2.25.

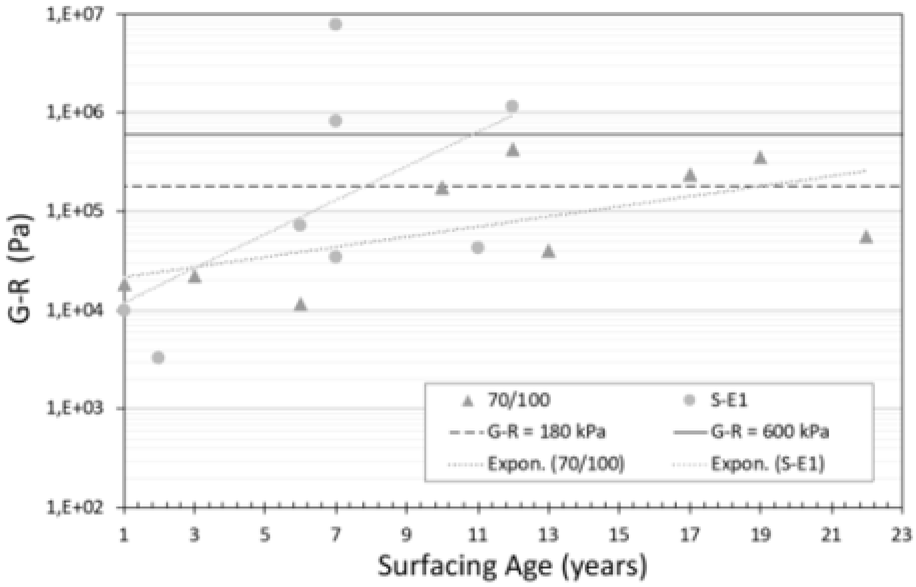

Figure 2.23: Glover-Rowe Parameter versus the Age (Goosen and Jenkins, 2019)

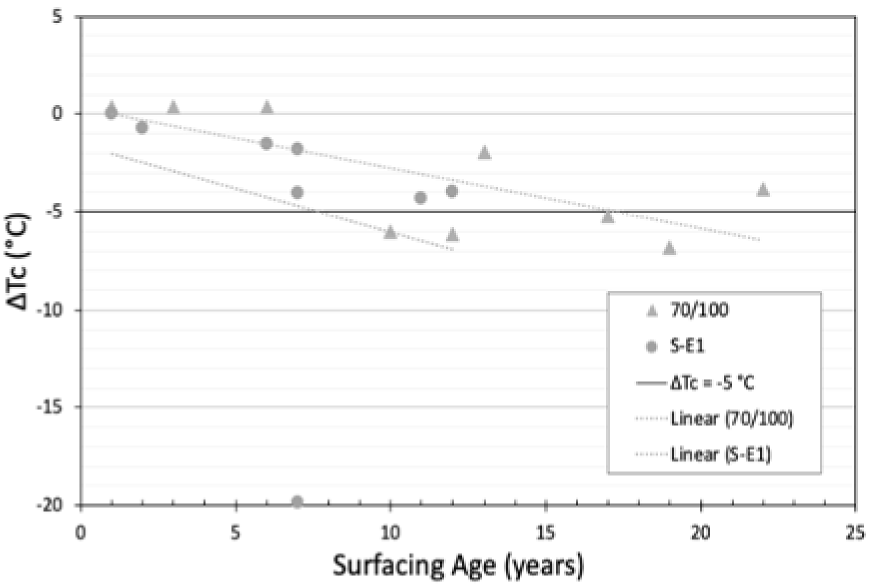

Figure 2.24: Change in Critical Temperature versus Age (Goosen and Jenkins, 2019)

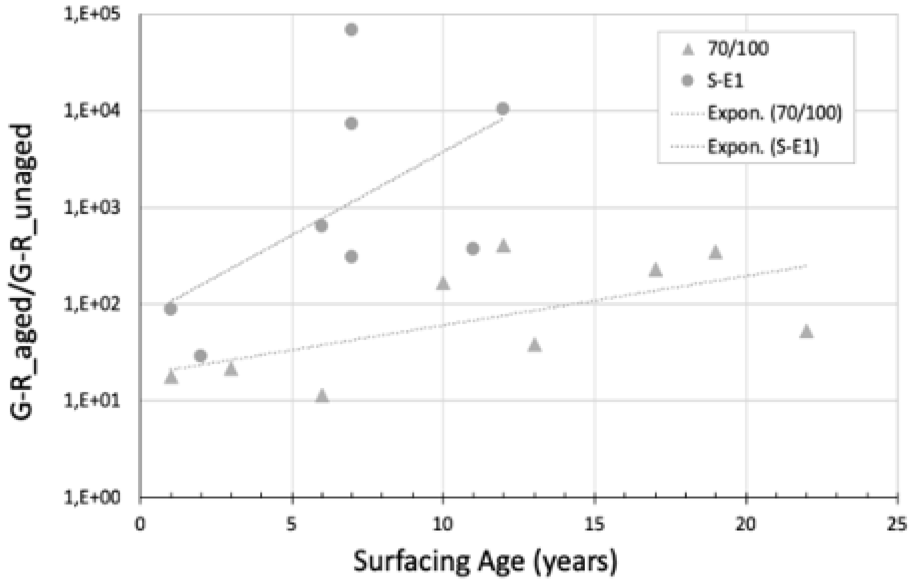

Figure 2.25: Ageing Ratios versus Age (Goosen and Jenkins, 2019)

Another important aspect to take note of includes the relationship between the stiffness of the binder and temperature. Generally, a 6°C increase or decrease in binder temperature results in the stiffness of the binder doubling or halving (Goosen and Jenkins, 2019).

2.5.6.2 Rheology Analysis

A common method to analyse the behaviour of bituminous binders at different temperatures and loading frequencies includes the construction of master curves (Engelbrecht, 2018). The complex modulus (G*) is plotted against the frequency which is along a logarithmic axis after which the isotherms are shifted to a reference temperature (T_{ref}) with the introduction of a shift factor to enable a continuous curvature (Hunter *et al.*, 2015). A typical G*-space master curve for a 70/100 binder can be seen in Figure 2.26.

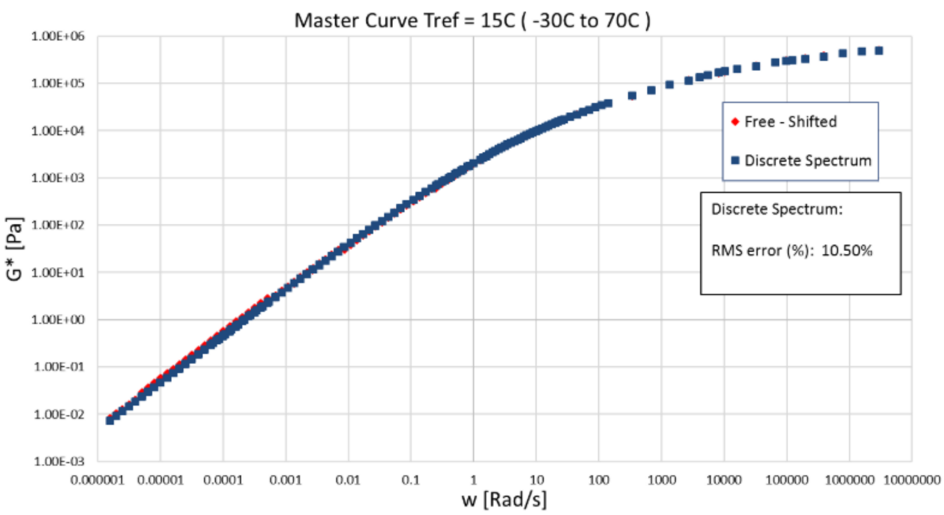

Figure 2.26: Typical master curve as per Engelbrecht (2018)

Cracking performance of binders can be determined by means of rheological measurements (Rowe *et al.*, 2014). Subsequently, to evaluate cracking together with material properties, Black Space diagrams are constructed by implementing a Complex Modulus (G*) versus Phase angle (δ) plot (Engelbrecht, 2018).

2.6 Aggregates

2.6.1 Introduction

According to Milne (2004), aggregates can be defined as the result of processed rock, either by crushing or sieving, that serves the purpose of a load bearing material and wearing course that can be constructed at surface level. Generally, aggregates used during the road building process include both natural and processed aggregate, which can consist of either gravel and/or rock. When investigating a typical pavement structure it is clear that each layer of substrate consists of a certain or specific type of aggregate. It should also be noted that aggregates used as surfacing material could differ from aggregates used in the structural layers. Thus, when investigating this section, two different types of aggregates are referred to, namely a structural layered (base) aggregate and a surfacing (seal) aggregate.

2.6.2 Origin

When choosing a suitable type of aggregate to be used during the construction of a pavement, aggregates within close proximity of the site will generally be considered due to transportation and economical reasons. As stated in Section 2.4.1, aggregates can be crushed, sieved or screened to obtain the desired form, shape and angularity that are required for the pavement. With regards to the binder used, minerals, which are the building blocks of all aggregates, are also of importance as they play a role in the adhesion between the binder and the aggregate. Therefore, to understand aggregates, a general understanding of minerals and aggregate types is required.

According to Tarbuck *et al.* (2014), minerals are defined as a natural occurring inorganic material that is in solid form, and consists of a crystalline structure with a definite chemical composition. The term *rocks*, in contrast with minerals, is more widely defined as a solid mass of mineral, or mineral-like material, that occurs naturally on earth. Thus, to obtain a definition for aggregates, the following can be stated: aggregates are joint minerals without losing individual mineral properties.

2.6.2.1 Sedimentary Rocks

According to geologists, most of earth's solid surface (roughly 75%) consists of sedimentary deposits or sedimentary rocks. Sedimentary rocks form when weathering of existing rocks take place. Gravity and erosion then continue to perform the weathering process by means of running water, wind and glacial movement. During the weathering and transportation process, the material particles break down. This means that the material is now called sediment, and it again turns into a rock. Examples of sedimentary rocks include sandstone, conglomerate, breccia and limestone.

2.6.2.2 Metamorphic Rocks

Metamorphism is a process where changes in mineralogy, texture and even the chemical composition of a parent rock occurs. The mineralogy changes due to new condition, such as elevated temperatures and pressures, which are much different from the conditions in which the parent rock was initially formed. The degree, to which a parent rock undergoes change, is referred to as the metamorphic grade. There are two types of grades including a low grade (low temperatures and pressures) and a high grade (high temperatures and pressures). Examples of metamorphic rocks include slate, hornfels and quartzite.

2.6.2.3 Igneous Rocks

These types of rocks form in two basic settings, namely the process when molten rocks crystallize at depth and when it solidifies. When magma crystallizes under the surface, at depth, intrusive (plutonic) igneous rocks are formed and when magma crystallizes at the surface, extrusive (volcanic) igneous rocks are formed. Examples of igneous rocks include basalt, gabbro, andesite and granite.

2.6.3 Granular Base Aggregate

The material classification system in South Africa emphasizes the origin of aggregate as a more important aspect than the layer (in the pavement) where it is implemented. High quality crushed stone, such as G1 and G2, as well as in-situ subgrade material (G10), are all classified according to the gradation criteria, Atterberg limits, resistance to abrasion, CBR (California Bearing Ratio) and different density requirements. The upper layers of a pavement system (base and subbase) will generally consist of G1 and G2 material for crushed stone, while consisting of G4 to G6 for natural gravels. The gradation classes for aggregate, as adapted from Theyse (2002), is shown in Table 2.7.

Table 2.7: Gradation classes of aggregate as per Theyse (2002)

Classification	Producing Process	Propeties
G1	Crushing and blending of solid, unweathered rock	Fracture rock faces. Only origin fines may be added to adjust gradation.
G2 **G3**	Crushing large boulders of rock and course gravel material.	>half of crushed particle mass (>4.75 mm) must have one fractured face. To adjust grading, fines from different parent material may be added.
G4 **G5** **G6**	Crushing of natural boulders or gravel that acquire crush potential.	Classification done per soaked CBR test and plasticity index (PI) adjusted by addition of cement, lime and sand. G4 is generally used in base while both G5 and G6 are used in subbase layers. All particles <63 mm.

Furthermore ,the gradation requirements for a base layer aggregate, as presented by Theyse (2002), are shown in Table 2.8.

Table 2.8: Base Layer Aggregate Gradation Requirements as adapted from Theyse (2002)

	Percentage passing by mass		
Sieve Size	**G1, G2, G3 nominal size (mm)**		**G4**
mm	**37.5**	**26.5**	
53.0	100	100	100
37.5	100	100	85 - 100
26.5	84 - 94	100	-
19.0	71 - 84	85 - 95	60 - 90
13.2	59 - 75	71 - 84	-
4.75	36 - 53	42 - 60	30 - 65
2.00	23 - 40	27 - 45	20 - 50
0.425	11 - 24	13 - 27	10 - 30
0.075	4 - 12	5 - 12	5 - 15

2.6.4 Seal Aggregate

According to the SABITA Manual 40 (2021), the main functions of aggregates in a seal surfacing layer are to:

- ensure adequate resistance to the wheel loads,
- transfer the wheel loads down to the underlying pavement layers,
- provide an adequate skid-resistance to improve the safety of road users,
- provide a structure for the bituminous binder to be applied, with sufficient voids to ensure no flushing of binder to the surface and
- provide adequate roughness and height to protect the binder from the ultraviolet rays of the sun.

In certain cases, aggregates may be applied in a surfacing seal to execute a functional value, such as prevent glare from sunlight rays and to define different demarcated areas. The influence of shape, nominal size, grading, spread rate, adhesion, strength, durability and wearing characteristics, as well as porosity and absorption is to be considered carefully.

2.7 Modelling Permanent Deformation

2.7.1 Overview

In a pavement layer, plastic strain causes permanent deformation. Furthermore, the influence of plastic strain is often referred to as rutting which tends to occur in unbound (granular), stabilised layers and asphalt layers throughout a pavement structure. In contrast with granular layers, asphalt is more susceptible to permanent deformation during the early trafficking periods. Therefore, asphaltic material may behave visco-plastically, irrespective of the usage thereof as a surfacing or lower layer, with the effect of permanent deformation depending on the loading degree, trafficking speed, trafficking temperature, layer thickness and binder age (Goosen, 2021).

2.7.2 Shakedown Theory

After initial permanent deformation in an unbound layer and with continuous loading cycles, the material behaves elastically with either no further permanent deformation or a gradual accumulation thereof, resulting in material breakdown or incremental collapse (Rudman, 2019). Originally, the Shakedown Theory was introduced by Semmelink *et al.* (1997) to describe the implementation of the k-mould to simulate loading. Thereafter, Werkmeister *et al.* (2005) reported on the Shakedown Theory in that is has been utilised to describe the behaviour of structural elements under repetitive cyclic loading phases. Therefore, the theory corresponds to the following material response categories:

1. purely elastic,
2. elastic shakedown,
3. plastic shakedown and
4. incremental collapse.

Furthermore, the Shakedown Theory is aligned in correspondence with the observed pavement material behaviour as adapted by Werkmeister *et al.* (2005). As a result, the following redefined boundaries are identified with a general conceptual description of each:

1. Plastic shakedown - Range A: Corresponds to the permanent plastic response for a finite number of load cycles. The plastic response becomes resilient after the post-compaction period.
2. Plastic creep - Range B: The response is characterised by a low, gradual or almost constant level within the first cycles.
3. Incremental collapse - Phase C: Corresponds to little or no decrease in the rate of permanent strain.

The behaviour of granular material, as described by Werkmeister *et al.* (2005), is graphically shown in Figure 2.27. The various phases, as adapted from Rudman (2019), are shown in Figure 2.28. Generally, for an adequate designed pavement, the Plastic shakedown (Phase A) is desired whilst Phase B is applicable if rutting can be quantified with increased accuracy levels. Phase C is undesirable (Rudman, 2019).

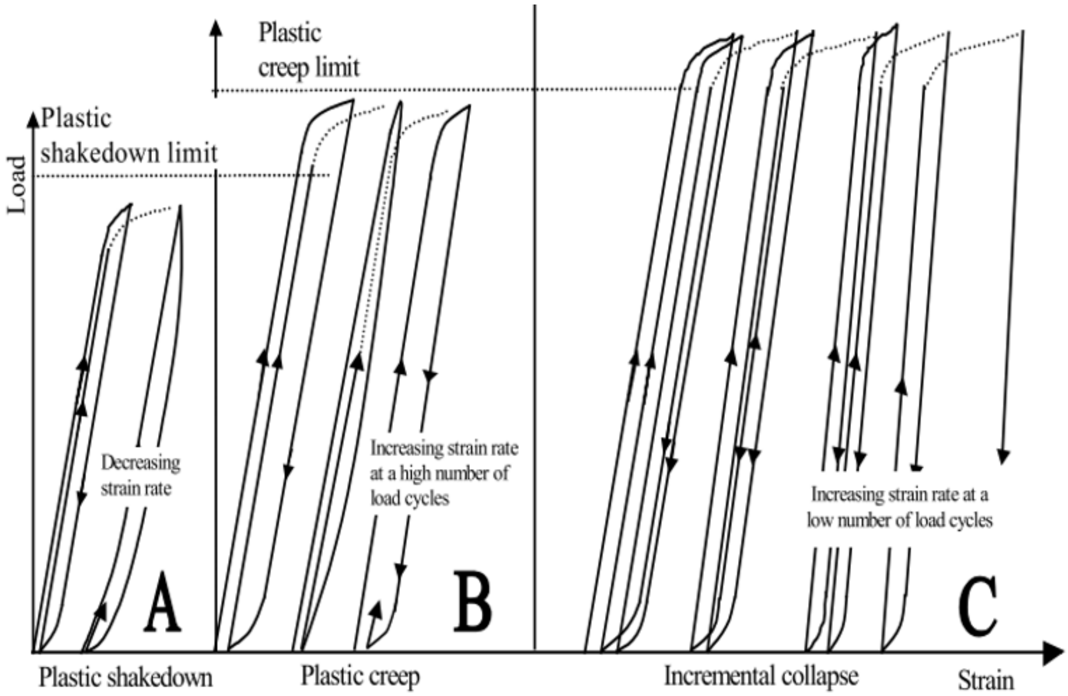

Figure 2.27: Granular material behaviour under repeated load cycles as per Werkmeister *et al.* (2005)

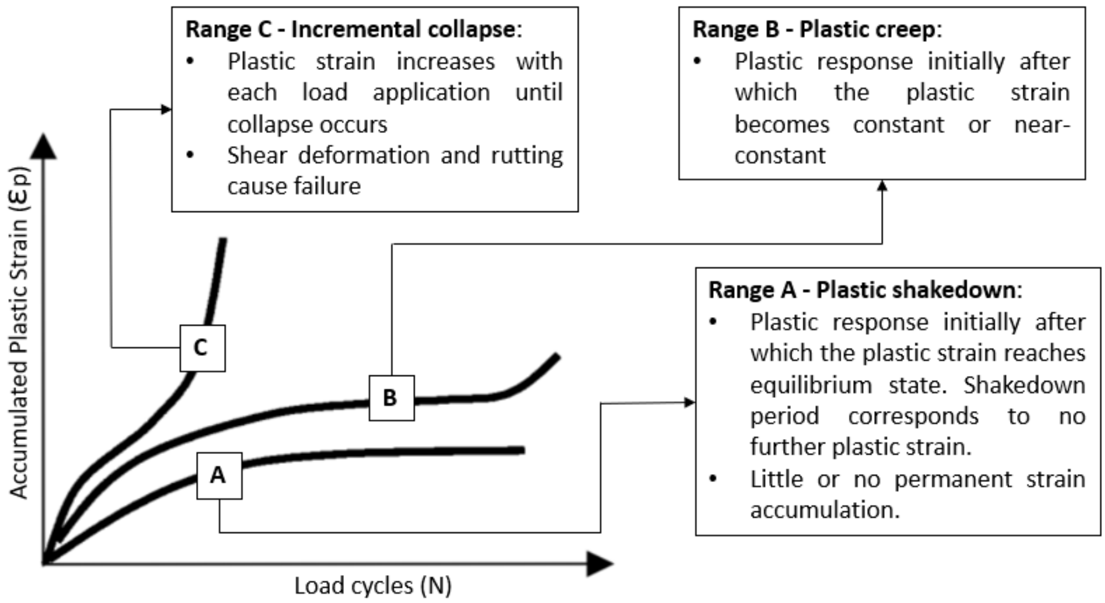

Figure 2.28: Concept of the Shakedown Theory applicable to elastic/plastic behaviour under repeated loading as adapted from Rudman (2019).

Currently, there is no direct indication of the usage of the Shakedown Theory and the applicability thereof on surfacing seals. However, with cyclic load repetitions by means of APT, and as a result thereof, texture loss occurring, the applicability of the theory and the alignment thereof with similarities to the modelling work done by Rudman (2019) and Werkmeister *et al.* (2005), may result in an adequate method of seal texture loss modelling.

2.8 Model Mobile Load Simulator (MMLS)

2.8.1 Background and History

The concept of implementing accelerated pavement testing (APT) followed a number of events, which started in 1988. During this period, the Texas Highway Department considered to develop a full-scale APT strategy. At the time, the only accelerated testing machinery available included the Heavy Vehicle Simulator (HVS) and the Accelerated Loading Facility (ALF). The HVS was initially developed in the 1960's in South Africa, while the ALF was used in both Australia and in the United States from the mid 1980's. Professor Fred Hugo, leader of the Texas project, returned to South Africa in the late 1980's and began developing a very unique closed loop loading system. A feasibility study was done on accelerated pavement testing, and Professor Fred Hugo and his team built a 1/10 scaled model of the mobile load simulator. After this model was presented to the Texas Steering Committee in 1990, a proposal was initiated to build a full-scale version of the model load simulator (MLS). This model was developed and named the Texas Mobile Load Simulator (TxMLS) (Kemp, 2006).

After the model for the MLS was completed, a decision was made to produce a fully operational laboratory mobile load simulator (MMLS1). In the Department of Civil Engineering at Stellenbosch University, the model was firstly utilized as a demonstration model only. According to Kemp (2006), this model was then sold to the University of Texas where it was used as an accelerated pavement testing machine whilst a second unit was used for research purposes at Stellenbosch University. Following the familiarity of these machines, the University of Arizona as well as the Indonesian Government acquired there own units following a Japanese sponsorship.

Due to feasibility issues relating to the MLS1, users suggested that another model be developed. The 1/10 scaled model was also being challenged in a laboratory environment. The scaling of materials and pavements layers were later questioned and subsequently, scaling issues were dealt with when developing the Model Mobile Load Simulator 3 (MMLS3). This unit was based on a third scale modelling of the original MLS concept. According to Kemp (2006), the first MMLS3 unit was completed in 1997 and then sold to the United States, after which units were sold to universities in Europe, America and to the Institute of Transport Technology (ITT) in Stellenbosch, South Africa.

2.8.2 Features and Attributes of the MMLS3

According to the MLS Test Systems (2016), the MMLS3 is a scaled down version intended for usage in accelerated pavement testing of full scale or model pavements. The owners manual describes that there are four bogies with one 1/3 scale tyre per bogie. The tyres are approximately 300 mm in diameter and they can typically apply 7200 realistic wheel loads per hour. The tyre can inflate to a maximum pressure of 800 kPa whilst the maximum wheel load is 2700 Newton. The MMLS3 machine consists of the following main mechanisms, as seen in Figure 2.29.

(a) A rigid frame with four adjustable leg standings.

(b) Loop guide rails mounted to the frame.

(c) Four bogies, each with a 300mm diameter pneumatic wheel and six guide wheels.

(d) Four link sections, each consisting of six guide wheels.

(e) Drive drum.

(f) Curved wheel guide.

(g) Lateral displacement mechanism.

(h) Detachable castors for ease of transport.

The link sections and the bogies are connected to form an endless chain, consisting of 48 guide wheels and four wheels. The guide wheels move along the two sets of guide rails, as seen in Figure 2.29. As soon as a single bogie moves along the bottom section of the rails, the tyre of the pneumatic wheel is in contact with the pavement layer while applying a load to it. When the drum rotates, the guide wheels move along in a very similar manner as with a gear system. The chain and the bogies are driven around. A 1.5 kW electric motor, with adjustable speeds, is used to drive the drum (MLS Test Systems, 2016).

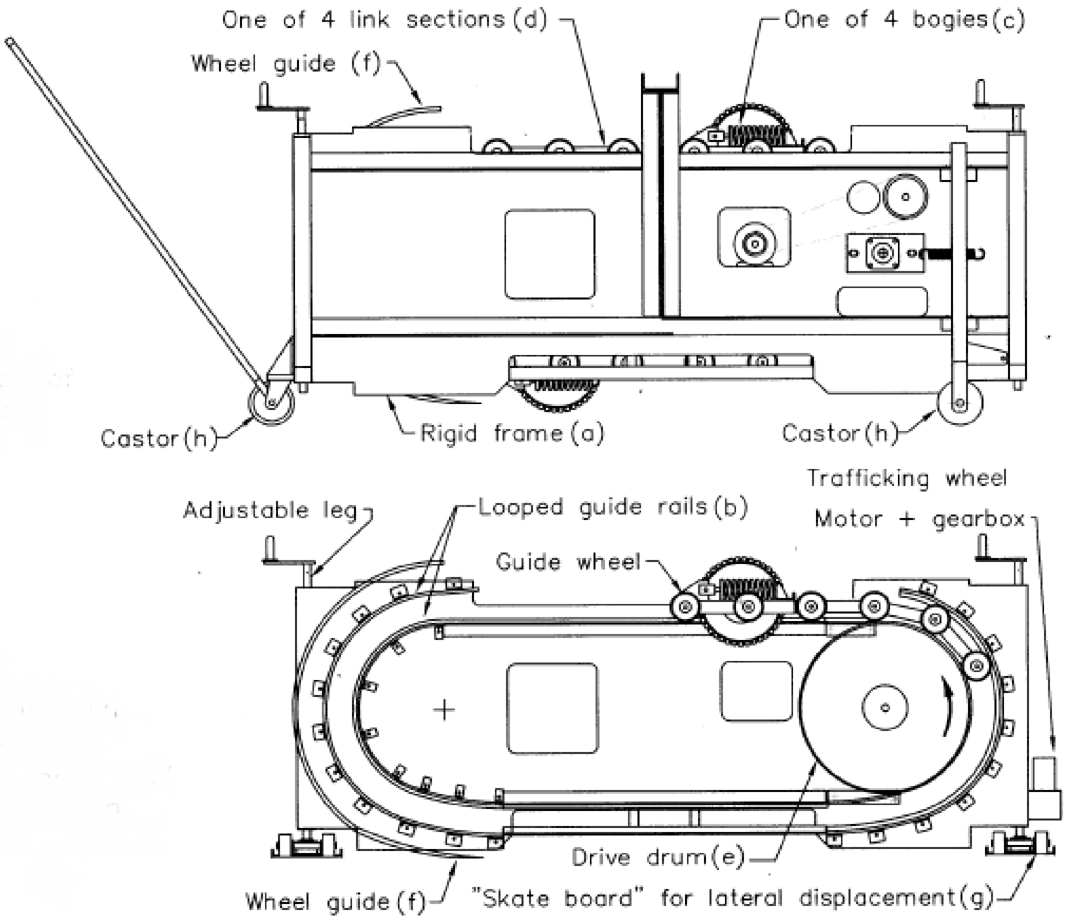

Figure 2.29: Side and Section View of the MMLS3 (MLS Test Systems, 2016)

Another important adjustable mechanism of the MMLS3, is the adjustable suspension system of the trafficking wheel. The maximum travel of the suspension corresponds to a value of 20 mm. Once the suspension has been set, the geometry of the suspension system makes the wheel load practically independent of the displacement within the 20 mm range. It is of note that during operation, the suspension is kept within its range by only adjusting the legs on the fixed frame.

2.8.3 Valuable MMLS research on seals

2.8.3.1 Towards modelling road surfacing seal performance

In 1998 performance testing, of surfacing seals, was done by identifying the usage of the MMLS3 and by developing a test method. Between 1998 and 2002, a test setup, using five different bituminous binders (with variation of the rubber bitumen manufacture process) and three temperature regimes, was developed. The goal was to develop a method to evaluate seal behaviour (Milne, 2004). The research assessed the South African seal design methodology whilst identifying areas where further research, development or updating is required to accommodate changing binder types, traffic conditions and environmental conditions.

Milne (2004) firstly set up a regime to identify the factors influencing seal performance and the identification of performance criteria. The controllable factors, non-controllable factors as well as the performance criteria can be seen in Figure 2.30. Using these identified factors and criteria for evaluating performance, Milne (2004) proposed a seal design method based on mechanistic material properties. A prototype of a numerical model using finite element analysis, was then also presented.

To verify the finite element data and to contribute to further seal design development, performance tests were developed using the MMLS3 machinery. The tests were performed on the most basic seal type, the single seal. Various binder types were also analysed. These included penetration grade bitumen, SBS, SBR, EVA binders and bitumen rubber. Each binder type was used to construct a single seal, which was then tested by implementing the MMLS3 and three different temperature regimes. The traffic loads of the MMLS3 single wheels were set to produce a load of 2.1 kN per axle while a tyre pressure of 600 kPa was decided upon. The MMLS machine was set to apply 200 000 load repetitions, with no lateral wander, which equates to an estimated five-year traffic load period, based on a 40 equivalent light vehicles (ELV) per 80 kN axle load. To be conservative, a factor of 3, owing to the effect of lateral wander, was also introduced and therefore contributed to the equivalency of 40 ELV to a single 80 kN axle load. The temperature regimes included an ambient temperature range (20 - 36°C), elevated temperature range (> 50°C) and cold temperatures (10°C). The influencing factors, that were both controllable and non-controllable, as well as the criteria to evaluate performance are shown in Figure 2.30.

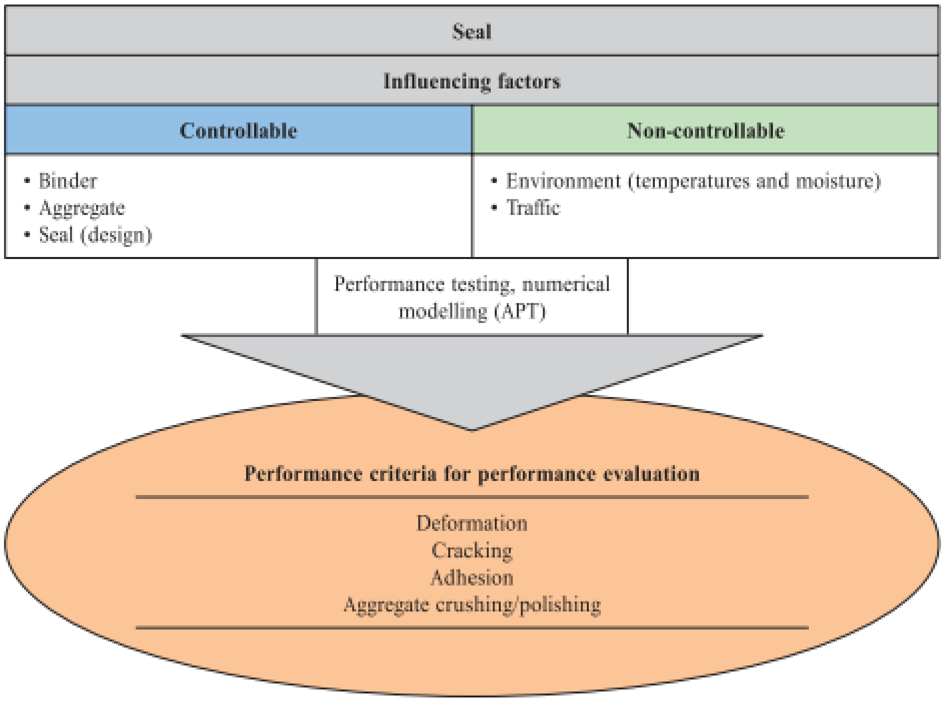

Figure 2.30: Influencing Factors and Performance Variables (Milne, 2004)

The results, as documented by Milne (2004), depict that each binder type has its own contribution towards seal performance at varying temperatures. Subsequently, the MMLS3 APT machine successfully enabled comparative testing regarding the performance of each binder type. Table 2.9 provides a summary of the seal performance, with each binder at different temperature regimes.

Table 2.9: Seal Performance Summary Milne (2004)

Summary		**Scale: 100 maximum best 0: minimum worst**		
Seal Performance		**Test Regime**		
Binder	**Overall Performance**	**10°C (cold)**	**Ambient**	**30°C (elevated)**
Binder modified 80/100 pen grade				
3% SBR	0 - 22	19	17 - 22	0 - 6
3% SBS	0 - 28	28	0 -16	6 - 15
3% EVA	11 - 28	17	11 - 28	11
20% bitumen rubber BR TOSAS COLAS	14 - 39 11 - 56	17	14 - 35 11 - 33	25 - 39 17 - 56
80\100 penetration grade	22 - 56	22	31	56

Milne (2004) reported the following performance results which could be of relevance to this study:

80/100 penetration grade: The binder performed the best overall at ambient temperatures. Similar embedment, slightly more stone loss and better visual ratings were recorded at ambient rather than elevated temperatures. At low temperatures, less embedment, stone loss, crushing and less orientation were recorded as well. Milne (2004) also described that a higher binder application rate allowed for a better performance as limited stone loss occurred.

3% EVA: The binder performed much better at elevated temperatures, possibly due to a higher softening point and subsequently, higher adhesion properties. At colder temperatures, more stone loss and visual unsettlement occurred when compared to ambient conditions. Milne (2004) also recorded that the binder application rate was not a major influence on the performance of the seal.

3% SBR: Better performance was recorded at higher temperatures. The binder also performed better at ambient than cold tests.

3% SBS: Less rotation and embedment was found at ambient temperatures than elevated. Stone loss was found when cold tests were performed while less embedment, or settling under the wheel load, was found at ambient temperatures. Milne (2004) reported that less flushing was displayed when lower applications of binder content were implemented.

20% bitumen rubber (COLAS): The binder performed the best at cold temperatures due to less flushing being recorded. At higher temperatures, the binder became more sensitive to higher application rates. Subsequently, the binder performed better for lower application rates.

20% bitumen rubber (TOSAS): Less flushing was reported at ambient temperatures than elevated. Better performance was recorded on a harder surface due to less embedment while a lower application rate resulted in less flushing and a better appearance.

Important conclusions made by Milne (2004) included the following:

- Penetration grade bitumen performed sufficiently in average environments where extreme conditions are not evident.
- The aggregate application rate should be considered carefully, especially with the aim at preventing aggregate orientation when the service temperature has exceeded the ring and ball softening point $T_{R\&B}$ temperature (°C).
- The use of the MMLS3 resulted in comparative seal performance tests under expected service environments. Milne (2004) also states that the MMLS3 would be able to assist in the determination of binder properties on seal performance, and the seal's ability to contribute to the performance of the overall pavement.

2.8.3.2 Embedment Evaluation using the MMLS3

Following from the work done by Milne (2004), another MMLS3 project was undertaken towards the development of a standard test protocol, involving the MMLS3 to evaluate the performance of surfacing seals. The primary aim of the project was to identify and develop a standard test protocol by which important surfacing seal performance variables could be measured (Abrahams, 2015).

The study involved various seal failure mechanisms. By identifying these mechanisms, improved testing is identified. Following this, along with the application of the MMLS3 device, certain applicable aspects to seal failure are targeted. Embedment, as a seal failure and behavioural characteristic was a focus point, and this study would result in the first which attempted to quantify embedment through APT testing. Abrahams (2015) implemented the MMLS3 device with the following properties as presented in Table 2.10.

Table 2.10: MMLS3 setup as per Abrahams (2015)

MMLS3 setup properties		
Wheel load (kN)	**Tyre pressure (kPa)**	**MMLS3 load cycles**
2.1	700	100 000 (5 years)

The experimental study which Abrahams (2015) followed, can be seen in Figure 2.31.

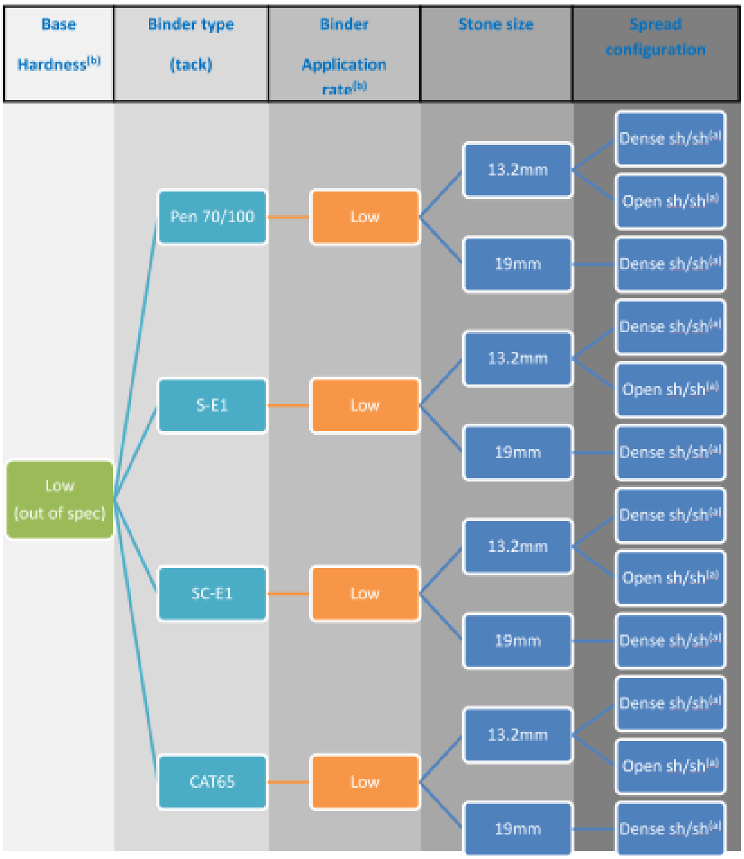

Figure 2.31: Experimental Design Summary (Abrahams, 2015)

From Figure 2.31, it is clear that careful consideration was given towards the base hardness, binder type, binder application rates, seal aggregate size and aggregate spread rate. Abrahams (2015) tested four binders, each with a 13.2 mm and 19 mm seal aggregate nominal stone size, over two aggregate matrices, namely an open and a shoulder-to-shoulder configuration.

To quantify the embedment, a laser texture meter (LTM) was used to measure the texture depth of the seal aggregate. Abrahams (2015) mentions that the software, together with the data from the LTM device, was implemented to obtain the z-coordinate values for each horizontal axis coordinate. The MMLS3 wheel load application intervals occurred up to 100 000 applications, each interval consisting of a laser scan. Consistent measuring points were identified within the wheel path to enable embedment calculations. This process was done by capturing images, after each trafficking phase, of the seal tiles. Individual aggregate particles were identified by colour coding and tracked throughout the trafficking phase by means of image processing.

Furthermore, Abrahams (2015) recorded a few interesting results which might be of importance to this study. It was noted that the design assumption of 50% of embedment potential (as measured by the ball penetration test) as observed during the construction phase, is potentially inaccurate. According to the results, the ball penetration test, which is related to base hardness, underestimates the embedment in a seal. This brought into question whether or not the test is a reliable method.

The binder type, according to Abrahams (2015), had an effect on the embedment of the seal. The hot applied binders, such as the penetration grade bitumen, outperformed the polymer modified SE-1. Both the hot applied binders appeared to be superior to the emulsions that were used. Adhesion problems and extensive embedment results were recorded when using emulsion. The adhesion problems resulted in stone orientation and in extreme cases stone loss, especially for a 13.2 mm CAT65 open aggregate configuration (Abrahams, 2015).

When investigating the influence of aggregate configuration, the practical testing was inconclusive. From the statistical analysis, the open aggregate matrix resulted in a higher probability of aggregate loss, especially for emulsions. This is intuitive since there is not good interlocking between aggregates in an open aggregate matrix (Abrahams, 2015).

Aggregate size played an important role in the embedment performance of the seal, but it was also influential in terms of aggregate orientation. Abrahams (2015) describes that the Flakiness Index added to the amount of aggregate orientation during the initial embedment. Another important factor was the difference in void content between the 13.2 mm and 19 mm aggregate. From the statistical analysis, the 19 mm aggregate showed a consistent negative embedment during the life of the seal. This was likely due to the flakiness and void content resulting in aggregate orientation. The void content and flakiness contributed to the 13.2 mm outperforming the 19 mm aggregate when investigating the resistance to embedment. The 13.2 mm aggregate was also more stable during the seal life after adhesion problems were encountered with the 19 mm stone.

2.8.4 The Protocol Guidelines for Asphalt Industry use

The Draft Protocol Guideline 1 (2008) is a description of the method used to investigate the rutting or deformation and moisture damage susceptibility, of bituminous pavements, by making use of the Model Mobile Load Simulator (MMLS3). The protocol was formulated and set up to be used by practitioners, in the asphalt industry, and is applicable to asphalt based mixtures containing penetration grade bitumen and modified bituminous binders (Draft Protocol Guideline 1, 2008).

The evaluation is performed under specific controlled environmental conditions. It is of note that the results should be analysed according to the specified environmental and trafficking conditions together with the in-service period of the pavement. To ensure adequate and realistic results, the materials, traffic conditions and environmental conditions in the laboratory should be representative of the actual conditions in practice. Both the Draft Protocol Guideline 1 (2008) and Abrahams (2015) describe different experimental test setups that could be used together with the implementation of the MMLS3

2.8.4.1 Test Setup

Laboratory cores and specimens: Cylindrical specimens should have a diameter between 149 mm and 150 mm and shall either be cored from an existing pavement or prepared in the laboratory. The thickness of the specimens shall range between 30 mm and 90 mm with a 2 mm deviation. The samples shall be sawed or trimmed using a planing blade to a tolerance of ± 0.5 mm. A schematic of a specimen can be seen in Figure 2.32.

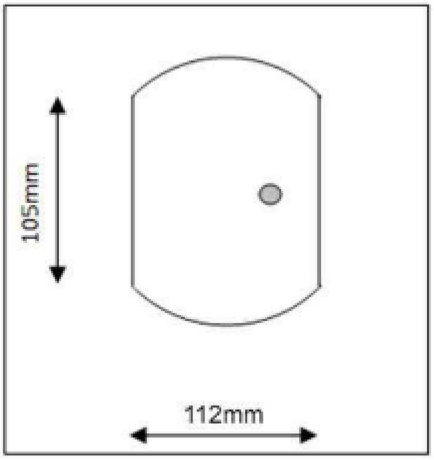

Figure 2.32: Cored Specimen according to the Draft Protocol Guideline 1 (2008)

Laboratory slabs: Although the Draft Protocol Guideline 1 (2008) does not completely describe a test method when constructing a layer system, Abrahams (2015) successfully performed an adequate and repeatable method. Slabs can be constructed, as a layered system, in the laboratory using sufficient compaction mechanisms, such as a roller compactor. Performance related variables and typical failure mechanisms, such as permanent deformation, embedment and aggregate orientation can then be measured after a desired number of load cycles have been applied. To exclude specimen variations, in terms of thickness, a layered test bed system should be constructed to avoid variation. This method is more promising than its predecessor for laboratory performance testing on surfacing seals (Abrahams, 2015).

Field testing: The MMLS3 could also be transported to a site to enable on-site testing. According to Abrahams (2015), this type of testing reduces variables such as temperature changes and wet trafficking along with other performance related variables which can not be replicated in a laboratory environment. Another advantage of on-site testing is the comparative relationships that can be obtained between on-site testing and laboratory testing (Abrahams, 2015).

2.8.4.2 Factors affecting performance relevant to MMLS3 testing

According to the Draft Protocol Guideline 1 (2008), the following factors need to be considered when evaluating the performance variables after MMLS3 trafficking.

Environmental conditions: Temperature has to be selected during testing due to it being a variable parameter. In practice, temperature changes occur frequently and are dependent on a number of factors such as elevation and geographical region. According to the Draft Protocol Guideline 1 (2008), wet trafficking increases the rutting of asphalt layers. Subsequently, rainfall patterns in terms of frequency, intensity and duration need to be accounted for. Wet trafficking could thus be more useful to provide information regarding the effects of moisture damage in seals, during MMLS3 loading.

Binder viscosity variations and temperature fluctuations result in periodic hardening and softening of the binder. This causes the bituminous binder in asphalt and surfacing seals to age. Milne (2004) describes four mechanisms causing ageing of binders: volatile losses, oxidation, porous seal aggregates and physical hardening of the binder. The Draft Protocol Guideline 1 (2008) states that geographical region and time play a great role in the ageing of binders and due to this, in-service ageing could have an effect on the rutting performance. Subsequently, provision is made for ageing by reducing the expected rutting, as estimated by the MMLS3, by 30%. This reduction is based on the increase in stiffness over time.

Traffic volume and axle loads: Traffic volumes and axle loads need to be selected with caution as they reflect the statistics pertaining the critical temperature phases, such as when the asphalt layer is above 40°C. The Draft Protocol Guideline 1 (2008) also mentions that careful consideration should be taken regarding the traffic during the early stages (< 30 days) as it impacts the critical primary rutting phase. Generally, only critical traffic is chosen to be replicated.

Lateral wander also affects the critical traffic parameter. This reduces the number of load repetitions at a specific location on the surfacing transverse profile. According to critical investigations, the deformation profile is generally Gaussian. Along with FEM analyses, lateral wander is considered less damaging when compared to channelised traffic flow. It should be noted that this is only for thick surfacing layers. Recently it was found that lateral wander on thin asphalt surfacings (< 40 mm) under high temperatures, caused significantly more damage in terms of permanent deformation. When using MMLS3 trafficking, lateral wander can be simulated by making use of transverse movement (Draft Protocol Guideline 1, 2008).

Traffic speed: The traffic that the surfacing layer has to carry, is selected to reflect the application service of the pavement layers. Average trafficking speed, gradients, vehicle volume, traffic flow and braking are all considered as factors. The following are recommended as influencing factors:

- Levelled flowing traffic.
- Gradient traffic flow.
- Slow moving intersection and inclination traffic flow.
- High contact stresses and runway thresholds at airport runways.

The Draft Protocol Guideline 1 (2008) considers free flowing traffic to be in excess speeds of 27 kPh and thus, when the MMLS applies 7200 load applications per hour, it classifies as free flowing traffic conditions.

Axle loads and tyre pressures: During conditions where moderate or low heavy vehicle traffic is found, 700 or 750 kPa tyre pressures can be used. The wheel load is another consideration since it has a profound effect on the footprint of the surface (De Beer and Fisher, 1999). High tyre pressures, such as 800 kPa, generally relate to high axle loads, such as 2.9 kN. The lower pressure situation requires a reduced wheel load of 2.7 kN per axle. Life cycle predictions are then made based on the resulting wheel loads (Draft Protocol Guideline 1, 2008).

Pavement Structure: According to the Draft Protocol Guideline 1 (2008), a thinner layer produces a better comparative relationship between the MMLS3 tyres and full scale tyres. Due to the limited depth of the stress profile related to the tyres of the MMLS3, the maximum layer thickness is 150 mm. The nominal maximum aggregate size should not exceed 50% of the asphalt layer thickness due to the stress profile as a result of tyre size (Draft Protocol Guideline 1, 2008).

2.9 MMLS Performance Variables for testing seals

To evaluate the influencing factors of MMLS3 trafficking, performance criteria, together with a method of evaluation is required. According to Milne (2004), the identification of factors influencing seal performance, from a theoretical, practical and numerical perspective, to be included in a numerical and experimental model, is an interactive process.

When modelling seal performance, a number of influencing factors should be evaluated and considered. According to Milne (2004), an APT schedule should be utilised to determine seal behaviour from a scaled down level when performing experimental modelling. FEM analyses methods to evaluate seal performance on a micro-mechanic scale should also be developed. Controllable and non-controllable factors are listed to determine potential critical variables when performing either experimental or numerical modelling. The performance variables can be seen in Table 2.11.

Table 2.11: Performance variables relating to the seal as adapted from Abrahams (2015) and Milne (2004)

Field	Component Variable	Performance Variable	Controllable
Bitumen	- Penetration grade: 70/100 - Emulsion: SC-E1, SC-E2 - Polymer modified: S-E1, S-E2 - Bitumen rubber: S-R1, S-R2	- Temperature - Viscosity - Adhesion - Cohesion - Ductility	- Field - MMLS3
Aggregate	- Type - ALD - Flakiness	- Strength - Adhesion - Wear - Texture	- Field - MMLS3
Seal Design	- Single seal - Binder application rate - Aggregate matrix and application rate - Void volume	- Binder application rate - Aggregate matrix and application rate	- Field - MMLS3
Substrate	- Material type - Material classification - Grading and stone size	- Density - Strength - Hardness	- Field (limited) - MMLS3
Traffic	- Equivalency factor - Contact stresses: footprint, pressure and load - Applications and time	- Tyre pressure - Axle load - Volume	- MMLS3
Environment	- Temperature variation - Moisture variation - Complex modulus (G*) per temperature zones	- Temperature effect - Ageing - Moisture effect	- MMLS3

As stated, the performance variables, as listed in Table 2.11, were needed to enable a guideline for a successful experimental design of this study. A good indication as to the controllable and non-controllable factors are of note.

2.10 Texture depth and Profile Depth

2.10.1 Macro-texture

Macro-texture is generally a result of seal aggregate stone (in this case) protruding in the surfacing layer. It corresponds to the pavement surface roughness as a whole. In comparison to the roughness wavelength less than 0.5 mm for the micro texture, the macro texture is defined as texture with a wavelength ranging between 0.5 mm to 50 mm (Van Zyl and Van der Gryp, 2015). Furthermore, the macro texture is evaluated for the following purposes as described by Van Zyl and Van der Gryp (2015):

- Skid resistance analysis.
- Suitable pre-treatment or reseal type selection.
- Binder application rate adjustments for seal design purposes.

The contribution of the macro texture to the skid resistance, as reported in the SABITA Manual 40 (2021), includes the following:

- It deforms the tyre which leads to an energy loss called hysteresis.
- It provides the run-off channels required to ensure adequate water dispersion, especially at higher speeds.

Based on the existing surface macro texture, additional binder is required to firstly fill the voids.

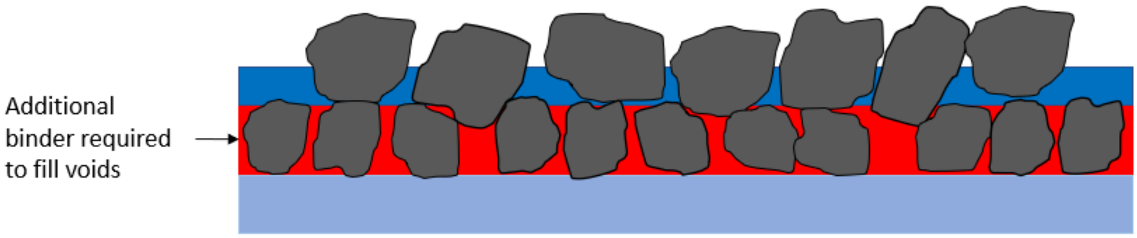

Figure 2.33: Additional binder required to fill voids as adapted from Van Zyl and Van der Gryp (2015)

Texture depth is often related to the term 'macro-texture' and there are different ways of quantifying it as explained in the following sections.

2.10.2 Volumetric Measurements

The SANS 3001-BT11 (2012) describes the volumetric patch method, related to the mean texture depth, as a volumetric approach to obtain the texture depth. It is obtained by spreading a known volume of sand or glass beads, conforming to a specific size, on a surface texture after which it is spread to ensure only the top peaks of the aggregate particles are visible. The volumetric texture depth is then obtained taking the ratio of the volume of sand or glass beads spread to the area that it covers when spread. ISO 10844, EN 13036-1 and ASTM E965 provide the standardized volumetric patch method. Furthermore, Van Zyl and Van der Gryp (2015) report that sand is no longer preferred, although still specified in the SANS 3001-BT11 (2012), as the usage of glass beads provide increased reproducibility. A visual representation of the method can be seen in Figure 2.34.

Figure 2.34: Volumetric texture depth (VTD) as per the SABITA Manual 40 (2021)

2.10.3 Laser Profile Measurements

According to Adams and Kim (2013), the mean profile depth (MPD) is a parameter that is used to accurately assess the seal surface texture by means of laser profile readings. The mean profile depth is defined as per the following relationship.

$$\text{MPD} = \left(\frac{\text{First peak level} + \text{Second peak level}}{2}\right) - \text{Average} \tag{2.1}$$

Where:
MPD = mean profile depth,
Peak level = the highest vertical aggregate point along a section and
Average = the average aggregate height along a section.

The parameters, as per Equation 2.1, can schematically be shown in Figure 2.35.

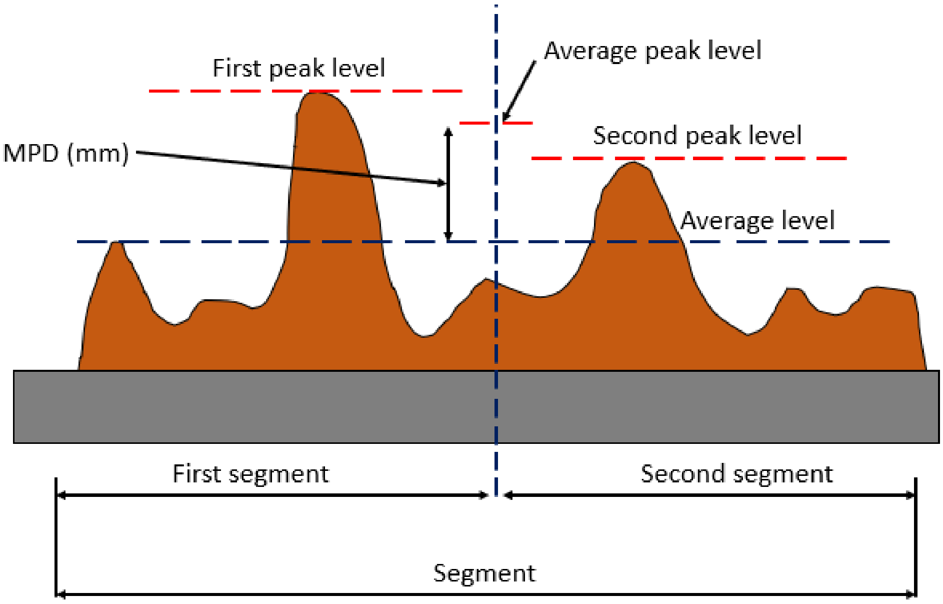

Figure 2.35: Mean Profile Depth Schematic as developed from Gransberg and James (2005)

The MPD calculation, as shown in Equation 2.1, is of value as it provides valuable information as to the macro-texture and the aggregate exposure depth. Both of these roughness parameters are required as they ensure adequate braking of vehicles. Seal aggregate exposure depth is related to potential embedment which is an important seal aggregate behaviour characteristic as it relates directly to the managing of aggregate whip off (stone loss) and bleeding. Apart from the results that Adams and Kim (2013) obtained, Figure 2.36 shows that the MPD decreases as the number of wheel passes increase for both field and MMLS3 testing. Although documented that this trend is related to aggregate loss and bleeding, a similar trend can be expected when investigating aggregate orientation and embedment.

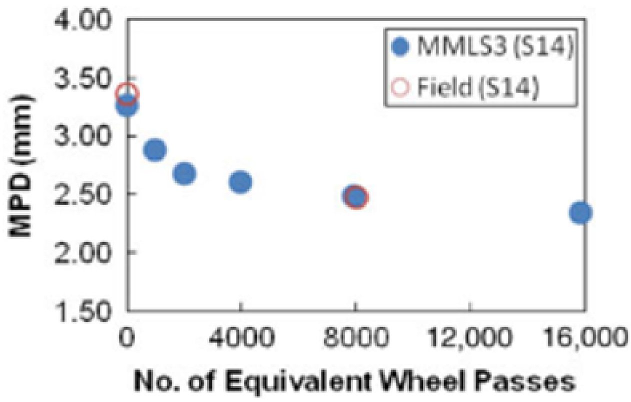

Figure 2.36: MPD decreases with an increase in traffic (Adams and Kim, 2013)

2.10.4 Estimated Texture Depth

The transformation equation, as reported by Van Zyl and Van der Gryp (2015), between the MPD and the estimated texture depth (ETD) is obtained, with reference to PIARC/ISO, by making use of Equation 2.2.

$$\text{ETD(mm)} = 0.2 + 0.8\text{MPD} \tag{2.2}$$

Furthermore, Van Zyl and Van der Gryp (2015) mention that for surfacing types with texture depths varying between 0.5 mm and 5.5 mm, good correlation between the MPD and volumetric texture measurements yielded, although different from the transformation equation as per Equation 2.2. From the laser profiling and the specified volumetric sand patch method, a potential more applicable transform equation is obtained by forcing the MPD and volumetric texture depth relationship line through the origin for both the sand (75 - 300 micron) and glass bead (100 - 300 micron) volumetric approaches. Equation 2.3 describes the relationship between the estimated texture depth and the mean profile as proposed by Van Zyl and Van der Gryp (2015). The equation is derived from both Figure 2.37 and Figure 2.38.

$$\text{ETD(mm)} = 0.2 + 0.8\text{MPD} \tag{2.3}$$

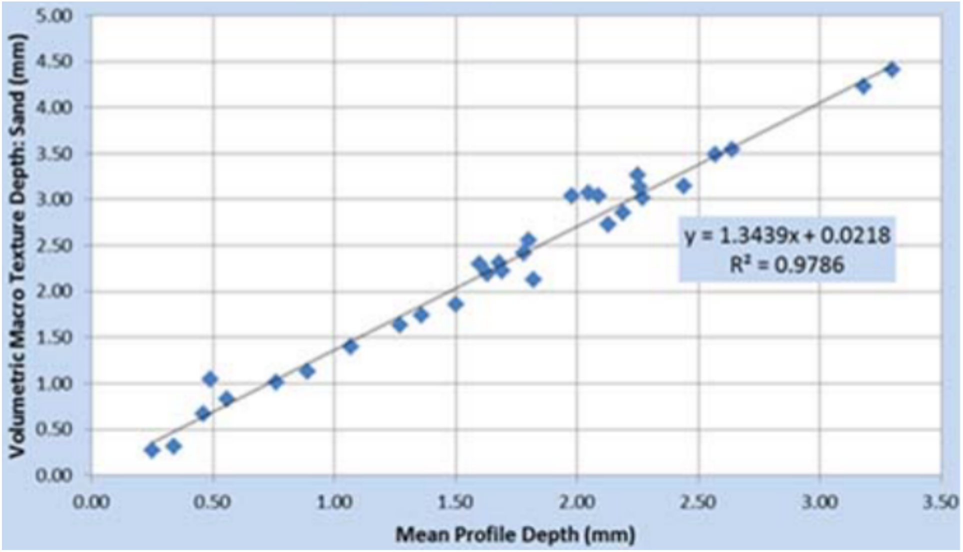

Figure 2.37: MPD versus volumetric texture depth (75 - 300 micron sand) as per Van Zyl and Van der Gryp (2015)

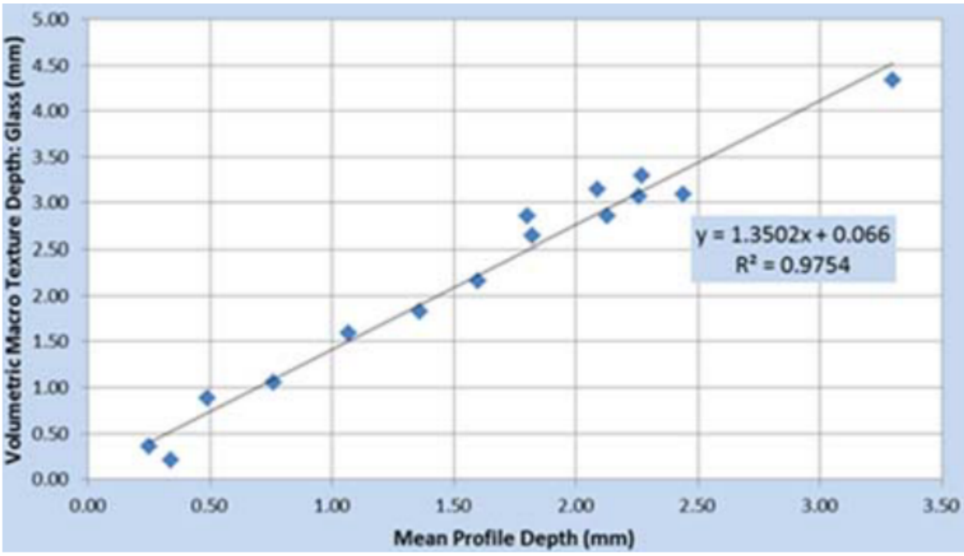

Figure 2.38: MPD versus volumetric texture depth (100 - 300 micron glass beads) as per Van Zyl and Van der Gryp (2015)

2.10.5 Mean Texture Depth versus Mean Profile Depth

Arendse (2016) conducted a study to establish a comparison between the mean profile depth (as measured and calculated by means of a laser unit) and the mean texture depth of both surfacing seals and asphalt. This was done for both the 50 ml and 100 ml volumetric sand patch tests. Both regression lines can be seen in Figure 2.39 and Figure 2.40. As obtained, the coefficient of determination for the 50 ml and 100 ml volumetric tests was 0.902 and 0.912, indicating a good relationship.

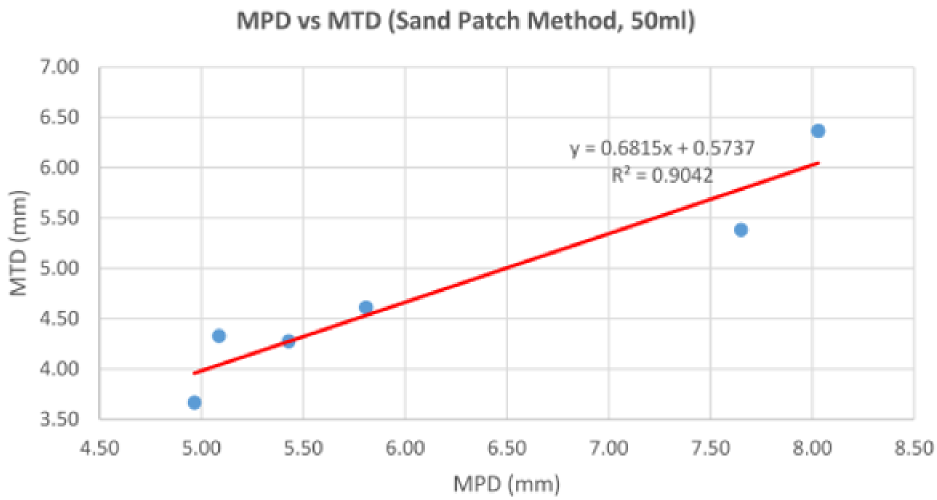

Figure 2.39: MPD vs MTD (50ml) (Arendse, 2016)

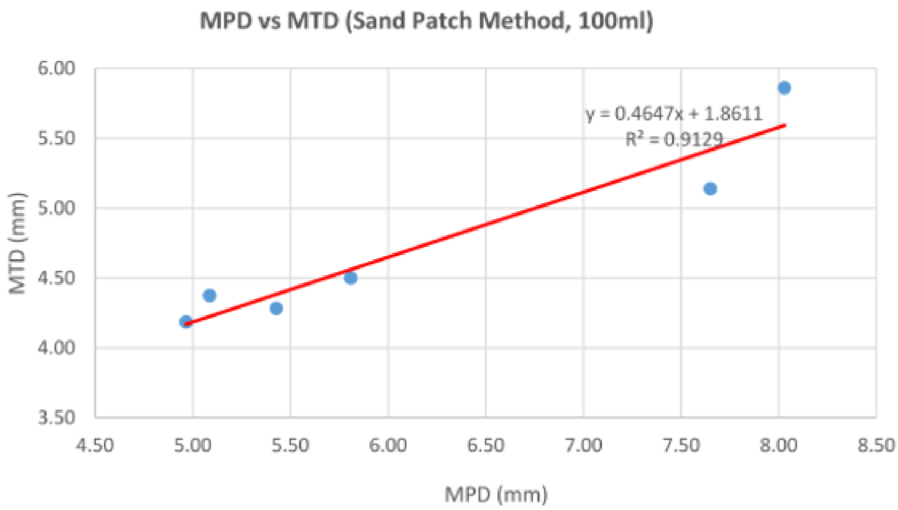

Figure 2.40: MPD vs MTD (100ml) (Arendse, 2016)

Furthermore, a regression analysis was performed resulting in the following two relationships between the MTD_{50ml} as well as the MTD_{100ml} and the MPD:

$$MTD_{50ml} = 0.6815MPD + 0.5737 \tag{2.4}$$

$$MTD_{100ml} = 0.4647MPD + 1.8611 \tag{2.5}$$

It was reported that a better regression was obtained between the MTD_{100ml} and the MPD due to a larger volume of glass beads or sand being used. It was furthermore concluded that positive regression was obtained between the MPD (laser reading) results and the MTD (sand patch) results. Thus, both methods are accurate and should produce a general trend as to the change in texture when evaluating surfacing seals.

2.11 Summary

The literature discussed provides the necessary background information regarding binders, seal and base aggregate, surfacing seals as well as accelerated pavement testing mechanisms such as the Model Mobile Simulator 3. Furthermore, it is of importance to understand that various aggregate and binder properties, together with seal behaviour in aggregate embedment and aggregate orientation, influence seal performance under various trafficking and environmental conditions. Surface measurement methods, such as the sand patch test and the calculation of the mean profile depth, provide valuable information regarding the possibility of implementing such methods to analyse decreases in texture and profile depth losses as a result of aggregate embedment and orientation.

Chapter 3

Experimental Design

3.1 Introduction

This chapter elaborates on the design considerations given to achieve the objectives as mentioned in Chapter 1. Following the design considerations, the experimental design includes the final design implementations. Lastly, an overview of the experimental design is provided.

3.2 Overview: Seal Aggregate Orientation

Aggregate orientation, in a surfacing seal, is a behavioural process occurring partially during the construction and partially during the in-service phase. It is dependent on the binder type, which relates to rheology, aggregate properties, trafficking- and environmental conditions and aggregate configuration. The process involves the concept that aggregate particles tend to orientate themselves onto their flattest side such that the particle's ALD is perpendicular to the horizontal surface. Aggregate orientation is important for seal design as it influences the void content in a seal surfacing layer. The void content is subsequently a design influencing factor as it is necessary for seal aggregate to accommodate bituminous volume changes during temperature increases to ensure that the binder does not move up and onto the surface.

The following factors are investigated to obtain a conclusion as to how it influences aggregate orientation:

- The type of hot modified binder used.
- The temperature conditions.
- Aggregate configuration.

Kumbargeri *et al.* (2019) emphasizes the importance that most of the chip seal aggregate particles orientate themselves to produce a one-stone thickness after compaction, to increase the desired performance potential of the surfacing seal. An optimum binder application rate and optimum aggregate application rate exists where the aggregate particles are allowed to orientate themselves to lie on their flattest side. It was shown that as the binder application rate increased, it would act as a lubricating fluid for the stone to orientate. But, this process reaches a certain binder application rate which is too high and would lead to texture loss and excessive binder moving out onto the surface causing bleeding and flushing.

The result of aggregate behaviour in a seal mat is also dependent on the tyre footprint, inflation pressure and the wheel load as described in literature by De Beer and Fisher (1999) and Hernandez *et al.* (2013). Furthermore, the movement of aggregate in a seal, for an over application aggregate matrix, is influenced by the 3-D mosaic packing of the aggregate and therefore the variation in vertical, longitudinal and transverse stresses contributes to the tyre-pavement contact relationship. When aggregate particles disorient themselves from their ALD, chip loss, skid resistance issues and uncomfortable driving conditions arise.

As stated in Section 2.4.1.2, modified binders influence aggregate orientation due to the elastic, flexibility and stiffness characteristics thereof. Aggregate particles tend to orientate between 5 - 10 years when an S-R1 surfacing is constructed due to significant elastic qualities that exist. Aggregate particles in an S-R1 binder, when slightly orientating under traffic loading, revert back to their original construction position. S-R2 modified bitumen rubber results in a very low viscous binder at construction, causing most of the aggregate particles to orientate during construction. Due to a higher polymer content in an S-E2 binder, and with increased elastic properties, the aggregate particles tend to not orientate during the high construction temperature. The lower polymer content in the S-E1 would still contribute towards the elasticity properties of the binder, but not to the extent as in an S-E2.

3.3 Construction Considerations

3.3.1 Introduction

To set up an experimental matrix that would result in quality data, testing recurrence and adequate feasibility, careful design- and construction consideration is necessary. The experimental matrix requires great detailing to ensure that the laboratory environment validates the testing and the results thereof.

The variables are carefully considered and the seal construction process was modified to represent in-practice construction within the limits of a laboratory environment.

3.3.2 Base Properties

As stated in Section 2.2.3.2, the structural layers of a pavement structure are expected to effectively transfer the imposed loads to the deeper layers. The upper layers, such as the base, are generally constructed from stiffer and high-strength material due to higher stresses from traffic loads. The large quantity of material, such as aggregate, required to construct the base are generally acquired from quarries within close proximity to the site to minimize transport costs. Careful consideration should however be taken when sourcing material close to the site as the material is not always of good and desirable quality. For the base construction of this project, a similar sourcing method will follow to acquire a good quality G2 or G3 material from the nearest quarry with a maximum aggregate particle size of 20 mm. Careful consideration should also be given as to how the base material should be prepared in terms of scalping off. Either scalping at the 20 mm after which the material will be crushed again and sieved as to ensure all aggregate particles are smaller than 20 mm, or whether all particles between 20 mm and 37.5 mm should be crushed and placed back into the base material of which the larger particles are already smaller than 20 mm.

Constructing a quality base layer can be an exacting procedure and the specifications should be stringently applied to enable the base to perform to its best potential whilst ensuring the cost-effectiveness thereof to be valid. Kleyn (2012) mentions the importance of accepting only in-specification material on site. Before commencing with the construction of the base, a clean, stabilized, level and dampened subbase as anvil should be prepared. A suitable and stable subbase material should be brought in and compacted as to provide a hard and compacted layer on which the base material could be constructed. The stabilisation of the base material is also to be investigated with the goal to construct a base layer which will not only provide adequate stiffness support, but also provide hardness to ensure that seal aggregate embedment is limited. The embedment behaviour of aggregate, in seals, are directly correlated to the base layer's upper section. Gerber (2016) states that the embedment characteristics of the base layer can be quantified by evaluating the hardness of the layer by means of the ball penetration test. This test method will be used to estimate the potential embedment of the seal aggregate to obtain a consistent and adequate initial embedment. For the purpose of evaluating the embedment characteristics of the base layer, a test-base can be constructed on which various ball penetration tests could be completed. This would provide an indication as to the mix design of the base layer and whether or not the stabilisation thereof is sufficient. As embedment is not the critical focus of this study, the initial embedment of the aggregate particles should be achieved as adhesion between the base and the seal aggregate is required. Due to embedment influencing the degree of aggregate orientation, a desired low ball penetration should be achieved as the particles should still be able to orientate without full embedment restrictions. To ensure better adhesion between the upper base and the constructed seal, a prime layer is also considered.

Slush-compaction, a process which involves using water with an adequate amount of energy to slush fines from a base course, is then used to complete a quality base. By expelling the fines through slush-compaction, maximum particle interlocking is assured leaving a strong aggregate matrix, with a mosaic after brooming that significantly reduces embedment of the seal stones. Abrahams (2015) mentions the difficulty of achieving a specific base hardness in a laboratory environment. Compaction methods would be established and evaluated to construct a G2 or G3 base in this project according to the correct specifications. An inadequately compacted base could result in unknown variables which are not desirable.

3.3.3 Seal Type

The SABITA Manual 40 (2021) states that the selection of an appropriate seal type is primarily based on the experience of the authorities and the practitioners designing and constructing the surfacing seals. For newly designed and constructed surfacings, it is of importance to note and understand the influencing factors and to identify surfacings which will preform well under the specified conditions. The SABITA Manual 40 (2021) mentions these influencing factors and states that the selection of a specific surfacing seal is based on a method of eliminating the inappropriate seal types. Subsequently, this again emphasizes the inability to accurately predict the conditions in which a surfacing seal is placed during its functional lifetime. The following guidelines are specified for the elimination process.

- Traffic
  - Vehicle volume
  - Vehicle action
- Road gradient
- Maintenance capability
- Required surface depth
- Viable construction techniques
- Quality of the pavement base
- Environmental conditions
- Cost comparisons based on the initial design
- Any other special condition which the surfacing seal might experience

The above-mentioned selection criteria corresponds largely to the influencing factors as mentioned and discussed in detail in Section 2.3.6. Furthermore, the SABITA Manual 40 (2021) states that the recommended surfacing seals are all based on historical performance that was classified as sufficient. With that, it does not necessarily indicate that a non-recommended surfacing seal will not perform adequately. Seal performance is largely based on the experience of the design team and the construction process and techniques implemented by the practitioners in a specific area.

Considerations regarding the seal type includes the constructibility thereof in a laboratory environment. Abrahams (2015) mentions that the in-service construction techniques are difficult to replicate in a laboratory environment and thus, the type of seal should carefully be considered given the small scale of construction. The newly constructed seal should reflect the properties of an in-practice surfacing seal by replicating the binder- and aggregate application together with the compaction process thereof.

Another consideration when following the elimination process of seal types, is to realise that multilayered seal types, such as double or Cape seals, could further implicate the measurements of depth as there multiple aggregate layers. Subsequently, the seal type is to be considered carefully and strategically to ensure quality data gathering and reworking.

3.3.4 Tack Coat (Binder Coat)

The tack coat, or binder coat, is the first bituminous layer to be applied onto the base of the pavement, after which the seal aggregate is applied and compacted. The tack coat is a thin bituminous layer that serves the purpose of binding the seal aggregate to create a strong matrix together with the protection of the base layer by acting as a waterproof layer to prevent moisture ingress. The choice of bitumen, or bitumen emulsion, is generally based on varying factors such as the type of seal, the environmental conditions, economical value of the binder, application convenience, aggregate compatibility, traffic conditions and the durability properties of the binder (SABITA Manual 40, 2021).

The application rate of the bituminous binder, irrespective of the type of binder, is influenced by the properties of the seal aggregate. These aggregate properties include the shape (flaky or rounded), the spread rate and the equivalent resulting texture depth thereof. The shape of the aggregate affects the void ratio in the aggregate mat. Subsequently, there is a decrease in voids between the aggregate particles when there is an increase in the flakiness value of the aggregate. With the voids influencing the accommodation of the binder, there is a need to apply or adjust the binder application rate to take aggregate properties into account (SABITA Manual 40, 2021).

Another careful consideration that is of importance, is the laboratory application of the tack coat. In practice, the application method of the tack coat includes the systematic drive and spray of the tack coat from a construction vehicle which carefully controls and monitors the application rate. This process, together with the application of the aggregate directly after the tack coat, can be seen in Figure 3.1.

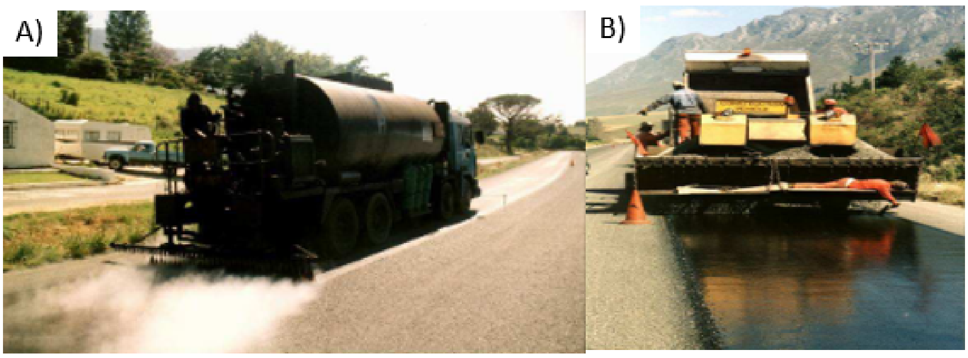

Figure 3.1: Where a) shows the application of the tack coat and b) the aggregate (Van Zyl, 2000)

The final compaction then occurs where the seal stones are initially embedded and orientated to a certain degree. This process could be difficult to replicate accurately in a laboratory environment. The small representative time period between the application of the tack coat and the application of the seal aggregate is vital as a too long period could result in adhesion problems between the binder and aggregate. This issue could result in unrepresentative test samples as aggregate orientation would also be affected.

3.3.5 Aggregate

3.3.5.1 Type and shape

The type of aggregate generally used in the construction of surfacing seals relates to the type of aggregate within the vicinity of the construction site. Again, the use of adequate aggregate, which is close to the construction site, minimises the transportation costs. The aggregate type and the mineral composition thereof, determines the resistance to weathering and erosion. Generally, aggregates with sufficient hardness properties are desired as they do not crush, break or chip under loading.

As mentioned previously, the aggregate shape affects both embedment and orientation during the construction period and during the in-service period. Aggregate orientation is influenced by the flakiness value of the seal aggregate as a high flakiness index would result in aggregate particles orientating themselves earlier onto their ALD under loading. The void content, in the seal mat, is a function of the aggregate flakiness and an increase in flakiness, as mentioned in Section 3.3.4, results in a decrease in void content which subsequently leads to binder problems such as bleeding. The effect of aggregate size on the orientation of aggregate particles is neither clear nor well investigated in literature but generally, larger aggregates are used under heavy vehicle loading due to a higher void content and therefore allowing for more binder to occupy with a decrease in void content as a result of embedment.

3.3.5.2 Spread Rate

The SABITA Manual 40 (2021) states that the application of aggregate should be at such a rate that a uniform mosaic cover is achieved. The individual particles should lie shoulder-to-shoulder, in a tight matrix in single layer. With a too high aggregate application rate, adequate adhesion between the tack coat and excess aggregate does not necessarily develop, allowing for the excess aggregate particles to be forced into the seal mat after which whip-off is more prominent. Degradation as a result of crushing and grinding of the aggregate and unnecessary waste of material could also occur due to an over application rate. An aggregate application rate that is too low will result in a loss of texture (due to less aggregate) and extensive cases of bleeding and flushing. Repeated traffic loading could also result in binder being whipped form the pavement causing surface damage.

The SABITA Manual 40 (2021) does not specify the recommended aggregate spread rate as it generally depends on various factors such as aggregate- and base properties, seal functionality and practitioner preference. Lawson *et al.* (2007) states, and as mentioned in Section 2.4.1.2, that the aggregate particles should be spread in such a manner that they do not touch one another but are still close enough to deny another particle to fit into the void space. Subsequently, as schematically shown in Section 2.4.1.2, there are two aggregate spread rate considerations:

- Shoulder-to-shoulder spread rate.
- Over application spread rate.

The SABITA Manual 40 (2021) also mentions that over chipping prevents aggregate orientation. This results in aggregate particles not orientating onto their respective ALD.

When over chipping occurs, the movement (and orientation) of the aggregate particles is governed by the binder and the aggregate strength as well as the influence of aggregate crushing and abrasive resistance. When a more open spread aggregate matrix exists, the bitumen is seen as a continuous phase with seal aggregate dispersed into it. The movement and orientation of the aggregate particles is then governed by the adhesion of the stone particle to the bituminous layer (Abrahams, 2015).

Kumbargeri *et al.* (2019) describes that an optimum aggregate spread rate exists where the aggregate particles orientate themselves to lie on their flattest side. As the aggregate application rate increases above the optimum application rate, the particles begin to disorient themselves. When the application rate is lower than the optimum rate, the particles orientate too easily due to the bituminous binder acting as a lubrication material.

3.4 Experimental Design

3.4.1 Introduction

After careful consideration of the design variables, as discussed in Section 3.3, the design matrix is identified. This matrix includes all of the construction properties of the seals as well as the implementation characteristics of the testing equipment. Subsequently, all construction variables are decided upon to ensure validity of the construction process and to produce a testing procedure which is repeatable and reliable.

A partial testing procedure is set up to ensure that all relevant and important aspects with regards to seal aggregate orientation is sufficiently covered. For the purpose of this study, the following test variables are identified and decided upon.

3.4.2 Base Properties

Before constructing the base material, it was decided upon to make use of a 150 mm sand layer as the subbase, compacted at OMC to ensure a suitable tipping subbase for the base layer. As mentioned in Section 3.3.2, the base construction procedure followed to ensure a quality G1 base course, would require a slush-compaction method which would be difficult to replicate in a laboratory, small-scale environment. As a result of this, a bitumen stabilised base (BSM-emulsion), with 3.5% emulsion and 1.5% cement is used together with a G2 granular material. The reason for constructing a 1.5% cemented, G2 BSM-emulsion, is to remove the punching effect of aggregate embedment as much as possible whilst maximizing the aggregate orientation behaviour of the particles as this is the main focus. If the base is too soft, the seal aggregate would embed under loading and the orientational effect thereof would be difficult to quantify. It is also decided to firstly construct a smaller BSM test base for the purpose of evaluating the ball penetration of the base layer. After careful consideration, the ball penetration of the base layer is limited to 1.5 mm for the purpose of maximizing orientation of seal aggregate. After the construction of the base, a hand controlled pedestrian roller is used to ensure sufficient compaction.

3.4.3 Seal Type

The process of selecting the appropriate seal type is mainly based on either a process of elimination, as described in the SABITA Manual 40 (2021), or the design team's preference. When focusing on aggregate orientation, it is beneficial to implement and construct a very simple seal type, to enable quality and sufficient orientation quantification by means of evaluating the changes in texture. Thus, when comparing multi-layered aggregate seal types and a single layered aggregate, it is more logical to construct a single seal. The basic structure of a single seal can be seen in Figure 3.2.

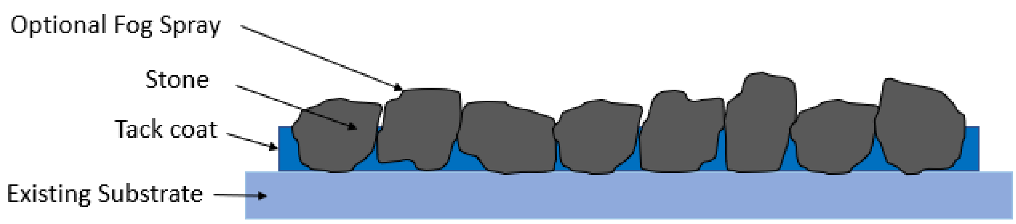

Figure 3.2: Single seal structure as adapted from the SABITA Manual 40 (2021)

As seen, the single seal consists of a tack coat applied to the top of the base layer, followed by a single layer of seal aggregate which is sprayed with a bituminous based cover spray of fog spray. The purpose of the fog spray (when using emulsions), is to lessen the likelihood of stone loss under trafficking conditions.

3.4.4 Tack Coat

This study is focused on the implementation of four hot polymer modified bituminous tack coats:

- SBR latex modified bitumen (S-E1).
- SBS modified bitumen (S-E2).
- Modified bitumen by means of bitumen rubber (S-R1).
- Modified bitumen by means of bitumen rubber (S-R2).

The application rate, of the tack coats, is based on the use of the seal design methodology as described by the SABITA Manual 40 (2021). To obtain an appropriate application rate, the ELV, corrected ball penetration value, macro texture requirement, aggregate hardness and the ALD of the seal aggregate is required.

The application rates for the different hot polymer modified binders will differ as some of the input parameters differ (such as the corrected ball penetration values) together with the conversion factors to obtain a hot modified binder application rate. These factors are dependent on the type of hot modified binder, the type of seal (single, double or split) and the ELV traffic. The application rates are also governed by the practical minimum and practical maximum rates.

Due to all of the binders being polymer modified bitumen, the seal aggregates are pre-coated. This process is generally followed to ensure better adhesion properties between the aggregate and the bituminous binder. Subsequently, Bitukote is selected as a bitumen-based pre-coat. This was recommended by the manufacturers together with the expert advise from Van Zyl (2021).

3.4.5 Aggregate properties

During in-practice seal construction, nearby material is generally sourced and if sufficient for construction, they are used. This process is also followed in terms of the aggregate type. Metamorphic andesite was sourced and decided upon to be used as the seal aggregate as it is in abundance in the Western Cape area and also commonly used during the construction of seals in the Western Cape.

As both the ALD and the flakiness index influences the bituminous binder application rate, the properties of the aggregate are used to determine the initial binder application rates according to the SABITA Manual 40 (2021). It is of importance to determine the initial binder application rates as they are a focus point in assessing to what extent they are to be adjusted to account for aggregate orientation. During the construction and testing of the seals, a single sized aggregate is used, namely a 14 mm nominal size. A 14 mm size is generally used in the construction of single seals as it is sufficient to accommodate bituminous binder in the void spaces whilst keeping noise levels to a minimum during trafficking conditions.

3.4.6 Aggregate application rate

The SABITA Manual 40 (2021) mentions that optimum binder application rate is dependent on the aggregate application rate. Generally, the usage of cubical aggregate particles, that are densely packed, results in less binder being accommodated before failure issues such as flushing start occurring. This process can be logically described in the sense that cubical particles, which are densely packed, lessen the void content between aggregate particles, and subsequently there is no space for the binder to fill and the probability of flushing or bleeding increases. When using flaky aggregate particles, less aggregate is required per unit area to obtain a dense packed aggregate mosaic. If flaky aggregates are orientated to lie flat, both the void and binder content decreases.

The SABITA Manual 40 (2021) also mentions two different basic aggregate spread rates, namely a dense shoulder-to-shoulder and an open spread rate. Subsequently, due to the different interpretation of these terms between road authorities, a more direct configuration approach is decided upon:

- Shoulder-to-shoulder (sh-sh): this configuration would see the aggregate particles packed on their respective ALD's in a mosaic pattern such that the individual particles touch each other but display an open spread rate. Only after compaction, when orientation takes place, does the matrix display a shoulder-to-shoulder configuration.

- Over application: this spread configuration would see an over application of aggregate in a mosaic pattern. A larger mass percentage (when compared to the sh-sh matrix) of aggregate particles would be used to obtain such a matrix with the desire to obtain as many contact points between the aggregate particles.

As supported by the SABITA Manual 40 (2021), and successfully implemented by Abrahams (2015), the volume of aggregate to be spread is determined visually. A simplistic, but accurate method, to determine the two different matrices is to make use of a predetermined area (generally 1 m^2) wherein a sh-sh aggregate matrix is achieved by placing stones, onto their ALD (such as after compaction), in a loose knitted matrix such that void spaces, to be filled with binder, can clearly be seen. The mass of the stone is then recorded. An over application matrix is then achieved by placing the same mass of aggregate (as per the sh-sh matrix) into the mould, in a very similar manner as to achieve ALD, after which individual stones are placed in the void spaces (still on ALD) up to the point where no stones can be added without wedging the neighbouring stone. The mass is then recorded. Subsequently, the over application aggregate matrix consists of a certain percentage mass additional stone mass compared to the sh-sh matrix. Thus, there is a sh-sh and an over application matrix for each of the four binder types, resulting in eight seals in total.

It is of note that the aggregate is to be applied in a quick and efficient manner to not allow for adhesion problems between the hot modified binder and the stone.

3.4.7 MMLS3 Implementation

3.4.7.1 Wheel pressure and load

As mentioned by Abrahams (2015), a wheel load of 2.7 kN, which is representative of a single wheel of a dual axle system of an E80, is decided upon. This wheel load is an input value on the MMLS machine. With regards to the tyre pressure and a range between 600 kPa and 750 kPa available on the MMLS3, a value of 750 kPa was decided upon to be conservative. A tyre pressure of 750 kPa is also a realistic value corresponding to a wheel inflation pressure of an E80 axle.

3.4.7.2 Load Applications

Due to the aggregate particles orientating and behaving differently when implemented together with different modified binders, it is of importance to determine and set respective measuring intervals along the load application process. The SABITA Manual 40 (2021) specifies the following relationship between light and heavy vehicles:

$$\mathrm{ELV} = \mathrm{L} + (40\mathrm{H}) \tag{3.1}$$

where:
ELV = equivalent light vehicles/lane/day
L = number of light vehicles/lane/day
H = number of heavy vehicles/lane/day
40 = equivalency factor between heavy and light vehicles.

It is usual practice to implement and construct surfacing seals to carry traffic volumes between 125 to 20 000 equivalent light vehicles per lane per day. Furthermore, lighter seal types, such as small aggregate seals, should only be implemented for roads carrying up to a maximum of 2000 ELV per lane per day. Based on the expertise knowledge of Van Zyl (2021), the equivalent light vehicles per lane per day is selected as 3000 ELV as it is representative of in-service trafficking conditions.

Based on the equivalency relationship between light vehicles and heavy vehicles, together with the goal to evaluate the MPD and MTD , the following load application intervals are selected as presented in Table 3.1.

Table 3.1: Time equivalent period based on 3000 ELV per lane per day

Reading Interval	Load Application	Equivalent Time Period (days)
1	0	Construction
2	100	2
3	500	7
4	2000	27
5	5000	67

To obtain quality measurements, especially during construction and the early stages of trafficking, readings are taken more frequently. This allowed for a better idea as to how the aggregate particles behave during the early stages, especially important for the very soft modified binders such as the S-R2 surfacing.

3.4.8 Trafficking Temperature

To analyse the various aggregate orientation behaviour of the seal aggregate for the different modified binders, three trafficking temperatures are selected to simulate common environmental conditions. These conditions are representative of actual trafficking conditions in the sense that a climate controlled chamber (insulating box) is constructed around the MMLS3. The trafficking temperatures are:

- 10°C (lower temperature boundary),
- 20°C (intermediate temperature) and
- 30°C (elevated temperature boundary).

By testing at these trafficking conditions, both the annual maximum and minimum average temperatures are covered.

3.5 Overview of Experimental Design

As seen in Figure 3.3, the overview and summary of the experimental design is given. The design includes each of the four initial different binders, binder application rates, nominal aggregate sizes and aggregate spread rates.

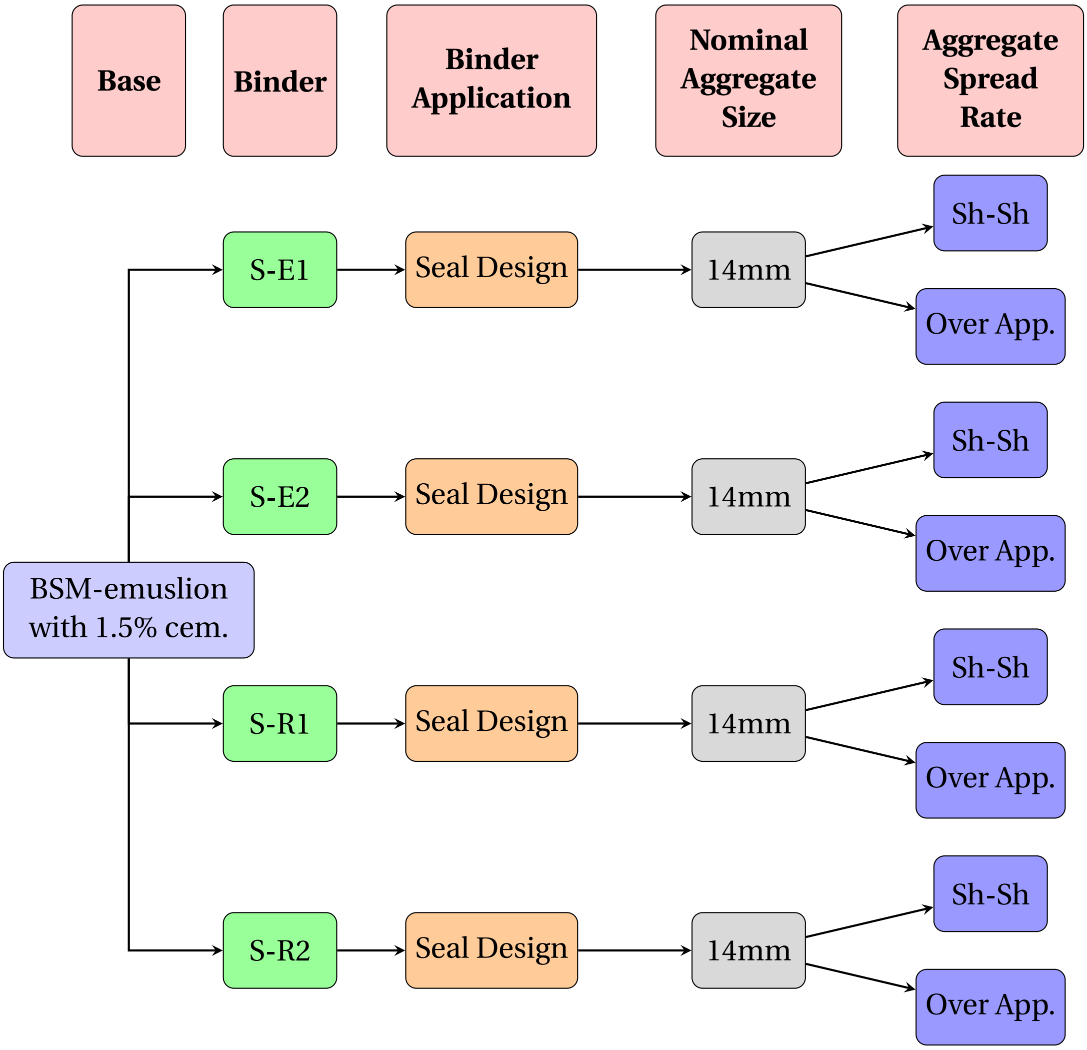

Figure 3.3: Experimental Design Summary

3.6 Summary

To enable a successful experimental design matrix in which aggregate orientation, as a focus point, is based off, it is of importance to evaluate all necessary design and construction considerations. A central construction consideration includes the BSM-emulsion base used to construct the surfacing seals on. The base contributes to the aggregate embedment and aggregate orientation behaviour in surfacing seals. Furthermore, seal and binder type with a focus on binder and aggregate application rate, is also of major importance whilst the trafficking conditions govern the experimental design setup.

Chapter 4

Experimental Test Setup and Process

4.1 Introduction

The test setup and test procedure, as explained in this chapter, required an easy, repeatable and constant methodology. This was especially necessary for the testing and data capturing phases of the test process. The following subsections describe the construction and testing phases of the experimental test process.

4.2 Equipment

The following equipment was used during the test setup and testing process of this research:

- BOMAG Pedestrian Roller 700
- 75 litre and 200 litre concrete mixer
- Model Mobile Load Simulator 3 (MMLS3) and its insulating panels
- Laboratory scale MMLS3 test bed
- Laser Profilometer (LPM)
- Mean texture depth apparatus

The full details of the MMLS3 system are described in Appendix B, Section B.3, but the full calibration and implementation thereof is elaborated on at a later stage in this chapter.

4.3 Test Matrix

Following the experimental design as shown in Section 3.5, a test matrix was set up to describe the pre-investigation, construction, testing and data reworking procedures. The test matrix consists of six phases, in which Phase A includes the pre-investigation and preparation section, Phase B and Phase C include the base and seal construction and Phase D and Phase E include the testing and data capturing methods. This process can be seen in Figure 4.1.

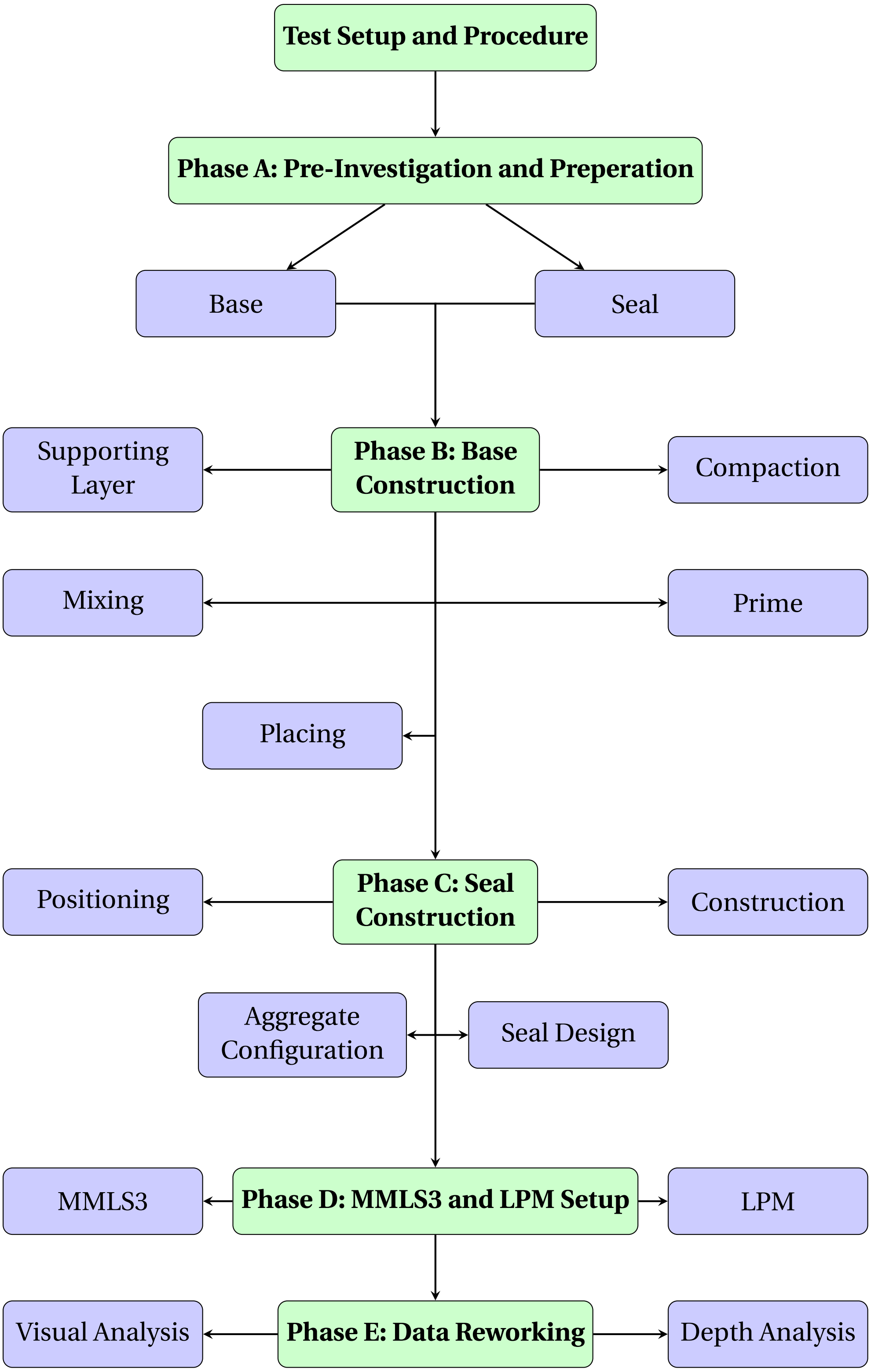

Figure 4.1: Test Matrix

4.4 Phase A: Investigation and Preparation

To ensure adequate base hardness, in terms of the ball penetration test or embedment, it was necessary to implement a pre-construction investigation. Subsequently, Phase A of the experimental test setup is explained in the following sections.

4.4.1 Base

A good quality G2 bitumen stabilised material (with emulsion) was constructed in a preliminary smaller test base. This was a necessary step in the test setup as it was used to evaluate whether the BSM-emulsion mix design was sufficient if based on the hardness of the base.

4.4.1.1 Crushing and Blending

To ensure quality G2 base material, a representative sample from the stockpile was taken and dried out. The G2 material was then quartered and passed through a 20 mm sieve after which all aggregate particles not passing were crushed and blended with the virgin material. Effectively, a G2 material was obtained with all material being < 20 mm. This blend was then used to construct the preliminary base.

4.4.1.2 Material Grading

Before performing a grading analysis on the G2 material, it was necessary to ensure that the material is dry and that no extra moisture, excluding the hydroscopic moisture, was present. A grading analysis, in line with Test Method A1 in the TMH 1 (1986) was done to ensure that the base material adhered to the grading of a G2 BSM base course. The grading is shown in Figure 4.2

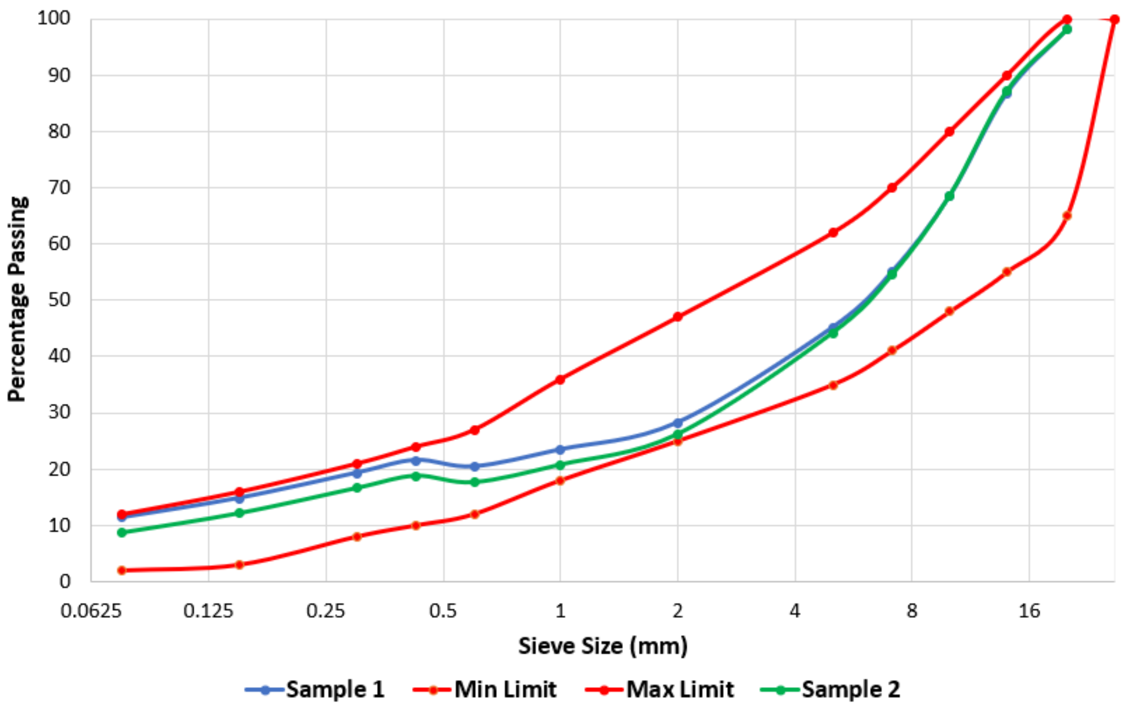

Figure 4.2: Sieve analysis of G2 material

4.4.1.3 Maximum Dry Density and Optimum Moisture Content

A good quality G2 base is largely dependent on the compaction thereof which relates to the moisture content of the material. Subsequently and due to this, the maximum dry density (MDD) and optimum moisture content (OMC) of the material was obtained by making use of Test Method A7 as provided in the TMH 1 (1986).

This method yields the relationship between the maximum density of the material and the moisture content required to achieve the maximum density. It should also be noted that the hydroscopic moisture and the determination thereof is also included in the total moisture content. The following measured results, as seen in Figure 4.3, were obtained from the test with full calculations shown in Appendix A.1.

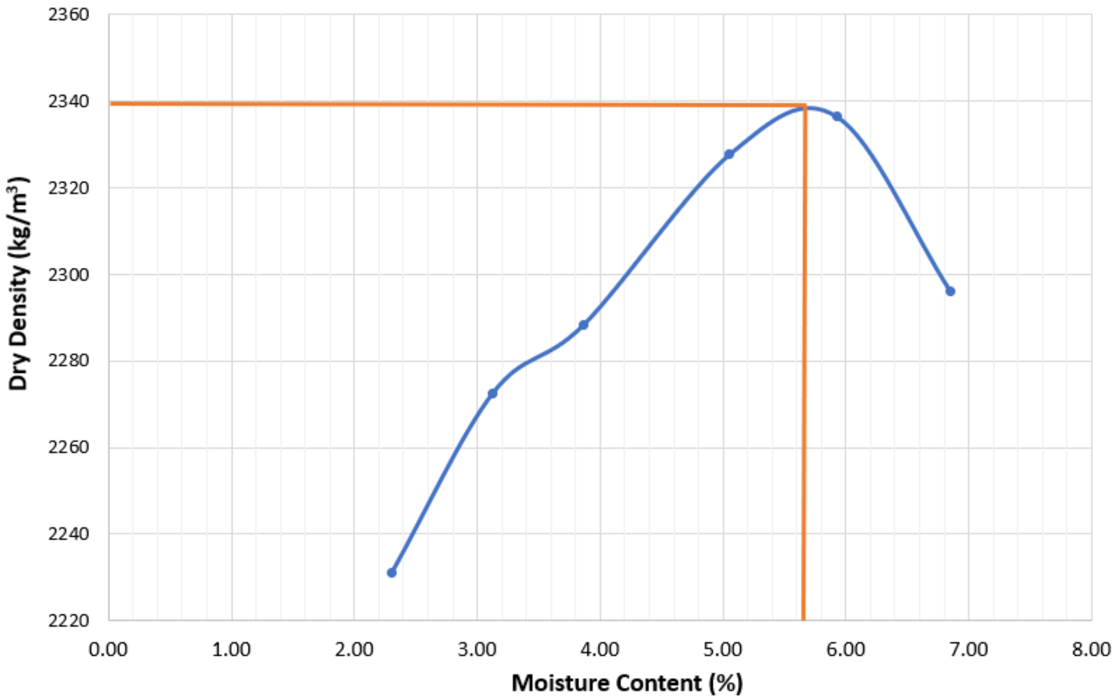

Figure 4.3: Measured Dry Density and Moisture Content

Subsequently, the following values were obtained for the MDD and the OMC:

MDD = 2340 kg/m^3 and,
OMC = 5.7%

4.4.1.4 Test Base Construction

To evaluate the effectiveness of the BSM base, a smaller test base was firstly constructed after which ball penetration tests were completed to determine the embedment potential of aggregates. Due to the embedment characteristics of the base being tested by means of the ball penetration test, failure of the target embedment could conclude that the mix design of the G2 base is insufficient and adjustments are required. Subsequently, when the MMLS3 base is constructed, the mix design is sufficient.

The test base is a 685 mm x 580 mm x 125 mm steel bed as graphically shown in Figure 4.4. To evaluate the embedment, it was only required to at least build up to a height of three times the maximum base aggregate size, being 60 mm.

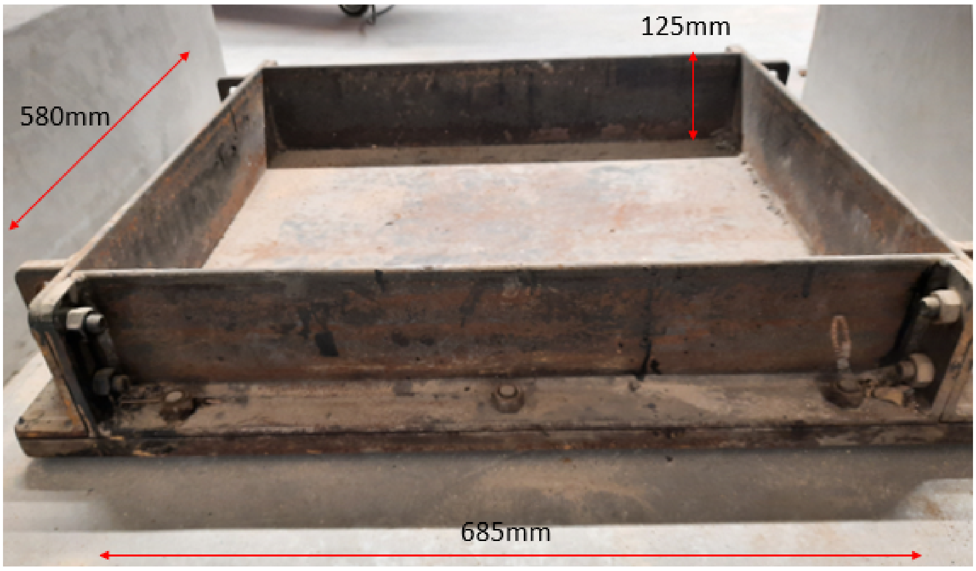

Figure 4.4: Test Base Dimensions

The volume filled with base material together with the total G2 base mass was then calculated as:

$$V = L * B * H = 0.685 * 0.580 * 0.06 = 0.0238\,m^3$$

The following mix design was then implemented for the G2 BSM-emulsion test base:

- Gross emulsion (SS60) content: 3.5%
- Moisture content: 5.85%
- Cement content: 1.5%

A moisture content of 5.85% was calculated as it includes the 5.7% optimum moisture content, whilst an extra 0.15% of water was also added, to delay the breaking of the emulsion, to enable better workability. Subsequently, the construction process was effectively controlled. A cement content of 1.5% was chosen to increase the hardness of the base to withstand the embedment forces of the aggregates under loading. The following masses, as shown in Table 4.1, were calculated for the test base whilst the full calculation can be found in Appendix A.2.

Table 4.1: Test base material mass

G2 Base (kg)	Emulsion (kg)	Cement (kg)	Water (kg)
79.27	2.774	1.189	1.744

All masses were then weighed and a 75 litre concrete mixer was used to produce the BSM-emulsion mixture. Firstly, it was necessary to clean the test base mould from all dust particles to ensure that the fines content of G2 base material is not changed throughout the process. Subsequently, the mixing process commenced by placing the G2 material into the concrete mixer, after which the 1.189 kg cement content was added. The mixer was then switched on and the material was mixed thoroughly to ensure an even distribution of the cement content throughout the G2 material. The 1.744 kg water, which contributes to the moisture mass together with the emulsion and hydroscopic moisture, was then gradually added. The concrete mixer was kept on, ensuring a good distribution of wet G2 material with cement. To ensure that less fines collect at the back of the concrete mixer, the mixer was stopped and the material was manually worked from the back to the front. Thereafter, the 2.774 kg emulsion was slowly added by means of a small container, ensuring a gradual and equal distribution thereof in the mix. A mixing time of 40 seconds to 60 seconds was then implemented as it resulted in a thorough and consistent mixture.

To compact the 60 mm layer effectively, sublayering was decided upon, the first one being 40 mm and the top layer being 20 mm. To complete the compaction process, it was necessary to use the most appropriate machinery for such a small environment, but most importantly, enough compaction energy was required. Subsequently, the vibratory hammer with a circular footing together with a rectangular hammer plate for the corners was used. Thus, by means of this compaction method, the maximum dry density of the test base was achieved at OMC. The final test base can be seen in Figure 4.5.

Figure 4.5: Test base after compaction

4.4.1.5 Test Base Embedment

An important aspect when trying to evaluate the orientation of aggregates in a surfacing seal, is to control or manage the embedment of the aggregate particles into the base layer. For the purpose of this study, it is necessary to limit embedment into the base. Subsequently, the cement content of the BSM-emulsion mix, as explained in Section 4.4.1.4, was 1.5% as it increases the hardness property of the base.

Another valuable aspect when evaluating embedment is to take base temperature into account and thus, ball penetration tests were performed on the test base at the following temperatures: 25°C, 30°C, 35°C and 40°C. To heat the BSM base up to the higher temperature reanges, the usage of infrared lighting was implemented. Three infrared lights were placed at a distance of 750 mm above the base to gradually increase the temperature, whilst assisting with the curing of the base by accelerating the breaking of the emulsion. Figure 4.6 shows the test base under the infrared lighting.

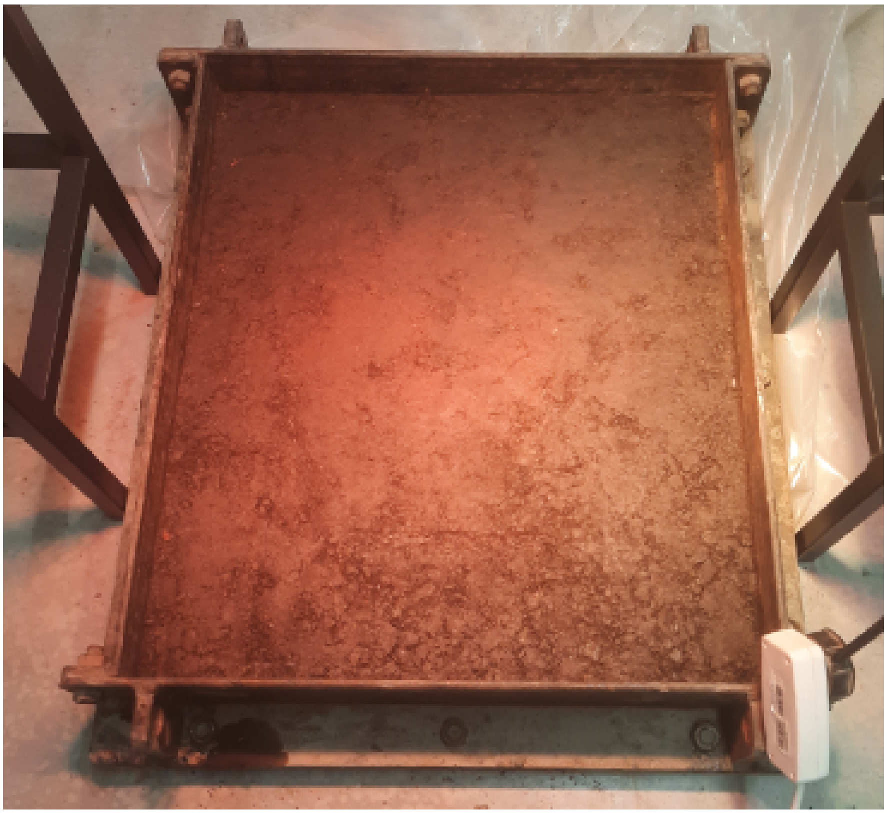

Figure 4.6: Heating up of the test base

The temperature is regulated effectively by means of insulating panels (of 75 mm thickness), which were constructed around the test base. This was of importance as it is not only the surface of the test base that is temperature regulated, but the base layer itself. The temperature of the test base was therefore often checked by means of an infrared thermometer to ensure that it reached the desired temperature and remained at the temperature for at least 24-hours. The heating process and temperature regulation was extended over a longer period of time to allow for sufficient base heating.

To differentiate between the 30°C, 35°C and 40°C temperatures, the number of infrared globes used varied. To obtain the 30°C, a single infrared globe was used over the 24-hour time period whilst three infrared lights were used to heat up the base to reach the 35°C and 40°C temperatures. This ensured a process that would keep the period of heating and temperature regulation constant. The insulating panels around the base together with the implementation of infrared lighting can be seen in Figure 4.7.

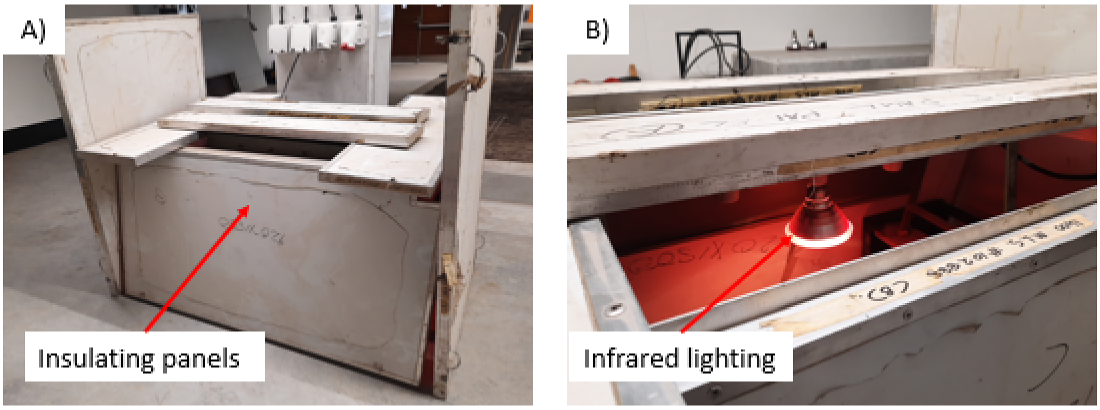

Figure 4.7: a) Shows the insulating panels around the test base and b) shows the infrared lighting used to heat up the base

Random areas on the test base were chosen thereafter to perform ball penetration tests. Firstly, the base was tested at 25°C after which it was heated up and tested at 30°C, 35°C and 40°C. A minimum of 9 ball penetrations was done per temperature test to ensure valid measurements across the whole surface of the base layer. It was necessary to ensure that the tests were done on both the rough and the smooth surfacing areas of the base to obtain representative results. Another important aspect, directly related to the ball penetration test, was to identify and find a factor which correlates the penetration values at 25°C to the rest of the temperature variances. Figure 4.8 shows the position as well as the number of test blows per temperature variance.

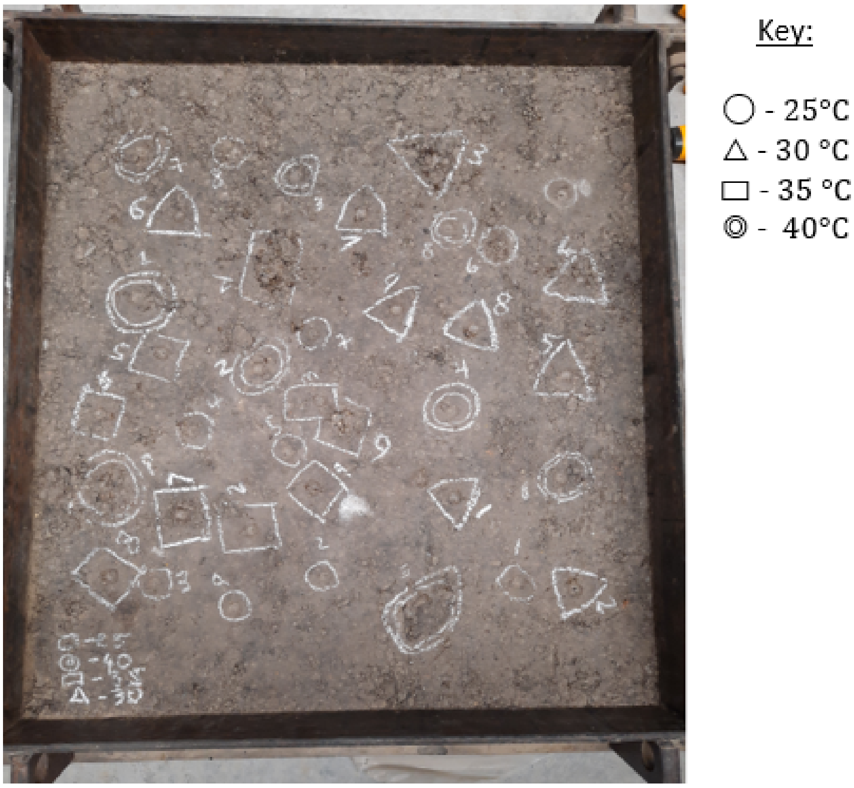

Figure 4.8: Ball penetration tests on the surface of the test base

4.4.2 Seals

4.4.2.1 Seal Moulds

The seal moulds used to construct the different seal types on top of the BSM-emulsion base layer was used in such a manner that the seal is wide enough for the MMLS3 trafficking action to cover the needed area together with a representative LPM measurement to take place. The wheel path of the MMLS3 is effectively 80 mm wide whilst the length of contact, taking into account the hammering action of the area where the wheel begins to make contact with the surface, is 1100 mm. Thus, a 300 mm x 600 mm wooden mould was built with a total surface area of 0.18 m^2.

4.4.2.2 Aggregate Grading

To determine the grading of the crushed metamorphic andesite, Test Method B4, as described by the TMH 1 (1986), was followed. This method describes the sieve analysis of a dried aggregate sample after it has been washed through the 0.075 mm sieve. It was of importance to ensure that the 14 mm nominal aggregate adhered to the 14 mm roadstone grading. The following sieve analysis result, as seen in Figure 4.9, was obtained.

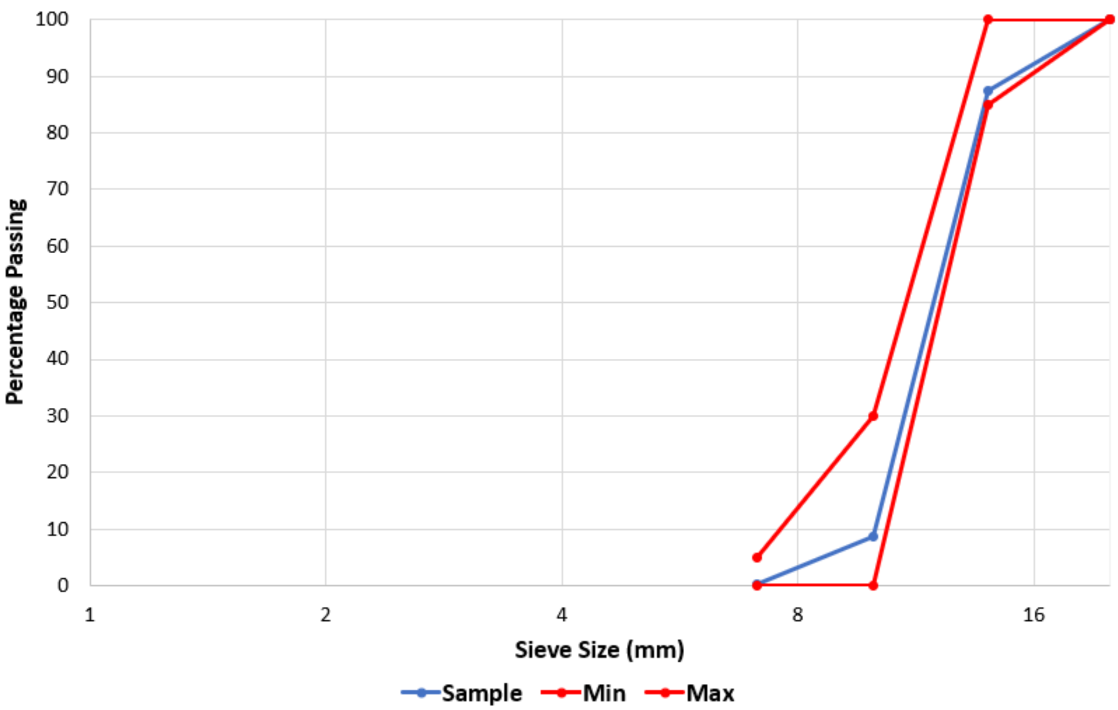

Figure 4.9: Sieve analysis on the seal aggregate

4.4.2.3 Average Least Dimension of Aggregate

The ALD of the seal aggregate was determined as per Test Method B18(a) (1986) in the TMH 1. The method describes the determination of the ALD of aggregate as the ratio between the sum of the smallest dimension of all the aggregate particles to the total number of particles. The full ALD calculation can be found in Appendix A.4.

ALD = 8.6 mm.

4.4.2.4 Flakiness of Aggregate

To determine the flakiness of the seal aggregates, Test Method B3T (1986), as explained in the TMH 1, was used. The method describes the calculation of the Flakiness Index, which is a representative percentage of the mass of aggregate as a percentage of the total aggregate mass, that passes through the slots of pre-specified widths for the specific fractions. The method specifies that the width of the slots are half that of the sieve openings through which the fractions pass through. The full calculation and data used to obtain the Flakiness Index can be found in Appendix A.4.

FI = 16.2%.

4.4.2.5 Aggregate Crushing Value

To obtain the resistance to crushing of aggregates, the Aggregate Crushing Value (ACV), as described by Test Method B1 (1986), was carried out. The full ACV calculations can be found in Appendix A.5.

ACV = 7.68%.

4.5 Phase B: Base Construction

Due to all the necessary information needed, as obtained during Phase A of the test setup, the construction of the BSM-emulsion base layer was undertaken. Two bases were constructed during Phase B of the test setup, each being 5000 mm x 2000 mm x 150 mm in volume.

4.5.1 Supporting Layer

Sufficient compaction of the BSM-emulsion base layer was only possible if an adequately stiff layer was constructed below. Subsequently, a 75 mm sand sub layer was placed to ensure an adequate and stable anvil to tip the BSM-emulsion base material onto whilst, simultaneously, not displacing itself. To compact the sand sublayer, water was sprayed on the surface after which the dry and wetter sections were thoroughly mixed to ensure an even distribution of moisture. A plate compactor was then used to compact the sand layer effectively. To ensure adequate compaction closer to the corners of the MMLS3 test beds, a vibratory hammer was used by setting it to its lowest energy. An indication as to the compaction degree of the sand layer was correlated from the extent of cracks on the sand surface. Subsequently, the sand layer was compacted and wetted until no major cracks were visually seen. The construction process, which includes the pre-compacted sand, the compaction process and the final sand sublayer, can be seen in Figure 4.10.

Figure 4.10: Where a) shows the uncompacted sand layer, b) is the plate compaction process, c) is the compacted sand with rough areas and d) is the final smooth compacted sand sublayer

4.5.2 Mixing

Following Phase A of the construction process, and especially the BSM-emulsion mix design as explained for the test bed in Section 4.4.1.4, the construction of the base commenced. Based on the dimensions of the MMLS3 test bed, the volume filled with BSM-emulsion was calculated as per the following:

$$V = 2 * 5 * 0.15 = 1.5\,\mathrm{m}^3$$

Where:
length = 5 m,
width = 2 m and
depth = 0.15 m.

Thus, as calculated, 1.5 m^3 of BSM-emulsion material was required at an MDD of 2340 $\mathrm{kg/m}^3$. To obtain a good mixed BSM-emulsion material, an industry concrete mixer with a total volume of 170 litre was used. The concrete mixer was used to ensure that a large quantity of BSM-emulsion was produced whilst still ensuring that the mixing process is thorough enough to not influence the performance thereof.

Due to the construction size of the BSM base being so large, whilst considering laboratory limitations, it was necessary to rather mix the base material in batches of 200 kg.

Thus, 18 x 200 kg G2 batches were mixed to obtain a total BSM mass of 3510 kg. According to the mix design, as explained in Section 4.4.1.4, the new contents and quantities for all batch material, including the cement, emulsion and water was calculated and is listed in Appendix A.3. From the calculations, the following masses, as presented in Table 4.2, were mixed per batch in the concrete mixer:

Table 4.2: Base material masses per 200kg batch

G2 Base (kg)	Emulsion (kg)	Cement (kg)	Water (kg)
200	7	3	4.275

The mixing process involved the addition of the 200 kg of G2 material into the concrete mixer after which a thorough mix was done by running the concrete mixer. The 3 kg of cement was then added and the concrete mixer was again turned on to allow for a thorough mix of the G2 material and cement. The concrete mixer generally mixed the finer material to the back when tilted and thus, it was necessary to move the fines to the middle and front of the mixer by hand when the machine was off. After the cement and the G2 was mixed sufficiently, 2 kg of the 4.275 kg total water mass was added to the mixture to ensure that the water was slightly mixed throughout before the emulsion was added. This was done due to the concrete mixer not mixing the water thoroughly through the material when all 4.275 kg was added and as a result, more clumped BSM-emulsion material formed. Thus, through trial and error, the addition of 2 kg of water before adding the emulsion proved successful. The emulsion was then added in 1 litre batches whilst keeping the concrete mixer on. The batch was mixed for a time period stretching between 40 seconds and 60 seconds, constantly increasing the tipping action of the mixer to ensure more material is mixed thoroughly whilst eliminating the chances of material getting collected in the back of the mixer. To ensure sufficient mixing of the BSM-emulsion batch, a constant quality check was done which involved the regular checking of clumped material which relates to the thorough mixing of the water, emulsion and G2 material. The mixing process can be seen in Figure 4.11.

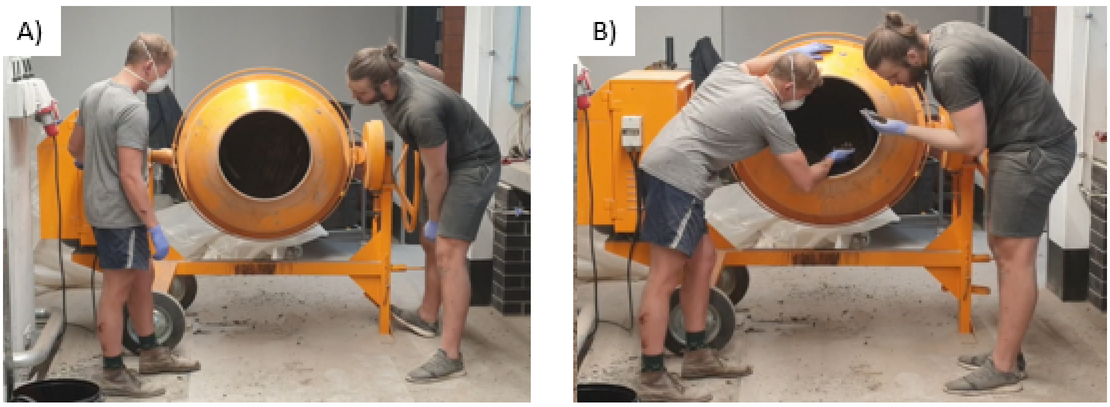

Figure 4.11: Where a) shows the mixing of the BSM-emulsion batch and b) shows the process of checking for clumped material

4.5.3 Placing

To move the mixed BSM-emulsion material in batches of 200 kg each to the MMLS3 test bed, wheelbarrows were used together with small steel ramps which provided ease of placement of the material into the test bed. Thus, the material was tilted into the wheelbarrow immediately after the mixing thereof, after which it was pushed onto the ramp and tilted into the MMLS3 test bed. To keep track of the amount of batches to be put in at a certain section in the test bed, it was decided to split the bed into three sections along the 5 m length thereof. Thus, when tipping the BSM-emulsion material into the test bed, 200 kg was added to each section before continuing to the next layer. Subsequently, 600 kg was tipped into the test bed to form a single filled layer. The ramp setup, together with a single tipped BSM-emulsion batch mixture can be seen in Figure 4.12.

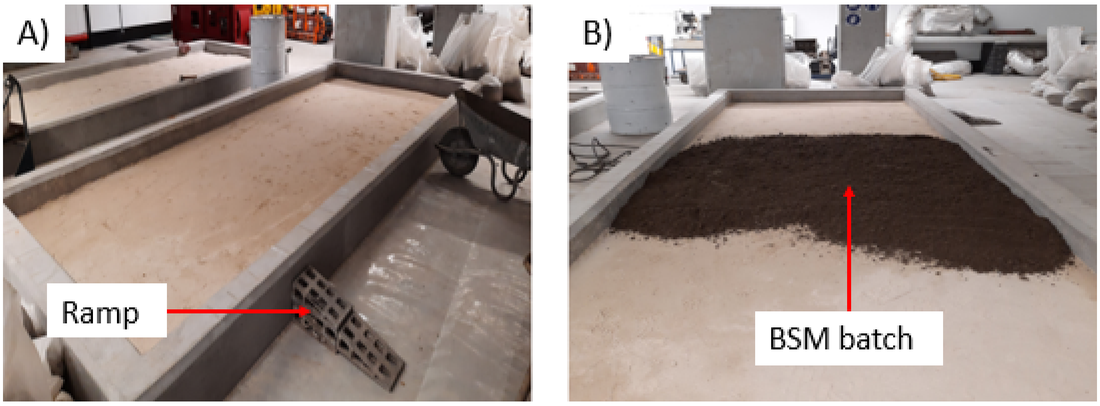

Figure 4.12: Where a) is the ramp and sand sublayer and b) is a single tipped BSM-emulsion batch

A shovel and a rake was used to manually move and spread the material to ensure an even distribution in the test bed. Due to the slight increase in water content that was initially added to the BMS-emulsion mix, more time was available to place the material without a high risk of the emulsion breaking. The manual working of the material can be seen in Figure 4.13.

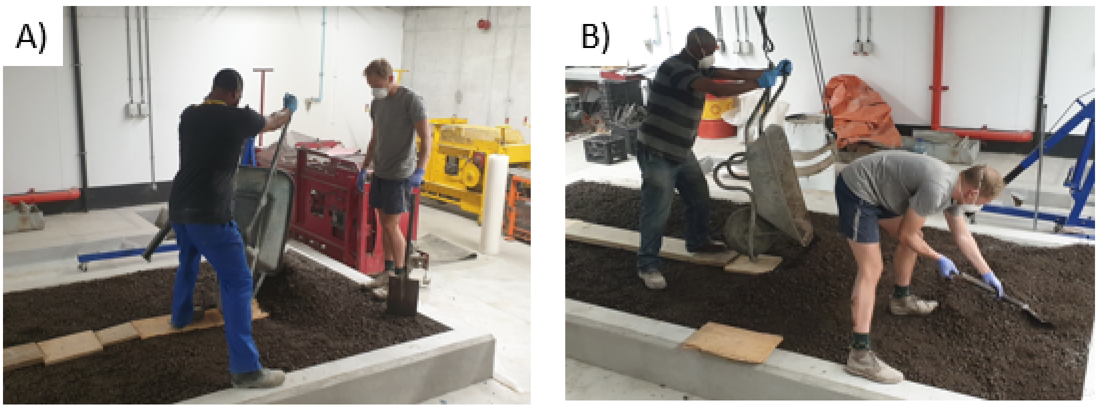

Figure 4.13: Where a) shows the tipping of the material and b) shows the spreading of the material

4.5.4 Compaction

For adequate compaction of the BSM-emulsion layer, it was necessary to compact the 150 mm layer in two sub layers. The first compaction cycle was performed on 2000 kg of material after which the next compaction cycle followed after the 3510 kg of material was added. A BOMAG pedestrian roller was mainly used as a compaction roller together with a vibratory hammer for the corners of the test bed. It was important to roughen the first compacted sublayer as to ensure better compaction and bonding when putting down the second sublayer.

To ensure a smooth base level, all large aggregate particles were raked off. This was also done to avoid the accumulation of large particles at the top of the base layer that could affect aggregate embedment and orientation behaviour. The vibratory hammer was mainly used to compact the edges and corners of the test bed whilst the roller was used to compact the larger areas. The compaction sequence of the roller involved the parallel movement of the roller to the long edge of test bed in an up and down sequence whilst moving side to side. The number of roller passes per section was kept constant over the width of the test bed in an attempt to obtain uniform compaction throughout. The compaction process and compaction sequence can be seen in Figure 4.14.

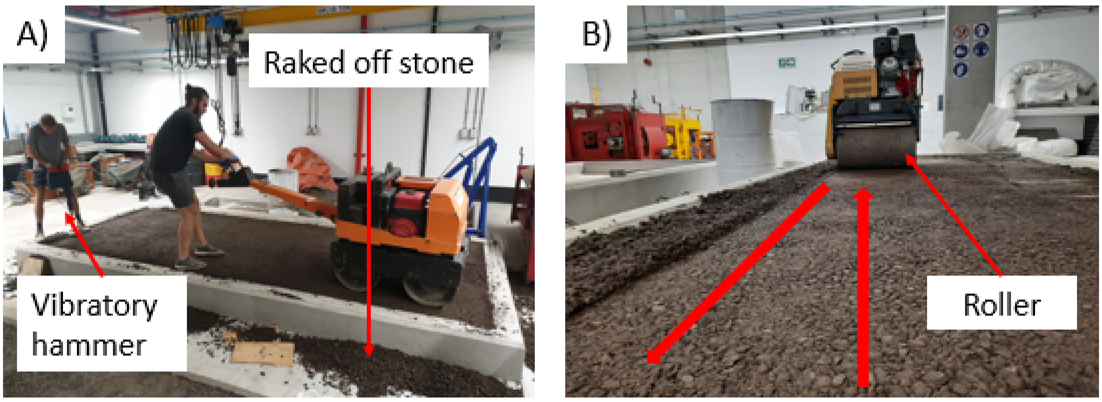

Figure 4.14: Where a) displays the compaction equipment and b) shows the compaction sequence

After the compaction process was completed, the base cured to reach the required hardness. For the emulsion to break completely, a minimum period of 4 weeks was allowed at ambient temperature without additional heating. According to the SABITA Manual 40 (2021), the OMC of the base material is to be reduced to 50% before any seal work commences. Thus, the time period allowed is more than sufficient. One way to also determine whether or not the base material reached an OMC of 50% is to perform ball penetration tests in certain intervals, such as days, and when the values remain similar, it can be stated that the base had attained its required strength and stiffness and seal construction could commence.

4.5.5 Priming

Priming new BSM bases prior to seal construction is also also standard practice. Preparing the base for a prime layer included a sufficient drying out period to prevent excess moisture entrapment which may lead to undesired moisture build up under the newly constructed seals and premature pavement distress. Together with the curing time, the base was also broomed to remove all loose material on the surface. The desired application rate for priming, with a Quick Drying Prime (QDP), according to the manufacturers, was 0.7 l/m^2. Subsequently, the base was divided into 1 m^2 blocks after which 700 ml of primer was sprayed and spread as seen in Figure 4.15. Before commencing with seal construction, the primer was left for at least four days to dry and set.

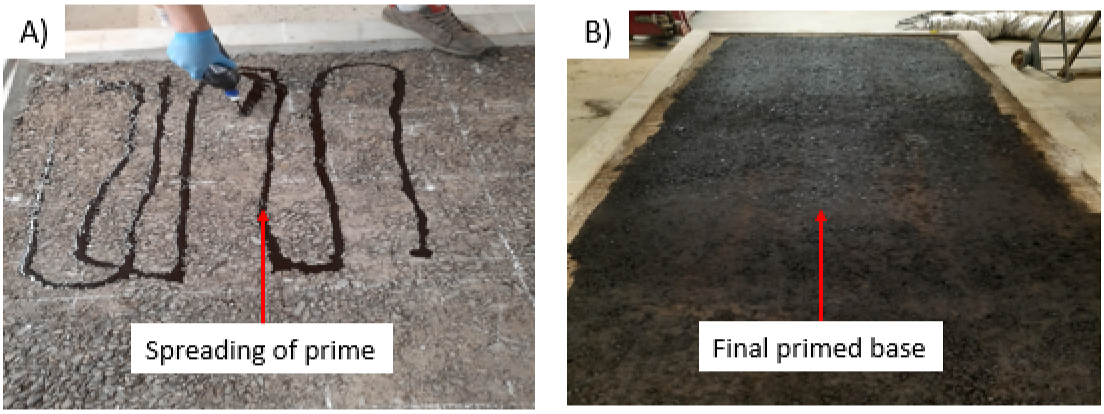

Figure 4.15: Where a) shows the spreading of the prime and b) the final primed surface

4.6 Phase C: Seal Construction

4.6.1 Process

In-practice seal construction is a process that is easily repeatable without the constraints as experienced in a laboratory environment. Therefore, to ensure quality construction of the S-E1, S-E2, S-R1 and S-R2 seals, a defined procedure, as shown in Figure 4.16, was followed. The seal construction process included the following main aspects:

- Seal positioning taking the MMLS3 position and physical size limitations into account.
- Aggregate configuration determination.
- Seal design procedure according to the SABITA Manual 40 (2021) and Van Zyl (2021).
- Sample preparation according to the SABITA Manual 40 (2021) and SABITA TG 1 (2019).
- Binder application methodology.
- Seal aggregate application methodology.
- Initial construction compaction.

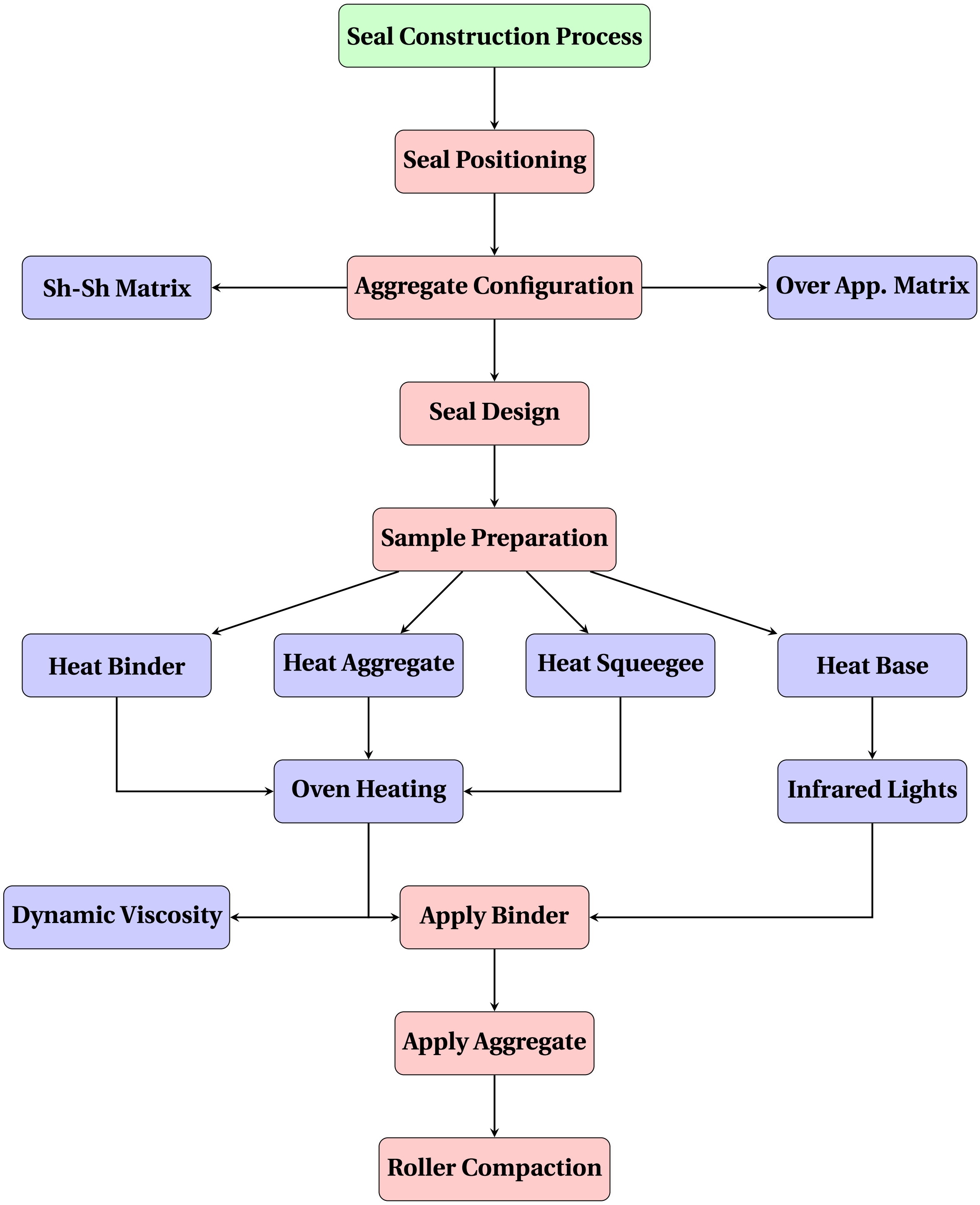

Figure 4.16: Overview of the seal construction process

4.6.2 Positioning

As described in Section 3.5, the experimental design overview described the different binders as well as the nominal aggregate size and the spread rate thereof. The planning of the seal positions and the layout thereof on the test bed was of importance because prior to deciding on the exact positioning of the seals and the practicality of the MMLS3 positioning and insulating panel placement, it was necessary to identify the most consistent sections on the BSM-emulsion base layer's surface. Therefore, the following seal test bed layout was proposed as seen in Figure 4.17.

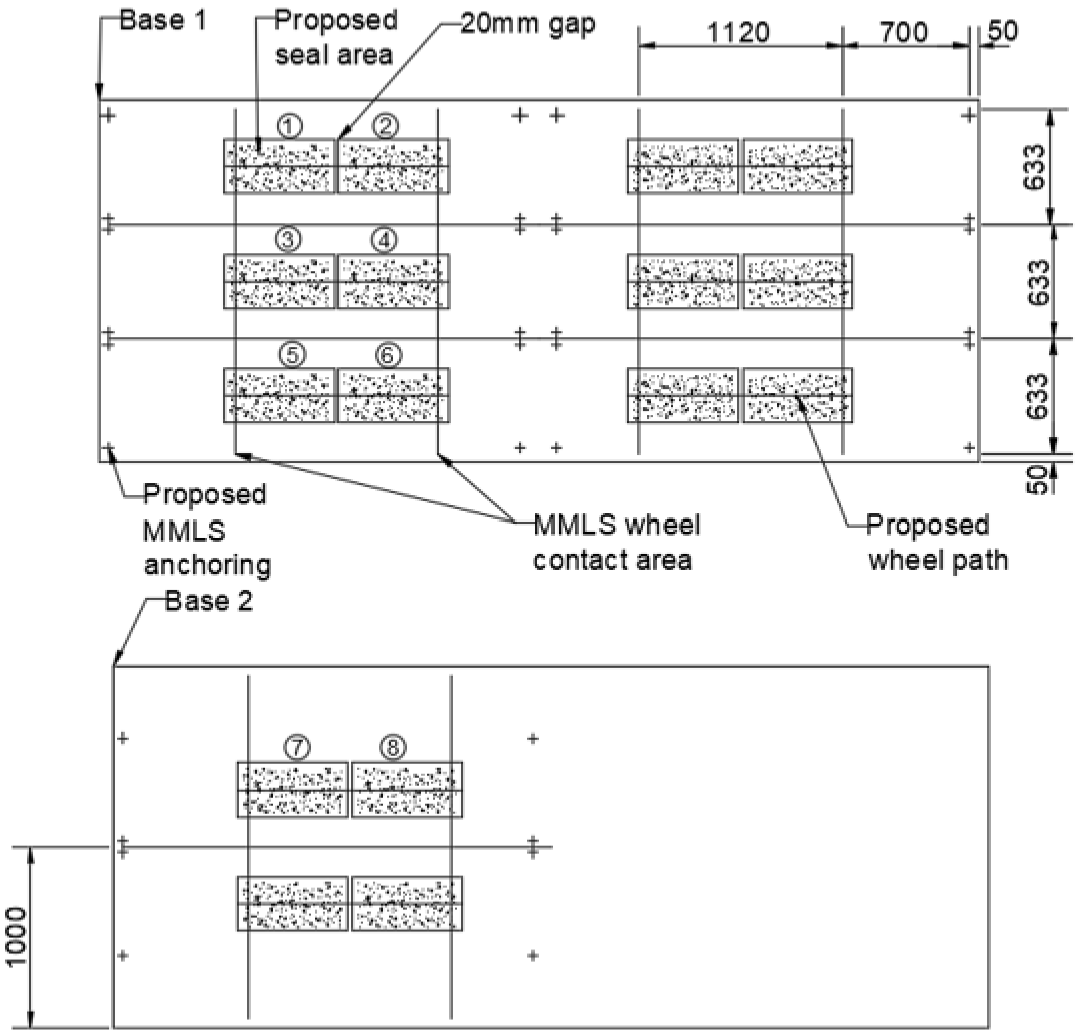

Figure 4.17: MMLS Schematic Plan

Together, with the schematic as presented by Figure 4.17, the proposed area of the MMLS3 placement, together with the positioning of the seal tiles, can be seen in Figure 4.18. The MMLS3 wheel path runs over two seal tiles simultaneously. To identify the seal tiles, a 20 mm gap was proposed as seen in Figure 4.17.

The positioning of the seal tiles, as such, was done to ensure efficient movement of the apparatus, such as the MMLS3 and the LPM, during testing. Two MMLS3 test beds were constructed, as shown in Figure 4.17, but only the seal positions numbered 1 - 8 were used in this study. The placement of the MMLS3 machine was also done in such a way that the footing positions were still a distance away from the edge of the MMLS3 test bed as to allow for better stability and pulling- and vibratory resistance.

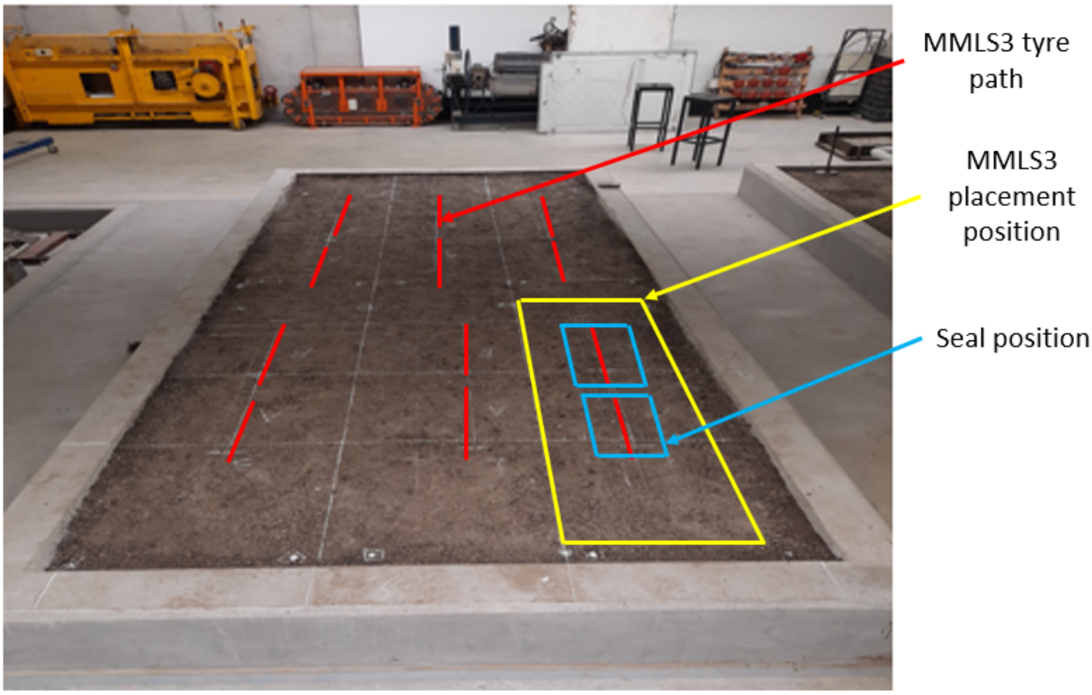

Figure 4.18: MMLS Testing Layout Plan

The following, as presented in Table 4.3, was the proposed positioning of the different seal types in correspondence with Figure 4.17.

Table 4.3: Seal positioning and properties

Seal Position	Binder Type	Aggregate Spread Rate
1	S-R2	Sh-Sh
2	S-R2	Over App.
3	S-R1	Sh-Sh
4	S-R1	Over App.
5	S-E1	Sh-Sh
6	S-E1	Over App.
7	S-E2	Sh-Sh
8	S-E2	Over App.

4.6.3 Aggregate Configuration

To determine how much aggregate is required per seal area (600 mm x 300 mm), the stones were individually placed onto their respective ALD in the wooden mould as seen in Figure 4.19. The mass of the aggregate placed was then measured and recorded as a sh-sh aggregate matrix. To determine the mass of aggregate required to construct an over application matrix, the aggregate quantity was increased and at 12%, no more stone could be added in the mould without disturbing the rest of the aggregate. Subsequently, Table 4.4 shows the aggregate masses required for each matrix.

Figure 4.19: Placing of aggregate onto ALD in the mould to determine the aggregate matrices

Table 4.4: Shoulder-to-Shoulder and Over Application aggregate masses per seal tile

Sh-Sh Aggregate Mass (g)	Over App. Aggregate Mass (g)
2170	(+12%) 2430

Subsequently, an aggregate mass of 2170 g was used for a sh-sh configuration whilst a 12% increase in the mass (total of 2430 g) was used for an over application aggregate spread rate. Due to the implementation of polymer hot modified binders, a pre-coating layer was required as per the TRH 1 (2019). Bitukote was chosen as the bitumen-based pre-coat at the following aggregate, water and pre-coat masses (as suggested by the manufacturers) as presented in Table 4.5.

Table 4.5: Pre-coating ratios by mass

Stone mass (g)	Water mass (g)	Bitukote (g)
1000	5	8.9

To ensure the pre-coating is mixed thoroughly, a bottle was used to simulate the mixing process as in a pre-coating plant. Firstly, the stone mass was measured and put in the bottle after which the water was added. The mixture was then shaken in a circular motion for at least 1-minute to ensure the stones were all wetted. The Bitukote was then added and the bottle was again shaken in a circular motion for at least 2 minutes. All aggregates were then dried by spreading them out for a time period of a week. The final pre-coated aggregate and the drying process can be seen in Figure 4.20.

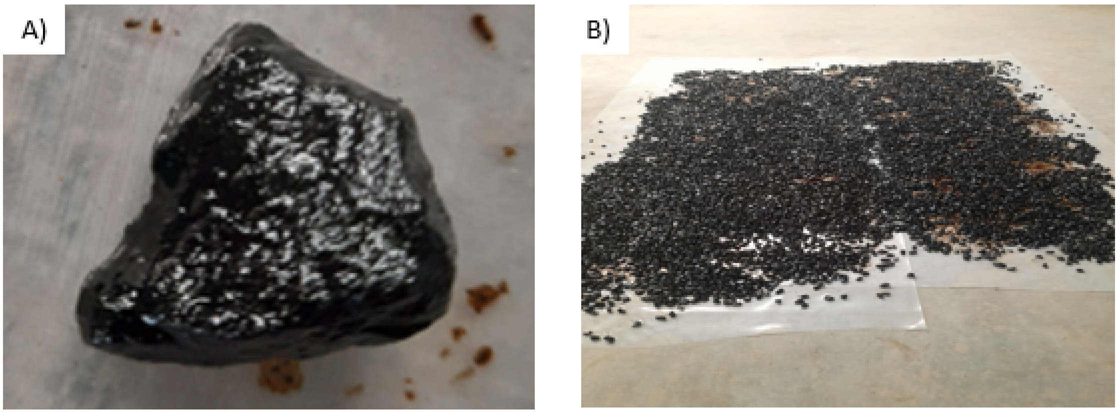

Figure 4.20: Where a) shows the pre-coated aggregate particle and b) the drying of the pre-coated aggregates

4.6.4 Seal Design

To obtain the correct binder application rates, the seal design methodology, as documented in the SABITA Manual 40 (2021), together with the input from Van Zyl (2021), was implemented. Together with the positioning of each seal, as shown in Figure 4.17, the following input parameters were obtained as listed in Table 4.6.

Table 4.6: Input parameters for seal design according to the SABITA Manual 40 (2021)

INPUT PARAMETERS FOR SEAL DESIGN					
SEAL	**CBP (mm)**	**ELV**	**ALD (mm)**	**Macro-texture required (mm)**	**10% FACT**
S-E1	2.17	3000	8.6	1	210
S-E2	2.43	3000	8.6	1	210
S-R1	2.17	3000	8.6	1	210
S-R2	2.17	3000	8.6	1	210

To obtain the CBP (Corrected ball penetration) values, a total of 25 ball penetration tests were done, in accordance to the method as explained in Appendix B.1, on the two BSM-emulsion bases. The ball penetration tests on the base of the S-E1, S-R1 and S-R2 seals, were recorded as the representative average of the BP1 values as shown in Appendix C, Table C.1. The average of the BP1 was used due to the surface showing very little displacement or crushing whilst a half moon indent was obtained. For the base on which the S-E2 seals were constructed, the ball penetration value was obtained by taking the average of the BP1 and BP2 readings as various half-moon, displacement and crushing surface effects were visible. These values can be found in Appendix C, Table C.2.

The equivalent light vehicle input parameter was chosen as 3000 vehicles as this was a representative trafficking volume for surfacing seals to carry. This decision was based on the recommendation from Van Zyl (2021). The ALD and the 10% FACT used, corresponded to the results obtained in Section 4.4.2.3 and as provided from the quarry. Van Zyl (2021) recommended the required macro-texture as 1 mm together with the support of the SABITA Manual 40 (2021) documentation.

Following the seal design procedure, as listed in Table C.3 in Appendix C, it can be seen that both the maximum and minimum binder application rate for a NCCB (net cold conventional binder) was calculated. Input from Van Zyl (2021) with regards to the seal design, resulted in the recommendation that all adjustments be made from the $NCCB_{min}$ value. As seen, the minimum NCCB values were all the same for the design of the S-E1, S-R1 and S-R2 as they were all constructed on the same base and subsequently, they all have the same input parameters. The S-E2 seals were constructed on the second base, and thus, the ball penetration value as input parameter, was the only difference. As a result of the different ball penetration values, a slightly lower $NCCB_{min}$ value was obtained. From the $NCCB_{min}$ values, the adjustments, with input from Van Zyl (2021) and as listed by the SABITA Manual 40 (2021), were introduced. These adjustments included the existing macro-texture, contractor's tolerance, heavy vehicle speed and channelisation.

Following the adjustments made, the conversion from NCCB to hot modified and from cold to hot spray was implemented based on the conversion factors as listed in the SABITA Manual 40 (2021) and as shown in Table C.3 in Appendix C.2. A summary of the application rates for each binder type can be seen in Table 4.7.

Table 4.7: Summary of hot spray application rates

HOT SPRAY APPLICATION RATES				
INFORMATION	**S-E1**	**S-E2**	**S-R1**	**S-R2**
Application Rate (l/m^2)	1.56	1.70	2.14	2.02
Mass Required (g) as per 600mm x 300mm mould	281	306	385	364

4.6.5 Construction

After the determination of the binder and aggregate application, the construction of the seals commenced. As seen in Figure 4.16, the sample preparation, binder application, aggregate application and compaction process formed part of the construction phase. Subsequently, the following method was used to prepare the seal samples, after which the construction thereof followed:

1. Before any seal construction commenced, the base area, on which the seal tiles were constructed, was swept to remove any loose material after which it was heated up by means of infrared lights and constantly monitored, by means of infrared laser guns, to ensure sufficient heating over the 600 mm x 300 mm mould area. The temperature was not allowed to exceed 45°C as it would start reaching the softening point of the prime.

2. To ensure sufficient viscosity to apply the binders, it was necessary to heat the binders in the oven to the specified temperature, as indicated by the manufacturers with support from the SABITA TG 1 (2019) and SABITA Manual 40 (2021). Table 4.8 presents the oven temperatures necessary to heat the different binders before application. As stated in Method MB-2 in the SABITA TG 1 (2019), the

binders were not left in the oven for more than 3 hours due to a risk of binder properties changing.

Table 4.8: Binder heating temperatures before application

	OVEN TEMPERATURES			
	S-E1	**S-E2**	**S-R1**	**S-R2**
Temperature (± 5°C)	180°C	180°C	200°C	185°C

To ensure conformed dynamic viscosity values, both Method MB-13 and Method MB-18, as specified in the SABITA TG 1 (2019) was performed. The results can be seen in Table C.4 in Appendix C.3.

3. As the binder temperature increased (up to the point where the viscosity was low enough), the pre-determined mass of binder was measured off by removing the 1-litre binder sample from the oven, thoroughly mixing it by means of a rod, pouring out the required mass and placing the poured out sample back into the oven to continue with the heating process. Infrared laser guns were also used to constantly record the temperature of the binder in the 1-litre sample container. This process was done for both the sh-sh and over application aggregate configurations. Subsequently, two exact binder masses (for each S-E1, S-E2, S-R1 and S-R2 binders) were measured off.

4. Together with the heating of the binders to reach optimum spray temperatures, the aggregate particles were also weighed off (for both the sh-sh and over application matrices) and heated in an oven to 40°C. This was done as to ensure the binders do not rapidly cool down, leading to adhesion problems between the binder and seal aggregate.

5. A squeegee was also heated up to binder temperature (lowering adhesion risks) and used to spread the binder directly after application thereof.

6. The seal construction commenced when the binder, aggregate, base and squeegee reached their specified temperatures. Firstly, the binder was removed from the oven, mixed and poured from side-to-side, along the length of the mould. The squeegee was then immediately used to spread the binder over the whole of the 600 mm x 300 mm mould area. Directly after spreading the binder, the aggregate was applied by dropping the particles from hand onto the binder. Subsequently, the aggregate configuration was random and no particles were placed individually by hand. When an over application of aggregate resulted in a specific area, some aggregate particles were picked up and moved to another area as to obtain either a sh-sh aggregate matrix or an over application matrix.

7. Directly after the aggregate was applied, the mould was removed and a rolling plate was used to compact the seal. A total number of 20 passes was completed, each pass consisting of three rolls over the length of the seal.

Figure 4.21 schematically shows the process followed to construct a seal.

Figure 4.21: Seal construction sequence

This process was then followed up until a sh-sh and over application aggregate matrix was constructed for each binder type.

4.7 Phase D: MMLS3 and LPM Testing

4.7.1 Overview

The following testing process, as illustrated in Figure 4.22, was followed for 10°C, 20°C and 30°C .

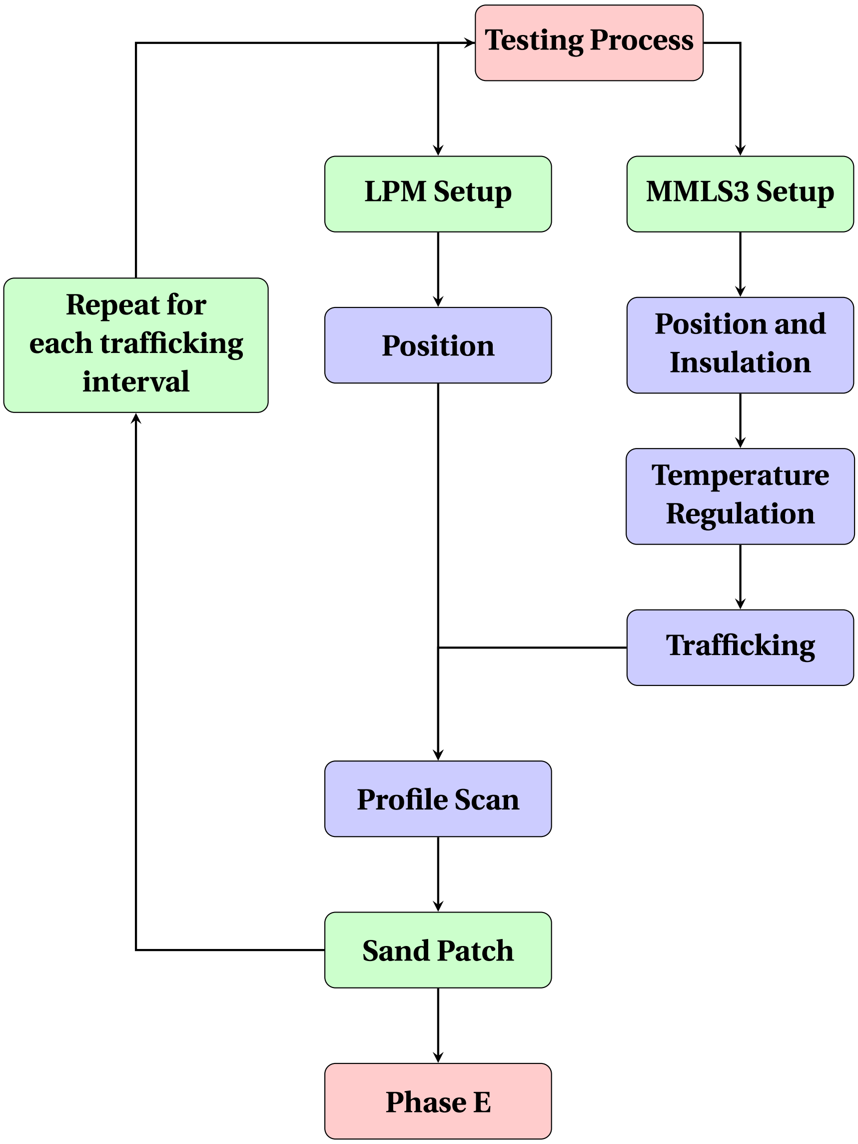

Figure 4.22: Testing overview per temperature

4.7.2 Laser Profilometer (LPM) Setup

The Laser Profilometer, as shown in Figure 4.23 a), consists of the following:

- Four framework stands.

- Framework with rails in both the x-and y-direction.
- Levelling bubble.
- Transportation handles.
- Laser and control unit ports as connected from the controlling device.
- Laser measuring unit in the z-direction.
- Control unit box.
- Controlling device with XYScanner software.

As seen in Figure 4.23 b), the LPM device is used to scan a surface with a pre-determined surface area after which the z-coordinates, corresponding to each of the x-and y-coordinates are plotted to produce a 3-D surface plot. The device is used in a laboratory environment but can also be utilised in-field by means of the battery-operated control unit. Furthermore, the scanning time is dependent on the scan area and therefore, careful consideration is given to obtain a sufficient scan matrix whilst taking testing time into consideration.

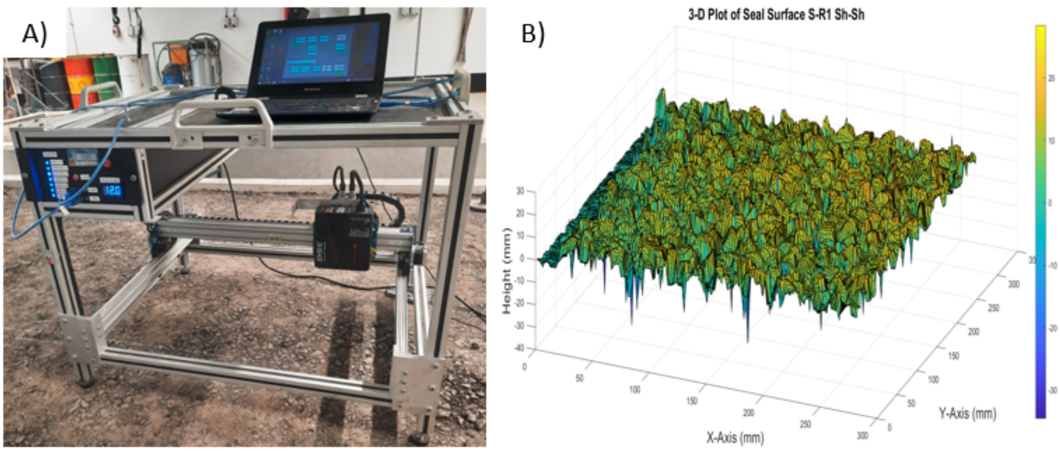

Figure 4.23: Laser Profilometer where a) shows the LPM device and b) a 3-D output of the scanned surface

To obtain a three-dimensional profile of the seal surface and to evaluate aggregate orientation by means of calculating the mean profile depth, the LPM system was implemented. The implementation was done after predetermined MMLS3 load applications, as explained in Section 3.4.7. A reference scan was obtained by making use of the LPM system before MMLS3 trafficking was done, after which scans were taken after the following load applications: 100, 500, 2000 and 5000.

The incremental steps and step counts, of the LPM laser, were set beforehand. Subsequently, the y-step was set to measure in increments of 1 mm for a total number of 300 steps whilst the increment for the x-step was set to measure every 2 mm for a total of 140 steps. The incremental setup can be seen in Figure 4.24.

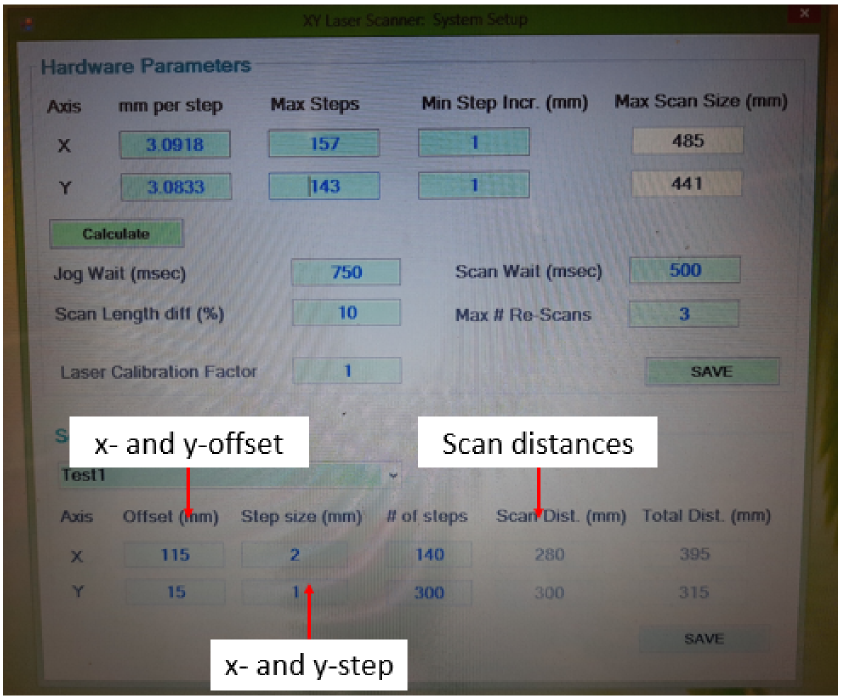

Figure 4.24: LPM step setup

Following the setup of the incremental x- and y-axis measurements, the laser was connected and the scan process commenced. The *Home* button moves the laser back to its origin after which the *Jog Scan Area* commands the laser to run on the outer border of pre-set distances in the x- and y-direction. After enabling the *Jog Scan Area* command, the laser returned to its starting position which is the position set from *Home* by means of an x- and y-offset.

Due to the layout of the seal tiles, the laser is positioned with an x- and y-offset of 115 mm and 15 mm respectively. Furthermore, the *Do Scan* button commands the laser to start the scanning process, starting in the y-direction (recording a z-coordinate every 1 mm) after which the laser moves in the x-direction (2 mm) and repeating the scan in the y-direction again. This start-up process of the laser can be seen in Figure 4.25

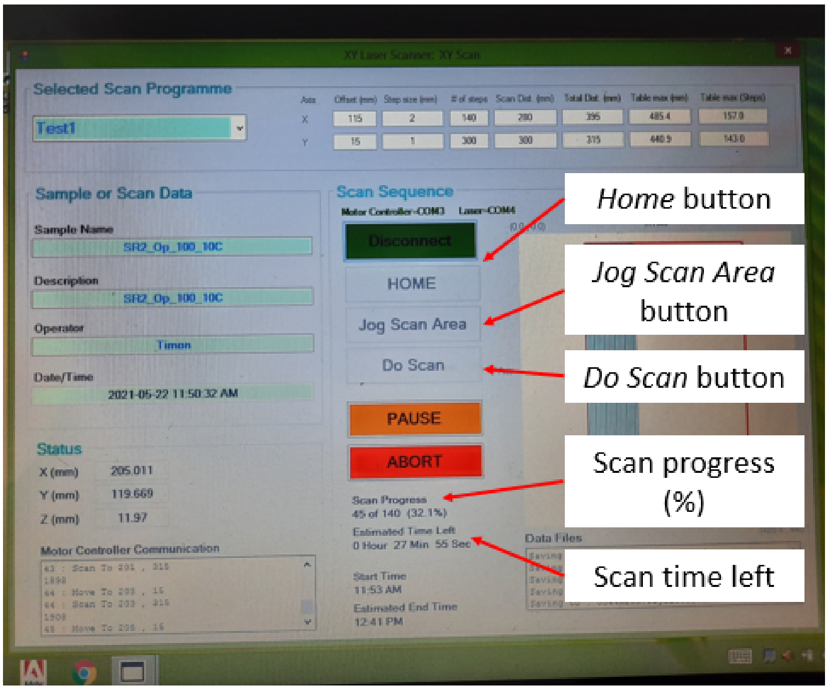

Figure 4.25: LPM start-up

To constantly scan the same seal surface area after each trafficking period, it was necessary to obtain reference points for both the laser and the footings of the LPM device. Subsequently, three reference points were identified including a single start point for the laser and two footing reference points. To ensure the laser is consistently placed in the same position for interval scanning, wooden footing moulds were made (for two of the four stands) and attached to the surface. Thus, the LPM was always in the same position whilst scanning the same area. These three reference point can be seen in Figure 4.26.

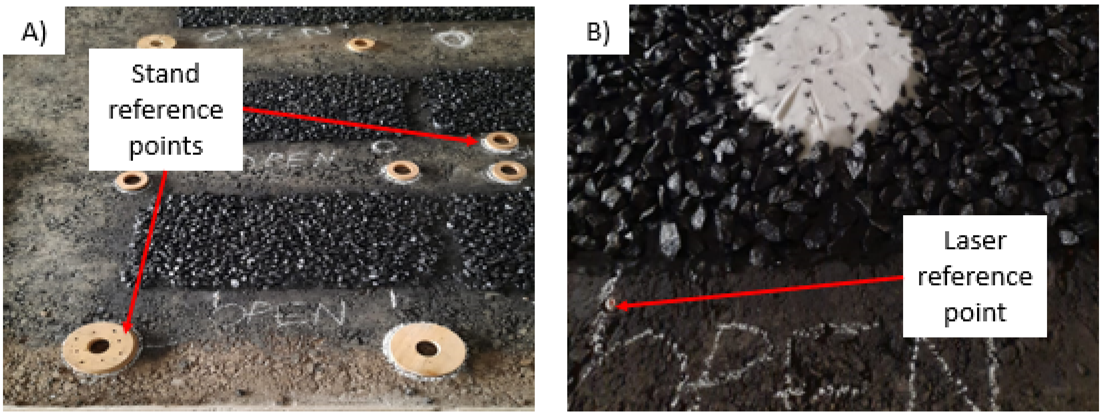

Figure 4.26: LPM placement where a) shows the footing references and b) the laser reference

4.7.3 MMLS3 Setup

The MMLS3 system was calibrated according to the Experimental Design as elaborated on in Section 3.4.7. All 4 tyre pressures were set to a pressure of 750 kPa and the wheel load, for each bogie system, was set to 2.7 kN as explained per the MLS Test Systems

(2016) and Appendix B.3. Both the spring mechanism and the calibration unit can be seen in Figure 4.27. The calibration process was completed each time the MMLS3 system was placed on the test bed.

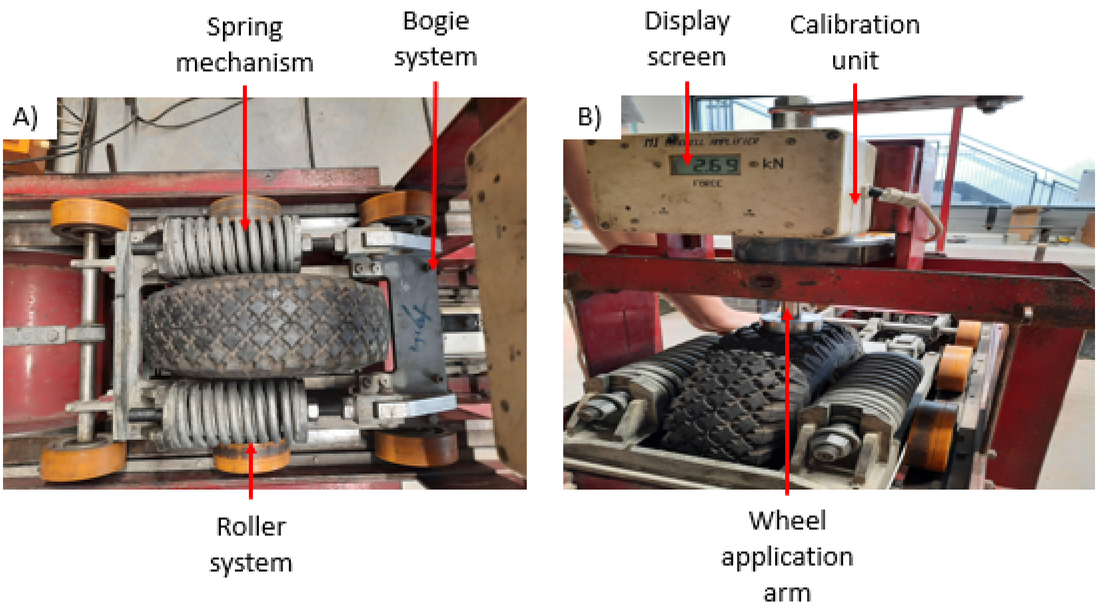

Figure 4.27: MMLS3 load setup

For free flow trafficking conditions, a speed of 7200 load applications per hour was selected (at a frequency of 48 Hz) and used. Based on the trafficking speed, the following run times were obtained for the load cycles, as identified in Section 3.4.7, Table 3.1. All MMLS3 trafficking was done at the trafficking temperatures 10°C, 20°C and 30°C as elaborated on in Section 3.4.8.

4.7.4 Testing Process

The testing process, as illustrated in Figure 4.22, which includes the MMLS3 trafficking, LPM scanning and the sand patch test, is described below:

1. Before any trafficking occurred, it was necessary to obtain a base reading of the seal tiles. Subsequently, the LPM system was placed over each seal tile individually and scans were completed. After the seal tiles were scanned, sand patch tests (mean texture depth readings) were performed.

2. Thereafter, MMLS3 trafficking commenced at 10°C, as the binder was still expected to be stiff and less orientation was expected to occur when compared to the 20°C or 30°C trafficking temperatures. The MMLS3 system was placed over two seal tiles (in length) simultaneously, together with the insulating box around it. To cool the air and the seal surfacings, an external cooling unit was attached to the insulating box and air was circulated throughout. The panels and cooling unit can be seen in Figure 4.28 A) - D). An infrared thermometer, with a temperature range between -30°C and 260°C, was used to monitor the temperature of the seal tiles, and when the surface reached 10°C (± 1.5°C) as shown per temperature regulation in Appendix C.4, the MMLS3 was started and 100 load repetitions was

applied. Generally, the seals took 1 hour to reach 10°C or 30°C. When trafficking at 20°C, the heating, ventilation and air conditioning (HVAC) system in the laboratory was used to keep the room temperature constant. This system was only used to regulate the temperature at 20°C as both the 10°C and 30°C was out-of-range for the HVAC to regulate. To allow trafficking at 30°C, the heating unit was used together with the insulating panels. Both the 20°C and the 30°C test setups can be seen in Figure 4.28 E) and F).

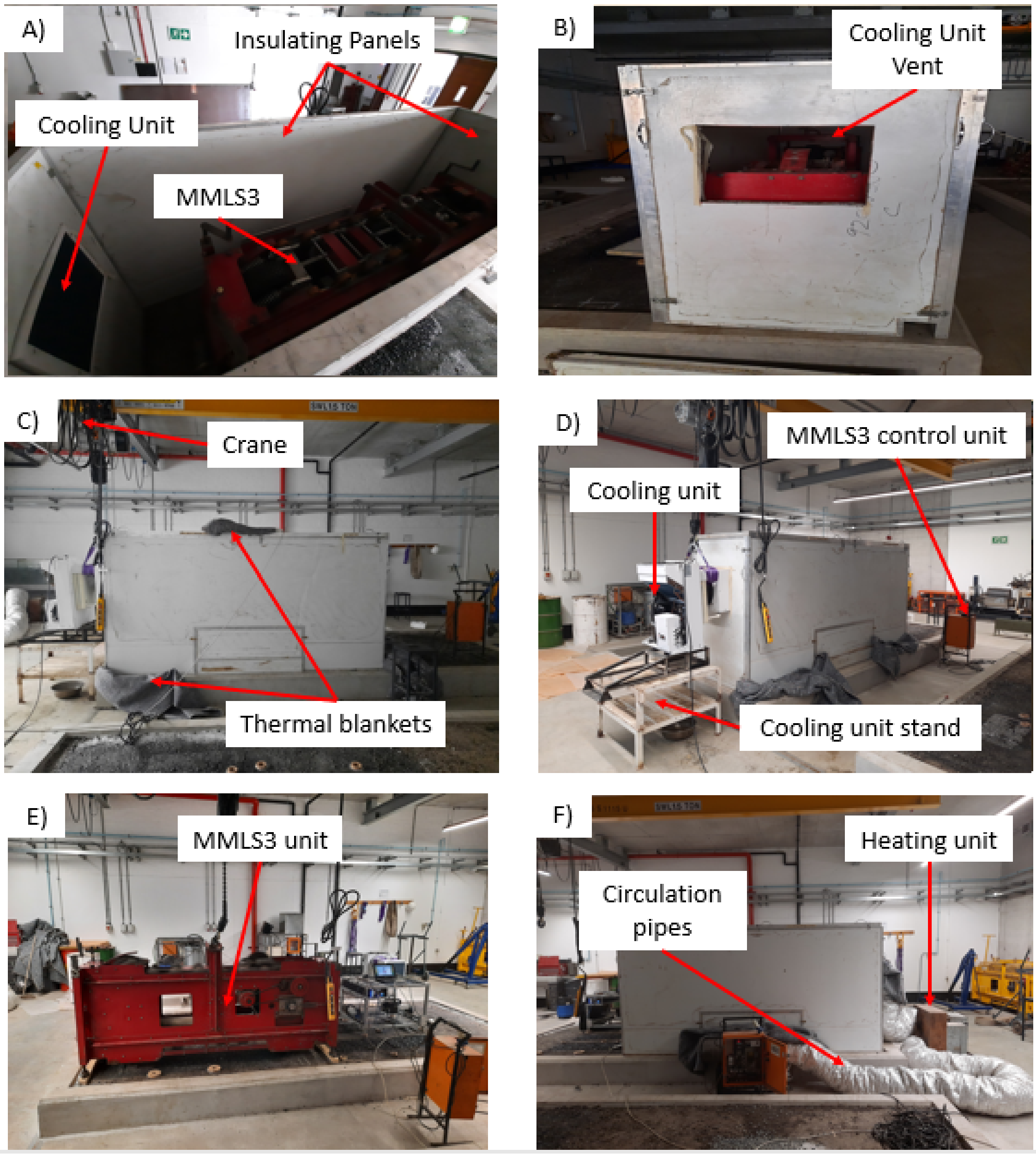

Figure 4.28: Where a) shows the top view of the setup, b) is the cooling unit's vent into the insulating box, c) shows the thermal blankets and the side view, d) shows the cooling unit, the stand thereof and the MMLS3 control unit, e) shows the MMLS3 for 20°C trafficking and f) shows the heating unit and circulation pipes for the 30°C trafficking

3. After the trafficking period, the MMLS3 system, together with the insulating box and the cooling unit (or heating unit in the case of the 30°C trafficking tempera-

ture), was moved on to the next seal tile combination and the temperature regulation and trafficking procedure continued. Simultaneously, the previous seals (that were trafficked already) were scanned individually by means of the LPM. Thus, trafficking and LPM measurements occurred at the same time as shown in Figure 4.29.

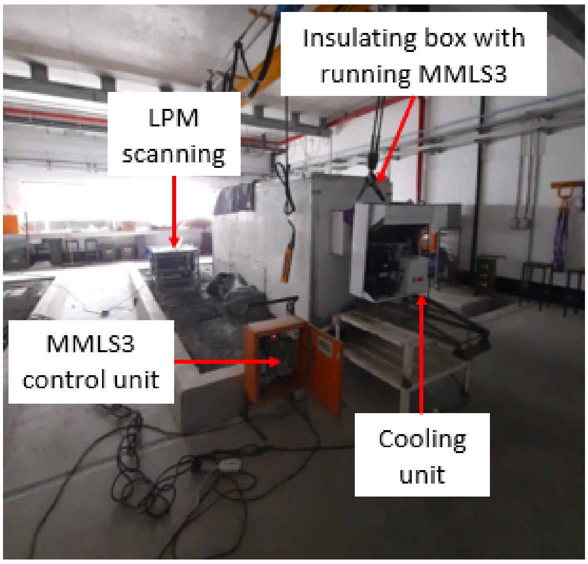

Figure 4.29: Cooling process together with the LPM

4. This procedure was followed until all seal tile combinations were trafficked after 100 load repetitions followed by the LPM measurements thereof.

5. Before commencing with the next set of load applications, it was necessary to perform sand patch readings on each of the seal tiles to obtain their respective mean texture depths.

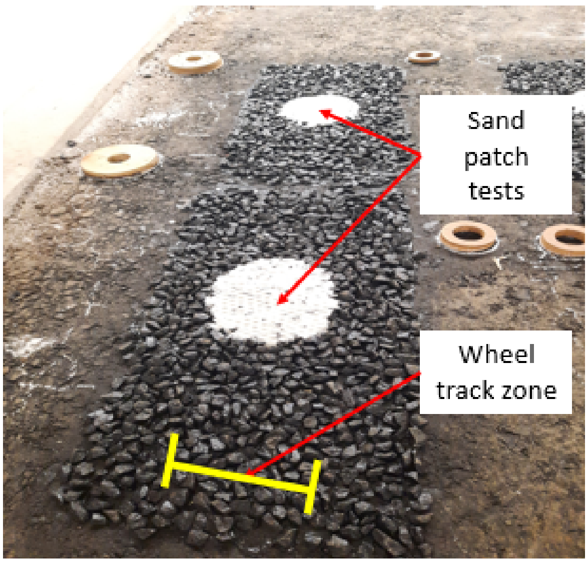

Figure 4.30: Mean texture depth test

6. Phase D of the test process was then followed for each of the load repetitions to follow (500, 2000 and 5000).
7. It was also of importance to check the tyre pressures and the wheel loads between load repetitions as to remain constant throughout testing.

4.8 Phase E: Data Reworking

The data reworking phase is done to determine the change in seal texture and profile depth over a range of temperatures and MMLS3 wheel load repetitions. These changes are then used to interpret rheological binder behaviour in terms of aggregate orientation and embedment.

4.8.1 Depth Analysis

The calculation of the MPD and MTD is of value as its relationship with MMLS3 wheel load repetitions provide an indication as to the change in mean profile depth and mean texture depth over traffic (or time). Subsequently, the change or the trend followed can be related to the rheological properties of the binder together with the influence of the polymer or rubber modification. Figure 4.31 illustrates the process followed to extract the data to obtain the MPD and MTD readings per seal tile, MMLS3 traffic interval and temperature.

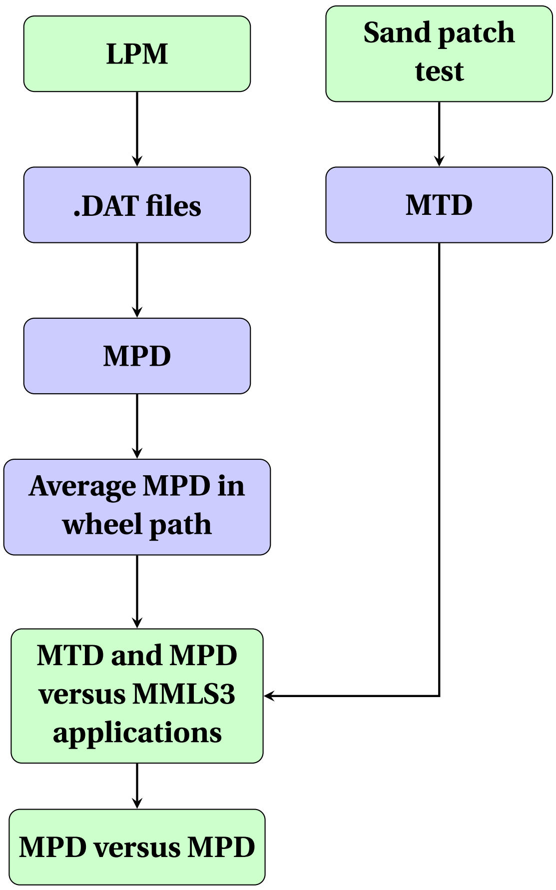

Figure 4.31: Overview of the data reworking and extraction process to obtain the MPD and the MTD

4.8.1.1 Extraction Process

As seen in Figure 4.31, the extraction process occurs after the LPM scans. The following start-to-end procedure is followed to obtain the MPD values in the MMLS3 wheel path:

1. After finishing a scan process of a seal tile, the compiled .DAT file is obtained from the LPM device where under the name of the seal tile is stored with reference to the aggregate configuration, MMLS3 application and testing temperature.

2. The .DAT file is then read into a MATLAB program which sorts the data into an array of z-coordinates along with the corresponding x- and y-coordinates. To calculate the mean profile depth along the y-direction, the sample length is set to 300 (referring to 300 mm in length). To enable the usage of Equation 2.1, a segment length, which refers to the length in which the 300 mm is divided in to obtain peaks, of 50 mm is defined, resulting in an MPD calculation consisting of six segments. An illustration of this process can be seen in Figure 4.32.

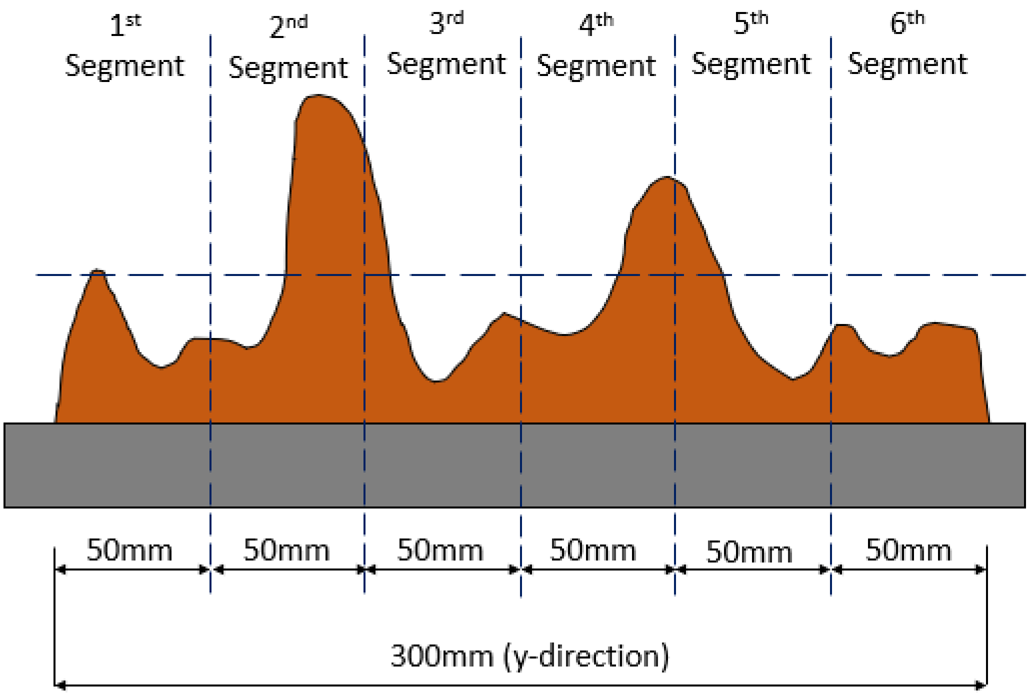

Figure 4.32: Six highest peak calculation at a given x-direction point

3. The following step involves the implementation of two "for" loops, the first running through the 140 x-direction points (280 mm in width) and another which runs through the 300 z-coordinates in the y-direction, dividing the length in the six segments and identifying the respective six highest segment peaks. The "for" loops continue in calculating the mean profile depth for each of the 140 x-direction points due to the x-step being 2 mm. Subsequently, the output from the program results in an array showing the x-direction point together with the mean profile depth in mm.

4. The array output for each seal tile is copied to an Excel spreadsheet after which the MMLS3 wheel path location is identified. Together with the positioning of the MMLS3 wheel path in the centre of the seal tile and the x= 115 mm and y=15 mm offset from the LPM, it is identified that the MMLS3 wheel path ranges between x = 131 mm and x = 211 mm for the S-E1, S-E2 and S-R2 seal tiles and between x = 95 mm and x = 175 mm for the S-E2 seal tile. The S-E2 seal tile wheel path differs due to practical constraints. The illustration of the wheel path is shown in Figure 4.33. Due to the x-step being 2 mm, the MMLS3 wheel path range consists of 40 x-coordinate lines in the y-direction. Subsequently, after copying the MPD data into the Excel spreadsheet, an average MPD value from the 40 wheel path MPD's is obtained. This process is followed for all eight seal tiles, all trafficking applications and all temperature ranges.

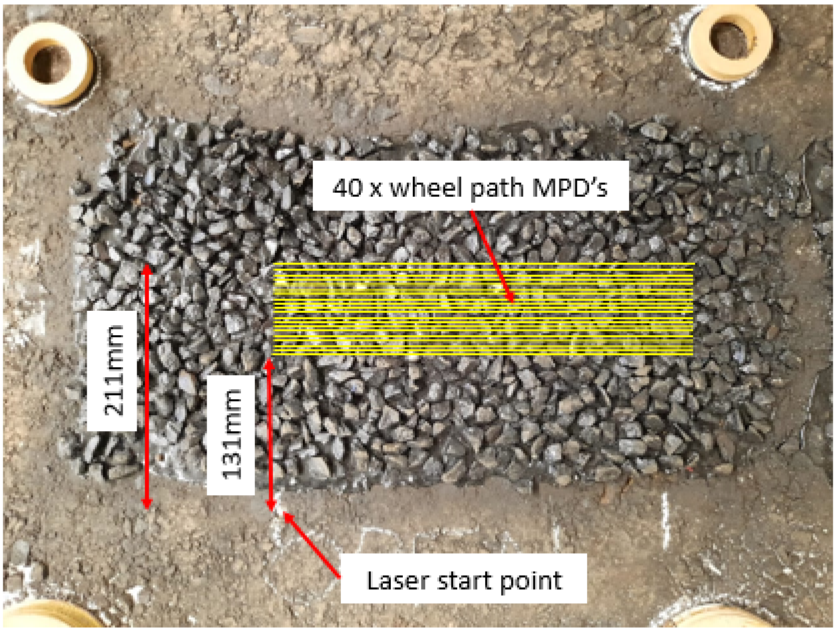

Figure 4.33: Wheel path range

5. To obtain comparative relationships between MPD and MTD and the relationships thereof with MMLS3 wheel load applications and temperature, all MPD values are summarised in a table.

4.8.1.2 LPM Reliability

Together with the data extraction process, the reliability of the LPM is also determined. This is done by evaluating the average MPD in the wheel path, of the same seal tile, after scanning it twice without any MMLS3 trafficking or changes in temperature. To obtain an average MPD value in the wheel path, the 40 MPD values between the distances x = 131 mm and x = 211 mm, in intervals of 2 mm, is obtained and averaged. Together with the evaluation of the average MPD in the wheel path, a visual analysis is performed on the MPD values over the x-axis. This is done by calculating the MPD, over the 280 mm x-distance length, in intervals of 2 mm. Subsequently, the visual analysis provides insight into the consistent scanning procedure of the LPM device.

To deem the LPM device a reliable device in terms of scanning quality, the percentage difference in average MPD value, as calculated in the MMLS3 wheel path, is to be sufficient. A low percentage difference value (< 1%) is desired to ensure quality data reworking.

4.8.1.3 Mean Profile Depth and Mean Texture Depth

The MPD and the MTD values are also plotted for each temperature as the MMLS3 trafficking applications occur. A correlation between the MPD and the MTD is then obtained by performing a linear evaluation analysis which included the evaluation of the coefficient of determination (R^2) as shown in Figure 4.34 for the S-R1 binder. As shown, the R^2 show a strong correlation for values above R^2 = 0.6.

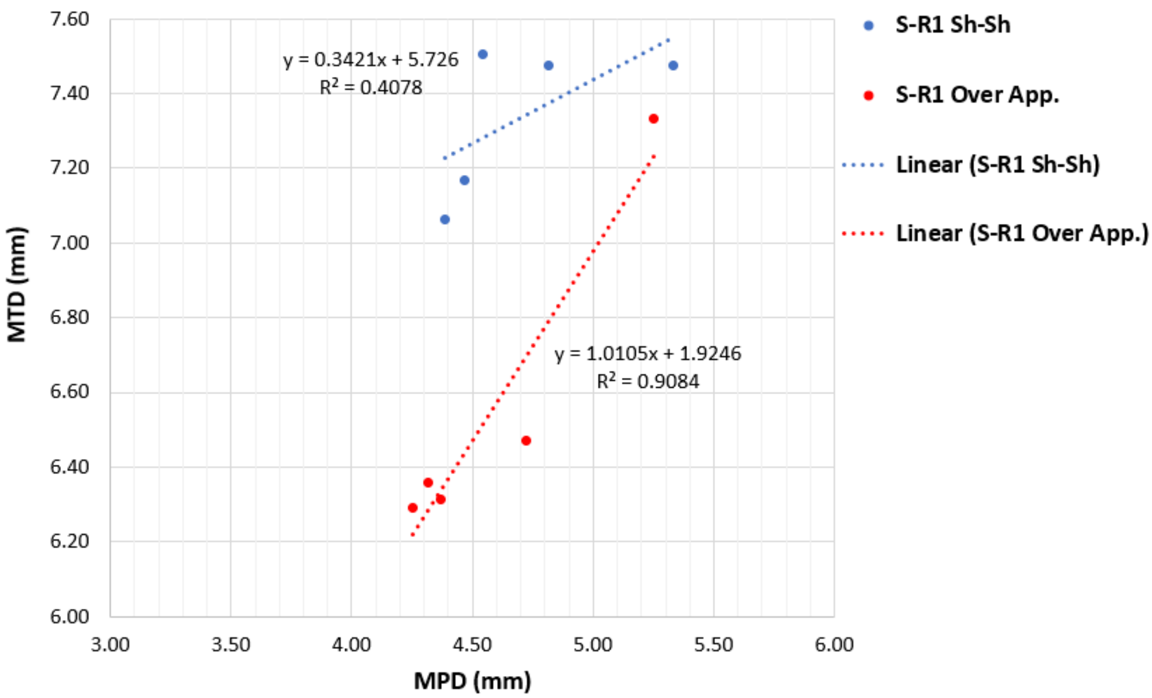

Figure 4.34: A typical relationship between the MPD and the MTD for S-R1 at 10°C

A linear relationship between the mean profile depth and the mean texture depth is then obtained. The evaluation of the relationship between the MPD and the MTD, for the binders, provides a better understanding as to the limitations and advantages of using both methods. Simultaneously, a general trend is also obtained as to the same positive correlation or negative correlation between the values. This is also shown in Figure 4.34. Together with the results and relationships obtained between the MPD and the MTD, a conclusion is also made as to accuracy and reliability of the methods.

4.8.1.4 Shakedown Theory Implementation

Similar to the implementation of the Shakedown Theory for permanent deformation, as elaborated on in Section 2.7, for unbound material, it is also implemented in the evaluation of the reduction in mean profile depth and mean texture depth based on the trends similar to those governed by the Shakedown Theory. The Shakedown period is therefore identified by analysing the reduction in MPD and MTD over MMLS3 load repetitions (N).

From the reduction in MPD, as elaborated on in Section 4.8.1.5, the Shakedown Theory (Phase 1) is implemented up to a constant MMLS3 load repetition after which there is a clear change in slope from a high rate of reduction in MPD to a lower rate of reduction in MPD. Furthermore, due to the Shakedown period occurring over such a short load repetition interval, the lengthier Steady State period is subdivided into a Phase 2 and Phase 3 to allow for more in-depth analysis. The Shakedown Theory concept is graphically shown in Figure 4.35.

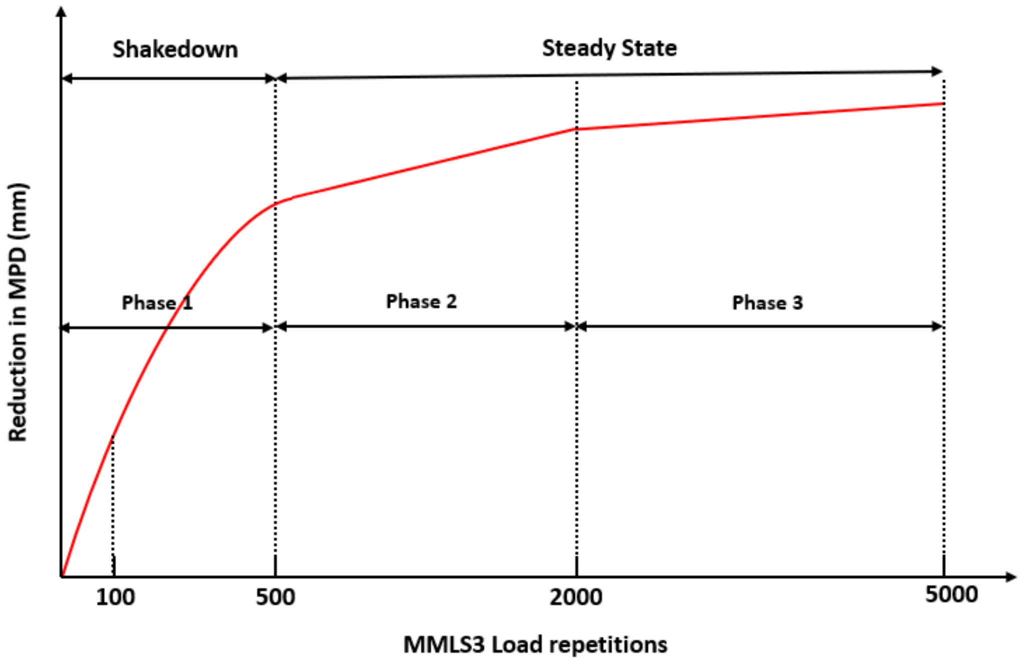

Figure 4.35: Conceptual implementation of the Shakedown Theory

4.8.1.5 Reduction in Mean Profile Depth

The seal aggregate behaviour is a function of accumulated trafficking, firstly at 10°C, then at 20°C and thereafter at 30°C. As a result thereof, it is necessary to apply an accumulation-process for the reduction in mean profile depth. Therefore, the following assumption is made to obtain normalised representative data:

- The reduction in mean profile depth after a specific MMLS3 load repetition set at a specific trafficking temperature, is an accumulation of the reduction experienced for the previous trafficking temperature sets (if applicable) and the current trafficking temperature.

Based on this assumption, representative reductions in mean profile depths are obtained by shifting the obtained averaged MPD values accordingly, to representative values, over 5000 MMLS3 load repetitions for the 10°C, 20°C and 30°C trafficking temperatures. To determine the reduction in MPD after a specific MMLS3 load repetition set, at any trafficking temperature, the following is implemented.

$$\Delta \text{MPD} = \text{MPD}_1 - \text{MPD}_2 \tag{4.1}$$

Where:
ΔMPD = the reduction in MPD (mm),
MPD_1 = the MPD value (mm) prior to MMLS3 trafficking at the specific temperature and
MPD_2 = the MPD value after a specific MMLS3 load repetition set for the same trafficking temperature.

Equation 4.1 is therefore used to determine the reduction in MPD at a specific temperature. Furthermore, to obtain the reduction in MPD at the intermediate trafficking temperature, the accumulated reduction in MPD is implemented by making use of Equation 4.1 as per Equation 4.2.

$$\Delta MPD_{INTER} = \Delta MPD + \Delta MPD_{COLD} \tag{4.2}$$

Where:
ΔMPD_{INTER} = the final reduction in MPD at the intermediate trafficking temperature,
ΔMPD = the reduction in MPD at the intermediate trafficking temperature as calculated according to Equation 4.1 and
ΔMPD_{COLD} = the reduction in MPD at the colder trafficking temperature as calculated according to Equation 4.1.

To obtain the reduction in MPD for the 30°C elevated trafficking temperature, the accumulation of MPD loss after a specific MMLS3 load repetition at 20°C, as calculated per Equation 4.2, is added to the reduction in MPD at 30°C. Therefore, Equation 4.3 is applicable.

$$\Delta MPD_{ELEV} = \Delta MPD + \Delta MPD_{INTER} \tag{4.3}$$

Where:
ΔMPD_{ELEV} = the final reduction in MPD at the elevated trafficking temperature,
ΔMPD = the reduction in MPD at the elevated trafficking temperature as calculated according to Equation 4.1 and
ΔMPD_{INTER} = the reduction in MPD at the intermediate trafficking temperature as calculated according to Equation 4.2.

To obtain representative MPD loss comparisons between different binders, aggregate matrices and trafficking temperatures, the reduction in MPD is calculated and compared after the initial trafficking period, that is the Shakedown period (Phase 1), as well as throughout the Steady State period which includes the evaluation after 2000 MMLS3 load repetitions (Phase 2) and 5000 MMLS3 load repetitions (Phase 3).

4.8.1.6 Rate of Change in Mean Profile Depth

Due to the Shakedown period occurring over the first 10% of trafficking per trafficking temperature, it is not analysed by means of the rate of change in MPD. It is rather based on the reduction in MPD indicating the initial MPD loss throughout the Shakedown period. Furthermore, to enable extrapolation for longer MMLS3 load repetition sets, the rate of change in MPD throughout Phase 2 and Phase 3 is obtained by making use of Equation 4.4

$$\Delta D = \frac{D_2 - D_1}{A_2 - A_1} \tag{4.4}$$

Where:
ΔD = the rate of reduction in MPD (mm/MMLS3 load repetition),
D_1 = the reduction in MPD (mm) after the first evaluated MMLS3 load repetition set as calculated per Equation 4.1 - Equation 4.3,
D_2 = the reduction in MPD (mm) after the second evaluated MMLS3 load repetition set as calculated per Equation 4.1 - Equation 4.3,
A_1 = the first set of MMLS3 wheel load repetitions and
A_2 = the second set of MMLS3 wheel load repetitions.

4.8.1.7 Normalised Reduction in MPD

To normalise the reduction during the Shakedown period, due to the greatest reduction in MPD occurring, the percentage reduction in mean profile depth is determined by means of Equation 4.5.

$$MPD_{\%} = \frac{\Delta MPD}{\Delta MPD_{5000}} * 100 \tag{4.5}$$

Where:
$MPD_{\%}$ = the percentage reduction in MPD after a specific set of MMLS3 wheel load repetitions during the Shakedown period,
ΔMPD = the reduction in MPD (mm) after the specific set of MMLS3 load repetitions as per Equation 4.1 - Equation 4.3 ,
ΔMPD_{5000} = the reduction in MPD value after 5000 MMLS3 wheel load applications as per Equation 4.1 - Equation 4.3.

4.8.1.8 Influence of Temperature

All data plots are completed to obtain comparable relationships between the following:

- Aggregate matrices.
- Polymer hot modified binders.
- Various MMLS3 trafficking load repetitions.
- Various trafficking temperatures

4.8.2 Visual Analysis

To visually determine the behaviour of the seal aggregate under the different MMLS3 wheel load repetitions for different trafficking temperatures, depth plots are made at the following positions:

- y-direction: A plot in the middle of the wheel path (x = 141 mm) is made for the binders after which an iteration process is followed along the plot to identify the behaviour of aggregate under the trafficking conditions.

- x-direction: Similar to the y-direction plot, a slice in the x-direction is plotted whilst an analysis continues on the edges of the wheel path (y = 131 mm and y = 211 mm). This allows for the identification of aggregate movement just outside the wheel path.

Furthermore, the plots include the change in depth (mm) for the MMLS3 wheel load repetition intervals of 0, 5000, 10000 and 15000. It is then used to analyse the movement of aggregate under each of the trafficking temperatures 10°C, 20°C and 30°C. It is noted that both aggregate matrices are evaluated in the wheel path for the y-direction plot whilst only the over application matrices are analysed on the edges of the wheel path.

4.9 Summary

A simplistic, repeatable and consistent test setup and procedure is required to enable data capturing and processing that is of quality. This chapter described the process used throughout the testing setup, including the pre-investigation phase, construction phases and MMLS3 and LPM testing phases after which the data reworking procedure is elaborated on. As mentioned, to allow for consistent results, the preparation and investigation of the seal and base construction phases are of major importance as they can influence the results obtained during the data extraction process.

Chapter 5

Results

5.1 Introduction

This chapter presents the results from the data reworking phase as discussed in Section 4.8. The analysis of the data is shown along with interesting observations. The full interpretation and discussion is presented in Chapter 6.

5.2 Influence of Temperature on Embedment

As described in Section 4.4.1.5, the relationship between embedment and base temperature is of major importance. From the ball penetration tests done, the following one-ball drop (BP1) and two-ball drop (BP2) values, as shown in Table D.1 - Table D.4 in Appendix D.1, for each temperature range is calculated. The results shown are all obtained for the respective temperature ranges within a deviation of ± 0.5°C. As seen in Figure 5.1, the behaviour of the surface indicates half-moon indents, together with the occasional crushing and displacement reaction after the ball drops. Subsequently, and with support from SABITA Manual 40 (2021), the average BP1 value, or E1 value, as listed in Table D.1 - Table D.4 in Appendix D.1, is a representative potential embedment value.

Figure 5.1: Test base surface reaction to ball penetration testing

Evaluating the BP1 and BP2 values, as shown in Table D.1 - Table D.4, it can be seen that the average BP1 values are the same for both the 25°C and 30°C tests, after which a slight increase in the value (from 1.50 mm to 1.56 mm to 2 mm) followed with an increase in temperature to 35°C and 40°C. At 40°C, the BP1 value is the largest, indicating a greater embedment potential. The BP2 values increased in a more linear manner, indicating that the relationship between the embedment potential and the 5°C interval change, is more gradual. As seen in Table D.1 - Table D.4, the increase in embedment, as the temperature increases, is in the range of 0.05 mm - 0.06 mm per temperature increase.

To obtain a graphical relationship between embedment potential and BSM-emulsion base temperature, The BP1 and BP2 values are plotted against base temperature as seen in Figure 5.2. From the plots, it is indicated that the BP1 values, with an increase in temperature, experience a sharp increase between the base temperatures of 35°C and 40°C whilst there is no increase between the temperatures of 25°C and 30°C. The BP2 values, as indicated previously, do not indicate the potential embedment due to the visual assessment of the surface reaction, but the values show a linear increase with an increase in base temperature of 5°C.

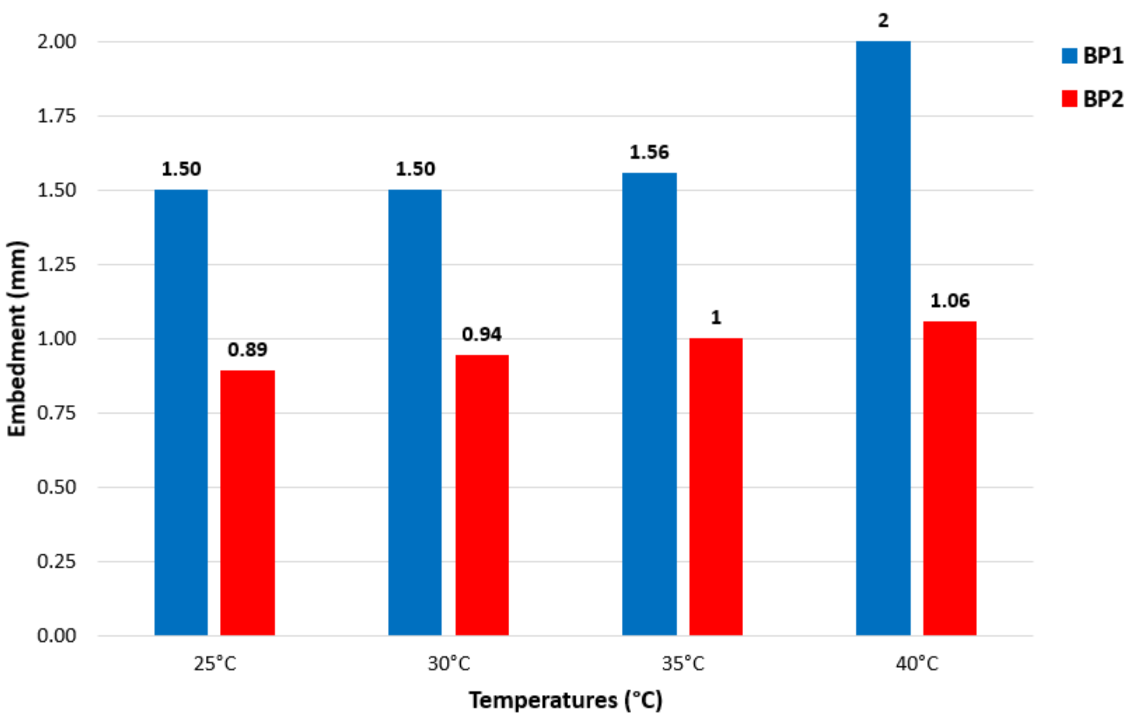

Figure 5.2: Embedment values

To obtain the potential embedment at a specified temperature, ratios between the ball penetration values are calculated. Table 5.1 a) and b) presents the ratios obtained using the 25°C average BP1 and BP2 results as base values. Subsequently, by knowing the BP1 and BP2 values at 25°C, the potential embedment at another base temperature is obtained by multiplying the BP1 and BP2 values with the corresponding ratio at the desired temperature.

Table 5.1: Ball Penetration Ratios
a) Ball Penetration 1 Ratios

	Ball Penetration 1 Ratios						
From / To	**25°C**	**30°C**	**35°C**	**40°C**	**Mean**	**Standard Deviation**	**COV**
25°C	1.000	1.000	1.037	1.333	1.084	0.161	0.149
30°C	1.000	1.000	1.037	1.333	1.084	0.161	0.149
35°C	0.964	0.964	1.000	1.286	1.046	0.156	0.149
40°C	0.750	0.750	0.778	1.000	0.813	0.121	0.149

b) Ball Penetration 2 Ratios

	Ball Penetration 2 Ratios						
From / To	**25°C**	**30°C**	**35°C**	**40°C**	**Mean**	**Standard Deviation**	**COV**
25°C	1.000	1.063	1.125	1.188	1.092	0.081	0.074
30°C	0.941	1.000	1.059	1.118	1.027	0.076	0.074
35°C	0.889	0.944	1.000	1.056	0.970	0.072	0.074
40°C	0.842	0.895	0.947	1.000	0.919	0.068	0.074

To obtain a ratio for lower, intermediate or higher base temperatures (other than 25°C, 30°C, 35°C or 40°C), the relationship between the ratios are plotted from a base temperature of 25°C, as seen in Figure 5.3 and Figure 5.4. It should be noted that these plots and relationships are obtained for a BSM-emulsion base, with a granular G2 grading correspondent to the grading in Section 4.4.1.2 together with the BSM mix as shown in Table A.2 in Appendix A.2.

From the linear BP1 analysis, as seen in Figure 5.3, the trend evaluation is done between 25°C - 35°C, followed by another between 35°C - 40°C. For this evaluation, it can be seen that with an $R^2 = 0.75$, the ratio determination between 25°C - 35°C indicates the following relationship.

$$\mathrm{Ratio}_{\mathrm{BP1}(25°\mathrm{C}-35°\mathrm{C})} = 0.0037\mathrm{T} + 0.9012 \tag{5.1}$$

Where:
$\mathrm{Ratio}_{\mathrm{BP1}(25°\mathrm{C}-35°\mathrm{C})}$ = the ratio required between 25°C - 35°C for BP1 and
T = the temperature at which the ratio is required.

The linear analysis for BP1, between the temperatures 35°C - 40°C, indicates a goodness of fit of $R^2 = 1$ with a temperature and ratio relationship as follows.

$$\mathrm{Ratio}_{\mathrm{BP1}(35°\mathrm{C}-40°\mathrm{C})} = 0.0593\mathrm{T} - 1.037 \tag{5.2}$$

Where:
$\mathrm{Ratio}_{\mathrm{BP1}(35°\mathrm{C}-40°\mathrm{C})}$ = the ratio required between 35°C - 40°C for BP1 and

T = the temperature at which the ratio is required.

From the second order polynomial trend analysis for the BP1 ratios, as seen in Figure 5.4, the goodness of fit increases to $R^2 = 0.9684$ whilst the following relationship is obtained.

$$Ratio_{BP1(25°C-40°C)} = 0.003T^2 - 0.1719T + 3.4556 \tag{5.3}$$

Where:
$Ratio_{BP1(25°C-40°C)}$ = the ratio required between 25°C - 40°C for BP1 and
T = the temperature at which the ratio is required.

The linear analysis of BP2, as seen in both Figure 5.3 and Figure 5.4 , indicates a strong correlation in that $R^2 = 1$. Subsequently, the relationship between temperature (T) and ratio is as follows.

$$Ratio_{BP2(25°C-40°C)} = 0.0125T + 0.6875 \tag{5.4}$$

Where:
$Ratio_{BP2(25°C-40°C)}$ = the ratio required between 25°C - 40°C for BP2 and
T = the temperature at which the ratio is required.

Equation 5.1 - Equation 5.4 can be used to determine the ratio required to obtain a potential embedment value when the ball penetration (BP1 or BP2) value is known at a BSM-emulsion base temperature of 25°C. The following mathematical expression is used to determine the ball penetration value at a desired temperature after obtaining the ratio.

$$BP_B = Ratio_B * BP_{A(25°C)} \tag{5.5}$$

Where:
BP_B = the required ball penetration value at temperature B,
$Ratio_B$ = the ratio determined from using Equation 5.1 - Equation 5.4 at temperature B and
$BP_{A(25°C)}$ = the known ball penetration value at temperature A = 25°C.

If the ball penetration value is known at a temperature (A) other than 25°C, the ratio required is obtained by taking the inverse of the ratio at the desired temperature (B) and multiplying it with the known ball penetration value. The mathematical expression is described as per the following.

$$BP_B = \frac{1}{Ratio_B} * BP_{A(\neq 25°C)} \tag{5.6}$$

Where:
BP_B = the required ball penetration value at temperature B,

$Ratio_B$ = the ratio determined from Equation 5.1 - Equation 5.4 at temperature B and $BP_{A(\neq 25°C)}$ = the ball penetration at temperature A which is not equal to 25°C.

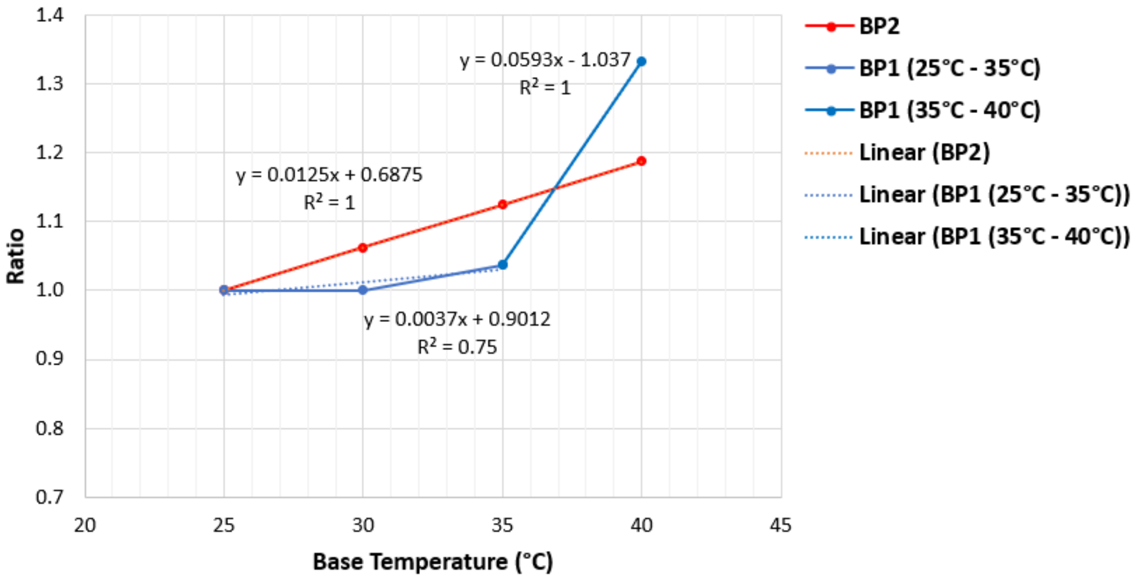

Figure 5.3: Ball penetration ratio trend from a 25°C base temperature with a linear BP1 analysis

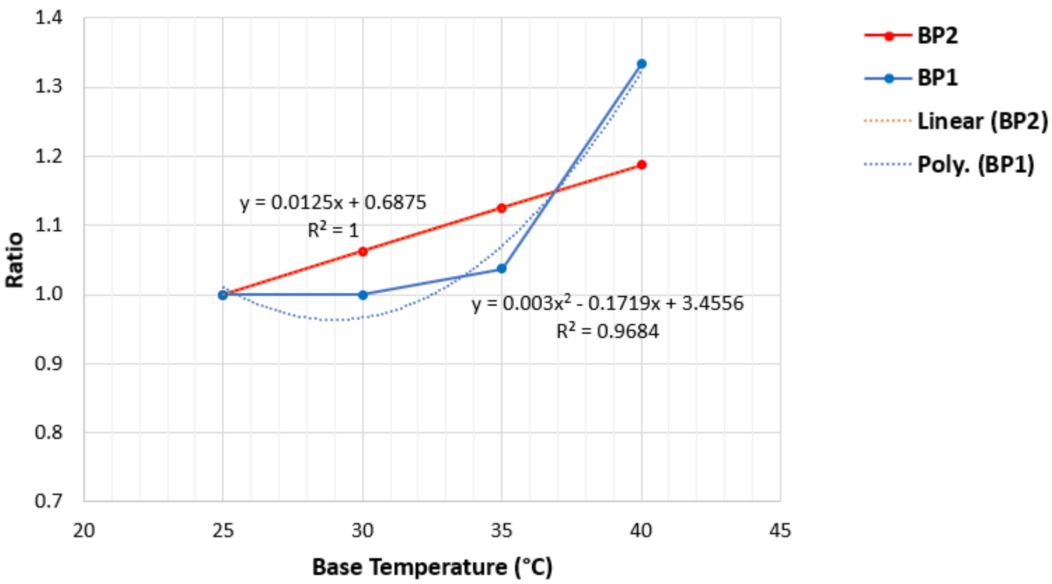

Figure 5.4: Ball penetration ratio trend from a 25°C base temperature with a polynomial BP1 analysis

5.3 Laser Profilometer Reliability

As elaborated on in Section 4.8.1, the reliability of the LPM device is evaluated by performing two re-scans on the S-E1 sh-sh and the S-R1 over application seal tiles without any influence of MMLS3 trafficking. The plots, as seen in Figure 5.5 and Figure 5.6, show the mean profile depth for each 2 mm interval, as calculated along the 280 mm x-distance.

Performing a visual analysis on the plots, it can be seen that various x-distance coordinate points indicate a higher or lower MPD value between the two plots. This anomaly occurs due to the laser, of the LPM device, recording an unusual reading at random positions. An indication thereof is shown when a z-coordinate is listed as a value of z = -180 mm, indicating that the measured seal position is above the laser. To correct this specific z-coordinate, the device performs an interpolation process between known z-coordinate values from the neighbouring y-coordinates. Due to this occurrence, it is possible for the two re-scans, as seen in Figure 5.5, to indicate a difference in z-coordinate.

Another indication, further justifying the reliability of the LPM device, is shown in Figure 5.5, where it can be seen that the two scans are near similar in the x-distance. Thus, the LPM device did not experience a horizontal shift or movement between the positioning of the first scan and that of the second. Thus, no horizontal shift is required as Abrahams (2015) indicated when using the Laser Texture Meter. Figure 5.6 confirms that the plots of the re-scans also initiated at the same x-distance position. This confirms the restriction in movement of the LPM device between scans, ensuring that the device starts the scanning process at the exact same coordinate as per the previous scan.

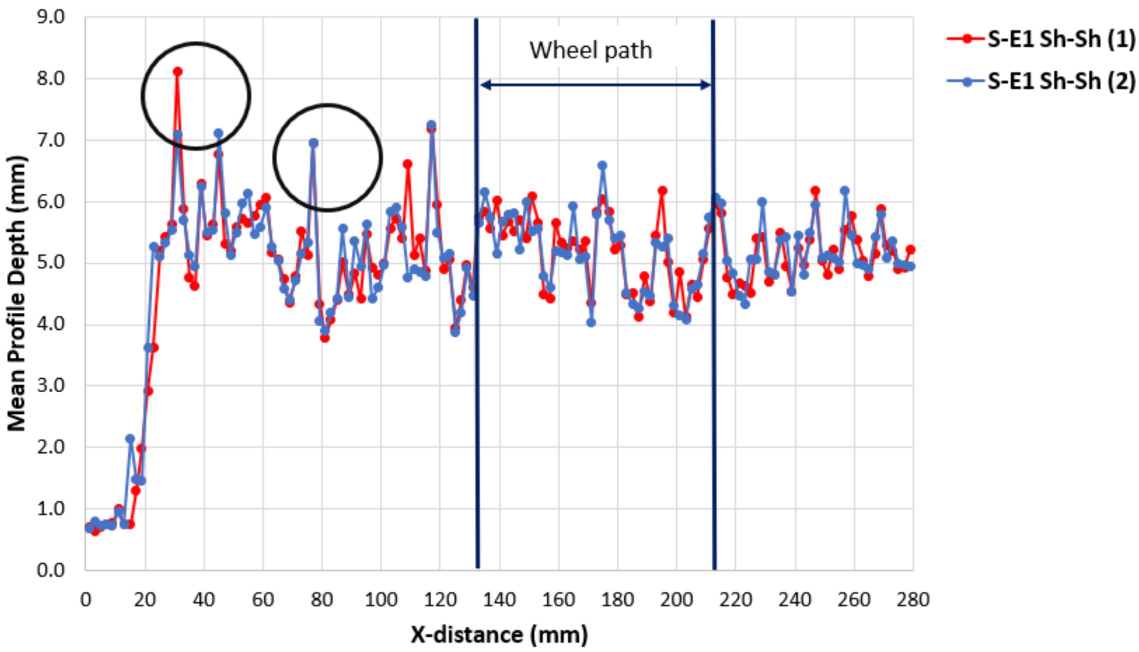

Figure 5.5: MPD plot across the x-distance for the S-E1 sh-sh matrix

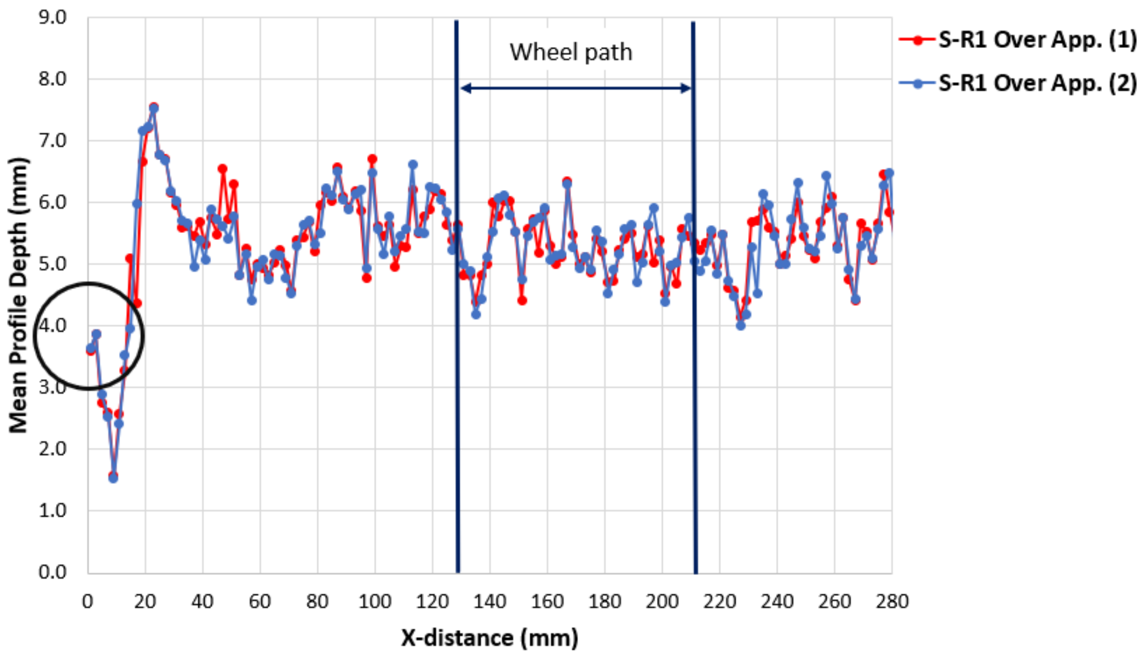

Figure 5.6: MPD plot across the x-distance for the S-R1 over application matrix

Due to the analysis of the mean profile depth occurring in the wheel path, it is necessary to evaluate the MPD of both the S-E1 and S-R1 binder. Subsequently, the wheel path positions, as indicated between the distances x = 131 mm and x = 211 mm, as shown in both Figure 5.5 and Figure 5.6, are analysed by obtaining the average MPD from the 40 individual wheel path MPD values as described in Section 4.8. The results are shown in Table 5.2. As seen, the S-E1 sh-sh matrix indicates a percentage difference in mean profile depth in the wheel path of 0.60%, whilst the S-R1 over application matrix shows a difference of 0.32% between the re-scans.

Table 5.2: Average MPD evaluation in the wheel path

Seal	Configuration	Wheel path MPD (mm)
S-E1	Sh-Sh	5.187
S-E1	Sh-Sh (2)	5.156
	Difference (%)	0.60
S-R1	Over Application	5.251
S-R1	Over Application (2)	5.267
	Difference (%)	0.32

5.4 Profile Depth versus Texture Depth

A linear regression analysis is done for all the binder types, aggregate configuration matrices and temperature ranges. The following sections discuss the results.

5.4.1 10°C Trafficking

The relationship between the MPD and the MTD, for all the seal binders up to 5000 wheel loads at 10°C, is shown in Figure 5.7 - Figure 5.10. The general trend seen, for all binders and aggregate application rates, show that as the MPD decreases, the MTD also decreases. All supporting MTD and MPD values can be found in Appendix D.2, Table D.5 - Table D.9 and Table D.20 - Table D.23 with a summary in Table D.32.

Applying a linear regression analysis, between the MPD and the MTD, yields the R^2 values as shown in Figure 5.7 - Figure 5.10. Figure 5.11 illustrates the comparison between the different binders and aggregate matrices in terms of R^2 values. An evaluation line is also inserted at a value of $R^2 = 0.6$ which indicates the minimum limit whereby the data points are too scattered (< 0.6) to obtain an accurate relationship between the respective MPD and MTD values.

From Figure 5.7 - Figure 5.10 and Figure 5.11, it is seen that the degree of correlation between the MPD and MTD values are high (> 0.6) for all over application aggregate matrices except for the S-E2 binder. No clear trend is defined between the MPD and the MTD values as Figure 5.11 also shows a high coefficient of determination value for the S-R2 sh-sh aggregate matrix. Further confidence in the trends include the identification of possible outliers, as indicated Figure 5.7, which results in a higher coefficient of determination, indicating that the trend's goodness of fit increases. Subsequently, for the 10°C trafficking temperature, the S-E1 sh-sh aggregate matrix increases from an $R^2 = 0.1439$ to a value of $R^2 = 0.336$ by means of outlier identification.

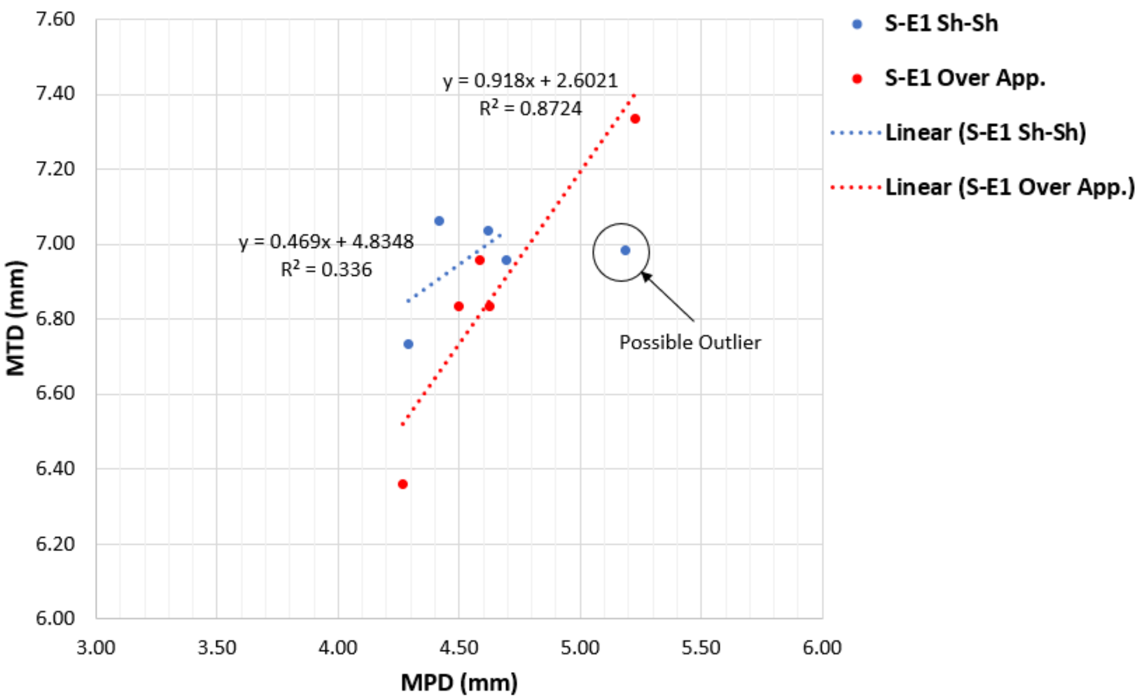

Figure 5.7: MPD vs MTD for S-E1 at 10°C

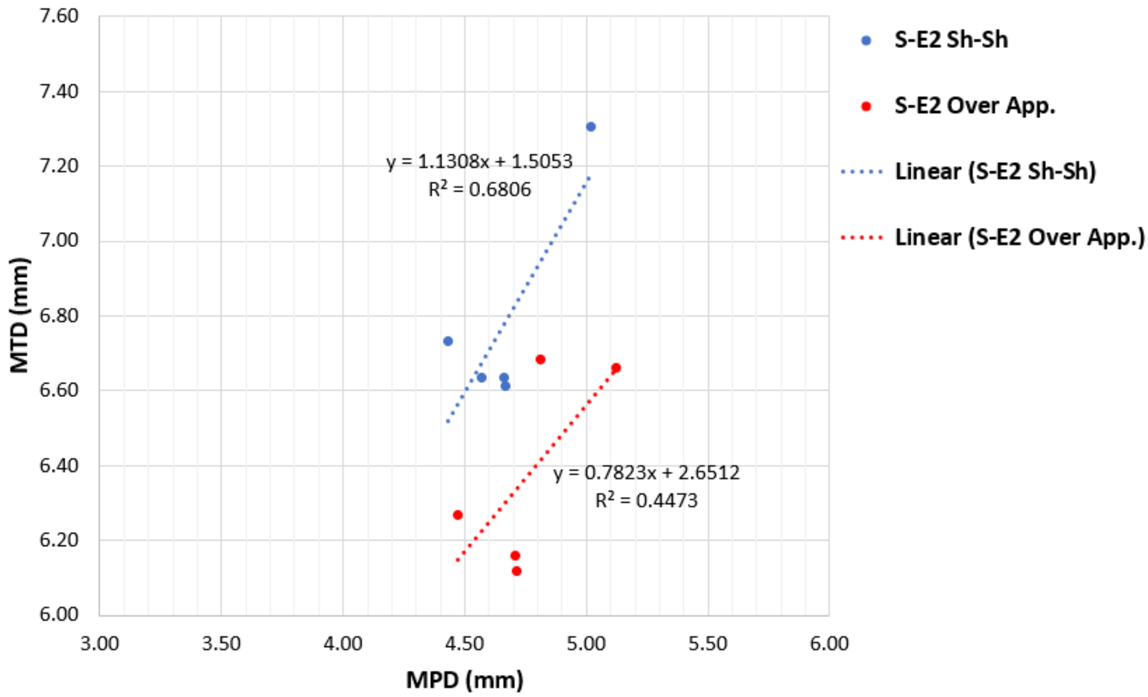

Figure 5.8: MPD vs MTD for S-E2 at 10°C

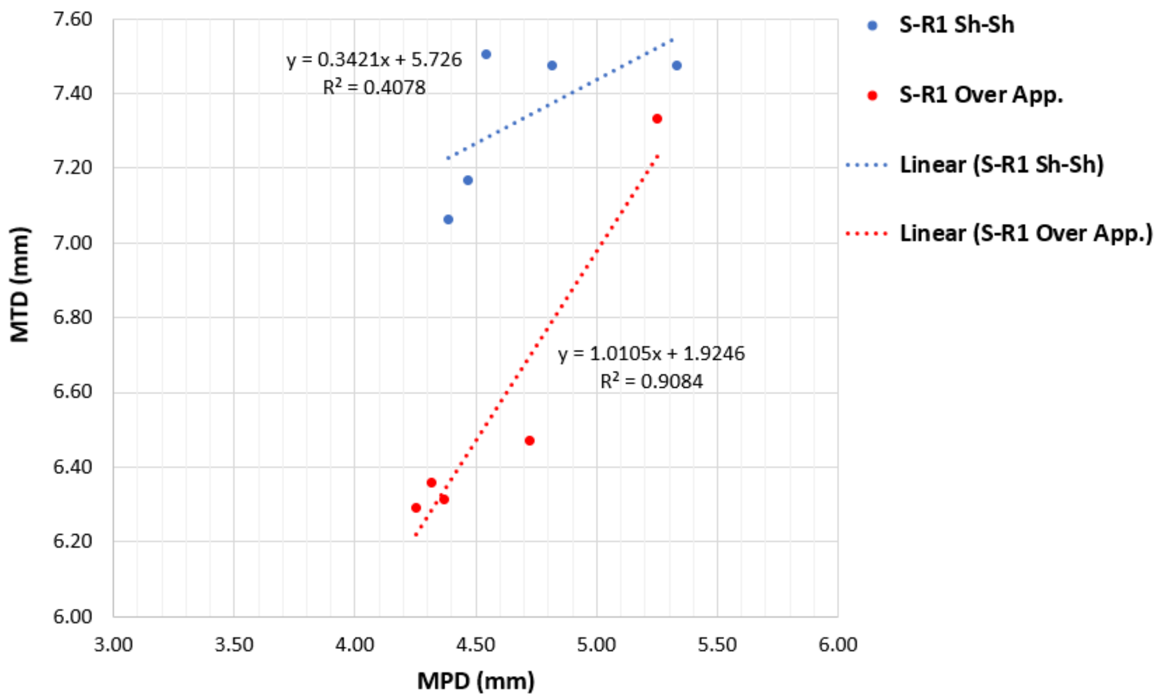

Figure 5.9: MPD vs MTD for S-R1 at 10°C

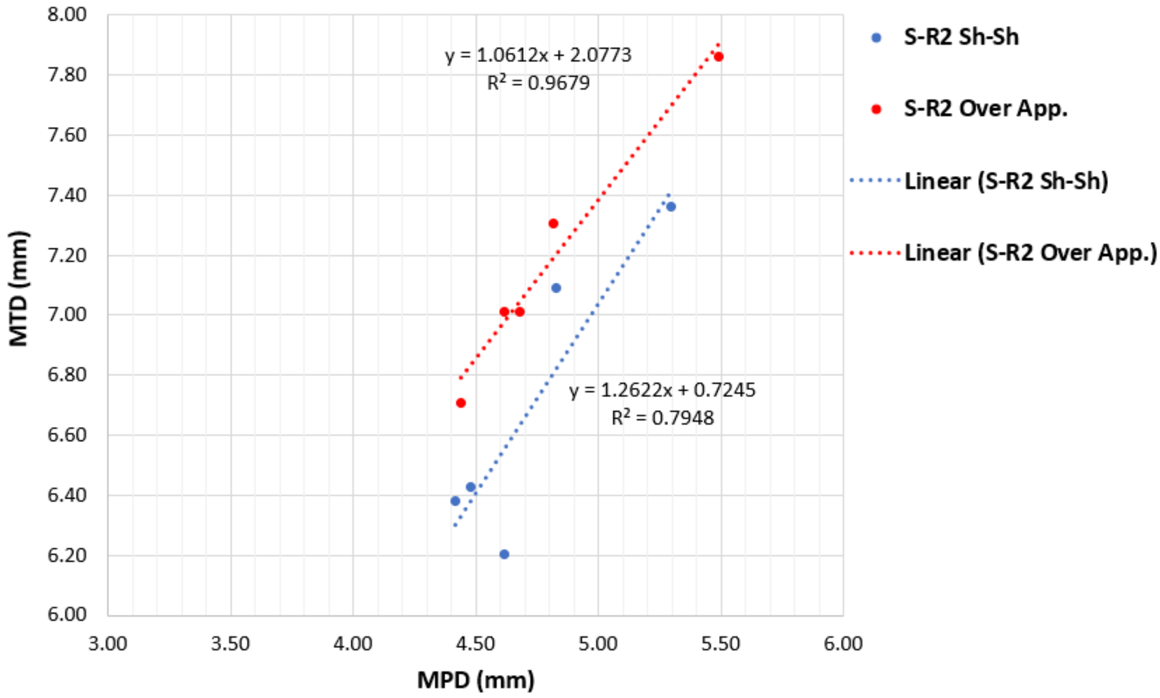

Figure 5.10: MPD vs MTD for S-R2 at 10°C

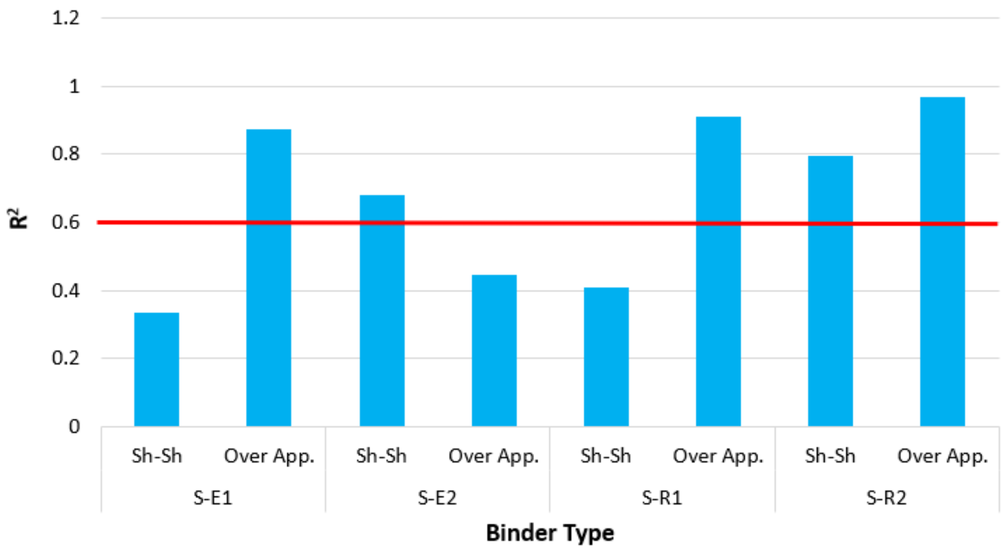

Figure 5.11: Comparative correlation coefficients R^2 at 10°C for each binder and aggregate configuration

Following the linear analysis, the relationship between the MPD and the MTD values are obtained for all binders and aggregate matrices with $R^2 > 0.6$ values. Subsequently, the following relationship is obtained for the S-E1 over application aggregate seal, with $R^2 = 0.8724$.

$$MTD_{S-E1(over-application)} = 0.918(MPD) + 2.6021 \tag{5.7}$$

Similarly, the following transformation equations are obtained for the sh-sh S-E2 binder, with a value of $R^2 = 0.6806$, and the over application S-R1 binder with a high degree of correlation ($R^2 = 0.9084$).

$$MTD_{S-E2(sh-sh)} = 1.1308(MPD) + 1.5053 \tag{5.8}$$

$$MTD_{S-R1(over-application)} = 1.0105(MPD) + 1.9246 \tag{5.9}$$

Both aggregate matrices for the S-R2 binder show a high degree of correlation. The following relationships, as described per Equation 5.10 and Equation 5.11, are obtained with values of $R^2 = 0.7948$ and $R^2 = 0.9679$ for the sh-sh and over application aggregate matrices respectfully.

$$MTD_{S-R2(sh-sh)} = 1.2622(MPD) + 0.7245 \tag{5.10}$$

$$MTD_{S-R2(over-application)} = 1.0612(MPD) + 2.0773 \tag{5.11}$$

5.4.2 20°C Trafficking

Following the same linear analysis as per the 10°C temperature range, the following MPD versus MTD relationships, as shown in Figure 5.12 - Figure 5.15, are obtained. All supporting MTD and MPD values can be found in Appendix D.2, Table D.10 - Table D.14 and Table D.24 - Table D.27 with a summary in Table D.33. Evaluating the coefficient of determination for each binder and aggregate configuration, it is seen that only four of the binder types, together with their specific aggregate matrix, resulted in an $R^2 > 0.6$. This is also illustrated in Figure 5.16.

From the MPD versus MTD plots, it is seen that the trend, as with the 10°C temperature range, continues in that the MPD and the MTD relationship is directly proportional as a decrease in the MPD with an increase in MMLS3 wheel loads also results in a decrease in MTD.

Furthermore, and as shown in Figure 5.16, the coefficient of determination, corresponding to the goodness of fit, is high (> 0.6) for all over application aggregate matrices, except the S-R2 binder, whilst the S-R2 sh-sh shows the only high degree of correlation for the sh-sh aggregate matrices.

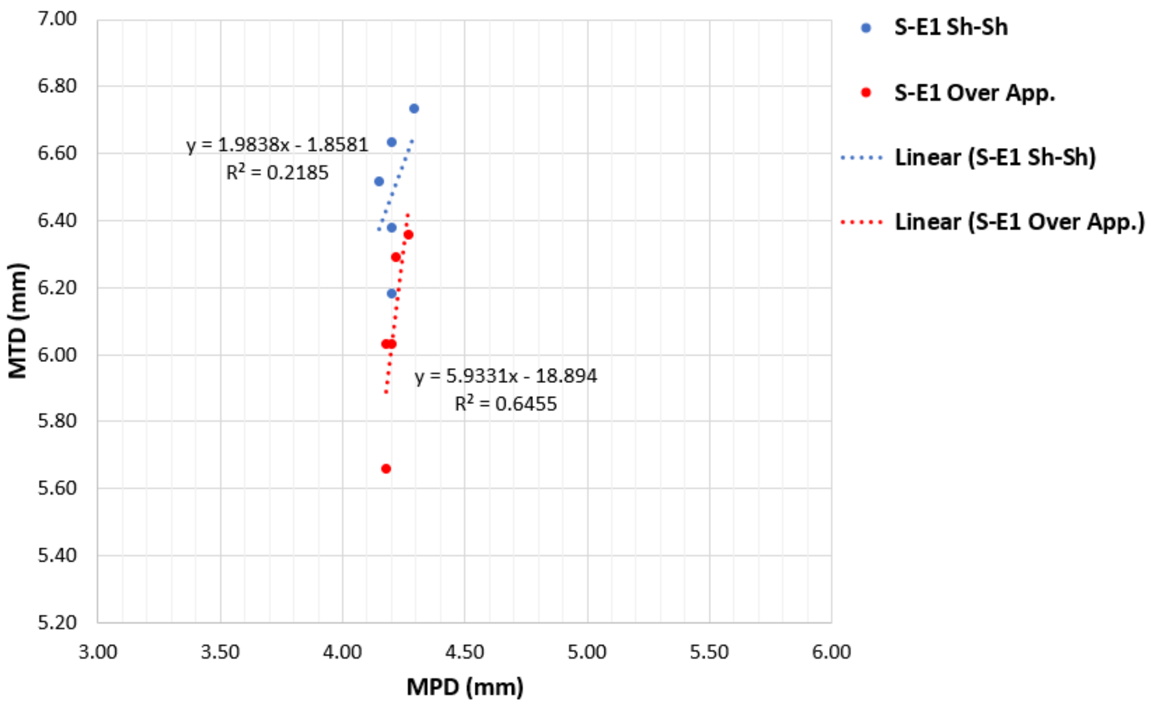

Figure 5.12: MPD vs MTD for S-E1 at 20°C

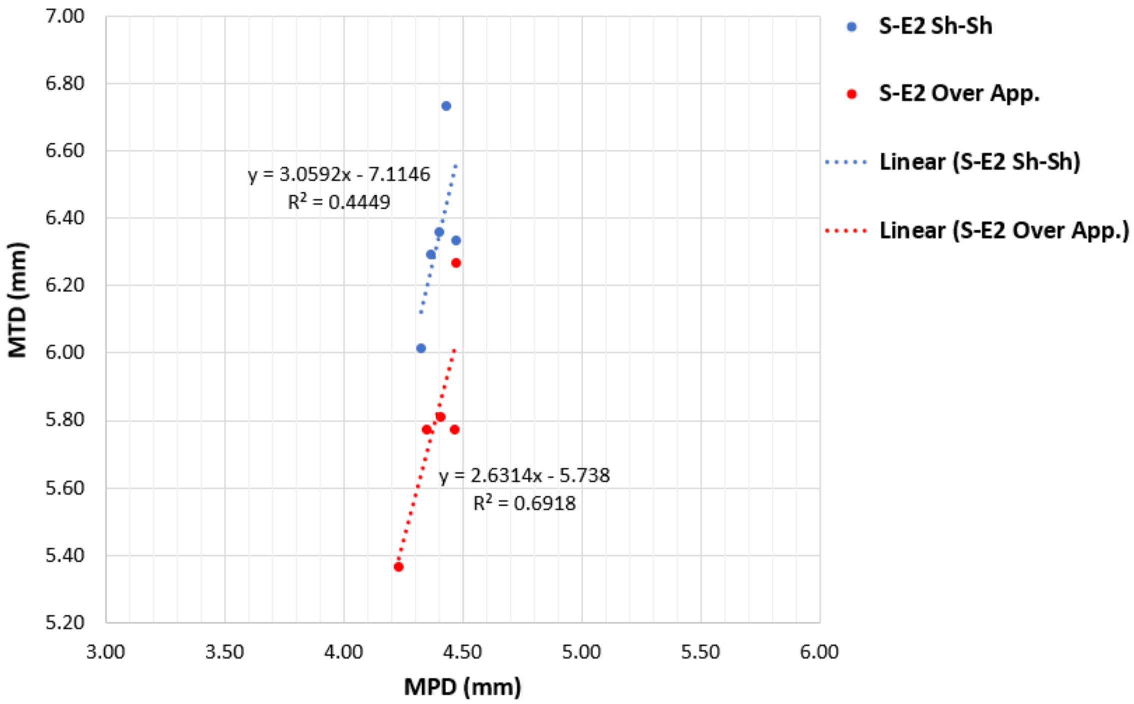

Figure 5.13: MPD vs MTD for S-E2 at 20°C

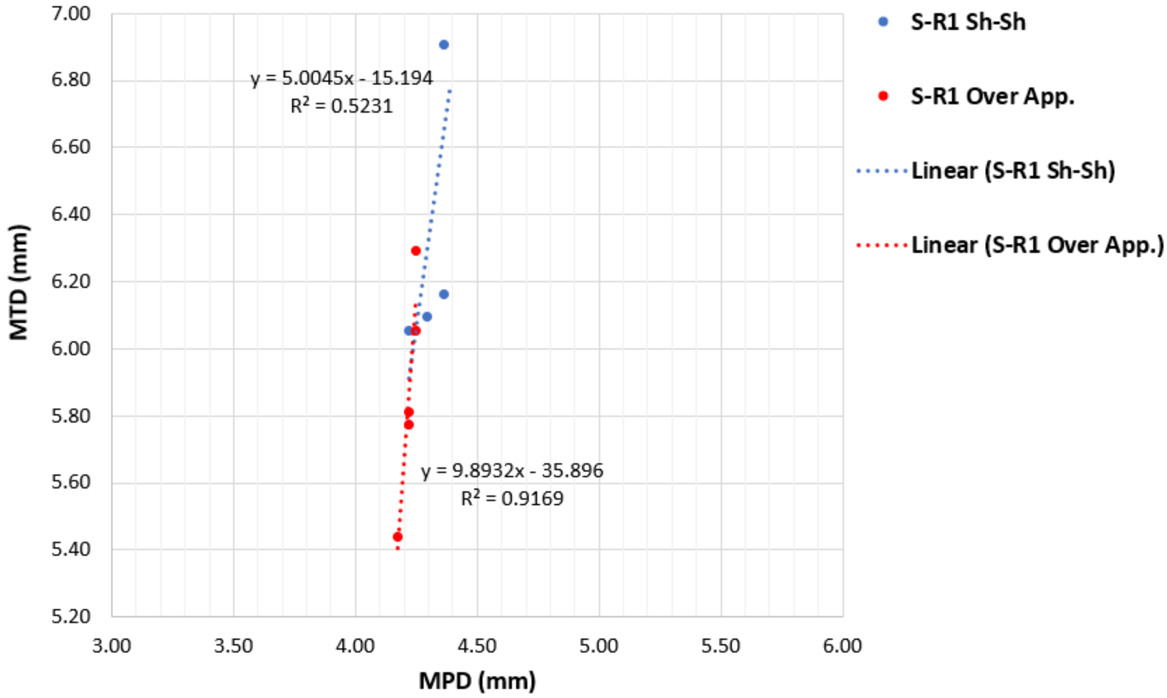

Figure 5.14: MPD vs MTD for S-R1 at 20°C

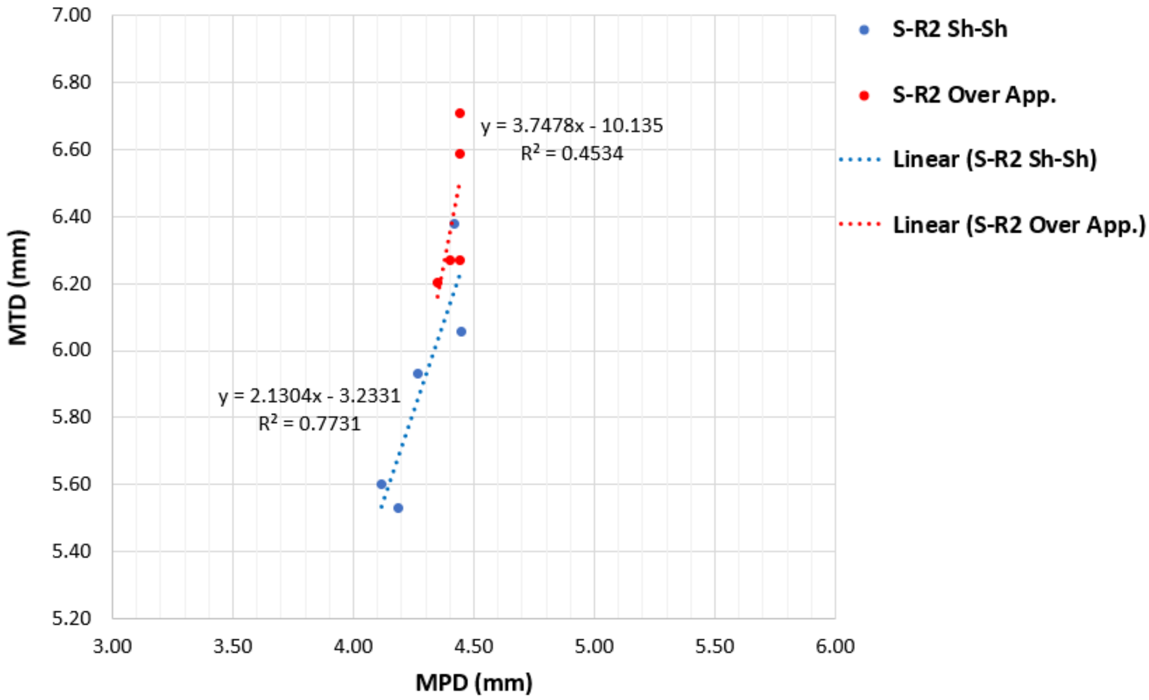

Figure 5.15: MPD vs MTD for S-R2 at 20°C

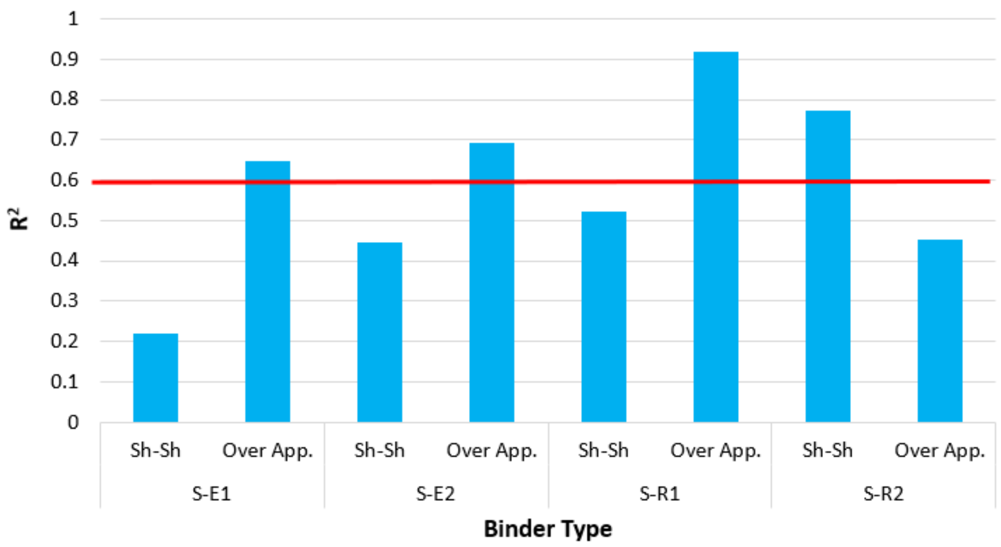

Figure 5.16: Comparative correlation coefficients R^2 at 20°C for each binder and aggregate configuration

To obtain accurate transformation equations between the MPD and the MTD for each binder, the R^2 is taken into consideration. For the S-E1 over application aggregate matrix, with $R^2 = 0.6455$, the following relationship is obtained.

$$MTD_{S-E1(over-application)} = 5.9331(MPD) - 18.894 \tag{5.12}$$

For the S-E2 binder, with an over application aggregate matrix, an R^2 value of 0.6918 is obtained resulting in the following relationship.

$$MTD_{S-E2(over-application)} = 2.6314(MPD) - 5.738 \tag{5.13}$$

The S-R1 over application matrix produced a value of $R^2 = 0.9169$ which corresponds to a high degree of correlation between the MPD and the MTD results. As shown in Figure 5.14, the following relationship is obtained.

$$MTD_{S-R1(over-application)} = 9.8932(MPD) - 35.896 \tag{5.14}$$

Similarly to what was obtained at the 10°C temperature range, the sh-sh aggregate matrix for the S-R2 binder produced a high degree of correlation, resulting in $R^2 = 0.7731$. Subsequently, the following transformation equation is valid for the S-R2 sh-sh binder at a trafficking temperature of 20°C.

$$MTD_{S-R2(sh-sh)} = 2.1304(MPD) - 3.2331 \tag{5.15}$$

5.4.3 30°C Trafficking

It was also necessary to determine the correlation between the MPD and the MTD values at the higher 30°C temperature range. The MPD versus MTD linear analysis is shown in Figure 5.17 - Figure 5.20 whilst a summary of the coefficient of determination is shown in Figure 5.21. All supporting MTD and MPD values can be found in Appendix D.2, Table D.15 - Table D.19 and Table D.28 - Table D.31 with a summary in Table D.34.

From the MPD versus MTD plots, as shown in Figure 5.17 - Figure 5.20, the general trend corresponds to the direct proportionality of the MPD and the MTD values. As the MMLS3 trafficking repetitions increase for a trafficking temperature of 30°C, both the MPD and the MTD decreases. Figure 5.21 shows that a good degree of correlation is obtained for all binder types and aggregate matrices except for the S-E1 and S-E2 over application matrices. An R^2 value lower than 0.6 is produced by the S-E1 over application matrix whilst $R^2 < 0.1$ corresponds to the S-E2 over application matrix. Figure 5.21 also shows that, similar to Figure 5.11 and Figure 5.16, both rubber binders, S-R1 and S-R2, including both aggregate matrices, show consistent R^2 results in that there is less variation when compared to the elastomer binders S-E1 and S-E2.

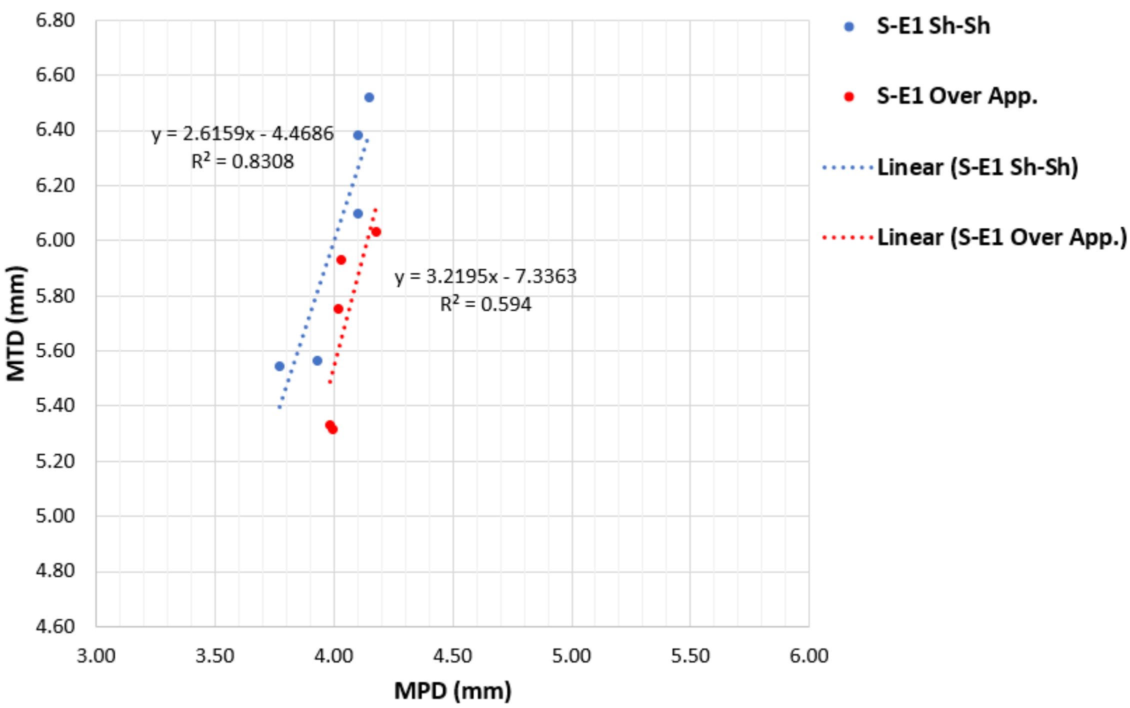

Figure 5.17: MPD vs MTD for S-E1 at 30°C

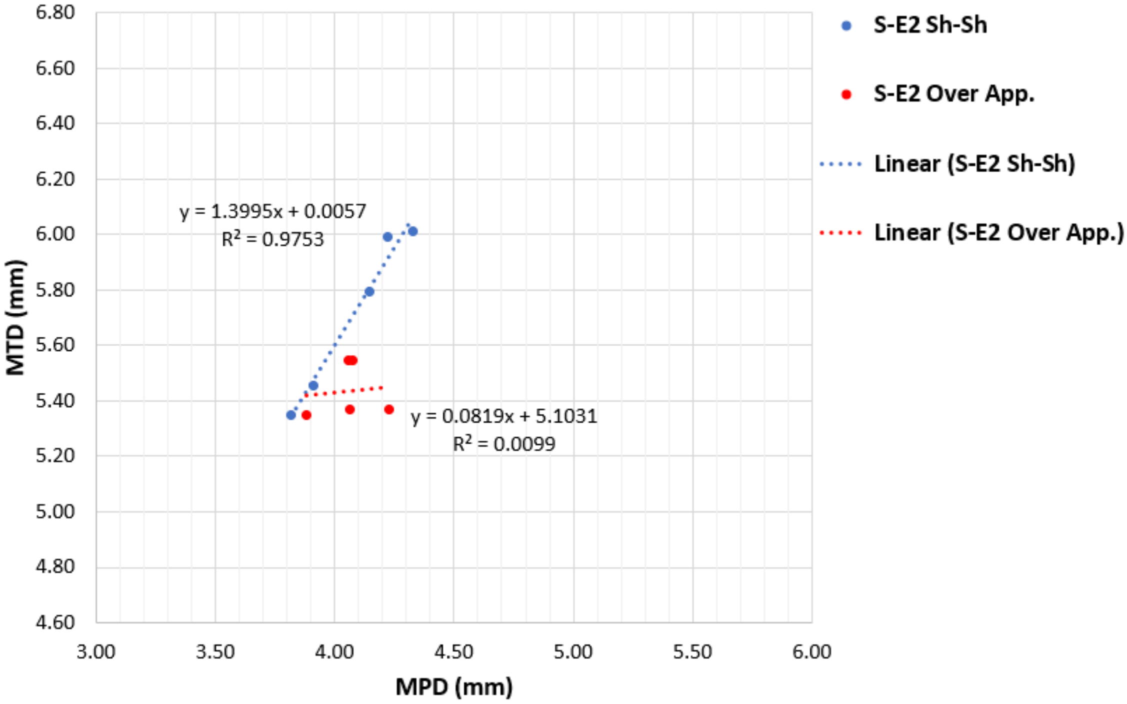

Figure 5.18: MPD vs MTD for S-E2 at 30°C

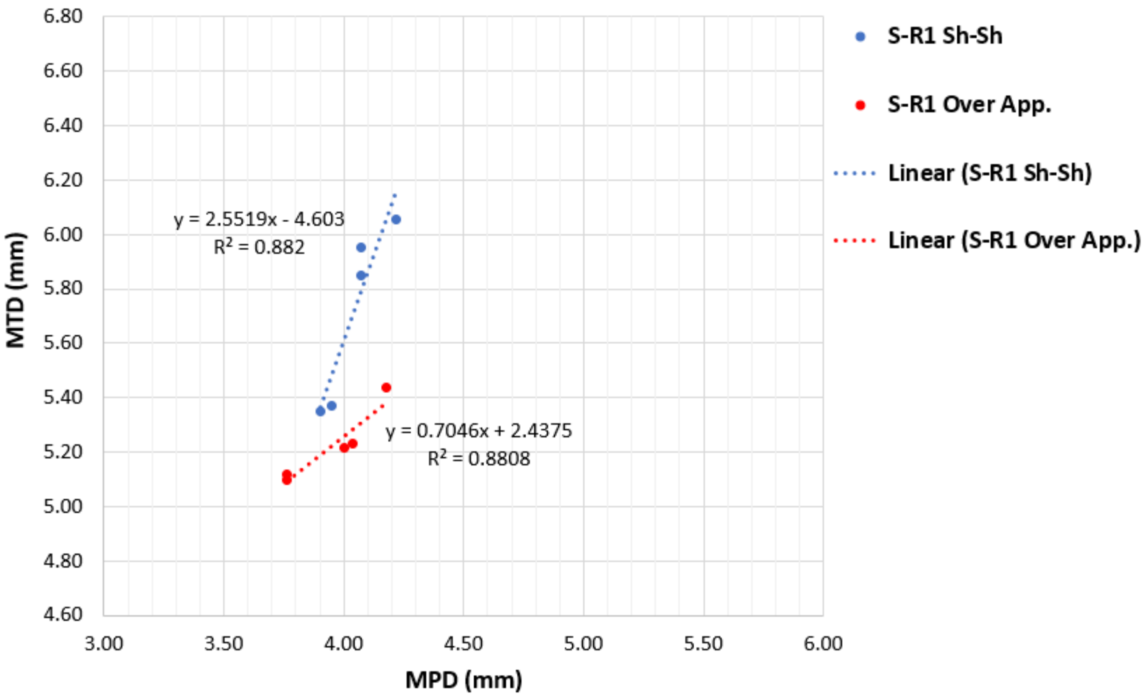

Figure 5.19: MPD vs MTD for S-R1 at 30°C

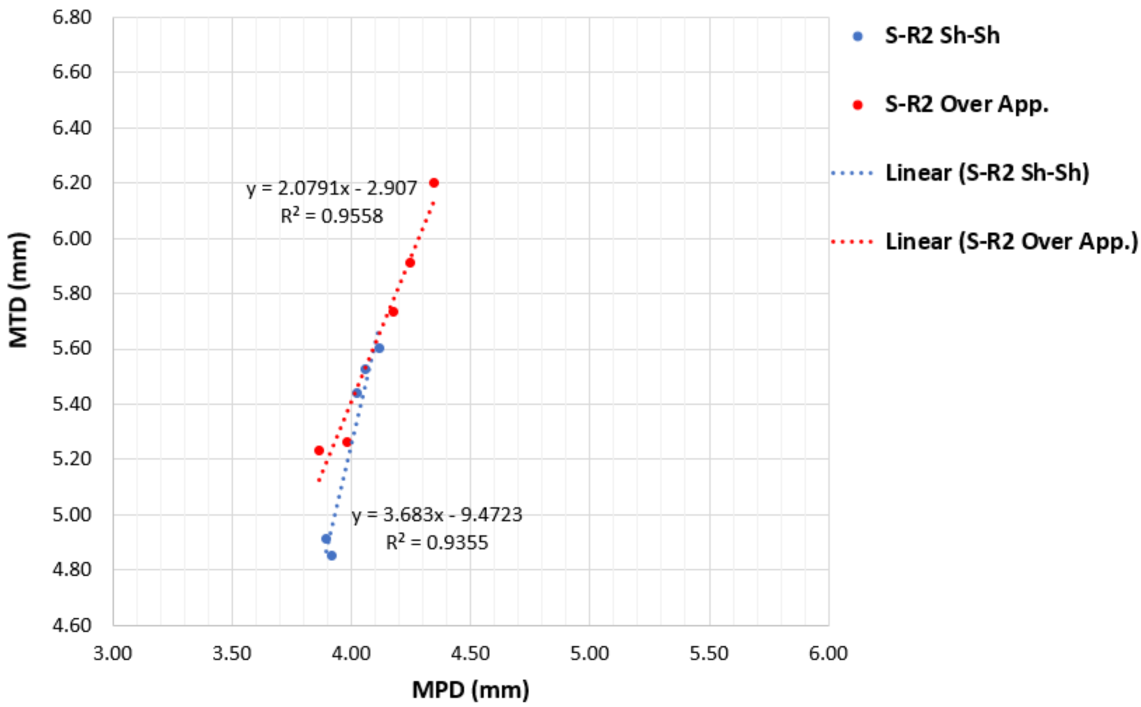

Figure 5.20: MPD vs MTD for S-R2 at 30°C

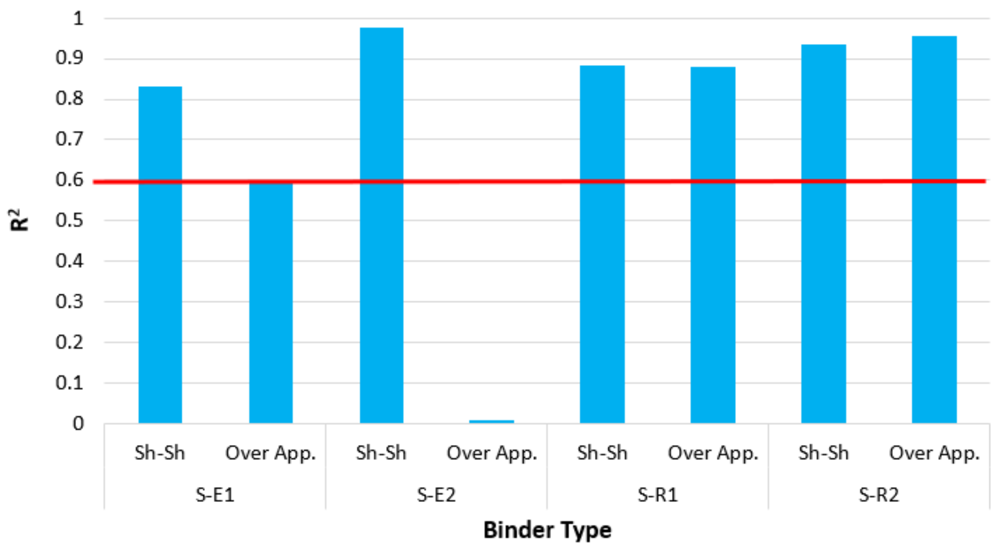

Figure 5.21: Comparative correlation coefficient R^2 at 30°C for each binder and aggregate configuration

From the evaluation of the transformation equations, the following is obtained for the S-E1 sh-sh and the S-E2 sh-sh seal binders with values of $R^2 = 0.8308$ and $R^2 = 0.9753$.

$$MTD_{S-E1(sh-sh)} = 2.6159(MPD) - 4.4686 \tag{5.16}$$

$$MTD_{S-E2(sh-sh)} = 1.3995(MPD) + 0.0057 \tag{5.17}$$

Both the S-R1 sh-sh and over application seals produce high coefficient of determination values ($R^2 = 0.882$ and $R^2 = 0.8808$) showing that there is a high degree of correlation between the MPD and the MTD values. Subsequently, the following relationships are obtained.

$$MTD_{S-R1(sh-sh)} = 2.5519(MPD) - 4.603 \tag{5.18}$$

$$MTD_{S-R1(over-application)} = 0.7046(MPD) + 2.4375 \tag{5.19}$$

Similar to the S-R1 binders, the S-R2 sh-sh and over application binders produce high degree of correlation values, resulting in the following transformation equations with values of $R^2 = 0.9355$ and $R^2 = 0.9558$.

$$MTD_{S-R2(sh-sh)} = 3.683(MPD) - 9.4723 \tag{5.20}$$

$$MTD_{S-R2(over-application)} = 2.0791(MPD) - 2.907 \tag{5.21}$$

5.5 Depth Analysis

The following subsections include the results obtained from analysing both the MPD and the MTD values over each of the different temperature ranges as MMLS3 load repetitions occur.

5.5.1 Trafficking History

As stated in Section 4.7, each seal tile undergoes 5000 MMLS3 load repetitions at the trafficking and surfacing temperatures of 10°C, 20°C and 30°C. A visual representation of the reduction in mean profile depth and mean texture depth, as seen in Figure 5.22 for the S-R1 binder as example, is plotted from the results in Appendix D.2, Table D.32 - Table D.34. The S-E1, S-E2 and S-R2 binder plots are presented in Appendix D.3, Figure D.1 - Figure D.3.

As a general trend for all binders, there is a clear reduction in both the mean profile depth and the mean texture depth over the 15000 MMLS3 load repetitions. As seen, the mean texture depth indicates a larger depth (mm) when compared to the mean profile depth. A discussion regarding the difference is provided in Chapter 6.

The evaluation per each trafficking temperature indicates that both the sh-sh and the over application aggregate matrices follow a similar trend in that there is a reduction with an increase in MMLS3 load repetitions. This is applicable to the mean profile depth and the mean texture depth for all binders.

As elaborated on in Section 4.8, a method to obtain comparable data (remove the trafficking history) is to shift the trafficking data at 20°C and 30°C to a similar trafficking level as at 10°C. This process is based on the assumptions as mentioned in Section 4.8.1.4 and Section 4.8.1.5. Therefore, the presented data is based on trafficking sets without history. Due to variability in the MTD data, as seen in Figure 5.22 and Figure D.1 - Figure D.3, the mean texture depth is not analysed according to the Shakedown Theory. The interpretation thereof is discussed in Chapter 6.

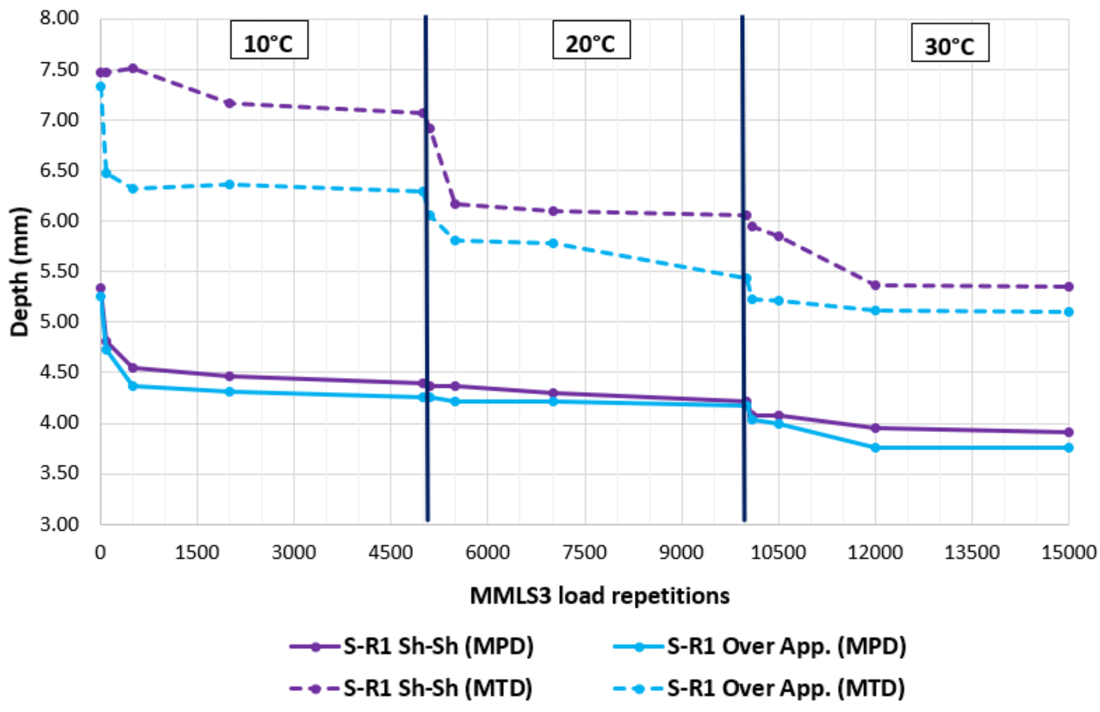

Figure 5.22: MPD and MTD reduction for S-R1

5.5.2 Reduction in Mean Profile Depth

To enable a phase related analysis, as explained in Section 4.8, it is of note to correspond the identified phases in line with a Shakedown-equivalent period and a Steady State period. Furthermore, to enable consistent data analysis, the phases for all binders are subject to the following MMLS3 load repetitions: 0 - 500 represents Phase 1 (Shakedown period), 500 - 2000 depicts Phase 2 as the initial stage of the Steady State period whilst Phase 3 occurs between 2000 - 5000 MMLS3 load repetitions, making up 60% of the trafficking period per temperature.

Figure 5.23 - Figure 5.26 graphically present the reduction in mean profile depth for each binder and corresponding aggregate spread rate matrix under 10°C, 20°C and 30°C MMLS3 trafficking. Furthermore, the trend shows that there are lower reductions in MPD at 10°C trafficking when compared to the higher trafficking temperatures over 5000 MMLS3 load repetitions.

Furthermore, and as seen in Figure 5.23 - Figure 5.26, Phase 1 shows a greater initial reduction in MPD whilst Phase 2 and Phase 3 illustrate a continuous reduction at a lower rate of change in MPD. From these trends, in-depth analyses follow with key trends identified during the phases for all binders. A full summary of the reduction in MPD can be found in Table D.35 in Appendix D.4.

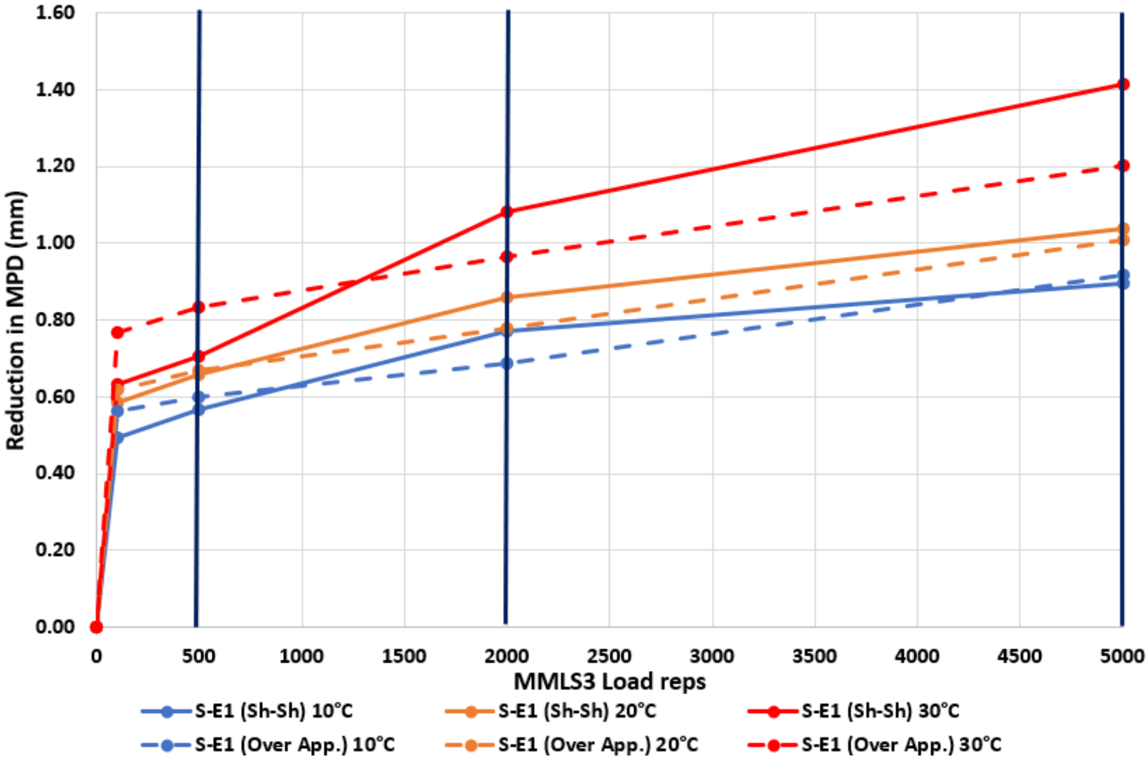

Figure 5.23: Reduction in MPD (mm) for the S-E1 binder

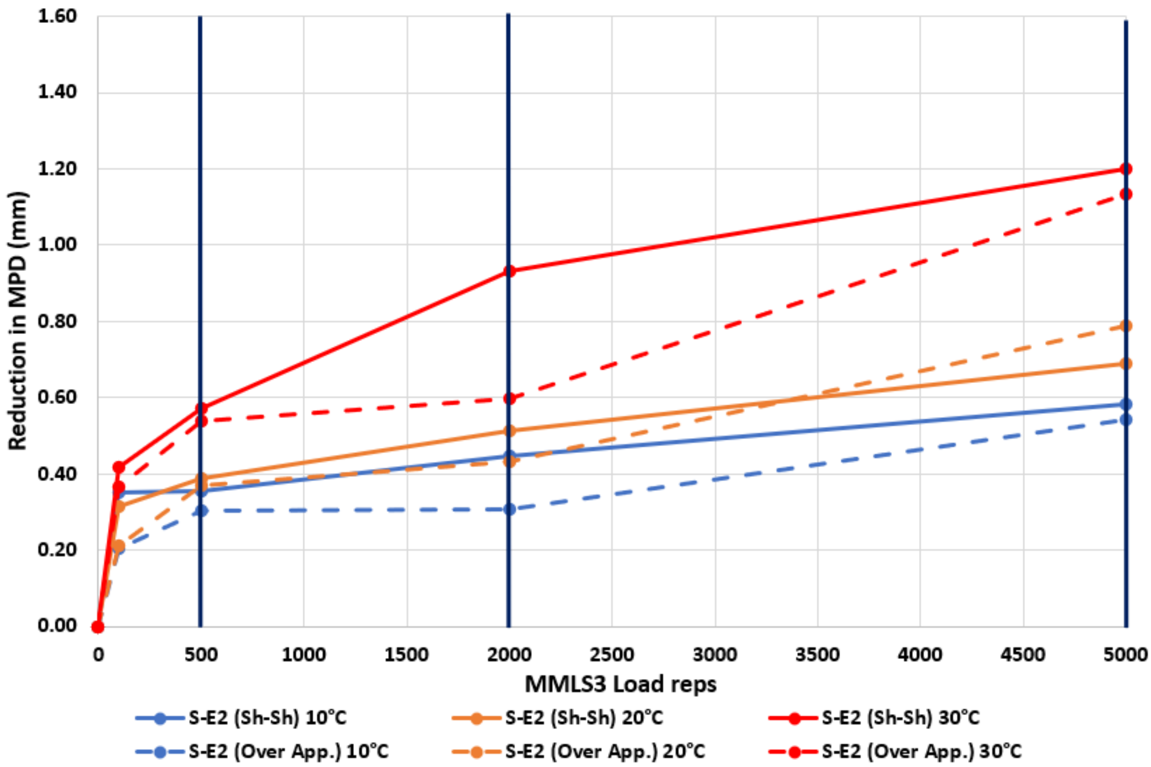

Figure 5.24: Reduction in MPD (mm) for the S-E2 binder

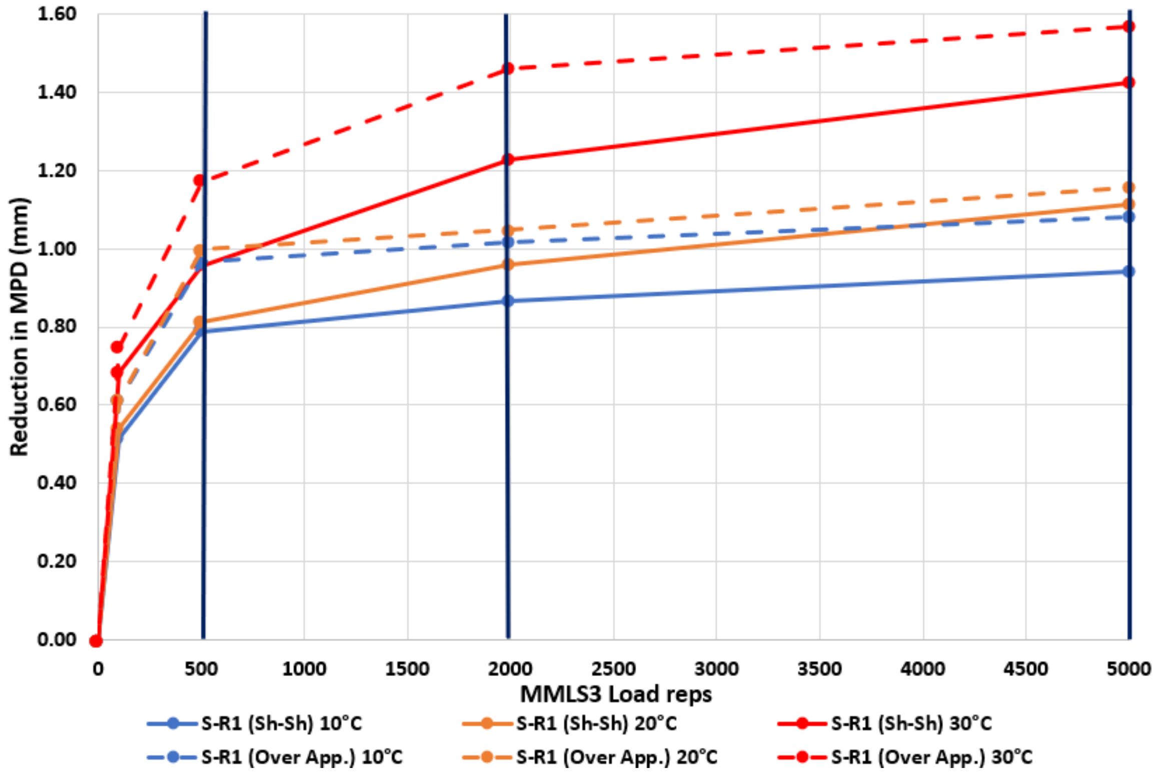

Figure 5.25: Reduction in MPD (mm) for the S-R1 binder

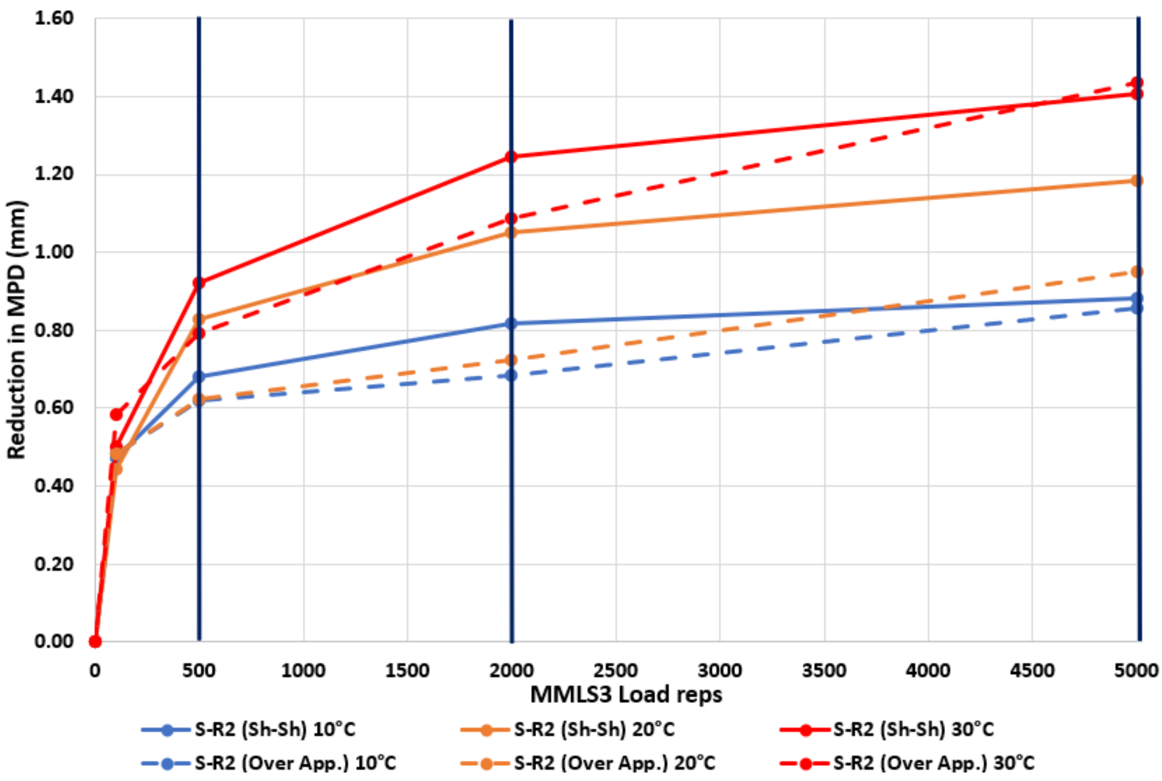

Figure 5.26: Reduction in MPD (mm) for the S-R2 binder

5.5.2.1 Phase 1: Shakedown

Analysing the reduction in mean profile depth, during the Phase 1 trafficking period, per binder over all trafficking temperatures, it is apparent that there is a greater reduction in the MPD with an increase in trafficking temperature as shown for both the sh-sh and over application aggregate matrices in Figure 5.27 - Figure 5.30. The trends also include variability during initial trafficking, as the over application matrices for the S-E1 and S-R1 binders show a greater reduction in MPD when compared to their sh-sh counterparts whilst, in contrast, the S-E2 and S-R2 sh-sh matrices show a greater reduction in MPD when compared to their over application matrices. Furthermore, it is evident that the S-E1 binder (including both aggregate matrices) experiences greater reductions in MPD when compared to the S-E2 binder, whilst the sh-sh matrices, for the S-R1 and S-R2 binders, experience similar reductions. A summary of the reduction in MPD (mm) after Phase 1 can be seen in Table 5.3.

Table 5.3: Reduction in MPD (mm) after 500 MMLS3 load repetitions

	Aggregate Configuration	S-E1	S-E2	S-R1	S-R2
10°C	**Sh-Sh**	0.57	0.36	0.79	0.68
	Over Application	0.60	0.30	0.97	0.62
20°C	**Sh-Sh**	0.66	0.39	0.81	0.83
	Over Application	0.67	0.37	1.00	0.62
30°C	**Sh-Sh**	0.71	0.57	0.96	0.92
	Over Application	0.83	0.54	1.17	0.79

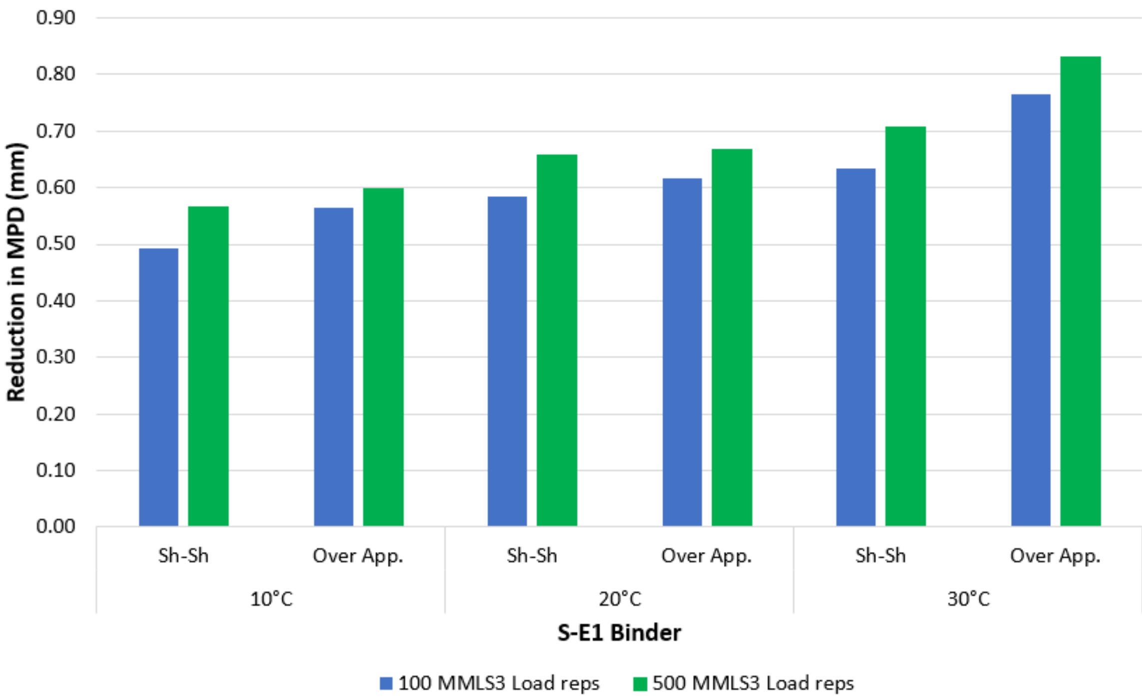

Figure 5.27: Reduction in MPD (mm) during Phase 1 for the S-E1 binder

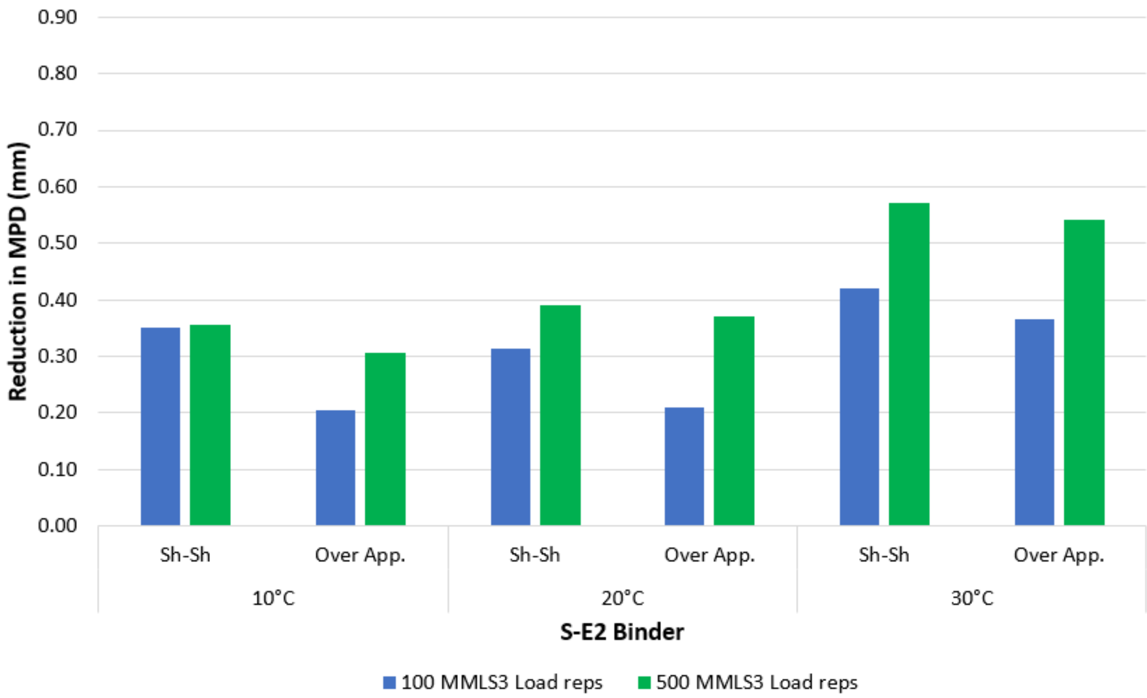

Figure 5.28: Reduction in MPD (mm) during Phase 1 for the S-E2 binder

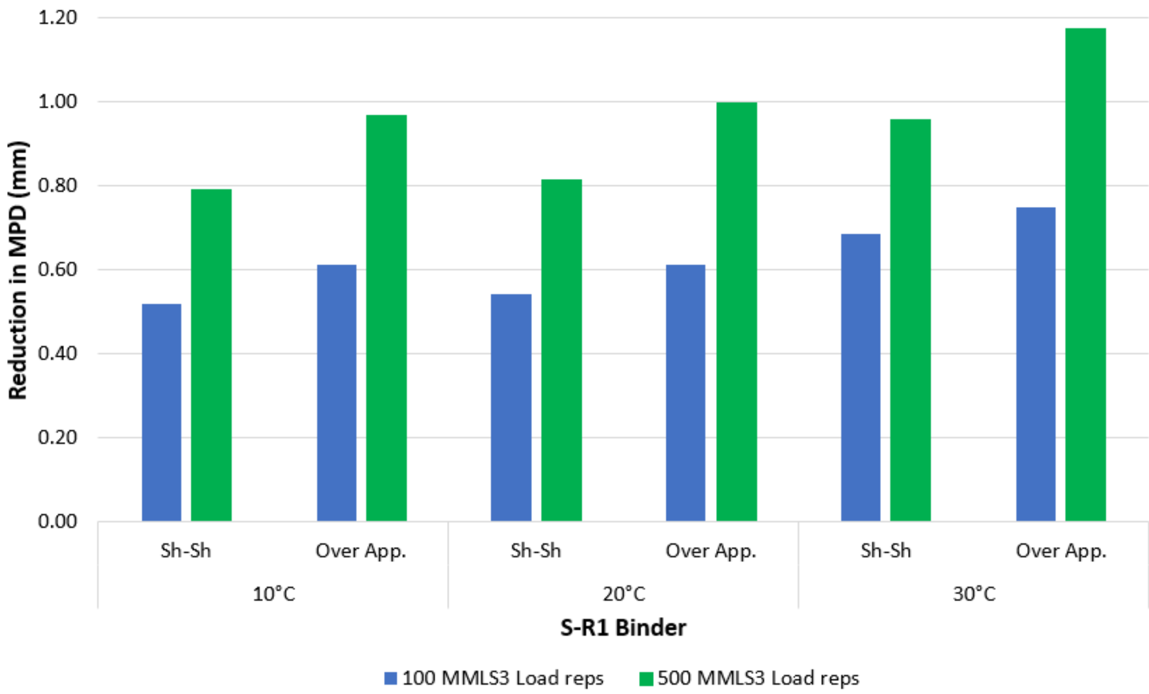

Figure 5.29: Reduction in MPD (mm) during Phase 1 for the S-R1 binder

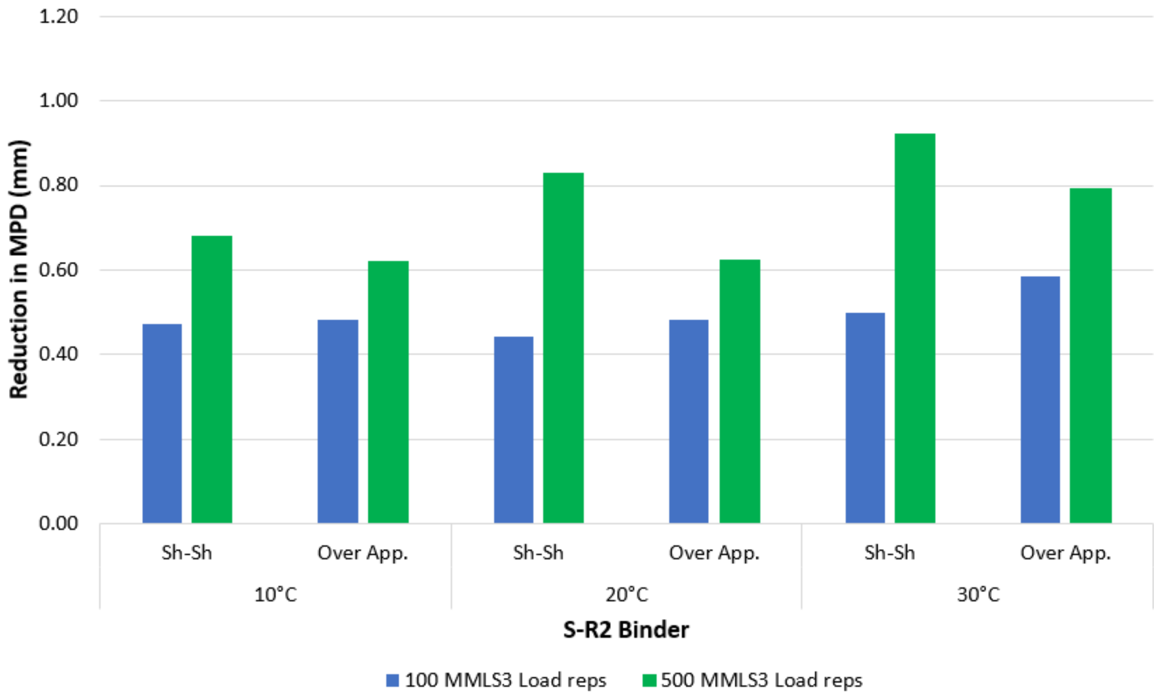

Figure 5.30: Reduction in MPD (mm) during Phase 1 for the S-R2 binder

5.5.2.2 Phase 2 and Phase 3: Steady State

Evaluating the reduction in MPD during Phase 2 and Phase 3 of Steady State, it is evident, as shown in Figure 5.31 - Figure 5.34, that with an increase in MMLS3 load repetitions and an increase in trafficking temperature, the reduction in MPD becomes greater. Furthermore, Figure 5.31 - Figure 5.34 shows that the MPD loss at 10°C and 20°C follow a gradual reduction whilst there is a subsequent greater reduction at 30°C. From the decreasing trends, as shown in Figure 5.23 - Figure 5.26 with support from Figure 5.31 - Figure 5.34, it is evident that the sh-sh aggregate spread rate indicates a greater reduction in MPD when compared to its over application counterpart at the same trafficking temperature. Comparing the binders, it is apparent that over the three trafficking temperatures, the S-E1 binder, including both the sh-sh and over application aggregate matrix, generally experiences a greater reduction in MPD when compared to the S-E2 binder. In comparison, it is evident that there is no significant difference between the sh-sh aggregate matrices of the S-R1 and S-R2 binders whereas the over application matrix, for the S-R1 binder, indicates a greater reduction at all trafficking temperatures.

Table 5.4: Reduction in MPD (mm) after 5000 MMLS3 load repetitions

	Aggregate Configuration	S-E1	S-E2	S-R1	S-R2
10°C	**Sh-Sh**	0.90	0.58	0.94	0.88
	Over Application	0.92	0.54	1.08	0.86
20°C	**Sh-Sh**	1.04	0.69	1.11	1.18
	Over Application	1.01	0.79	1.16	0.95
30°C	**Sh-Sh**	1.41	1.20	1.43	1.41
	Over Application	1.20	1.13	1.57	1.43

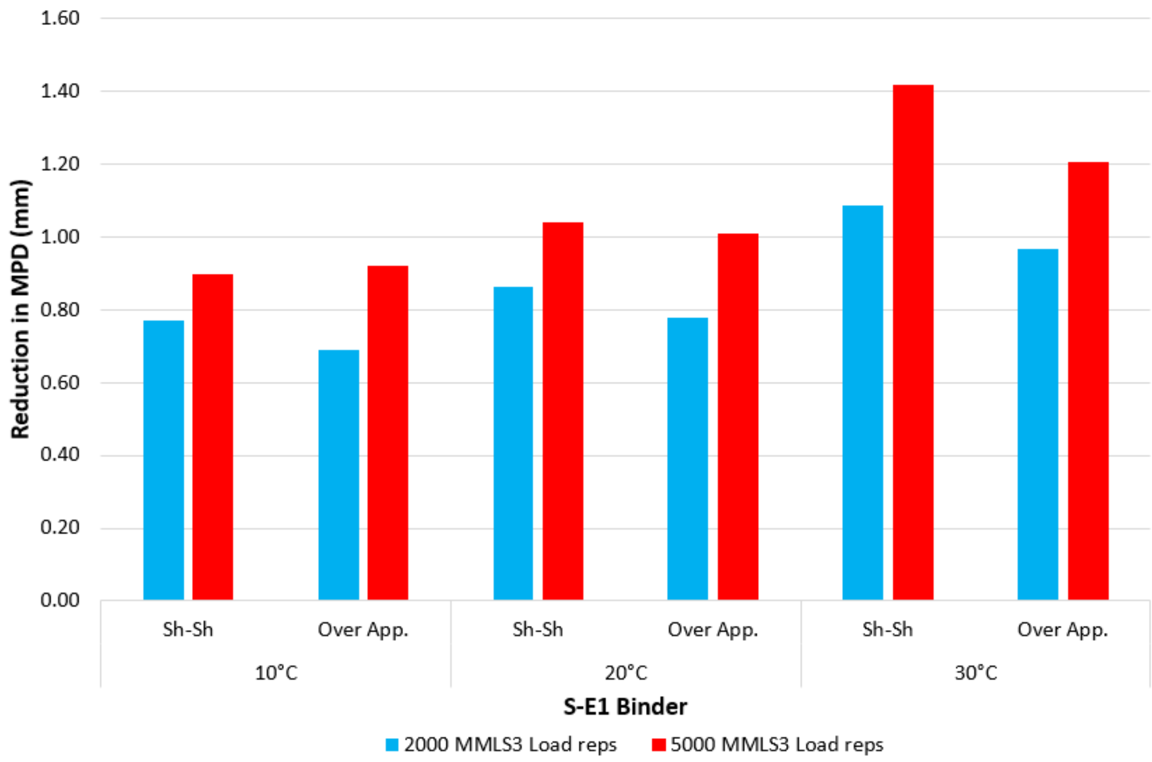

Figure 5.31: Reduction in MPD (mm) during Phase 2 and Phase 3 for the S-E1 binder

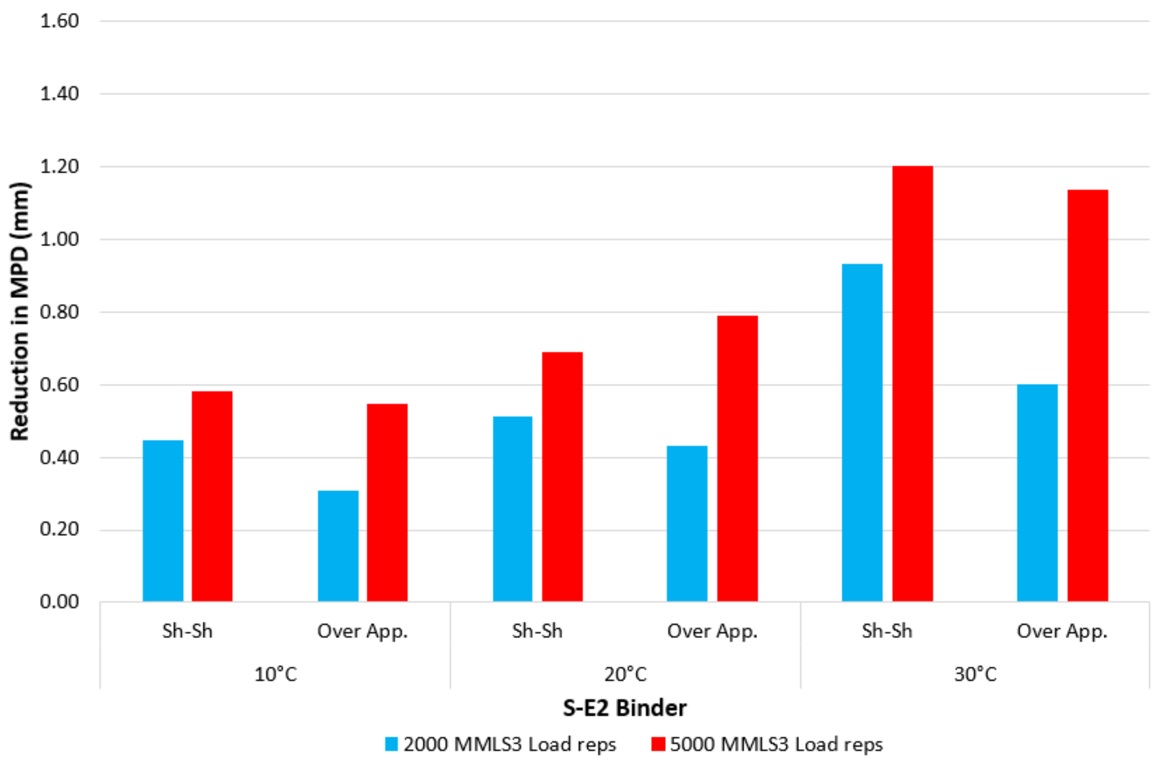

Figure 5.32: Reduction in MPD (mm) during Phase 2 and Phase 3 for the S-E2 binder

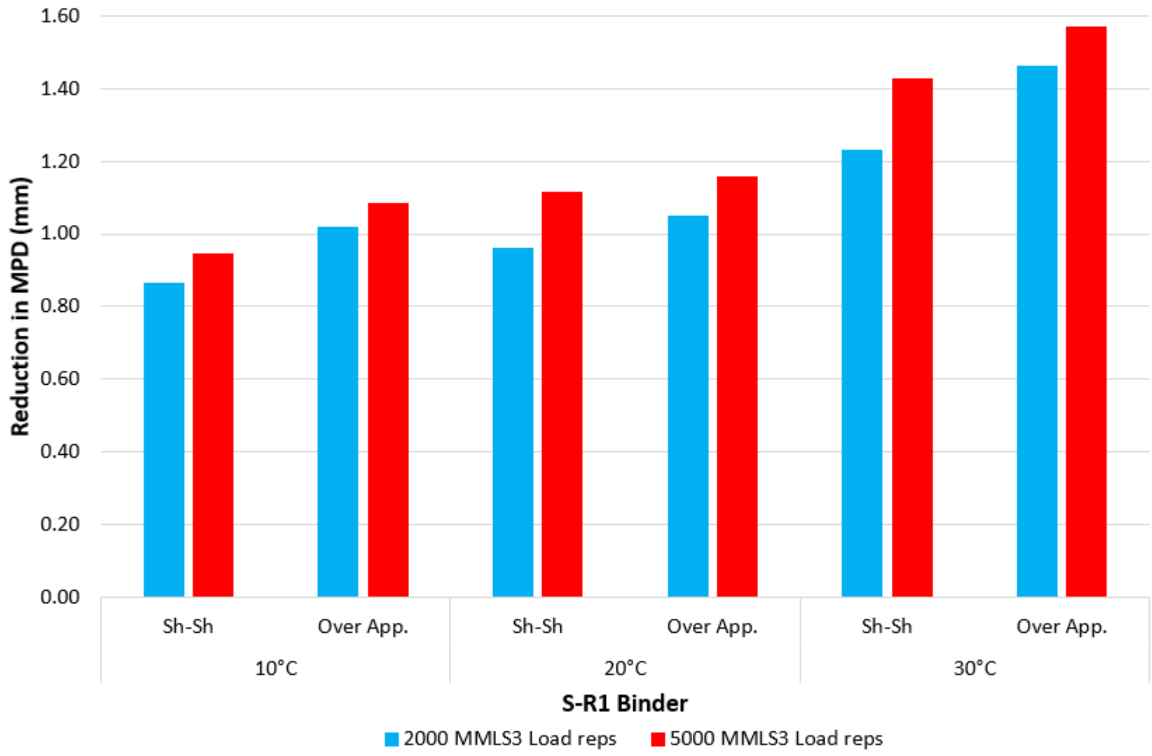

Figure 5.33: Reduction in MPD (mm) during Phase 2 and Phase 3 for the S-R1 binder

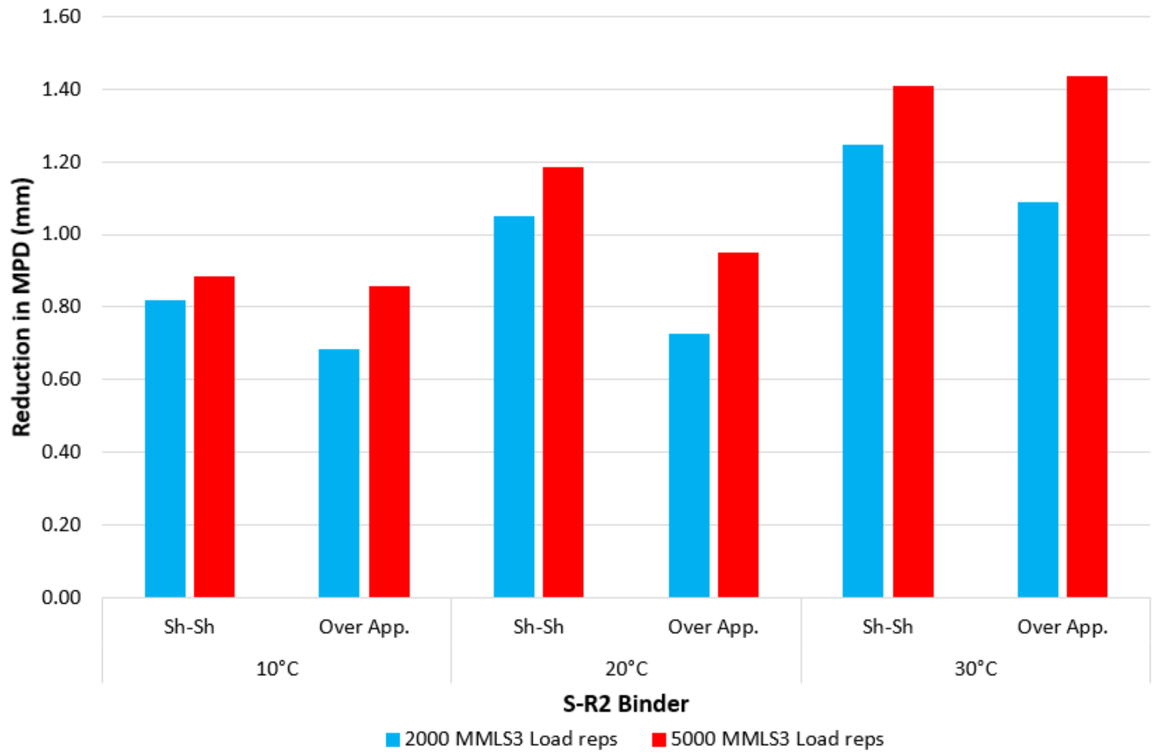

Figure 5.34: Reduction in MPD (mm) during Phase 2 and Phase 3 for the S-R2 binder

5.5.3 Rate of Change in Mean Profile Depth

The rate of change in MPD, as discussed in the following subsections, during the longer trafficking phases of the Steady State, is summarised in Table D.36 in Appendix D.5.

5.5.3.1 Phase 2: Steady State

From the rate of change results during Phase 2 trafficking, as plotted for the elastomers in Figure 5.35, it is evident that the sh-sh aggregate matrices show a higher rate of MPD loss when compared to the over application matrices. With an increase in trafficking temperature, variability is apparent for the S-E2 binder as the over application matrices show higher rates of change at 20°C whilst the initial trend continues in that the sh-sh matrices, at a trafficking temperature of 30°C, experience a higher rate of change. Furthermore, with an increase in trafficking temperature, there is also an increase in the rate of MPD loss for the elastomer binders.

From the rate of change in MPD evaluation, for the rubber binders, as graphically presented in Figure 5.36, it is apparent that an increase in trafficking temperature corresponds to an increase in the rate of MPD loss for both aggregate matrices. Furthermore, the trend shows that the sh-sh aggregate matrices experience higher rates of MPD loss whilst an increase in trafficking temperature, to 30°C, shows that the over application matrix, for the S-R1 binder, yields a higher rate of MPD loss. Furthermore, the S-R2 binder shows higher rates of MPD loss at all trafficking temperatures and for all aggregate matrices in comparison with the S-R1 binder.

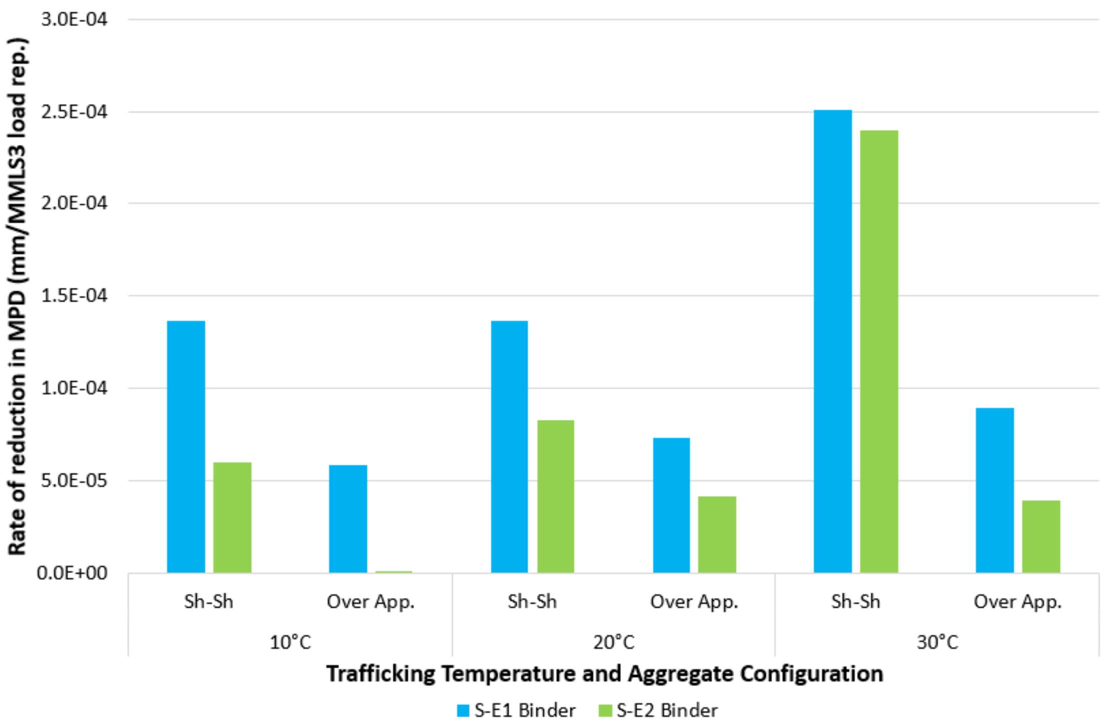

Figure 5.35: Rate of change (mm/MMLS3 load rep.) in MPD during Phase 2 for the S-E1 and S-E2 binders

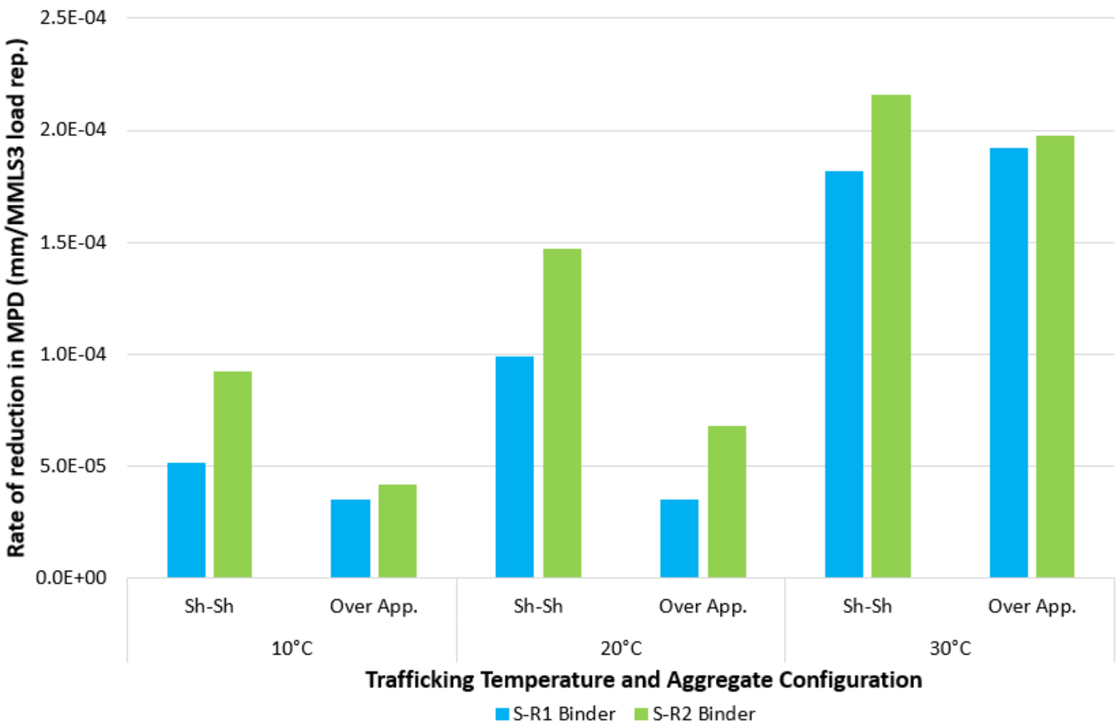

Figure 5.36: Rate of change (mm/MMLS3 load rep.) in MPD during Phase 2 for the S-R1 and S-R2 binders

5.5.3.2 Phase 3: Steady State

During the Phase 3 trafficking period of Steady State, as shown for the S-E1 binder in Figure 5.37, it is evident that a greater rate of MPD loss is shown for the over application matrix at colder temperatures whilst the trend continues in that an increase in trafficking temperature relates to higher rates of MPD loss for the over application matrix. The S-E2 over application matrix shows a higher rate of MPD loss when compared to its sh-sh counterpart over all trafficking temperatures. It is apparent when comparing the rate of change in MPD between the S-E1 and S-E2 binder, that similar rates are experienced during the 10°C trafficking period with an increase in trafficking temperature relating to an increase in variability.

Evaluating the rate of change in MPD during Phase 3 for the S-R1 binder, as shown in Figure 5.38, it is evident that the sh-sh aggregate matrix experiences a higher rate of MPD loss when compared to its over application matrix over all trafficking temperatures. In contrast, the S-R2 binder shows that the over application aggregate matrix indicates, similar to the elastomers, a higher rate of MPD loss compared to its sh-sh matrix over all trafficking temperatures.

In general, there is variability in the rate of change in MPD when comparing the rubber binders. With an increase in trafficking temperature, there is a general increase in the rate of change of MPD.

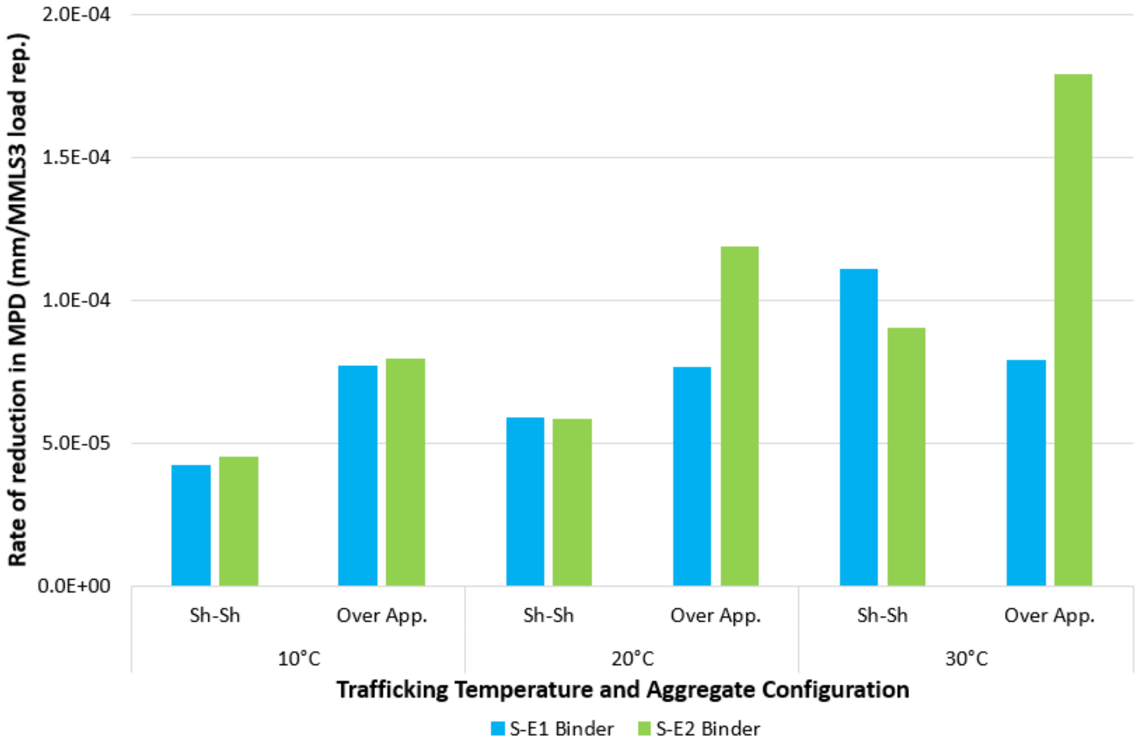

Figure 5.37: Rate of change (mm/MMLS3 load rep.) in MPD during Phase 3 for the S-E1 and S-E2 binders

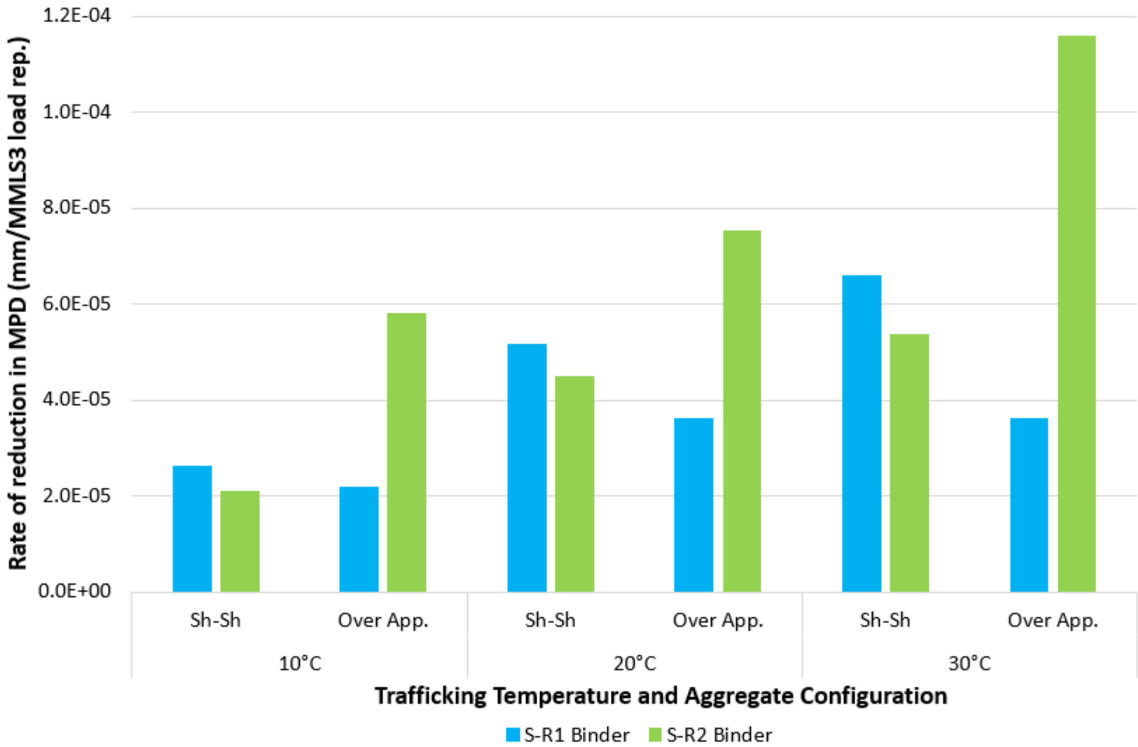

Figure 5.38: Rate of change (mm/MMLS3 load rep.) in MPD during Phase 3 for the S-R1 and S-R2 binders

5.5.4 Binder Comparison

The evaluation of the reduction in MPD, for each binder and aggregate matrix, is done after the Shakedown period (Phase 1) and the initial and final stages of the Steady State period (Phase 2 and Phase 3). In that, due to the short trafficking period during Phase 1, the reduction in MPD is related to the MPD loss (mm) whilst the reduction in MPD after Phase 2 and Phase 3 is analysed according to both the MPD loss (mm) and the rate of change in MPD for potential extrapolation purposes.

5.5.4.1 Phase 1: Shakedown

Comparing the different hot modified binders, as per the reduction in MPD for the sh-sh aggregate matrices after Phase 1, as graphically shown in Figure 5.39, it is apparent that both rubber binders, over all trafficking periods, experience a greater reduction in MPD when compared to the elastomers. Furthermore, there is an indication that the S-R1 and the S-R2 binders indicate similar reductions in MPD whilst the S-E1 binder shows a greater reduction when compared to the S-E2 sh-sh matrix.

Similar to the occurrence for the sh-sh aggregate matrices after 500 MMLS3 load repetitions, the S-R1 over application matrix shows a greater reduction in MPD when compared to the other binders as shown in Figure 5.40. This is applicable at all trafficking temperatures, with the 30°C temperature indicating the greatest reduction in MPD. Furthermore, the S-R2 over application matrix shows consistency between 10°C - 20°C in that the reduction in MPD is similar whilst there is an increase at 30°C. Furthermore, the S-E1, at all trafficking temperatures, similar to the occurrence for the sh-sh aggregate matrices, shows a greater loss in MPD when compared to the S-E2 binder.

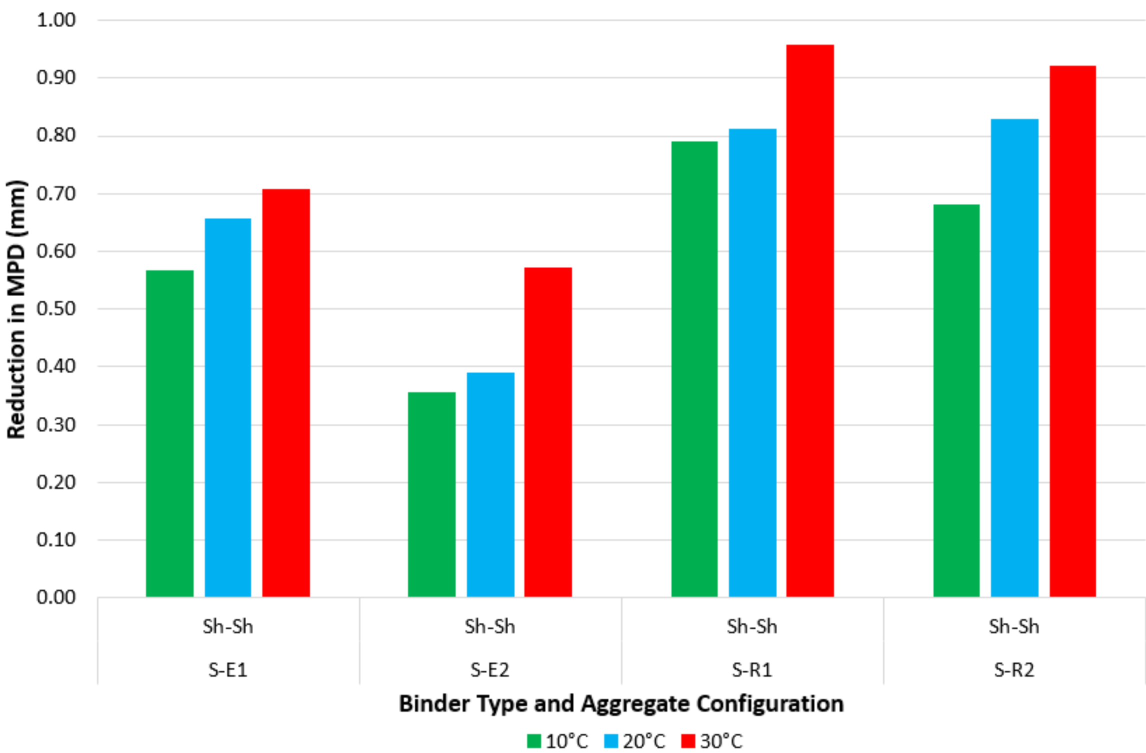

Figure 5.39: Reduction in MPD (mm) after Phase 1 for sh-sh aggregate matrices

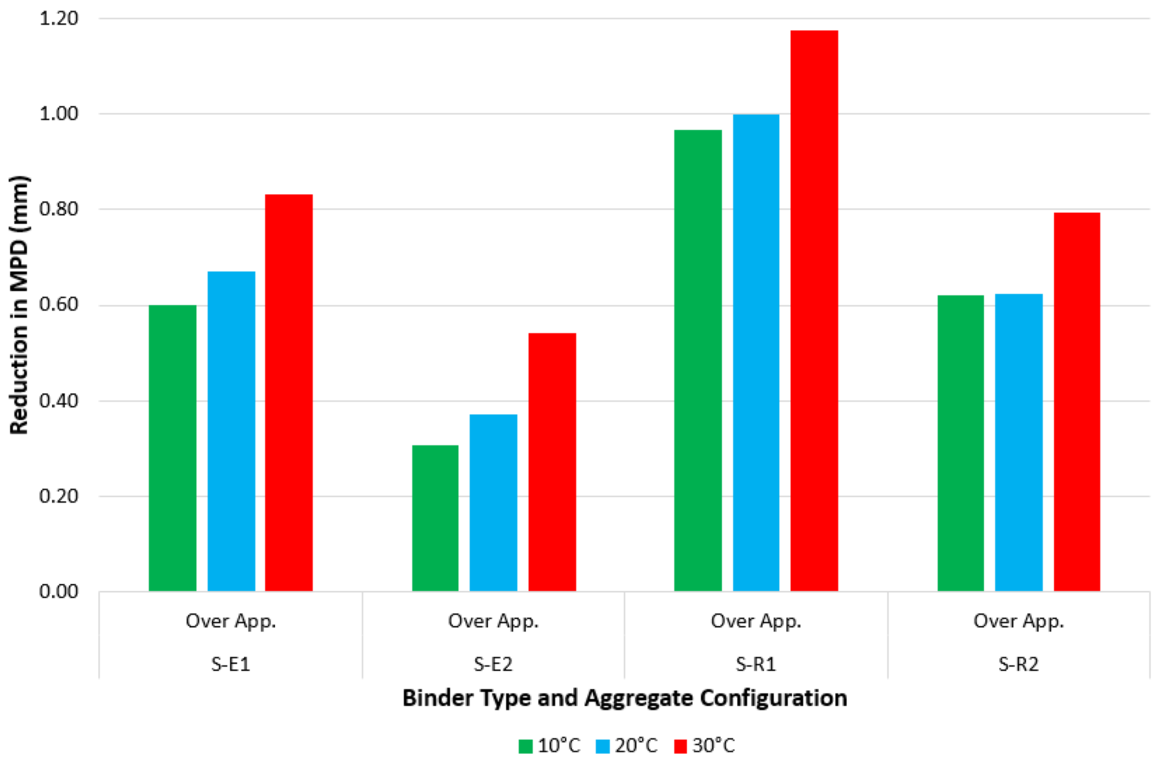

Figure 5.40: Reduction in MPD (mm) after Phase 1 for over application aggregate matrices

5.5.4.2 Phase 2: Steady State

From the analysis of the reduction in MPD (mm), as indicated by the sh-sh aggregate matrices after Phase 2 trafficking, it is apparent that the rubber binders experience a greater loss in MPD when compared to the elastomer binders, especially for the intermediate and elevated trafficking temperatures of 20°C and 30°C. Furthermore, all binders experience similar reductions in MPD at 10°C, whilst the S-E2 binder indicates a lower MPD loss at all trafficking temperatures.

With an increase in load repetitions, as shown for the rate of reduction in MPD (mm/MMLS3 load rep.) for the sh-sh aggregate matrices in Figure 5.42, there is an increase in rate of reduction in MPD. It is apparent that the elastomer binders show higher rates of reduction in MPD when compared to the rubber binders at 30°C.

Evaluating the reduction in MPD (mm) for the over application aggregate matrices, as seen in Figure 5.43, it is evident that the rubber binders show greater reductions in MPD when compared to the elastomers at elevated trafficking temperatures. In particular, the S-R1 over application matrix indicates the greatest loss in MPD, over all trafficking temperatures, whilst the S-E2 binder yields the lowest reduction in MPD.

Furthermore, the analysis of the rate of change in MPD (mm/MMLS3 load rep.) for the over application matrices yields that with an increase in trafficking temperature, there is an increase in the rate of reduction in MPD. As a general trend, both rubber binders show a higher rate of MPD loss at 30°C, whilst all binders experience lower rates of reduction in MPD at colder and intermediate temperatures.

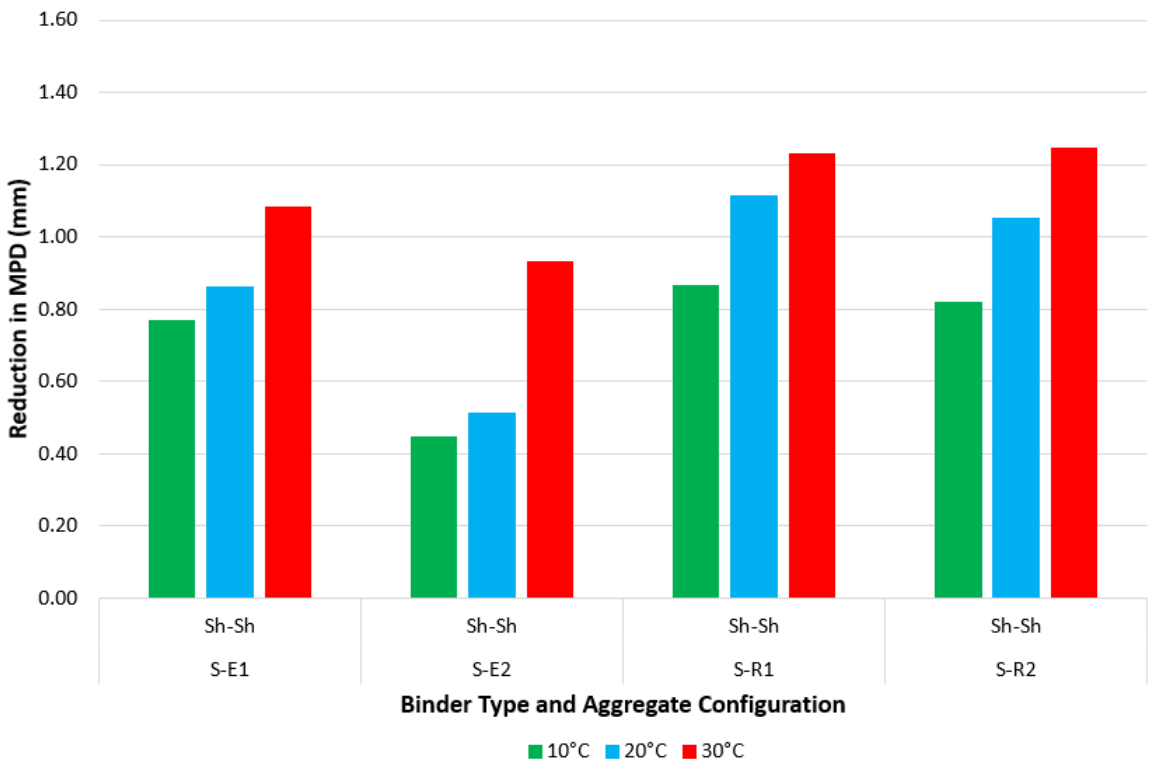

Figure 5.41: Reduction in MPD (mm) after Phase 2 for sh-sh aggregate matrices

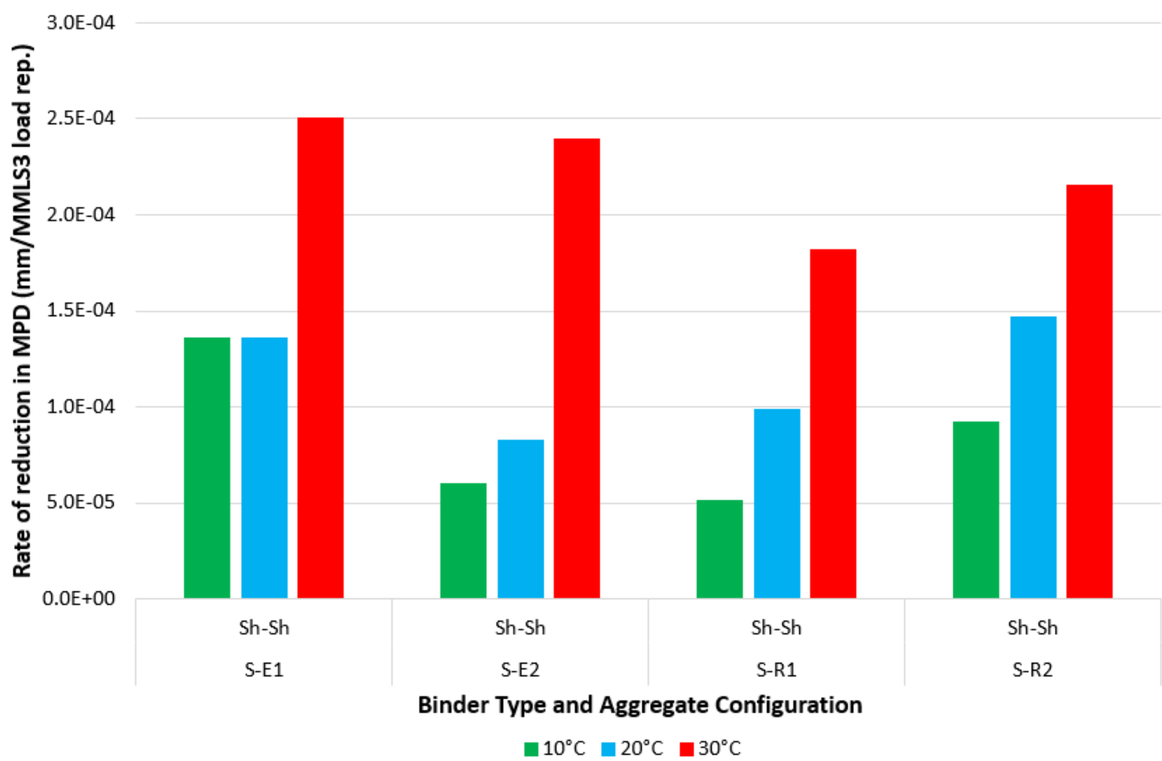

Figure 5.42: Rate of change (mm/MMLS3 load rep.) during Phase 2 for sh-sh aggregate matrices

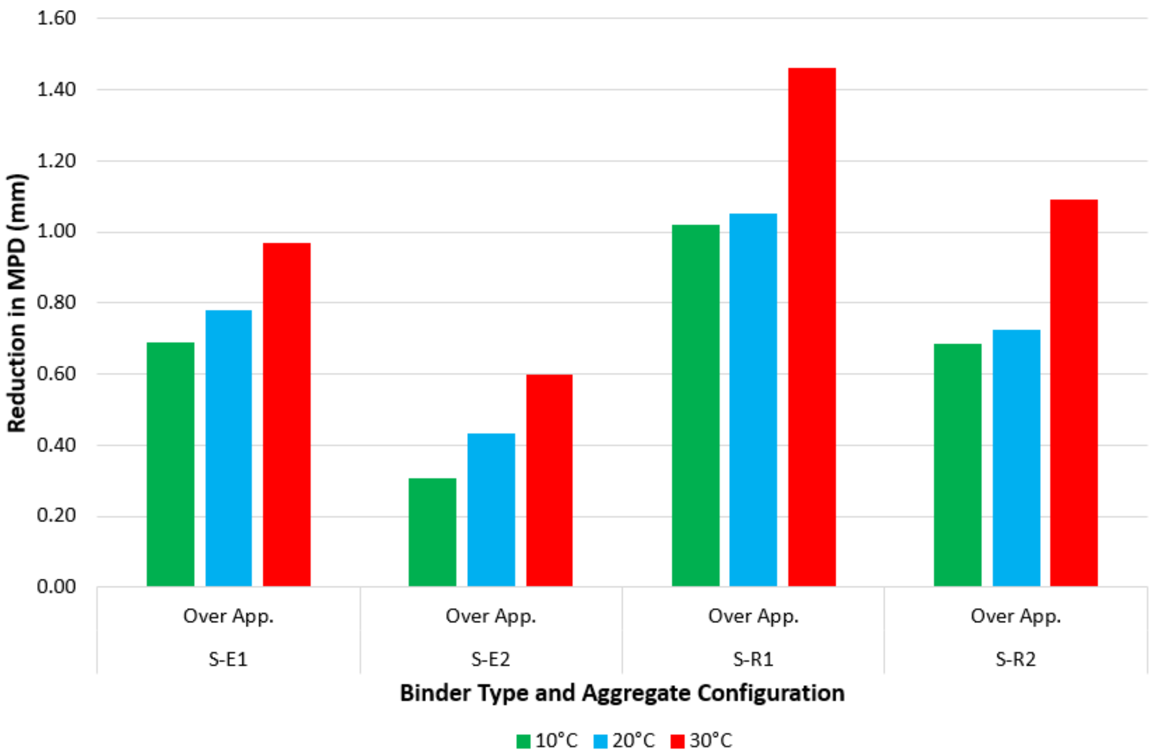

Figure 5.43: Reduction in MPD (mm) after Phase 2 for over application aggregate matrices

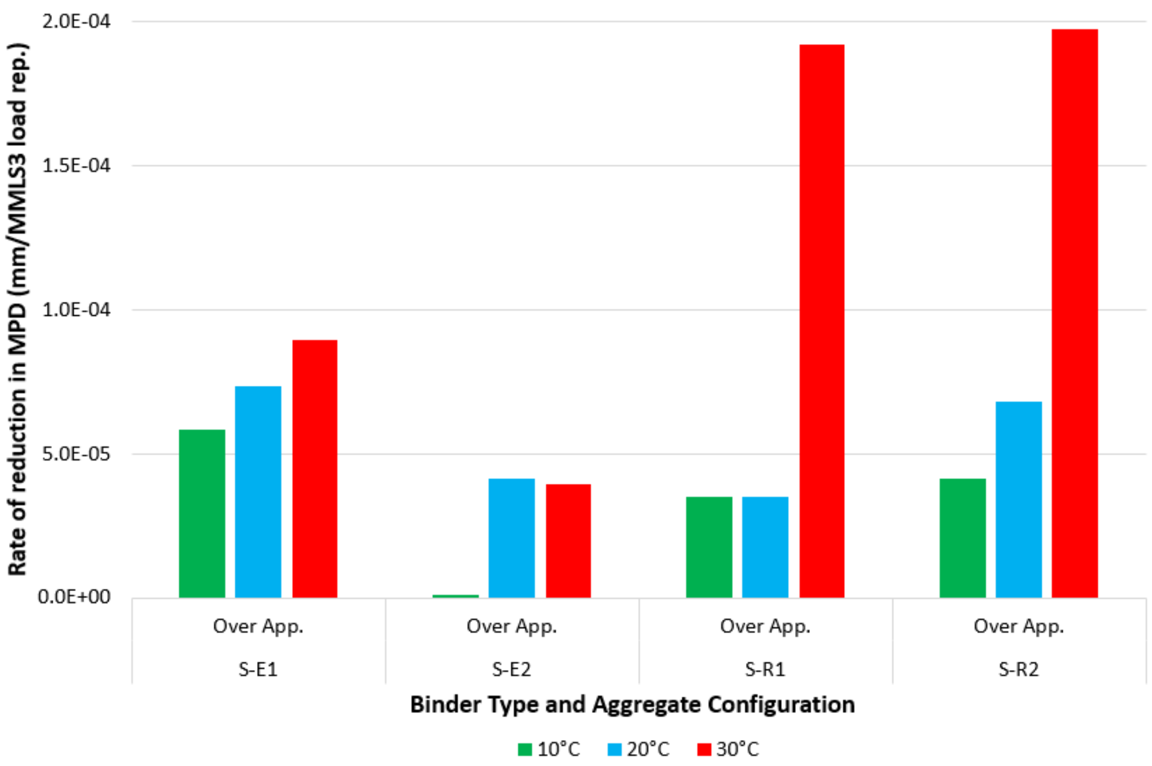

Figure 5.44: Rate of change (mm/MMLS3 load rep.) during Phase 2 for over application aggregate matrices

5.5.4.3 Phase 3: Steady State

Analysing the reduction in MPD (mm) during Phase 3, as shown for the sh-sh aggregate matrices in Figure 5.45, it is evident that after 5000 MMLS3 load repetitions, the rubber binders experience similar reductions in MPD (mm) over all trafficking temperatures whilst the S-E1 sh-sh matrix shows a similar reduction at 30°C with slightly less MPD loss at 20°C trafficking. Furthermore, the S-E2 binder shows the lowest reduction in MPD over all trafficking temperatures.

Evaluating the rate of change in MPD (mm/MMLS3 load rep.) for the sh-sh aggregate matrices, as shown in Figure 5.46, it is apparent that the elastomer binders show a higher rate of change during Phase 3 in comparison to the rubber binders, with the S-E1 binder indicating the highest rate of MPD loss at the elevated trafficking temperature of 30°C. Furthermore, the elastomer binders experience similar rates of MPD loss at 10°C and 20°C whilst the same trend is seen for both the S-R1 and the S-R2 rubber binders at the colder and intermediate temperatures. Both rubber binders, at the 10°C trafficking temperature, indicate lower rates of MPD loss when compared to the elastomer binders. With an increase in trafficking temperature, there is an increase in the rate of reduction in MPD for all sh-sh binders.

Analysing the over application matrices and in particular the reduction in MPD (mm) as presented in Figure 5.47, it is apparent that the rubber binders, S-R1 and S-R2, experience greater reductions in MPD at the elevated trafficking temperature of 30°C when compared to the elastomer binders. In general, the S-E1 over application matrix produces a reduction in MPD that is greater than that of the S-E2 binder at the colder and intermediate trafficking temperature whilst both elastomer binders experience similar reductions at the elevated temperature of 30°C.

From the evaluation of the rate of change in MPD (mm/MMLS3 load rep.) for the over application aggregate matrices, as graphically shown in Figure 5.48, there is an indication that the level of variability increases with an increase in trafficking temperature for all binders. Furthermore, it is apparent that with an increase in trafficking temperature, there is an increase in the rate of reduction in MPD for all binders. The S-R1 rubber binder, in general, produces the lowest rate of MPD loss when compared to all other binders whilst the S-E2 binder indicates the highest rate of reduction in MPD. It is prominent that the rate of change in MPD is similar for the S-E1 and S-R1 binders, over all trafficking periods.

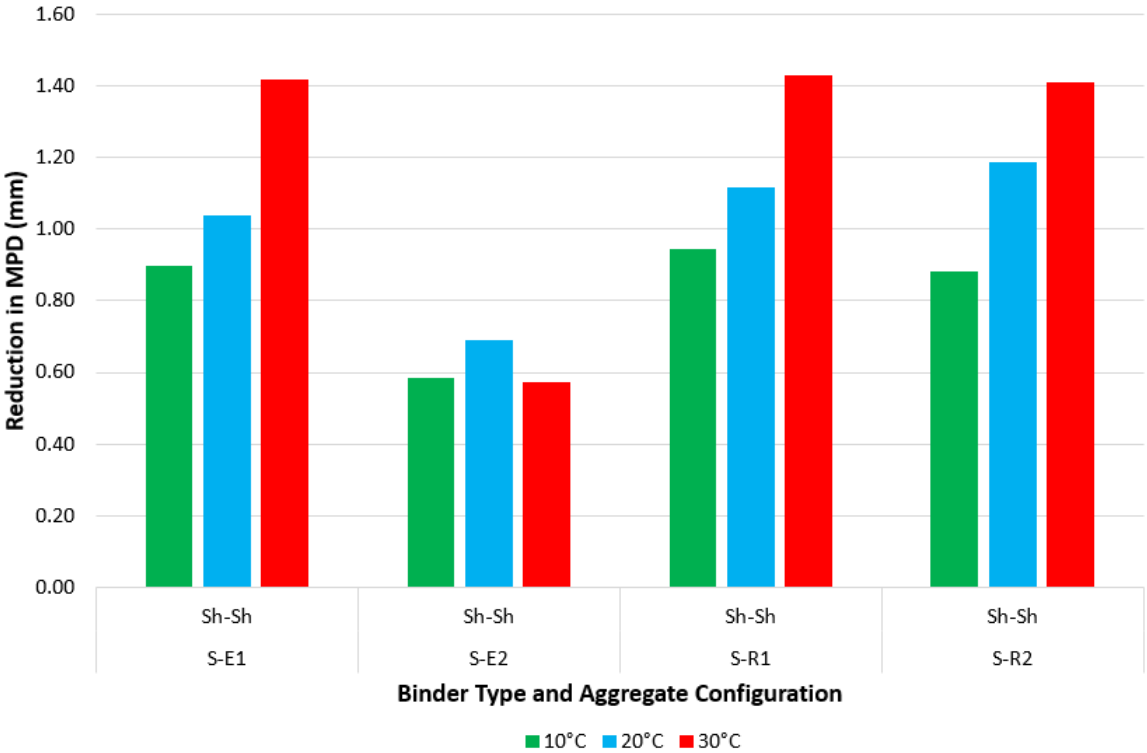

Figure 5.45: Reduction in MPD (mm) after Phase 3 for sh-sh aggregate matrices

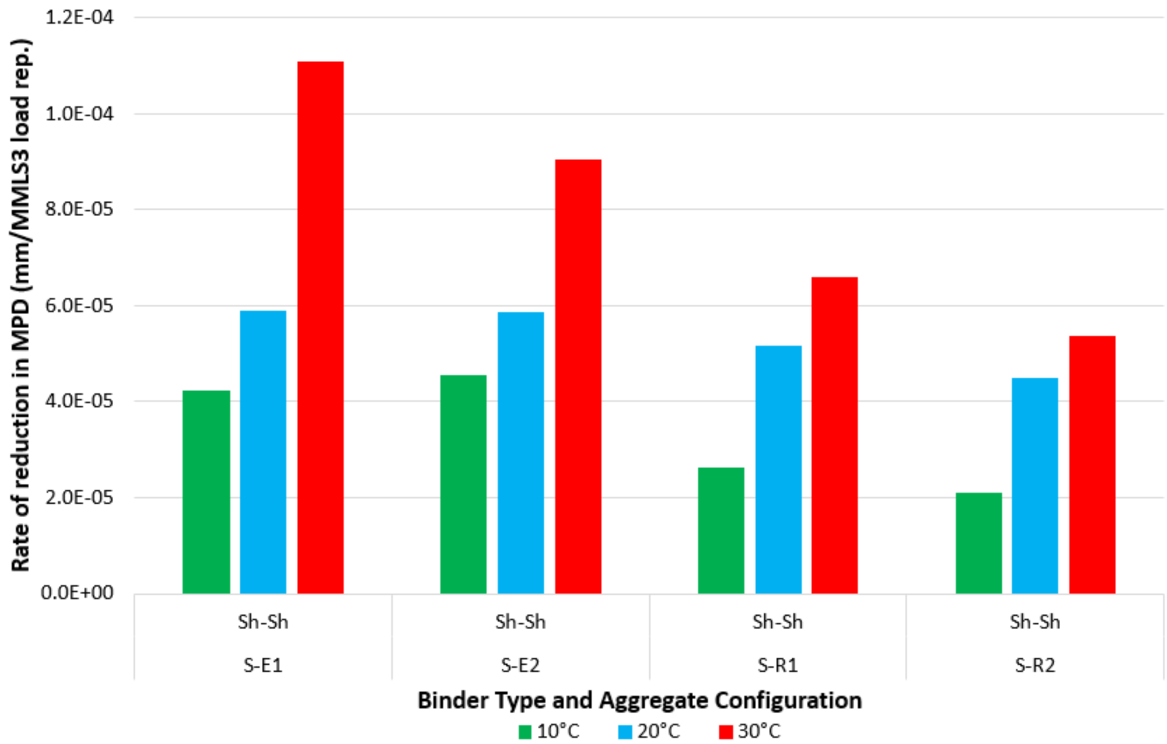

Figure 5.46: Rate of change (mm/MMLS3 load rep.) during Phase 3 for sh-sh aggregate matrices

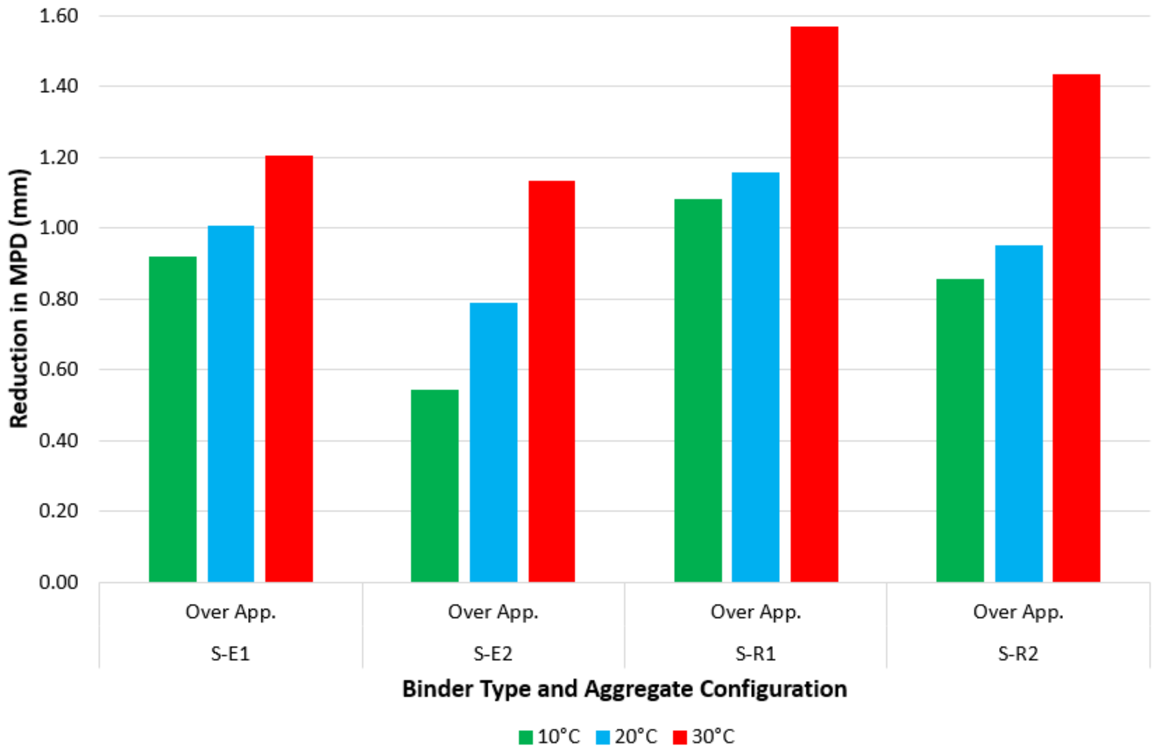

Figure 5.47: Reduction in MPD (mm) after Phase 3 for over application aggregate matrices

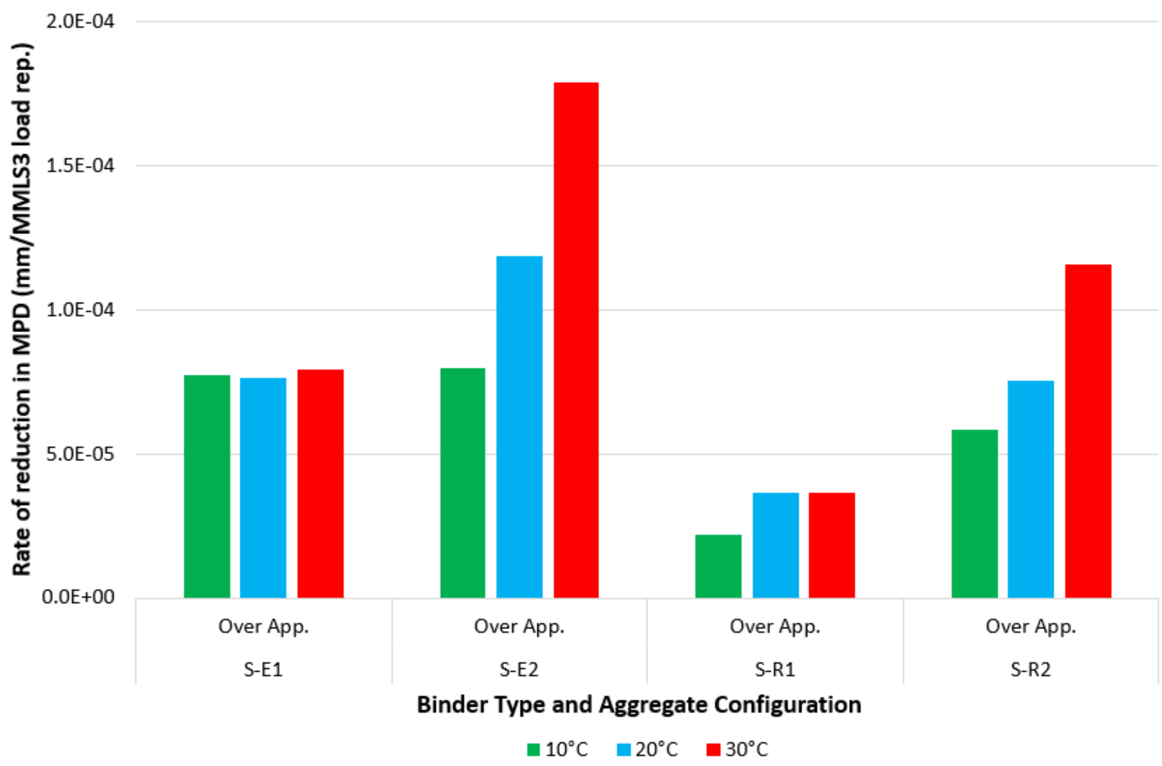

Figure 5.48: Rate of change (mm/MMLS3 load rep.) during Phase 3 for over application aggregate matrices

5.5.5 Depth Summary

Table 5.5, Table 5.6 and Table 5.7 show a summary of the depth analysis results.

Table 5.5: Summary of the reduction in MPD (mm)

Traffic Interval	Reduction in MPD (%)	Trafficking Temperature
Phase 1: 500	>45% for elastomers >55% for rubbers	Variation in reduction in MPD (mm) between sh-sh and over application aggregate matrices.
Phase 2: 2000	>75% for sh-sh elastomers >55% for over app. elastomer >88% for sh-sh rubbers >77% for over app. rubbers	Greater reduction for sh-sh with an increase in trafficking temperature compared to the over application.
Phase 3: 5000		Greater reduction for sh-sh with an increase in trafficking temperature compared to the over application.

Table 5.6: Summary of the rate of change in MPD (mm/MMLS3 load rep.)

Traffic Interval	Aggregate Configuration	Trafficking Temperature
Phase 2: 500 - 2000	Elastomers - S-E1 and S-E2: Sh-Sh aggregate matrices show higher rates of MPD loss. Rubbers - S-R1 and S-R2: Sh-Sh aggregate matrices show higher rates of MPD loss.	Elastomers - S-E1 and S-E2: Increase in trafficking temperature results in an increase in the rate of reduction in MPD. Rubbers - S-R1 and S-R2: Increase in trafficking temperature results in an increase in the rate of reduction in MPD.
Phase 3: 2000 - 5000	Elastomers - S-E1 and S-E2: Over application matrix show a higher rate of reduction in MPD. Rubbers - S-R1 and S-R2: Higher rate of reduction in MPD for S-R1 sh-sh whilst higher rate of reduction in MPD for S-R2 over application matrix.	Elastomers - S-E1 and S-E2: Increase in trafficking temperature results in an increase in the rate of reduction in MPD. Rubbers - S-R1 and S-R2: Increase in trafficking temperature results in an increase in the rate of reduction in MPD.

Table 5.7: Summary of the binder comparison results

Traffic Interval	Decrease in MPD (mm)	Rate of Change in MPD (mm/MMLS3 load rep.)
Phase 1: 500	Greater decrease for sh-sh and over application rubber matrices.	Too little trafficking for representative capturing.
Phase 2: 2000	Greater decrease for sh-sh rubber binders with increases in trafficking temperatures. S-E2 binder continues to produce the lowest decrease in MPD.	Elastomers (sh-sh) yield higher rates of reduction in MPD at elevated trafficking temperatures. S-R2 (sh-sh) indicates high rate of reduction at intermediate trafficking temperature. Rubber binders show higher rate of reduction in MPD at elevated trafficking for over applied matrices.
Phase 3: 5000	Similar decreases in MPD for the sh-sh rubber binders with variation in the elastomers. The S-E2 sh-sh indicates the lowest reduction in MPD. Over application rubber binders indicate greater reductions in MPD at elevated trafficking temperatures.	Higher rate of reduction in MPD for elastomer sh-sh matrices over all trafficking temperatures. temperatures.

5.6 Visual Analysis

5.6.1 Wheel Path Analysis

5.6.1.1 Shoulder-to-Shoulder Aggregate Matrix

In the S-E1 sh-sh aggregate matrix, at a slice of x = 141 mm in the wheel path, as seen in Figure 5.49, it is seeming that between the distances y = 100 mm and y = 105 mm, there is a reduction in depth over the 15000 MMLS3 load repetitions with little to no visual horizontal displacement. Furthermore, between y = 110 mm and y = 113 mm, the peak experiences a reduction in depth up to 10000 MMLS3 load repetitions after which there is a forward displacement and downwards movement, as seen after 15000 MMLS3 load repetitions. An extended analysis of the S-E1 sh-sh matrix, between the distances y = 265 mm and y = 268 mm, as shown in Figure 5.50, indicates that initially there is a reduction in depth after 10000 MMLS3 load repetitions, after which horizontal movement occurs in the direction of trafficking, as experienced after 15000 MMLS3 load repetitions.

An analysis of the sh-sh aggregate matrix for the rubber binder, S-R1, as seen in Figure 5.51, shows that between the distances y = 74 mm and y = 76 mm, there is a similar reduction in depth followed by a horizontal movement as indicated after 15000 MMLS3 load repetitions. Between the distances y = 238 mm and y = 242 mm, as seen for the S-R1 binder in Figure 5.52, it is evident that a horizontal and rotation movement occurs with an increase in MMLS3 load repetitions.

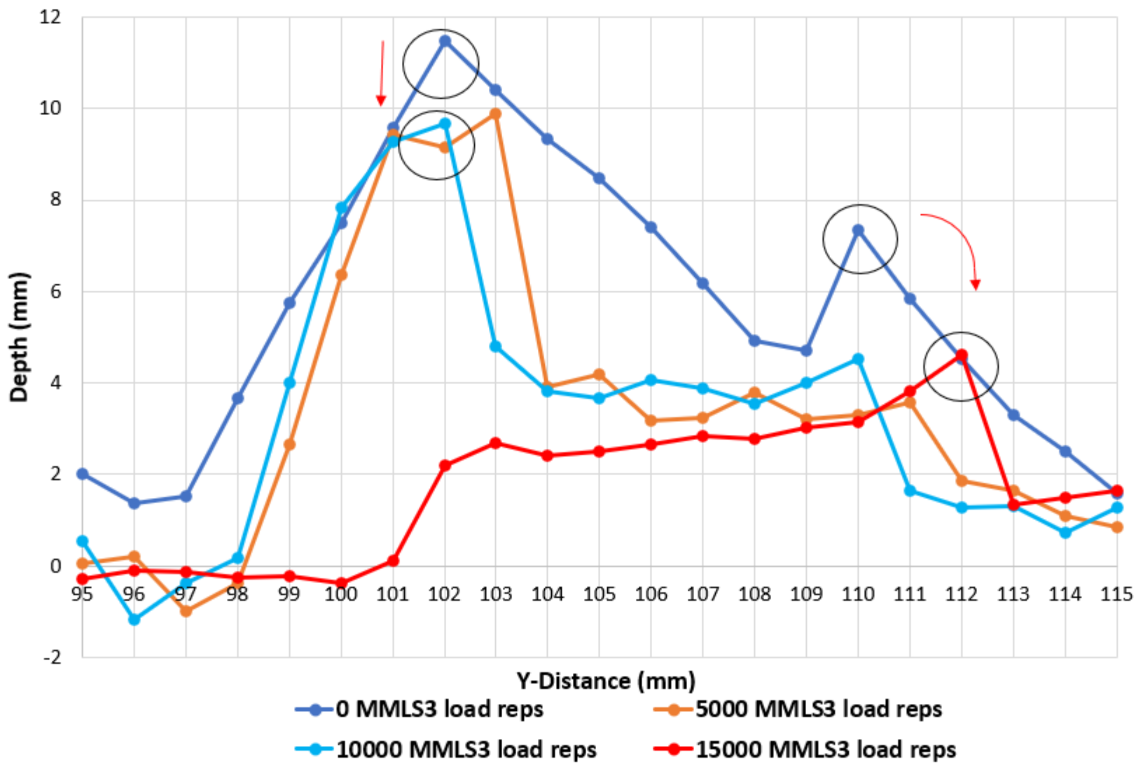

Figure 5.49: Movement of the aggregate in the S-E1 sh-sh matrix at x = 141mm

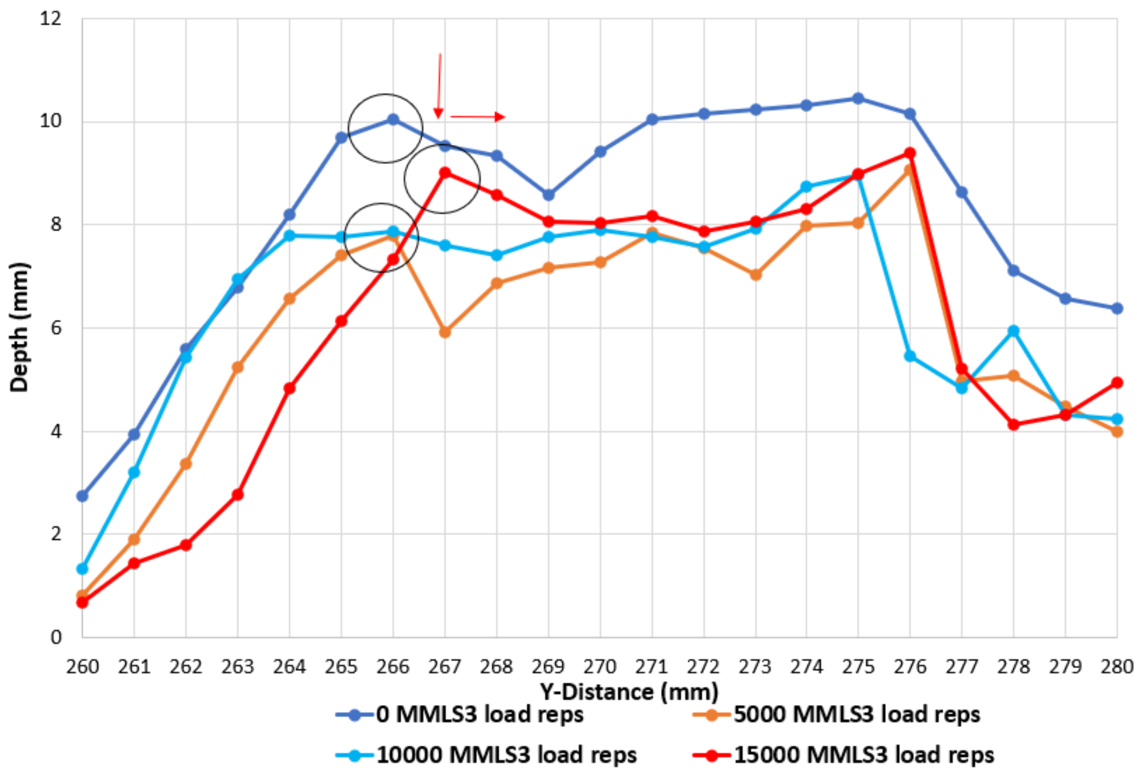

Figure 5.50: Movement of the aggregate in the S-E1 sh-sh matrix at x = 141 mm

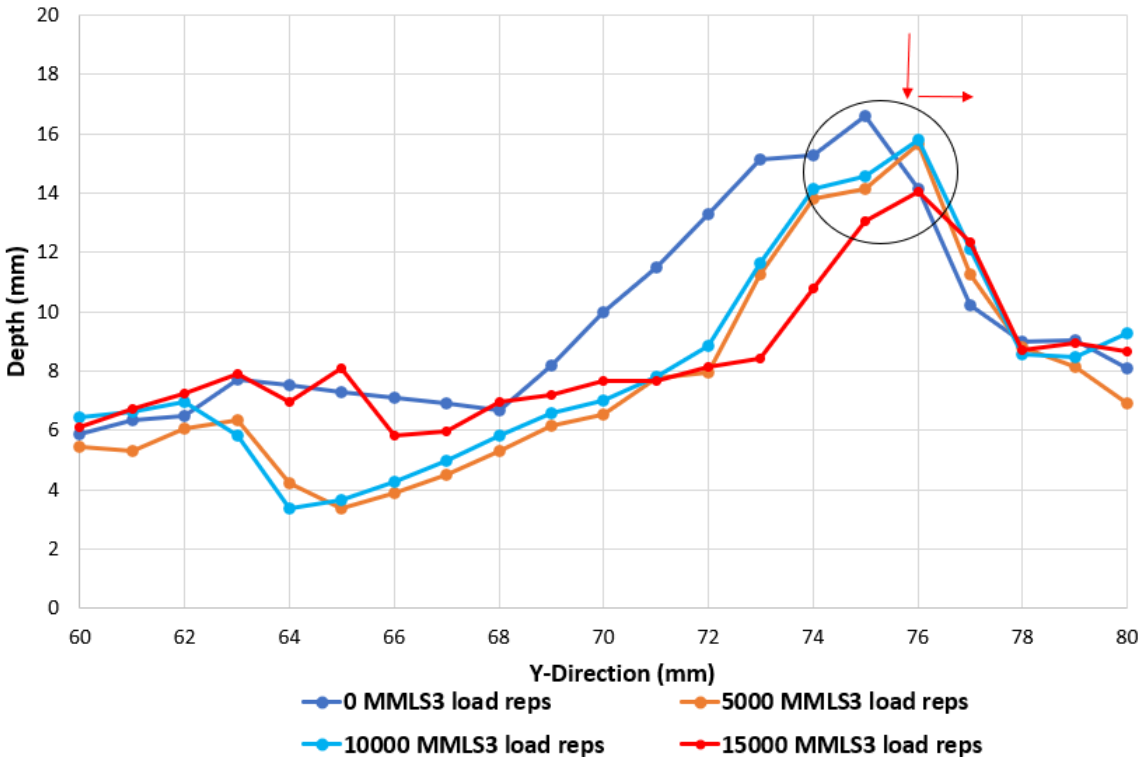

Figure 5.51: Movement of the aggregate in the S-R1 sh-sh matrix at x = 141mm

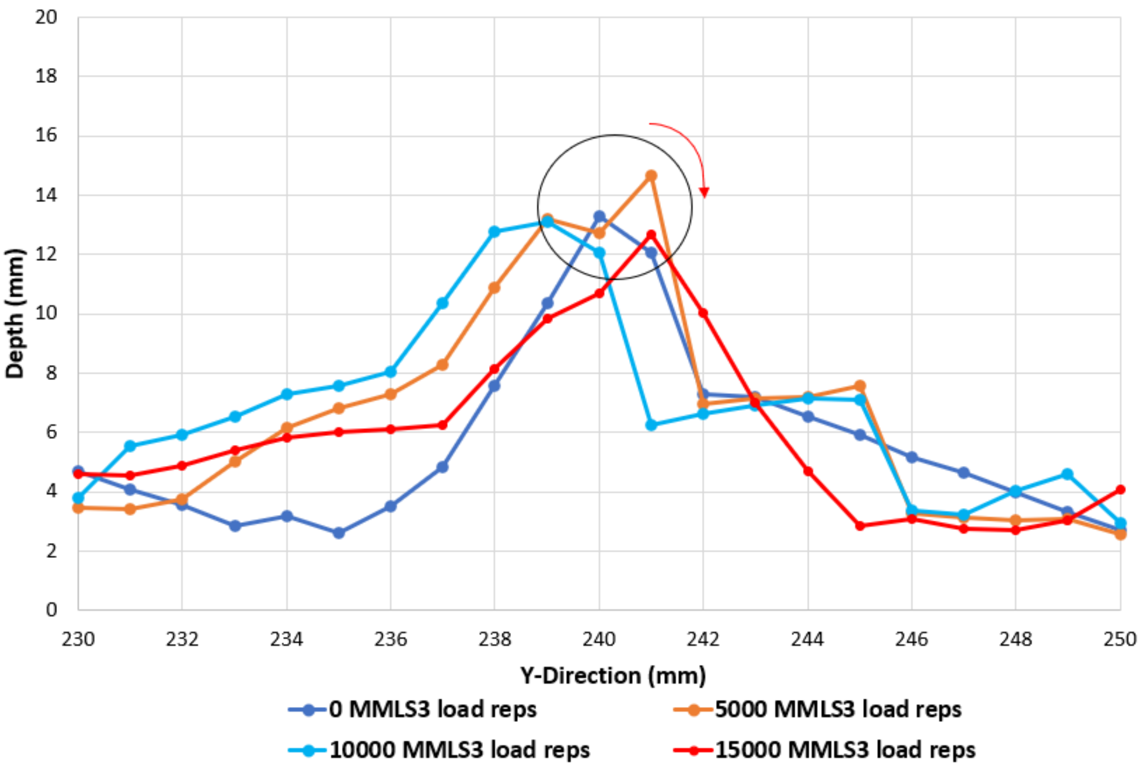

Figure 5.52: Movement of the aggregate in the S-R1 sh-sh matrix at x = 141 mm

5.6.1.2 Over Application Aggregate Matrix

Evaluating the over applications matrices at an x-slice distance of x = 141 mm, it is seen, as illustrated for the S-E1 binder in Figure 5.53, that between the distances y = 172 mm and y = 176 mm, there is a horizontal movement in the direction of trafficking with an increase in MMLS3 load repetitions. The shape of the profile, under evaluation, does not change and the peak position is similar in depth after 15000 MMLS3 load repetitions. Furthermore, there is no indication of a definite reduction in depth or rotation movement.

Evaluating the S-R1 over application aggregate matrix, as graphically shown in Figure 5.54, it is evident that between y = 45 mm and y = 48 mm, there is a definite reduction in depth with an increase in MMLS3 load repetitions. Furthermore, between the distances y = 53 mm and y = 57 mm, there is an increase in depth with an increase in MMLS3 load repetitions. The visual forming of a peak occurs after 5000 MMLS3 load repetitions, whilst there is no prior indication of a peak (before MMLS3 trafficking). After 5000 MMLS3 load repetitions, the depth reduces again although the shape of the profile is maintained with an increase in MMLS3 load repetitions.

Similar aggregate behaviour can be seen between the distances y = 70 mm and y = 80 mm for the S-R1 binder in Figure 5.55. The initial, pre-trafficked profile shows a gradual reduction in depth after which the profile depth increases after 15000 MMLS3 load repetitions, indicating an upwards movement.

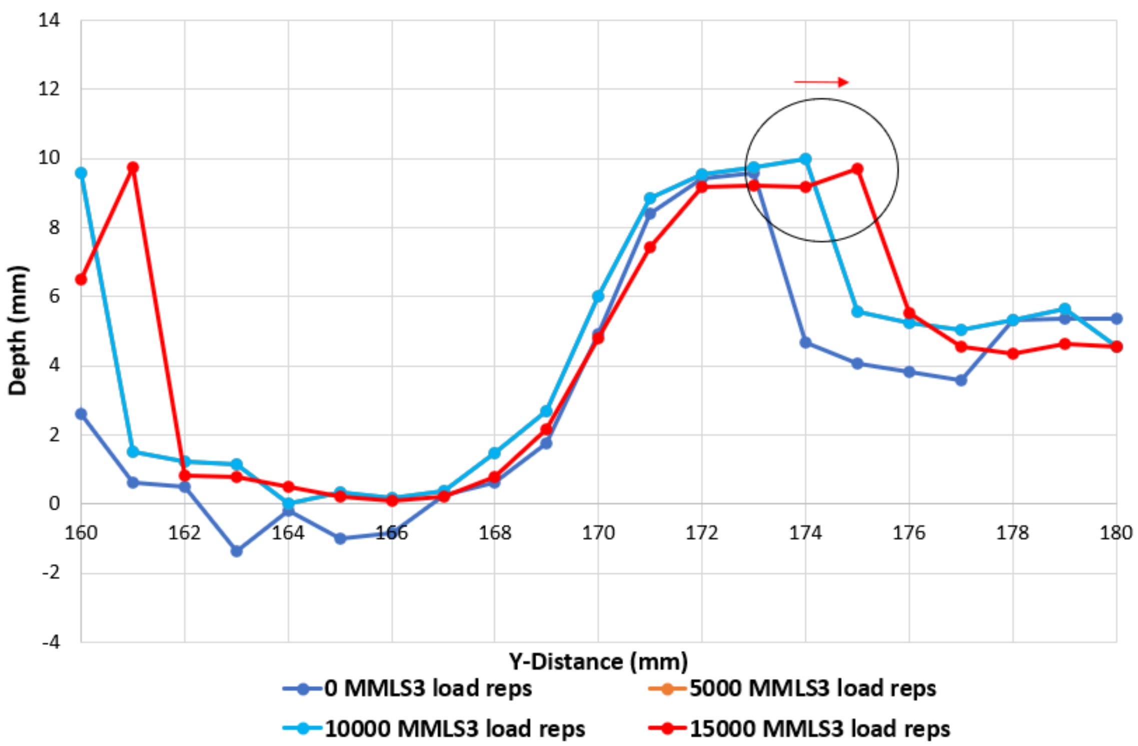

Figure 5.53: Movement of the aggregate in the S-E1 over app. matrix at x = 141mm

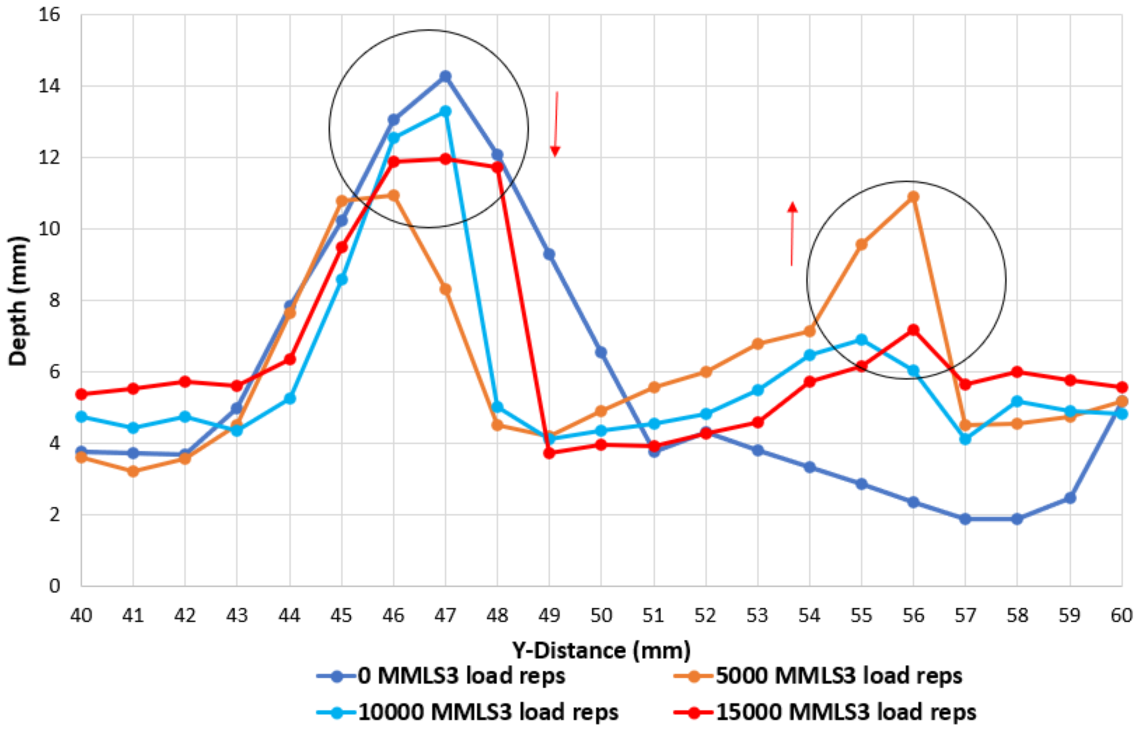

Figure 5.54: Movement of the aggregate in the S-R1 over app. matrix at x = 141mm

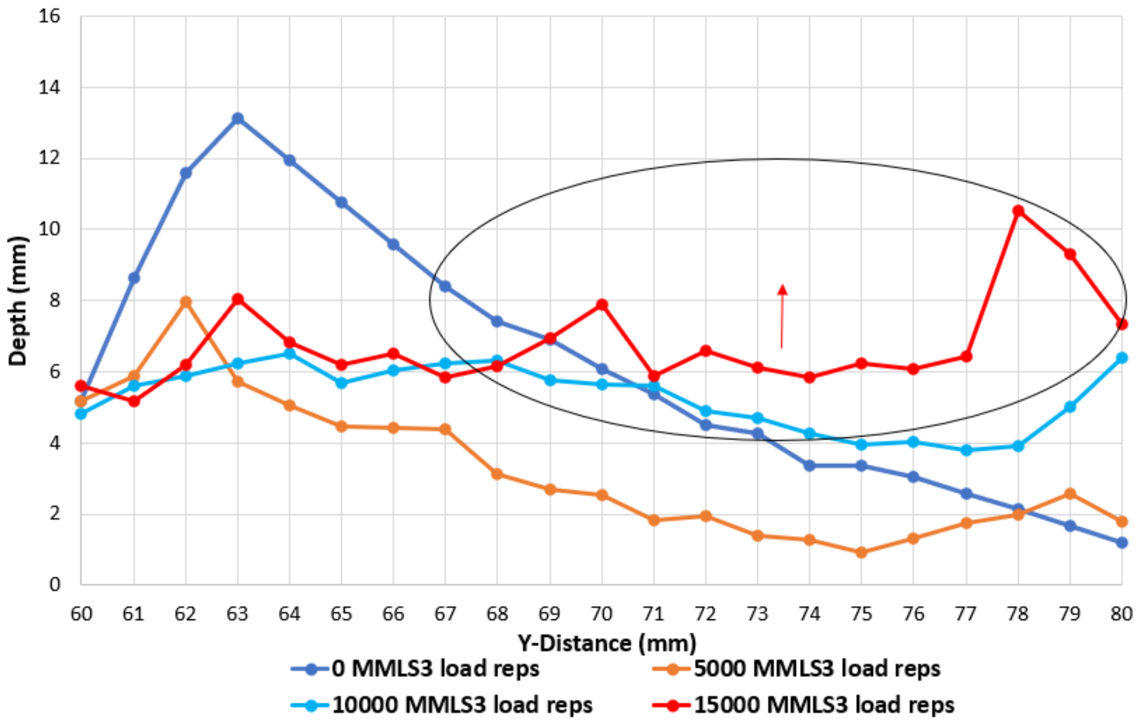

Figure 5.55: Movement of the aggregate in the S-R1 over app. matrix at x = 141 mm

5.6.2 Cross-Section Analysis

As shown for the S-R1 over application matrix in both Figure 5.56 and Figure 5.57, following 15000 MMLS3 load repetitions throughout the trafficking temperature periods, there is transverse movement in the seal mat. The movement, as predominantly indicated within 15 mm outside the wheel path, occurs not only in an outwards direction as indicated in Figure 5.57, but it also causes an uplift in the profile, as shown in Figure 5.56. The evaluated sections, between the coordinates x = 120 mm and x = 140 mm and x = 205 mm and x = 229 mm, are specifically presented as they illustrate the movement within the seal mat clearly. Subsequently, Figure 5.56 illustrates the movement at a cross-sectional slice of y = 147 mm in the x-direction whilst Figure 5.57 shows the movement on the opposite side of the MMLS3 wheel path, at a slice of y = 136 mm.

Similar to the S-R1 over application matrix, the movement is indicated in the S-R2 and S-E1 over application matrices as seen in Figure 5.58 and Figure 5.59. The S-R2 over application matrix indicates that between the coordinates x = 120 mm and x = 140 mm, at a cross-sectional slice of y = 116 mm, there is an outwards transverse and uplifting movement in the seal mat profile with an increase in MMLS3 load repetitions. It is evident that initially, the peak position sits at x = 131 mm after which it is displaced to x = 129 mm with increased trafficking.

Similarly and as shown in Figure 5.59 between x = 115 mm and x = 135 mm, the S-E1 over application matrix contributes to the transverse movement in an over application matrix in that there is a movement in an upwards direction whilst an outwards displacement, with an increase in MMLS3 load repetitions, is apparent.

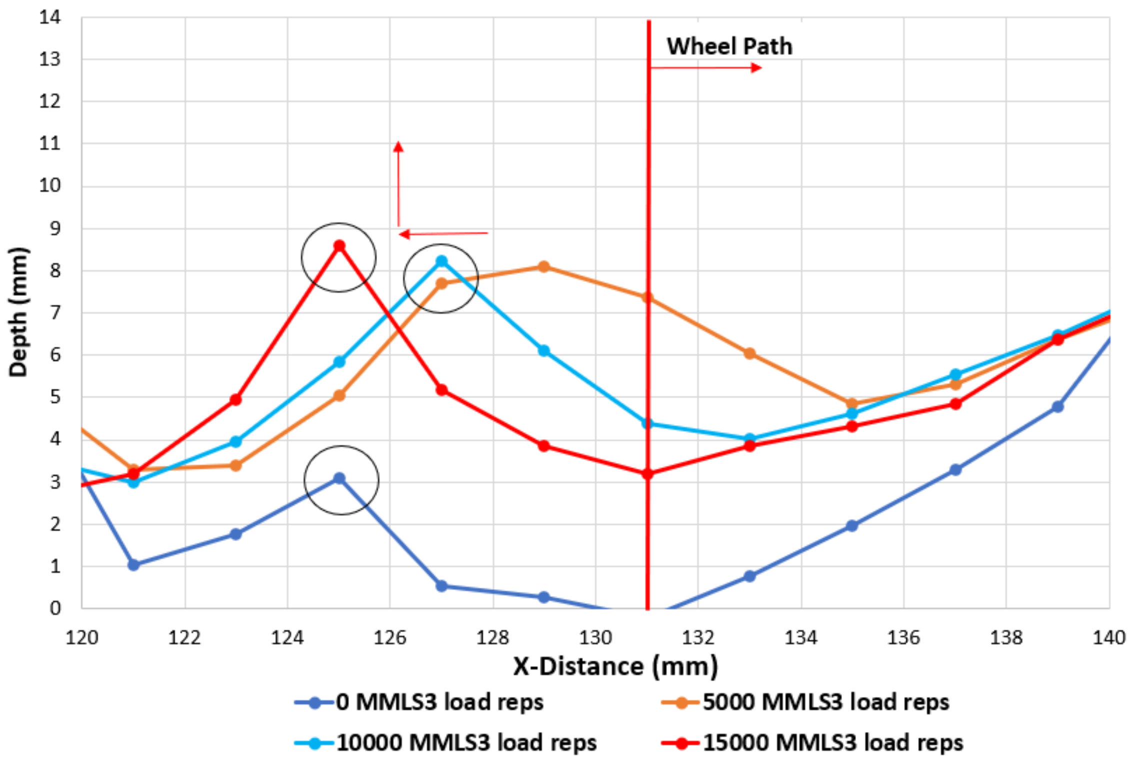

Figure 5.56: Movement of the aggregate in the S-R1 over app. matrix at y = 147 mm

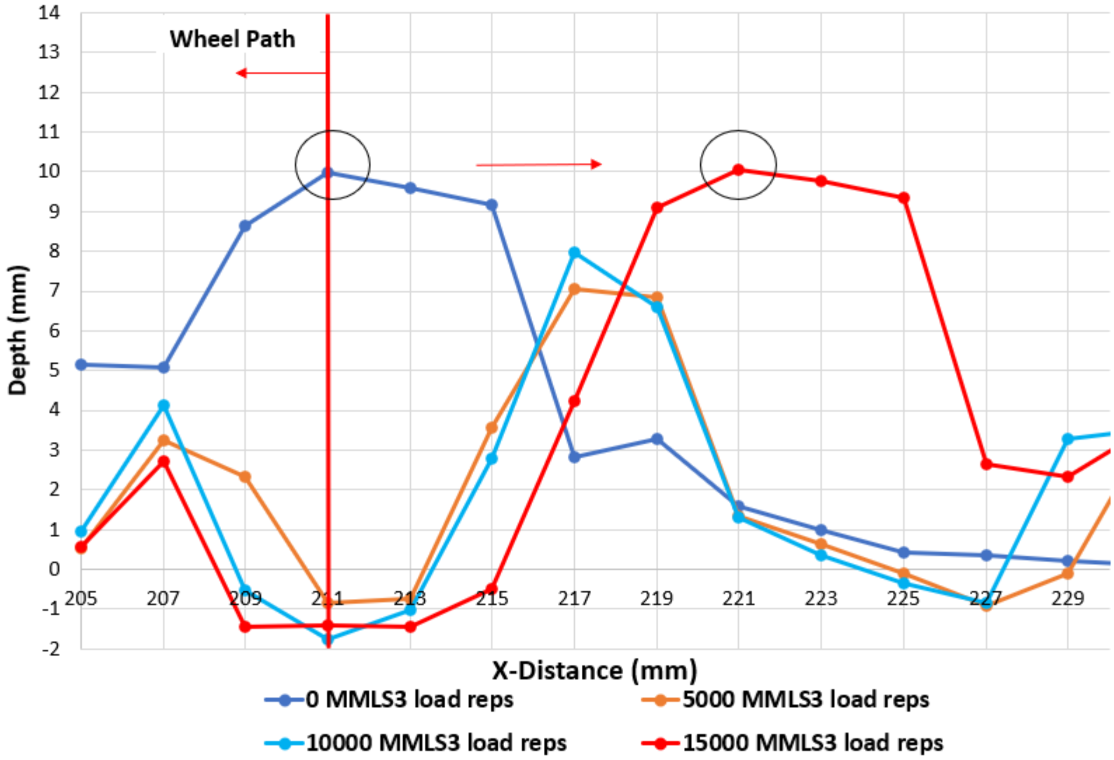

Figure 5.57: Movement of the aggregate in the S-R1 over app. matrix at y = 136 mm

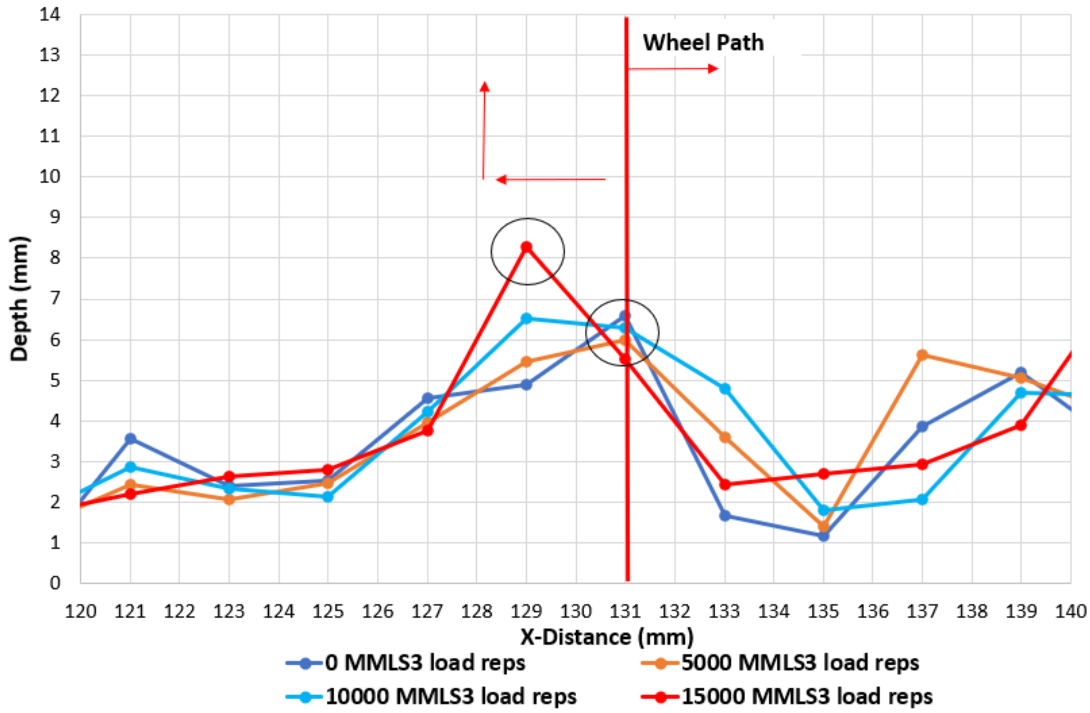

Figure 5.58: Movement of the aggregate in the S-R2 over app. matrix at y = 116 mm

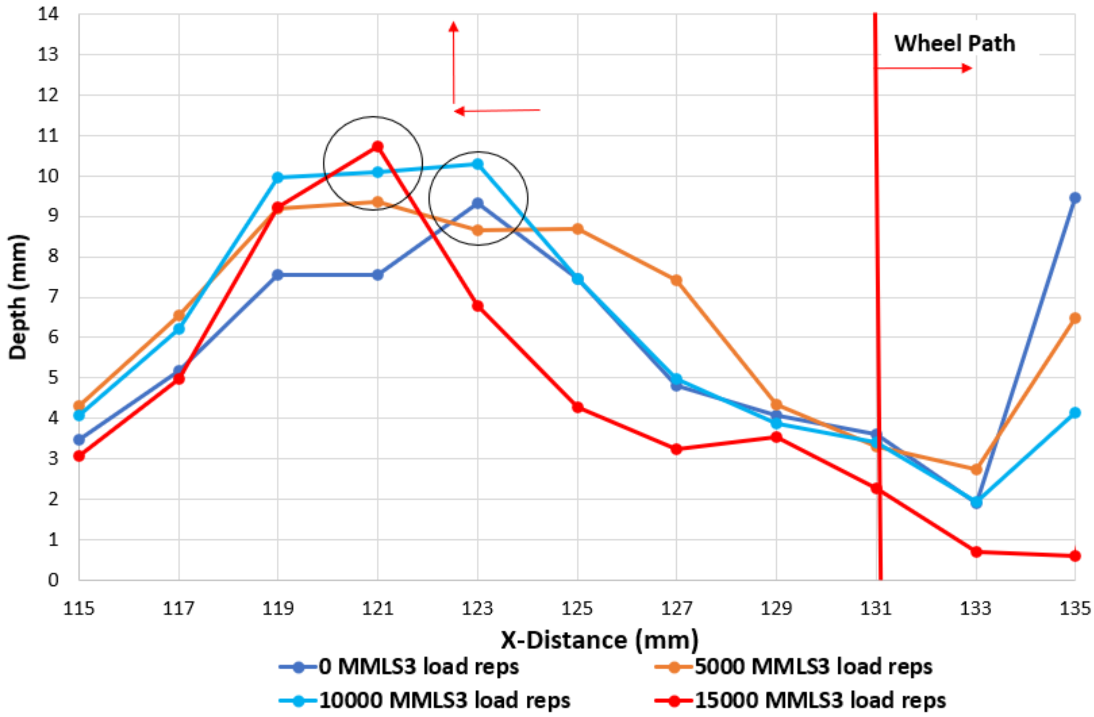

Figure 5.59: Movement of the aggregate in the S-E1 over app. matrix at y = 96 mm

5.6.3 Visual Analysis Summary

Table 5.8 presents a summary regarding the results of the visual analysis.

Table 5.8: Summary of the movement in the seal mat

Aggregate Configuration	In-wheel path	Cross-section
Shoulder-to-Shoulder	- Vertical reduction in depth. - Horizontal movement in the direction of trafficking. - Orientation movement in the direction of trafficking.	Only evaluated for over application matrices.
Over Application	- Horizontal movement in the direction of trafficking. - Vertical reduction in depth. - Vertical increase in depth.	- Transverse movement within 15 mm out of wheel path. - Vertical increase in depth within 15 mm out of wheel path.

5.7 Summary

The results section includes different analyses, all of which contribute to the output of the data capturing processes. Firstly, the influence of temperature on the BSM-emulsion embedment is shown after which the reliability of the Laser Profilometer is determined and presented. Furthermore, the relationship between the mean texture depth and the mean profile depth, for all binders and aggregate matrices at all trafficking temperatures, according to pre-set trafficking intervals, are determined. Thereafter, a depth analysis is done with a focus on the rate of MPD loss and the reduction in MPD. The MTD results are not analysed in-depth due to the interpretation of data as explained in Chapter 6. A visual analysis is lastly performed to determine the physical movement of aggregate in the seal mat. All data interpretation and discussion is presented in Chapter 6.

Chapter 6

Interpretation and Discussion

6.1 Introduction

The following sections elaborate on the data interpretation and discussion for the results presented in Chapter 5. All relevant observations are described and discussed in detail, with potential reasons as to the occurrence thereof.

6.2 Embedment Potential

From Figure 5.2 in Section 5.2, it is seen that with an increase in the temperature of the BSM-emulsion base, the embedment (mm) increases for both the one-ball drop (BP1) and two-ball drop (BP2) values. Due to the behaviour of the surface of the base, reacting in such a way that the extent of the ball drop indents show half-moon circles with little displacement or crushing, the embedment potential is based on the one-ball drop values. This is in accordance with SABITA Manual 40 (2021).

The transfer equations used to obtain the ratios between the BP1 values, as described in the linear Equation 5.1, show that between the 25°C - 35°C tests, a linear relationship is obtained with a gradient of 0.0037 which indicates that the rate of embedment potential increases gradually over the 10°C temperature interval. For a BSM-emulsion base temperature, in excess of 35°C, a sharper gradient is applicable in that of Equation 5.2 being 0.0593. As seen, Equation 5.3 describes the relationship to obtain the ratio between the temperatures 25°C - 40°C by means of a second-order transfer equation with an $R^2 = 0.9684$. Both the linear and second-order transfer equation yield high R^2 values but for improved accuracy, the linear transformation is preferred due to extrapolation purposes.

A potential reason for the sharper increase in the embedment potential, for a BSM-emulsion base temperature in excess of 35°C, as noted by Goosen and Jenkins (2019), includes the halving or doubling in binder stiffness with an increase or decrease of 6°C in binder temperature. Thus, when the BSM-emulsion binder reaches a temperature of 40°C, when compared to the 25°C, the binder stiffness has decreased, resulting in a softer BSM-emulsion base. Subsequently, the closer the temperature of the binder to its softening point, the less stiff it becomes, resulting in a softer binder.

6.3 Profile and Texture Readings

Evaluating the relationship between the mean profile depth, as obtained from the laser profilometer and the mean texture depth, as obtained from the volumetric sand patch test per SANS 3001-BT11 (2012), it is evident that a high degree of correlation is not always obtained for all binders and aggregate matrices. From the results, as described in Section 5.4, there is no clear trend, indicating that the variation in results reflect the sand patch test at specific seal tiles. In contrast, the low coefficient of determination is likely to be related to the sand patch test and not the laser readings as obtained from the LPM. Therefore, to eliminate all potential deviances and variation, the reliability of the laser profilometer is confirmed by performing re-scans on both the S-E1 sh-sh aggregate matrix and the S-R1 over application matrix, without trafficking or temperature changes, as discussed per Section 5.3. The repeatability results show that after scanning the seal tile and performing the mean profile depth data reworking phase, percentage differences of $< 1\%$ are obtained for the average MPD in the wheel path. Consequently, laser profilometer technology, with better accuracy levels, enables data collection at a higher quality when compared to the sand patch test.

The MTD trends, as seen in Figure D.1 for the S-E1 binder, show variability in that there is an increase in MTD. This trend is highly unlikely to occur under MMLS3 trafficking. Therefore, the evaluation of the MTD data will show scattered and unrepresentative trends if any. Based on the variable results obtained from the visual inspection of the MTD data, no Shakedown Theory implementation was performed thereon. Arendse (2016) mention that between the 100 ml and 50 ml sand patch tests, the 100 ml resulted in a higher coefficient of determination when performed on seals. Subsequently, even though a 100 ml volume of glass beads was used, the results still produce low R^2 values after all trafficking temperatures. Apart from human error, a reason contributing to the inaccuracy of the sand patch test method relates to the overlapping of the glass beads into the undisturbed seal tile region outside of the wheel path. With an increase in MMLS3 load repetitions, the seal aggregate undergoes a loss of texture depth due to aggregate behaviour such as orientation and embedment. Simultaneously, the diameter of the 100 ml glass bead volume, used to perform the sand patch test, increases due to the loss of texture depth. Initially, when the texture of the seal mat is rough and before aggregate orientation and embedment occurs, the glass beads are within the wheel path. This is where the test is performed, but due to a decrease in texture depth, the glass beads begin to overlap into the undisturbed section as seen in Figure 6.1. A conceptual explanation for the occurrence can be seen in Figure 6.2. With an increase in MMLS3 load repetitions, the glass beads overlap more into the untrafficked region, resulting in a restricted spread of beads as a large volume is spread into the voids of the undisturbed seal mat. Therefore, the diameter obtained is not a full representation of the mean texture depth although it also includes a significant trafficked wheel path. As a result of this occurrence, it is expected that the values obtained, especially with an increase in MMLS3 load repetitions during the 20°C and 30°C trafficking temperatures, a single mean texture depth value is produced as a function of both the trafficked and untrafficked regions.

Although the case for a glass bead volume of 100 ml, the usage of 50 ml, when preliminary tested, resulted in inadequate readings due to higher void contents present in the rough seal mat and therefore, the glass beads occupied the volume without forming a representative circular patch. Therefore, the lesser volume glass bead volumetric test contributed to the consideration and final decision in using 100 ml.

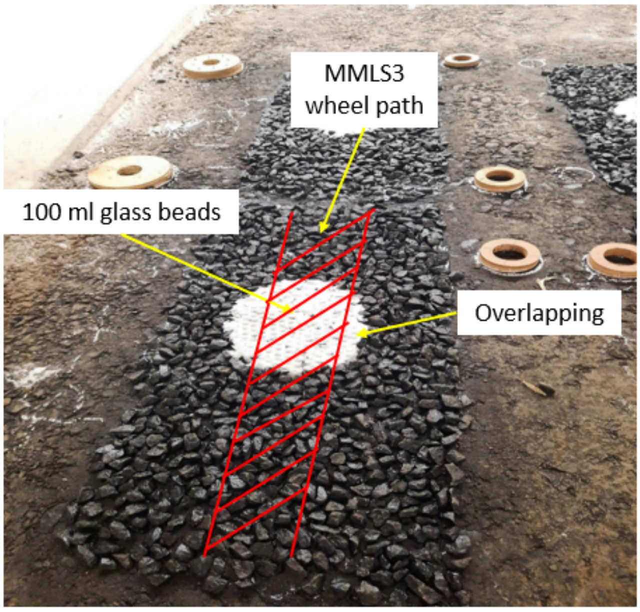

Figure 6.1: Overlapping of glass beads into the un-trafficked region outside the wheel path

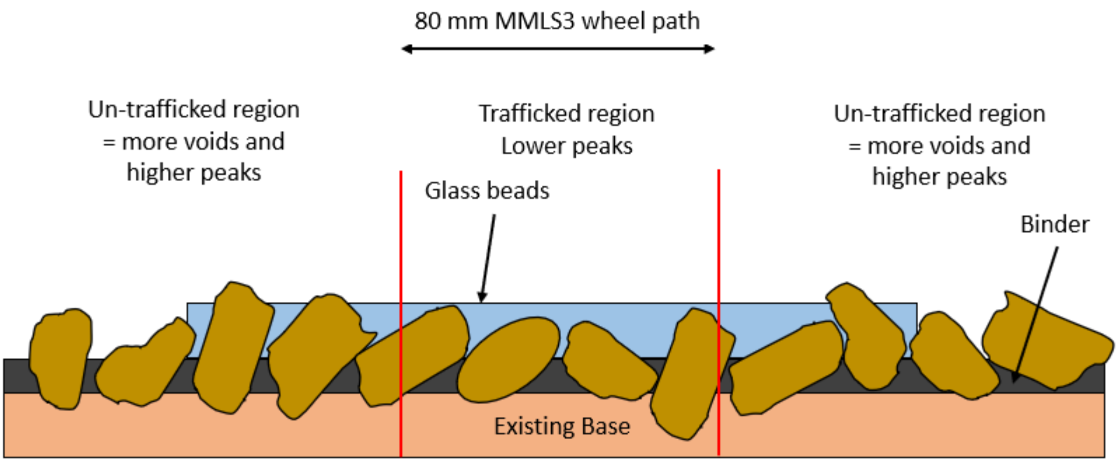

Figure 6.2: Conceptual illustration showing the overlapping of glass beads into the un-trafficked region

6.4 Binder Stiffness

An analysis of the binder stiffness is done using rheological models e.g. applying Abatech Rhea software, with a frequency input parameter of $\omega = 2$ Hz due to two MMLS3 load repetitions making surface contact per second. The stiffness parameter output relates to the Complex Shear Modulus (G*). A summary of the G* results is presented in Table 6.1 whilst the G* decrease, for the elastomer binders, with an increase in temperature, can be seen in Figure 6.3 and the G* decrease, for the rubber binders, are shown in Figure 6.4. The values are all obtained from the master curves as determined by Van Der Spuy (2021) and presented for each binder in Figure E.1 - Figure E.12 in Appendix E.1.

In general, both elastomer binders indicate higher G* values when compared to the rubber binders, over all trafficking temperatures. All binders, with an increase of 10°C in trafficking temperature, experience a reduction in G* greater than 50% except for the S-R1 binder at the temperatures of 20°C and 30°C. Comparing the elastomer binders, it can be seen that the S-E2 binder shows a higher G* for all trafficking temperatures, indicating that the binder is stiffer. Similarly, the S-R1 shows higher G* values, over all trafficking temperatures, compared to the S-R2 binder. The S-R2 binder also produces the lowest G* value at 30°C in comparison with all other binders.

Table 6.1: G* values for the seal binders for each trafficking temperature

	10°C	20°C	30°C
S-E1	16249094.7	3449115.6	22485.3
S-E2	27496772	7448428.4	1728834.4
S-R1	237004	51981.5	51981
S-R2	198800	42885.2	10885.5

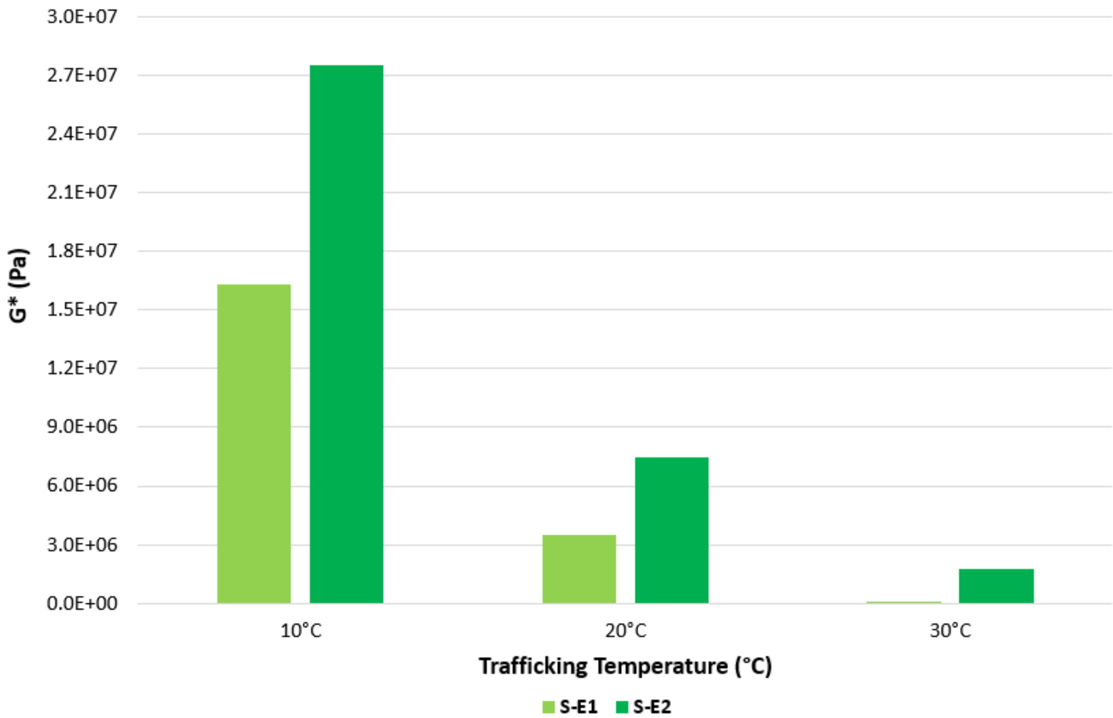

Figure 6.3: Complex Shear Modulus (G*) for the S-E1 and S-E2 binders

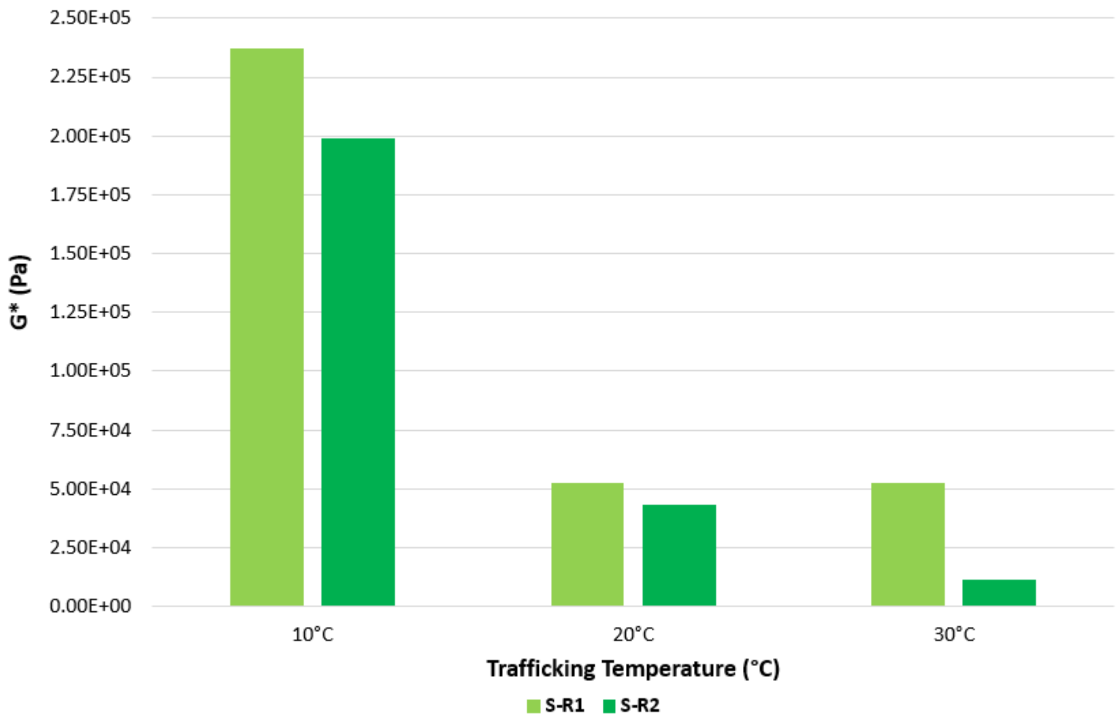

Figure 6.4: Complex Shear Modulus (G*) for the S-R1 and S-R2 binders

6.5 Aggregate Influence

6.5.1 Shoulder-to-Shoulder vs Over Application

From the visual analysis results, as described in Section 5.6.1, it can be seen that the shoulder-to-shoulder aggregate matrices predominantly experience more embedment over the lower trafficking temperature of 10°C after which horizontal and orientation movements are apparent at 20°C and 30°C. These observations are made as a result of the trends seen in Figure 5.49 - Figure 5.52.

From the summary in Table 5.5, it is apparent that the shoulder-to-shoulder aggregate matrices experience greater reductions in MPD with an increase in trafficking temperature between 500 - 2000 and 2000 - 5000 MMLS3 load repetitions, depicting the Phase 2 and Phase 3 trafficking period that is the Steady State. Therefore, is it expected that with an increase in voids in the seal mat, the reduction in MPD is a function of not only embedment, but also aggregate orientation. Shoulder-to-shoulder aggregate behaviour is schematically described in Figure 6.5. As seen, this aggregate matrix allows for aggregate particles to orientate to ALD. In a perfect matrix, all particles orientate to lie on their flattest side but due to three-dimensional mosaic packing, contact points between aggregate particles restrict orientation, resulting in a trafficked aggregate matrix which consist of partially orientated aggregates to ALD, whilst others are still orientating. From the analysis of the rate of change in MPD (mm/MMLS3 load rep.), it is apparent that the shoulder-to-shoulder aggregate matrices, for both the elastomer and rubber binders, experience more orientation during Phase 2 and Phase 3 of trafficking when compared to over application spread rate.

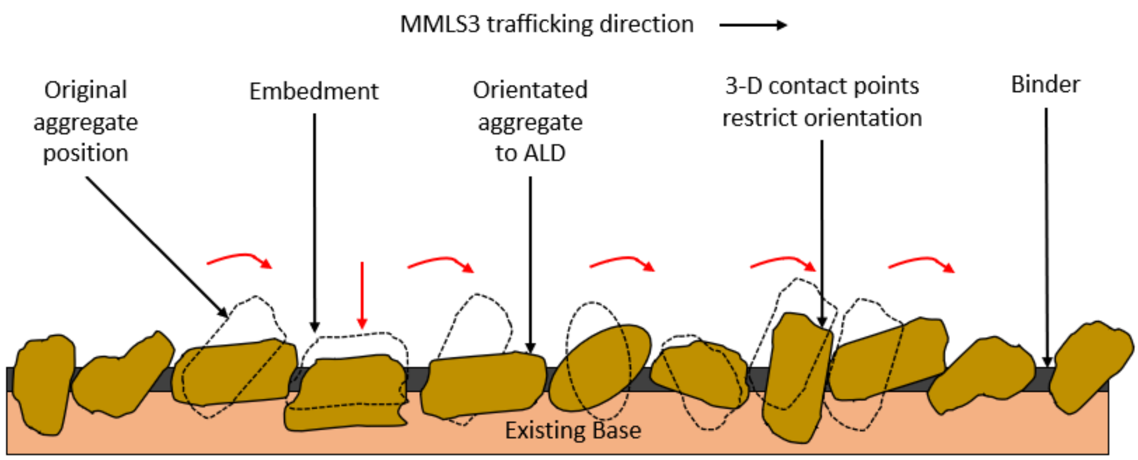

Figure 6.5: Aggregate movement in the wheel path for a shoulder-to-shoulder aggregate matrix

The visual analysis results, as presented in Figure 5.53, Figure 5.54 and Figure 5.55 in Section 5.6.1, show that the over application aggregate matrices experience horizontal aggregate movement in the direction of MMLS3 trafficking. Due to a tightly knit mosaic matrix, as a result of an increase in three-dimensional contact points between aggregates, further aggregate orientation is restricted. A schematic illustrating the behaviour of aggregate in an over application matrix is shown in Figure 6.6. A potential reason as to the uplifting movement in the seal mat is due to the embedment behaviour causing the neighbouring particle to lift and rotate. Again, this behaviour is largely a result of tyre footprint, tyre pressure and wheel load as described by De Beer and Fisher (1999). The tyre footprint induces, as mentioned by Hernandez *et al.* (2013), non-uniform longitudinal, transverse and vertical stresses which could potentially depict the behaviour of aggregate in a seal mat and cause the uplifting movement. This occurrence is unique to the over application aggregate matrix as a result of the extra 12% of aggregate added per area.

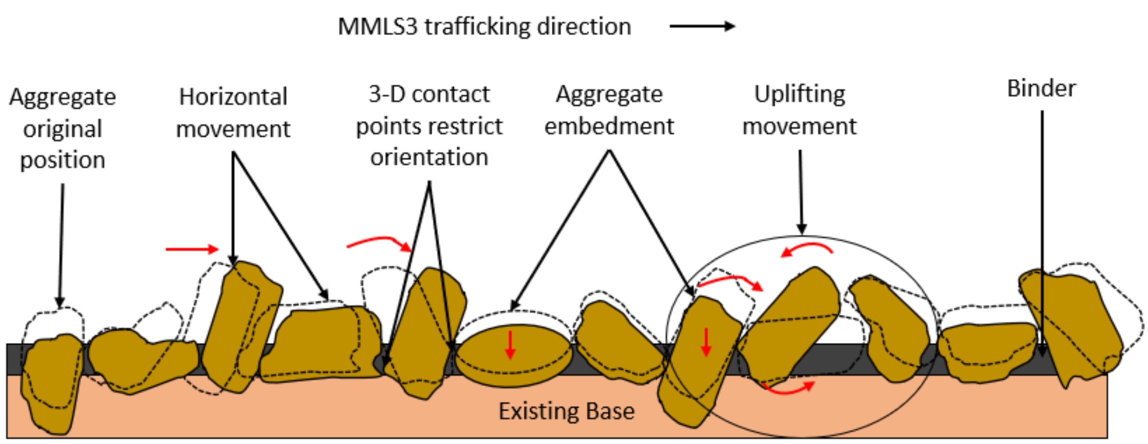

Figure 6.6: Aggregate movement in the wheel path for an over application aggregate matrix

6.5.2 Lateral Movement

As described by the results in Section 5.6.2, there is an indication that the over application aggregate matrices experience horizontal (outwards) movement in the lateral direction, just outside the MMLS3 wheel path. The movement is seen in Figure 5.56 - Figure 5.59.

Furthermore, there is also an indication of upwards movement of aggregate from the seal mat, 15 mm outside the wheel path. To describe the horizontal and upwards movement of aggregate, Figure 6.7 is schematically presented. Again, the uplifting movement of aggregate, just outside the wheel path, is potentially a result of the MMLS3 tyre footprint inducing non-uniform transverse stresses as described by De Beer and Fisher (1999) and Hernandez *et al.* (2013). Therefore, the displacement movement together with the transverse and vertical stresses potentially causes aggregate movement outside the wheel path.

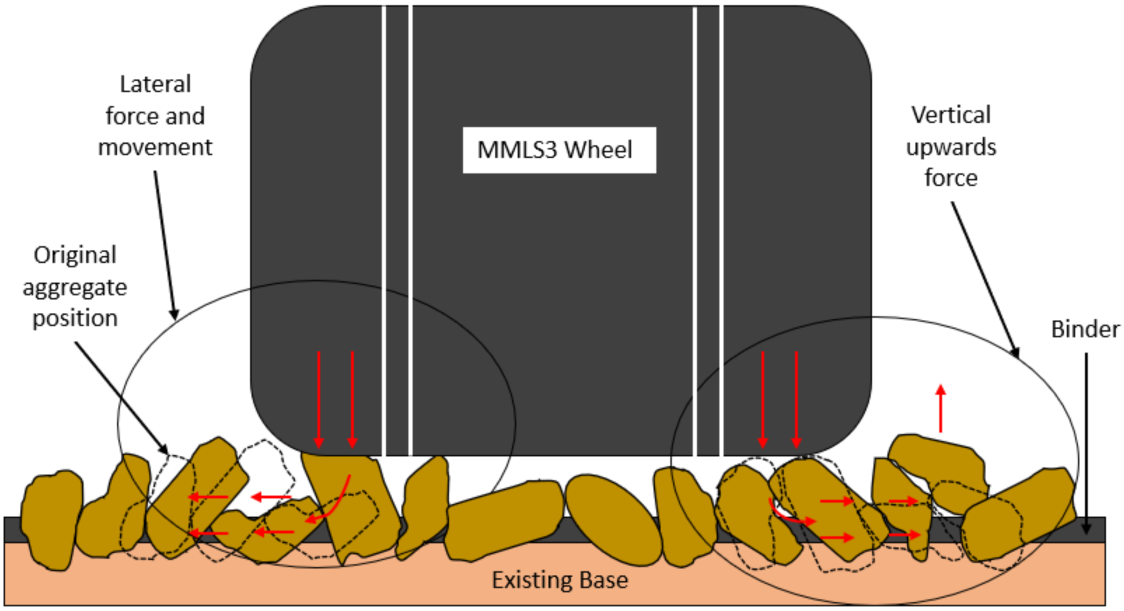

Figure 6.7: Horizontal displacement and upwards movement just outside the wheel path of the over application aggregate matrix

6.5.3 Aggregate Properties

It is recognized that there are additional factors influencing volumetrics, such as aggregate shape, texture, rugosity etc., however, this study is not focused on these. Generally, a single nominal size seal aggregate is desired to initiate a good interlocking aggregate matrix, such as for the shoulder-to-shoulder aggregate matrices in this study (SABITA Manual 40, 2021).

Furthermore a high aggregate flakiness, such as the 16.2% Flakiness Index obtained in this study, results in a more equal stress distribution when compared to the stress distribution of non-flaky aggregate which has not orientated. This corresponds to Abrahams (2015) findings. Similarly, the flaky metamorphic andesite aggregate limits the critical stress concentration points in the base layer allowing for the load to distribute over a larger area, especially for the orientated aggregate in a shoulder-to-shoulder matrix.

In an over application matrix, there is potentially an increase in critical stress points in the base layer, as flaky seal aggregate particles tend to not orientate to the same degree as per the shoulder-to-shoulder matrix. Therefore, shear stress in the base layer is more prominent in an over application matrix. Furthermore, the flaky aggregate in this study contributes to the orientation study as the aggregate limits the embedment potential into the base layer.

6.6 Binder Comparison

6.6.1 Rubber binders

As described in the binder stiffness comparison, as mentioned in Section 6.4, the binder and aggregate dominate the behaviour with a higher G* at the colder trafficking temperature of 10°C. With an increase to intermediate and elevated temperature ranges, the rubber modification begins to contribute to the behaviour in that there is an increase in flexibility and elasticity characteristics (Van Zyl, 2021). During the Shakedown period of trafficking, it is clear that both S-R1 and S-R2 binders experience a normalised percentage reduction in MPD greater than 55%. The behaviour of the higher G* binders during the Shakedown period at colder trafficking temperatures, is shown in Figure 6.8.

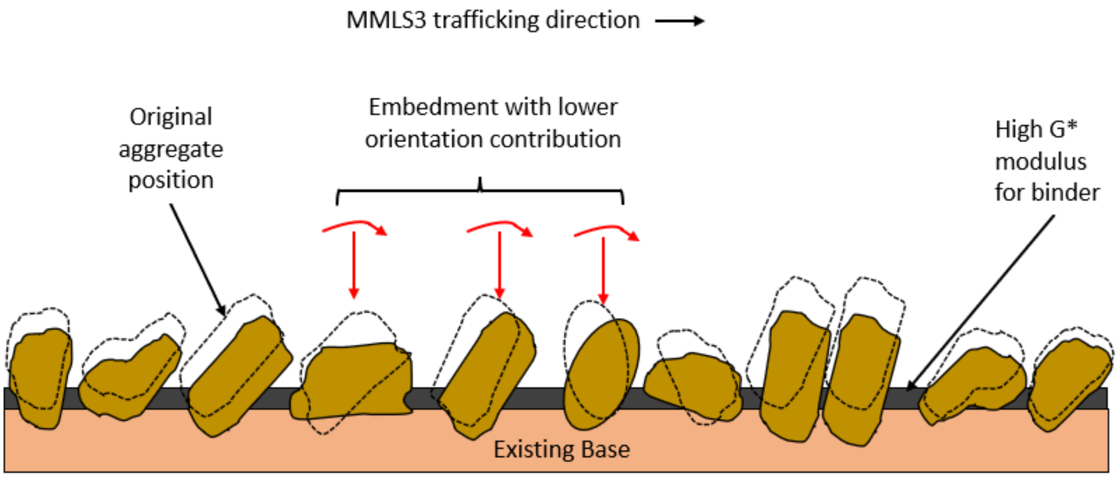

Figure 6.8: Embedment behaviour as a result of a stiff binder at 10°C

Furthermore, the Shakedown period is thus a period over which the greatest reduction in MPD is prominent. The reduction in MPD is a function of both aggregate embedment and aggregate orientation.

With an increase in MMLS3 load repetitions, as experienced by the rubber binders throughout Phase 2 of trafficking, it is evident that higher rates of MPD loss is apparent with a reduction in G* values and an increase in trafficking temperature. Therefore, aggregate orientation is more likely to dictate the behaviour in a seal mat, especially at 30°C. Throughout Phase 2 trafficking, it is evident that the rate of reduction in MPD, for the S-R1 binder, is lower than that of the S-R2 binder for all trafficking temperatures. This is applicable to both aggregate matrices. Therefore, the less stiff

S-R2 binder shows a greater reduction in MPD (mm) and a higher rate of reduction in MPD, linking the overall reduction in MPD potentially to more aggregate orientation. Furthermore, with an increase in temperature, the S-R1 binder becomes more flexible and elastic with increasing rubber modification contribution. Therefore, the lower rate of reduction in MPD is potentially due to the properties of the rubber modification in the S-R1 binder dominating behaviour. Throughout Phase 3 trafficking, it is seeming that variation exists for both binders. The S-R2 shoulder-to-shoulder matrix indicates lower rates of reduction in MPD when compared to the S-R1 rubber whilst the over application matrix continuously, over all trafficking temperatures, yields higher rates of reduction in MPD, indicating that movement in the less stiff S-R2 is prominent.

Furthermore, in comparison with the elastomer binders, the lower G* rubber binders experience greater reductions in MPD (mm) during the Shakedown period after which the elastomers experience greater reductions in MPD as shown after the Steady State period.

6.6.2 Elastomer binders

Similar to the rheological behaviour of the rubber binders, the polymer modification of the S-E1 and S-E2 binders contribute to the behaviour in the seal mat with an increase in trafficking temperature. Again, the higher G* values, as shown in Figure 6.3, indicate that the binder and aggregate predominantly determine the behaviour at colder trafficking temperatures.

Throughout the trafficking phases, the lower polymer modification in the S-E1 binder experiences greater reductions in MPD for all trafficking temperatures. The S-E1 binder also corresponds to a lower G* value. Both elastomers, similar to the rubber binders, experience a reduction in MPD greater than 45% during Phase 1, indicating that the Shakedown period continues to produce a significant influence on mean profile depth loss, irrespective of binder type. Throughout Phase 2 of trafficking, it is seeming that the S-E1 binder with a lower G*, yields higher rates of reduction in MPD for the shoulder-to-shoulder matrix in comparison with the S-E2 binder. Furthermore, the trend continues into Phase 3 of trafficking, indicating that the S-E1 binder potentially, as a result of a lower G* value and increased load repetitions at higher temperatures, experiences more aggregate orientation. Again, the rate of change in MPD is variable for the over application matrices. Furthermore, the larger embedment potential, as determined from the ball penetration tests on the S-E2 base, potentially allows for the S-E2 aggregate to experience more embedment during the Shakedown period, restricting aggregate orientation during the Steady State period.

Variability in the rate of change in MPD increases with increases in trafficking temperature and MMLS3 load repetitions. The elastomer over application aggregate matrices, throughout Phase 3 trafficking, show variation whilst there is an indication that lower rates of reduction in MPD is prominent for the elastomers throughout Phase 2 trafficking compared to the rubber binders.

6.7 Binder Application Rate

From the seal design methodology, as listed in SABITA Manual 40 (2021) and performed in Table C.3 in Appendix C.2, it is seeming that binder application rate, obtained from using conversion factors from NCCB to hot modified, is an influencing factor when evaluating a reduction in mean profile depth as a result of seal aggregate embedment, orientation and transverse displacement. The seal design method, as per Appendix C.2, resulted in the following binder application rates and conversion factors for both the shoulder-to-shoulder and over application aggregate matrices, as graphically presented in Figure 6.9.

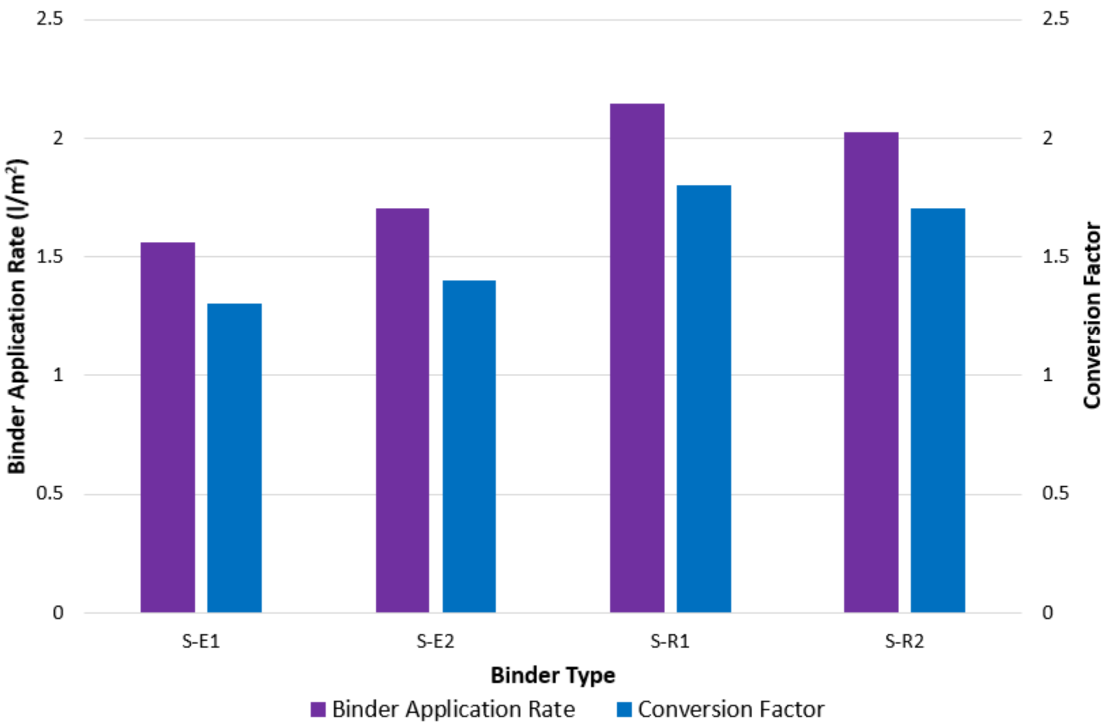

Figure 6.9: Binder application rates and conversion factors

It is evident that both rubber binders require higher binder application rates when compared to elastomer binders. It is of note that although this binder application rate is applicable to both the shoulder-to-shoulder and the over application aggregate matrices, adjustments in binder application rate are required to account for the aggregate application rates. Furthermore, the higher rate of binder application is a function of higher conversion factors from NCCB to hot modified. The need to evaluate the link between binder application rate (or conversion factor), aggregate application rate and seal aggregate behaviour is evident.

6.8 Summary

From the data analysis and data interpretation section, it is clear that aggregate orientation is an important component of seal design. The following relevant aspects are reported:

- The rate of embedment potential into the BSM-emulsion base layer increases for base layer temperatures in excess of 35°C based on the visco-elastic nature of the base material. This is also based on the addition of bitumen to the granular material. The embedment potential increases, as noted by Goosen and Jenkins (2019), in that the binder stiffness halves with an increase in the BSM-emulsion base layer temperature of 6°C.

- The sand patch test method is not a sufficiently accurate method to evaluate texture depth, related to repeatability and reproducibility, and it should only be used as an indication method. Furthermore, the test is also less appropriate when performed on a seal which has been subjected to channelised traffic. Laser profiling of the profile depth is more reliable, as noted by Abrahams (2015), making it more appropriate for research analyses.

- Aggregate application rate, as mentioned by Milne (2004), is considered carefully when evaluating aggregate orientation. Although a single nominal aggregate size and flakiness is used in this study, the influence thereof on aggregate behaviour is generalised but applicable in that it provides insight as to the influence thereof on orientation and embedment.

- Interpreting the data shows that a reduction in profile or texture depth is a function of both aggregate embedment and orientation, but it also includes the horizontal displacement in an outwards manner from the wheel path for an over applied aggregate matrix. This observation is also noted by the work done by Abrahams (2015).

- Movement in the seal mat is governed by orientation at higher temperatures as a result of lower G* values. Embedment is seeming at lower temperatures, with restricted orientation, due to the binder and aggregate dominating the behaviour as the polymer or rubber modification, resulting in increased binder elasticity and flexibility properties, do not dictate the movement of aggregate at colder temperatures.

- A greater reduction in MPD, by means of aggregate embedment and aggregate orientation, occurs during the Shakedown period.

- During Phase 2 (Steady State) trafficking, the shoulder-to-shoulder matrices show accelerated reduction in MPD compared to the over application matrices. Therefore, accelerated orientation was seeming for the shoulder-to-shoulder matrices after initial trafficking and the observation was necessary to gain an understanding of the behaviour with an increase in load repetitions.

- The rubber binders show lower rates of reduction in MPD as a potential result of higher levels of flexibility and elasticity properties for the elevated temperature during Phase 3 trafficking. The increased elasticity and flexibility properties correspond to the expected behaviour as noted by Van Zyl (2021).

- The S-E1 binder experiences greater reductions in MPD compared to the S-E2 binder.

- The rubber binders experience greater reductions in MPD compared to the elastomers.

- Milne (2004) mention that 20% bitumen rubber became sensitive to higher application rates with an increase in temperature. Although binder application rate is not a variable in the study, both S-R1 and S-R2 binders show lower rate of reduction in MPD at elevated trafficking temperatures, potentially indicating that the application rates, as per the seal design, is sufficient to limit early in-service trafficking orientation and therefore ensure sufficient skid resistance.

- With an increase in trafficking temperature and MMLS3 load repetitions, there is also an increase in the variability of the over application matrices when evaluating the rate of change in MPD.

- The binder application rate, as a result of the conversion factors from NCCB to hot modified binders, contributes to aggregate orientation behaviour.

Chapter 7

Conclusions and Recommendations

The behaviour of aggregate in surfacing seals, under different trafficking and environmental conditions, include both aggregate embedment and aggregate orientation. This study aims to evaluate the decrease in mean profile depth and mean texture depth for polymer hot modified binders. Subsequently, the objectives of the study are recalled below.

- Determine the behaviour of aggregate by constructing both shoulder-to-shoulder and over application aggregate matrices for each binder.
- Make use of the Model Mobile Simulator 3 to implement pre-determined trafficking sets on all seals at three different trafficking temperatures.
- Implement the usage of the Laser Profilometer after each trafficking set, together with the sand patch test, to evaluate both the mean profile depth and the mean texture depth.
- Investigate and analyse the mean profile depth and mean texture depth over the trafficking periods.
- Identify and report on the aggregate orientation behaviour in the different seal binders for different aggregate matrices and trafficking temperatures.
- Comment on the appropriateness of current conversion factors from net cold conventional binder to hot modified binders based on the aggregate orientation results.

Guidelines, as reported in the SABITA Manual 40 (2021), suggest that seal design is still largely based on industry experience and there is still much to learn. Subsequently, the BSM-emulsion base construction and the seal design methodology, as documented in detail, was done in such a manner as to replicate in-practice processes. The data analysis phase used to obtain mean profile depth and mean texture depth relationships are of value whilst the evaluation of the mean profile depth produced valuable information as to the behaviour of surfacing seals. Furthermore, visual analyses produced valuable information regarding the physical aggregate behaviour in a seal mat.

7.1 Conclusions

From this study, the following main conclusions can be drawn:

- Reductions in mean profile depth are both a function of aggregate orientation and aggregate embedment in shoulder-to-shoulder aggregate matrices, whilst transverse displacement of aggregate is prominent for over application aggregate matrices.

- The shoulder-to-shoulder aggregate matrix allows for aggregate orientation as a result of voids being present in the seal mat.

- At the lower trafficking temperature of 10°C, the stiffer binder and aggregate dominates the behaviour of the surfacing seal aggregate. The colder temperatures produces a high Complex Shear Modulus (G*) value. At elevated trafficking temperatures, the polymer or rubber modification dominates seal aggregate behaviour. As a result, the G* value decreases, leading to less stiff binders, potentially allowing for more aggregate orientation.

- Both shoulder-to-shoulder rubber binders yield lower rates of MPD loss in comparison with the elastomers, during 30°C trafficking, for the Steady State period. This potentially corresponds with increased flexibility and elasticity properties, especially for the S-R1 binder with a higher G* at elevated temperatures.

- The S-E1 binder yields a greater reduction in MPD in comparison to the S-E2 binder.

- The combined findings of this research show that seal binder type plays a significant role in the selection of binder conversion factors for seal design. The evidence is compelling, taking account of controlled variables such as trafficking temperature, loading properties, aggregate size and shape, binder application rate and seal aggregate configuration. In order to use these findings to determine conversion factors that are binder dependent, additional phase analysis will be required as mentioned in the recommendations.

7.2 Recommendations

There is still testing and data analysis to be done to fully understand the behaviour of aggregate in hot modified binder seals under different trafficking conditions. The following key aspects are recommended for further studies:

- The implementation of Finite Element Method analyses (FEM) to evaluate the distinct aggregate orientation behaviour in surfacing seals. This would enable the determination of FEM models to analyse the behaviour of aggregate in single seals for a specific set of trafficking and environmental conditions.

- The evaluation of aggregate orientation by means of physical sectioned cuts as well as CT scans of surfacing seals.

- A scope including the comparison between different nominal seal aggregate sizes relating to different ALD and flakiness properties. The determination of orientation behaviour as a result of stone properties can be analysed.

- Construct individual seal tiles for each binder at each of the trafficking temperatures. Therefore, multiple seals with the same binders are constructed to be tested independently at each trafficking temperature. This enables a normalised testing setup without having to accumulate reduction in profile or texture depths with increases in trafficking temperature.

- Enable a test matrix to obtain a clear distinction between aggregate orientation and aggregate embedment by making use of laser scanning devices and the MMLS3. Similarly, the test matrix should also identify the contribution of aggregate embedment and aggregate orientation to the loss of macro texture.

- Further experimentation of different seal types such as double and Cape seals.

- Improvement on the data analysis and data reworking phase to lessen time taken to execute the processing thereof.

- Together with the work of Van Der Spuy (2021), there is a need to determine the exact rheological properties of the S-E1, S-E2, S-R1 and S-R2 binders to enable a representative link between aggregate orientation and binder rheology.

List of References

Abrahams, M.S. (2015). *Towards the Development of a Standard Test Protocol : Application of the MMLS3 for Evaluating the Performance of Surfacing Seals*. Masters Thesis, Stellenbosch University.

Adams, J.M. and Kim, Y.R. (2013). Mean profile depth analysis of field and laboratory traffic-loaded chip seal surface treatments. *International Journal of Pavement Engineering*, vol. 15, no. 7, pp. 645–656. ISSN 1477268X.

Arendse, R. (2016). *Texture Depth of Seals - Measurement versus Modelling*. Skripsie Thesis, Stellenbosch University.

De Beer, M. and Fisher, C. (1999). Evaluation of non-uniform tyre contact stresses on thin asphalt. *Africa*, pp. 1–30.
Available at: `https://bit.ly/3znzu9i`

Draft Protocol Guideline 1 (2008). DPG1: Method for evaluation of permanent deformation and susceptibility to moisture damage of bituminous road paving mixtures using the Model Mobile Load Simulator (MMLS3). Tech. Rep..
Available at: `https://bit.ly/3jgUSrl`

Engelbrecht, F. (2018). *Age-related performance of typical seal binders in South Africa by*. Masters Thesis, Stellenbosch University.

Fawzy, N., Habib, H.F. and Mokhtari, S. (2021). Performance evaluation of electric vehicle model under skid control technique. *World Electric Vehicle Journal*, vol. 12, no. 2. ISSN 20326653.

Gerber, J.A. (2016). *Numerical modelling of performance and failure criteria for surfacing seals*. Masters Thesis, Stellenbosch University.

Glover, C.J., Davison, R.R., Domke, C.H., Ruan, Y., Juristyarini, P., Knorr, D.B. and Jung, S.H. (2005). Development of a New Method for Assessing Asphalt Binder Durability with Field Validation. Tech. Rep. 2, Texas Department of Transportation, Austin.
Available at: `https://static.tti.tamu.edu/tti.tamu.edu/documents/0-1872-2.pdf`

Goosen, E. (2021). PLASTIC STRAIN IN FLEXIBLE PAVEMENT DESIGN. *Society of Asphalt Technology (SAT) (Unpublished)*, , no. 1.

Goosen, E. and Jenkins, K. (2019). Extraction and Recovery of Bituminous Binders from Chip Seal Samples. *12th Conference on Asphalt Pavements for Southern Africa*.
Available at: `https://www.capsa2019.co.za/wp-content/uploads/2019/10/CAPSA'19 - Papers Accepted For The Conference.pdf`

Gransberg, D. and James, D. (2005 apr). *Chip Seal Best Practices*. August. Transportation Research Board, Washington, D.C. ISBN 978-0-309-09744-4.
Available at: `http://www.nap.edu/catalog/13814`

Hernandez, J.A., Al-Qadi, I. and De Beer, M. (2013 jun). Impact of Tire Loading and Tire Pressure on Measured 3D Contact Stresses. In: *Airfield and Highway Pavement 2013*, February 2017, pp. 551–560. American Society of Civil Engineers, Reston, VA. ISBN 9780784413005.
Available at: `http://ascelibrary.org/doi/10.1061/9780784413005.044`

Herrington, P., Ball, G., Patrick, J. and Towler, J. (2012). Aggregate Breakdown As a Cause of Chip Seal Flushing. In: *25th ARRB Conference: Shaping the future: Linking policy, research and outcomes*, vol. l, pp. 1–12.
Available at: `https://bit.ly/3DgdEqx`

Hoffmann, P. and Potgieter, C.J. (2007). Bitumen Rubber Chip and Spray Seals in South Africa. *SATC 2007 - 26th Annual Southern African Transport Conference: The Challenges of Implementing Policy*, , no. July, pp. 225–238.

Hunter, R., Self, A. and Read, J. (2015). *The Shell Bitumen handbook*. Six edn. ICE Publishing: Thomas Telford. ISBN 978-0-7277-5837-8.
Available at: `http://books.google.com/books?id=bA1tIkRJL8kC&pgis=1`

Ignatavicius, S., Kavanagh, A., Brennan, M.J., Colleran, D., Sheahan, J. and Newell, S. (2021). Experimental investigation of optimum adhesion properties for anionic emulsions in road maintenance applications. *Construction and Building Materials*, vol. 304, no. September, p. 124678. ISSN 0950-0618.
Available at: `https://doi.org/10.1016/j.conbuildmat.2021.124678`

Kane, M., Artamendi, I. and Scarpas, T. (2013). Long-term skid resistance of asphalt surfacings : Correlation between Wehner Schulze friction values and the mineralogical composition of the aggregates. *Wear*, vol. 303, no. 1-2, pp. 235–243. ISSN 0043-1648.
Available at: `http://dx.doi.org/10.1016/j.wear.2013.03.022`

Kashaya, A.A. (2013). *Surface Run-off Behaviour of Bitumen Emulsions used for the construction of seals*. Masters Thesis, Stellenbosch University.

Kemp, M. (2006). *Concept to Reality - MLS10*. Skripsie Thesis, Stellenbosch University.

Kim, N. (2014). Chemical Characterization of Gilsonite Bitumen. *Journal of Petroleum & Environmental Biotechnology*, vol. 05, no. 05. ISSN 21577463.
Available at: `https://bit.ly/3Bf9I7U`

Kleyn, E. (2012). Basecourse Construction. *31st South African Transport Conference (SATC 2012)*, , no. July, pp. 110–118.
Available at: `https://bit.ly/3sOxG6A`

Kumbargeri, Y., Boz, I. and Kutay, M. (2019). Investigating the effect of binder and aggregate application rates on performance of chip seals via digital image processing and sweep tests. *Construction and Building Materials*, vol. 222, pp. 213–221. ISSN 09500618.
Available at: `https://doi.org/10.1016/j.conbuildmat.2019.06.089`

Lawson, W.D., Senadheera, S. and Leaverton, M. (2007). Maintenance Solution for Bleeding and Flushed Pavements Surfaced with a Seal Coat or Surface Treatment. *Center for Multidisciplinary Research in Transportation*, vol. 91, no. February, pp. 399–404.
Available at: `https://bit.ly/3zp9xq4`

Milne, T. (2004). *Towards a Performance Related Seal Design Method For Bitumen and Modified Road Seal Binders*. Doctoral, Stellenbosch Univerisity.

MLS Test Systems (2016). MMLS3 Operator's Manual. Tech. Rep..
Available at: `https://bit.ly/2XWEJz0`

Neaylon, K. (2012). Ball Penetration Test. Tech. Rep. October.

Organisation for Economic Co-operation and Development (2005). *Economic evaluation of long-life pavements: Phase 1*, vol. 9789264008. Organisation for Economic Co-Operation and Development. ISBN 9789264008588.

Robertson, R.E. (1991). Chemical Properties of Asphalts and Their Relationship to Pavement Performance. Tech. Rep., Westent Research Institute.
Available at: `http://onlinepubs.trb.org/onlinepubs/shrp/shrp-91-510.pdf`

Roque, R., Anderson, D. and Thompson, M. (1991). Effect of Material, Design, and Construction Variables on Seal Coat Performance. *Transportation Research Record*, , no. 1300, pp. 108–115. ISSN 0361-1981.
Available at: `http://trid.trb.org/view.aspx?id=359577`

Rowe, G.M., King, G. and Anderson, M. (2014). The influence of binder rheology on the cracking of asphalt mixes in airport and highway projects. *Journal of Testing and Evaluation*, vol. 42, no. 5. ISSN 00903973.

Rudman, C. (2019). *Aspects of self cementation of recycled concrete aggregate when applied in roads*. Ph.D. thesis, Stellenbosch University.

SABITA Manual 2 (2012). *Bituminous binders for road construction and maintenance*. September, 5th edn. Southern African Bitumen Association (Sabita). ISBN 9781874968610.

SABITA Manual 40 (2021). *Design and Construction of Surface Treatments*. February, 2nd edn. Southern African Bitumen Association (Sabita). ISBN 9781874968771.

SABITA TG 1 (2019). *Technical Guideline 1: The Use of Modified Bituminous Binders in Road Construction*. January, 4th edn. Southern African Bitumen Association (Sabita). ISBN 9781874968740.

SANS 3001-BT10 (2013). SOUTH AFRICAN NATIONAL STANDARD Civil engineering test methods Part BT10 : Ball penetration test for the design of surfacing seals. 014. SABS Standards Division. ISBN 9780626294632.

SANS 3001-BT11 (2012). SOUTH AFRICAN NATIONAL STANDARD Civil engineering test method - Part BT11 : Texture depth measurement for the design of surfacing seals. 1st edn. SABS Standards Division. ISBN 978-0-626-37752-6.

SANS 4001-BT1 (2016). SOUTH AFRICAN NATIONAL STANDARD Civil engineering specifications Part BT1 : Penetration grade bitumen. 1st edn. SABS Standards Division. ISBN 9780626329877.

SAPEM (2014). *SAPEM: South African Pavement Engineering Manual*. October, 2nd edn. South African National Road Agency. ISBN 9781920611002.

Semmelink, C., Jooste, F. and De Beer, M. (1997). Use of the K-mould in determination of the elastic and shear properties of road materials for flexible pavements. *International Conference on Asphalt Pavements*, vol. 8, pp. 1643–58.
Available at: `https://trid.trb.org/view/501720`

Tarbuck, E., Lutgens, F. and Tasa, D. (2014). *Earth: An Intoruduction to Physical Geology*. Eleventh edn. Pearson. ISBN 10: 1-292-02094-6.

Test Method A7 (1986). TMH 1: Test Method A7. In: *TMH 1*, pp. 27 – 34. Department of Transport.

Test Method B1 (1986). TMH 1: Test Method B1. In: *TMH 1*, pp. 119 – 120. Department of Transport.

Test Method B18(a) (1986). TMH 1: Test Method B18(a). In: *TMH 1*, pp. 157 – 160. Department of Transport.

Test Method B3T (1986). TMH 1: Test Method B3T. In: *TMH 1*, pp. 123–124. Department of Transport.

Theyse, H.L. (2002). Stiffness, Strength, and Performance of Unbound Aggregate Aaterial: Application of South African HVS and laboratory results to California flexible pavements. Tech. Rep. July, University of California, Pretoria.
Available at: `http://www.ucprc.ucdavis.edu/PDF/Unbound Aggregate Theyse.pdf`

TMH 1 (1986). *TMH 1: Standard Methods of Testing Road Construction Materials*. Department of Transport, Pretoria.

Transit New Zealand (2005). *Chipsealing in New Zealand*. Tranzit New Zealand, Road Controlling Authorities and Roading New Zealand. ISBN 0-478-10562-2.

TRH 1 (2019). *TRH 1: Guidelines for primes and stone precoating fluids*. April, 2nd edn. South African National Road Agency Limited.

Van Der Spuy, H. (2021). *Seal Binder Rheology at Intermediate Temperatures and Influence on Stone Orientation*. Masters Thesis (Unpublished), Stellenbosch University.

Van Niekerk, A.A. (2002). *Mechanical Behaviour and Performance of Granular Bases and Subbases in Pavements*. Doctoral, Delft Technical University, Delft.
Available at: `https://bit.ly/3gvFe9q`

Van Zyl, G. (2000). Seal and thin surfacing technology. In: *TRB Workshop 153: South African Highway Technology and Practice*. South African National Road Agency Limited.
Available at: `https://www.nra.co.za/media-room/presentations/`

Van Zyl, G. (2021). Personal Communication.

Van Zyl, G. and Jenkins, K. (2015). Overview of Long Term Seal Performance. *Conference on Asphalt Pavements for Southern Africa (CAPSA)*, , no. August 2015, pp. 1–13.
Available at: `https://bit.ly/3DfdaB4`

Van Zyl, G. and Van der Gryp, A. (2015). Correlation between mean profile depth estimated macro texture depth. , no. August 2015, p. 6p.
Available at: `https://trid.trb.org/view/1404793`

Van Zyl, G.D., Fourie, H.G. and Bredenhann, S.J. (2015). Recommended Practice For Winter Sealing in South Africa. Tech. Rep..
Available at: `https://bit.ly/3sJJEyA`

Van Zyl, S. (2018). *Relationship Between the Age Related Performance of a Typical Bituminous Binder in South Africa and the Fatigue Performance of Asphalt Mixture*. Masters Thesis, Stellenbosch University.

Werkmeister, S., Wellner, F. and Dawson, A.R. (2005). Permanent deformation behaviour of granular materials. *Road Materials and Pavement Design*, vol. 6, no. 1, pp. 31–51. ISSN 21647402.
Available at: `https://doi.org/10.1080/14680629.2005.9689998`

White, G., Ward, C. and Jamieson, S. (2019). Field evaluation of a handheld laser meter for pavement surface macro texture measurement. *International Journal of Pavement Engineering*, vol. 0, no. 0, pp. 1–10. ISSN 1477268X.
Available at: `https://doi.org/10.1080/10298436.2019.1654103`

Wirtgen (2012). *Cold Recycling: Wirtgen Cold Recycling Technology*. 1st edn. Wirtgen GmbH.

Wood, T.J., Janisch, D.W. and Gaillard, F.S. (2006). *Minnesota Seal Coat Handbook 2006*. 2nd edn. Minnesota Department of Transportation.
Available at: `https://www.lrrb.org/pdf/200634.pdf`

Woodward, W., Woodside, A., Yacoob, H. and Maguire, S.J. (2000). Smaller stone size surface dressings for high stone surface mixes DEVELOPMENT OF A LABORATORY TEST TO PREDICT TYRE / ROAD NOISE. pp. 1–11.
Available at: `https://bit.ly/38bDVYX`

Appendices

Appendix A

Tests on Materials

A.1 Maximum Dry Density and Optimum Moisture Content

To obtain the dry density (DD) and the moisture content (MC), Test Method A7 (1986) was used.

$$DD = \frac{W}{d + 100} * F$$

$$W = (\text{mould} + \text{material}) - (\text{mould})$$

$$MC = \frac{a - b}{b - c} * 100$$

Where:
W = wet material mass,
d = moisture content as a percentage of the dry material,
F = 43.2 = the mould factor,
a = mass of the container and wet material,
b = mass of the container and dry material, and
c = mass of empty container.

Table A.1 shows the calculations for the moisture content and dry density whilst Figure A.1 provides the theoretical dry density versus moisture content plot.

Table A.1: OMC and MDD calculations

Information	Unit	Sample					
		1	2	3	4	5	6
Mould mass	g	4882	4882	4882	4882	4882	4882
Factor	-	43.2	43.2	43.2	43.2	43.2	43.2
Moisture	%	2%	3%	4%	5%	6%	7%
Moisture mass	g	140	210	280	350	420	490
Mould mass and material	g	10165	10307	10384	10543	10611	10561
Material mass	g	5283	5425	5502	5661	5729	5679
Dry density	kg/m^3	2238	2275	2285	2329	2335	2293
Container mass	g	236.7	236.8	235.6	212.7	178.4	196.6
Container mass and wet material	g	841.9	748.5	894.1	815.4	861.5	931.5
Container mass and dry material	g	828.3	733	869.6	786.4	823.3	884.4
Actual moisture	%	2.30	3.12	3.86	5.05	5.92	6.85
Actual dry density	kg/m^3	2230.97	2272.61	2288.43	2327.88	2336.53	2296.093

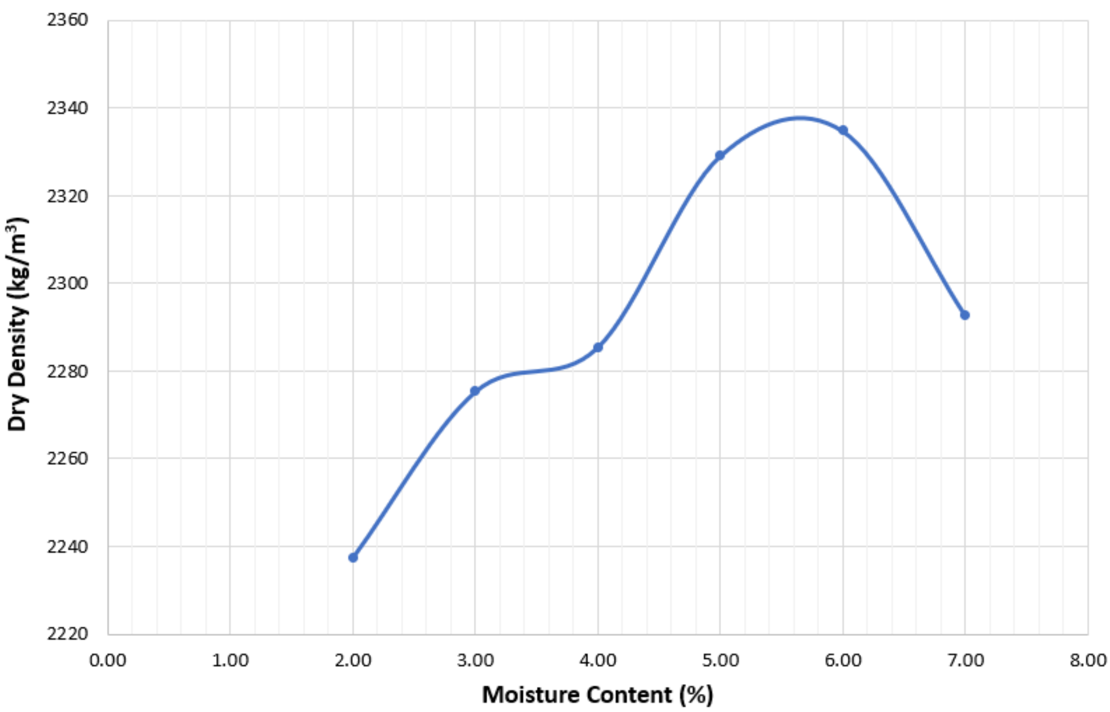

Figure A.1: Theoretical DD vs MC

A.2 Test Base Mix Design

The following masses and contents, as presented in Table A.2, were calculated for the test base:

Table A.2: Test Base Contents

Content	Calculation	Information
G2 Test Base	2340 kg/m^2 * (0.0238 + 0.001679)m^3 = 79.27 kg	
Moisture content	5.7% + 0.15% = 5.85%	OMC = 5.7% with the addition of 0.15% to prevent breaking of the emulsion
Moisture mass	79.27kg * 5.85% = 4.637kg	
Hydroscopic content	((1053-237) - (1051-237))/ (1051-237) = 0.25%	Container mass = 237g Wet sample and container mass = 1053g Dry sample and container mass = 1051g
Hydroscopic mass	0.25% * 79.27kg = 0.198kg	
Emulsion mass	79.27kg * 3.5% = 2.774kg	
Water mass	(4.637kg - 2.774kg - 0.198) + 0.1% * 79.27kg = 1.744kg	0.1% addition of extra water for wastage
Cement mass	79.27kg * 1.5% = 1.189kg	1.5% for extra hardness in the base layer

A.3 BSM Base Construction

The following masses and contents, as presented in Table A.3 were used for the construction of the BSM base.

Table A.3: Base contents

Content	Calculation	Information
As per the MMLS3 test pit		
G2 Base	2340 kg/m^3 $*$ 1.5m^3 = 3510 kg	Total G2 material required per base
As per a single batch of 200kg G2		
G2 Base	18 * 200kg batches	The batches were used for mixing convenience
Moisture mass	200kg* 5.85% = 11.7kg	5.85% total moisture
Hydroscopic content	0.21% as calculated per batch. 0.21% * 200kg = 0.425kg	Hydroscopic moisture as calculated per batch
Emulsion mass	200kg * 3.5% = 7kg	
Water mass	11.7kg - 7kg - 0.425kg = 4.275kg	Moisture mass - hydroscopic mass - emulsion mass
Cement mass	200kg * 1.5% = 3kg	1.5% for extra hardness in the base layer

A.4 Average Least Dimension and Flakiness Index

To obtain the ALD, Test Method B18(a) (1986) was used.

$$ALD = \frac{A}{B}$$

Where:
ALD = average least dimension (mm),
A = the sum of the smallest dimension of the aggregate particles (mm) and
B = the number of aggregate particles measured.

Following Method B18(a), 200 representative aggregate particles were obtained after which their ALD was individually measured by means of a caliper. The following results, as shown by Table A.4, was obtained.

Table A.4: Average Least Dimension of seal stones

Stone	ALD (mm)	Stone	ALD (mm)	Stone	ALD (mm)	Stone	ALD (mm)	Stone	ALD (mm)
1	9	**21**	9	**41**	**9.5**	61	**8**	81	**6.9**
2	6.8	**22**	6	**42**	**6.7**	62	**12.1**	82	**8**
3	8.7	**23**	7.8	**43**	**12**	63	**13**	83	**7.8**
4	7.2	**24**	8.3	**44**	**8.9**	64	**11.5**	84	**7.1**
5	8.8	**25**	7	**45**	**9**	65	**12.1**	85	**11**
6	7.5	**26**	10	**46**	**12**	66	**10**	86	**5**
7	8.8	**27**	10	**47**	**9.8**	67	**5**	87	**3.2**
8	10.8	**28**	9.8	**48**	**10.8**	68	**11**	88	**8**
9	10.22	**29**	9.8	**49**	**9.8**	69	**8**	89	**7**
10	8.1	**30**	9	**50**	**8.8**	70	**12.3**	90	**8.2**
11	9.4	**31**	8	**51**	**12**	71	**6.1**	91	**6.8**
12	6.1	**32**	8.2	**52**	**7.9**	72	**8.8**	92	**9.2**
13	5	**33**	9.1	**53**	**9.2**	73	**12**	93	**8.7**
14	8.1	**34**	12	**54**	**10**	74	**8.8**	94	**7**
15	8.8	**35**	10	**55**	**9**	75	**6.2**	95	**8.6**
16	7.2	**36**	7.5	**56**	**11.5**	76	**8.4**	96	**8.8**
17	8.5	**37**	9.6	**57**	**8.1**	77	**10**	97	**7.3**
18	8.5	**38**	6.1	**58**	**6.1**	78	**7.9**	98	**9.6**
19	7.5	**39**	5	**59**	**7.1**	79	**9**	99	**8.8**
20	11	**40**	4.9	**60**	**11.5**	80	**12.2**	100	**4**

Stone	ALD (mm)	Stone	ALD (mm)	Stone	ALD (mm)	Stone	ALD (mm)	Stone	ALD (mm)
101	8	**121**	8.5	**141**	**5.9**	161	**8**	181	**10**
102	10.5	**122**	11	**142**	**9.8**	162	**8**	182	**8.5**
103	7.1	**123**	8.8	**143**	**6.3**	163	**9.6**	183	**6.7**
104	9.9	**124**	7.8	**144**	**12.5**	164	**12**	184	**10.1**
105	5.1	**125**	8.8	**145**	**8.2**	165	**8**	185	**7.3**
106	6.8	**126**	5.1	**146**	**5.9**	166	**9.1**	186	**8.9**
107	8.8	**127**	6.1	**147**	**9.8**	167	**7.2**	187	**9**
108	8.7	**128**	6.1	**148**	**9.8**	168	**9.1**	188	**10.1**
109	9.7	**129**	11.5	**149**	**6.8**	169	**9.1**	189	**9.5**
110	6.2	**130**	11	**150**	**9.5**	170	**6.1**	190	**9.1**
111	7.1	**131**	5	**151**	**8.2**	171	**7.3**	191	**11**
112	10	**132**	5.1	**152**	**8.1**	172	**9.1**	192	**12**
113	11	**133**	7.5	**153**	**11.5**	173	**9.2**	193	**6**
114	7.2	**134**	8	**154**	**3.1**	174	**8.2**	194	**8**
115	4.1	**135**	8.7	**155**	**12**	175	**8.1**	195	**9.2**
116	7	**136**	7	**156**	**8**	176	**6.1**	196	**9**
117	13.1	**137**	9.5	**157**	**10.8**	177	**12.1**	197	**7.5**
118	9	**138**	9	**158**	**6.2**	178	**9.6**	198	**5.5**
119	13	**139**	8.8	**159**	**10.5**	179	**7.3**	199	**10**
120	11	**140**	4.4	**160**	**13**	180	**6.1**	200	**9.2**

Thus, ALD = 8.6mm.

The Flakiness Index was calculated using the following equation as described per the Test Method B3T (1986).

$$FI = \frac{M}{N} * 100$$

Where:
FI = Flakiness Index (%),
M = sum of the mass of the aggregate passing the slots (mm) and
N = test sample mass (mm).

The following results, as presented by Table A.5, were obtained.

Table A.5: Flakiness Index Calculations

Sieve Size	Sieve Mass	Mass sieve and aggregate	Mass of aggregate	Slot Width	Mass through slots	Flakiness Index
mm	g	g	g	mm	g	%
14	1672.8	1855.4	182.6	10	88.7	
10	1472	3511.7	2039.7	7.1	295.6	
7.1	1621.4	1882.7	261.3	5	18.1	
5	1751.4	1753.7	2.3	3.5	0.6	
TOTAL			**2485.9**		**403**	**16.21**

Thus, FI = 16.21%.

A.5 Aggregate Crushing Value

The ACV was determined by making use of Test Method B1 (1986). The following equation was used.

$$\mathrm{ACV} = \frac{\mathrm{B}}{\mathrm{A}} * 100$$

Where:
ACV = Aggregate Crushing Value (m/m),
B = mass aggregate passing the 2.36 mm sieve (g) and
A = total test sample mass (g).
The following results, as presented by Table A.6 were obtained.

Table A.6: ACV Calculations

Test	Unit	1	2	3	4
Filling the Cylinder					
Mass of cylindrical measure	g	5090.1	5090.4	5090.4	1478.3
Mass of cylindrical measure and sample	g	8082.4	8060.2	8084.6	4495.1
Mass of aggregate	g	2992.3	2969.8	2994.2	3016.8
Sieving of Material					
Mass of pan	g	780.2	1478.7	1478.7	1478.3
Mass of pan and material	g	1043.7	1702.5	1708	1680.8
Mass of fraction -2.36 mm	g	263.5	223.8	229.3	202.5
Aggregate Crushing Value					
A	g	2992.3	2969.8	2994.2	3016.8
B	g	263.5	223.8	229.3	202.5
C	%	8.81	7.54	7.66	6.71
Averaged	%	7.68			

Appendix B

Test Setup Procedures and Equipment

B.1 Ball Penetration Test

This method describes the test used to measure the penetration resistance of a pavement surface and the results may be used in the design process of a surface treatment for a road. The standardised method for the ball penetration test is included in the SANS 3001-BT10 (2013). This test is generally applied to estimate the potential embedment of seal aggregate into the underlying base layer under in-service trafficking conditions. The test is manually operated and can be conducted at random positions or even at specific areas where surfacing seals would be applied. Currently, the ball penetration test is the only empirical test available to estimate aggregate embedment. The test apparatus consists of the following mechanisms as listed in the SANS 3001-BT10 (2013):

- A 19 mm diameter steel ball.
- A 125 mm circular tripod stand with a cross bar.
- A depth gauge measuring in mm's.
- A thermometer graduated in Celsius (10 to 80°C).
- A standard Marshall compaction hammer as specified in the SANS 3001-AS2: Marshall Flow, stability and quotient.

The SANS 3001-BT10 (2013) describes that a minimum of 10 tests be performed in a specific area with a minimum road temperature of 25°C. The test is performed by placing the steel ball at the position where the penetration is to be determined after which a circular tripod is positioned over the ball so that the ball is in the centre of the circular frame. The crossbar is placed in the slots that are provided so that the edge of the bar is vertically over the ball. The first reading, d1, is then taken by making use of the depth gauge from the top of the crossbar to the top of the ball. The crossbar is then removed and a single Marshall hammer blow is applied. The distance is again measured and is noted as d2. A second Marshall hammer blow is then applied and the distance is measured as d3. The pavement surface and its reaction under the ball should be observed in terms of the embedment of the ball, the crushing of the surface and the displacement thereof. All obvious observations should be recorded. Equation

B.1 and B.2 shows the relationships used to obtain the ball penetration after the first and second Marshall hammer blow.

$$E1 = d2 - d1 \tag{B.1}$$

$$E2 = d3 - d1 \tag{B.2}$$

To obtain the one- and two-blow ball penetration values over the area of investigation, Equation B.3 and B.4 can be used:

$$BP1 = E1 \tag{B.3}$$

$$BP2 = E2 - E1 \tag{B.4}$$

The penetration of the base layer, and the hardness of the base, is then quantified by performing the ball penetration test at least another ten times. To select an applicable or representative penetration value, the following recommendations as seen in Figure B.1, as described in the SABITA Manual 40 (2021), is used:

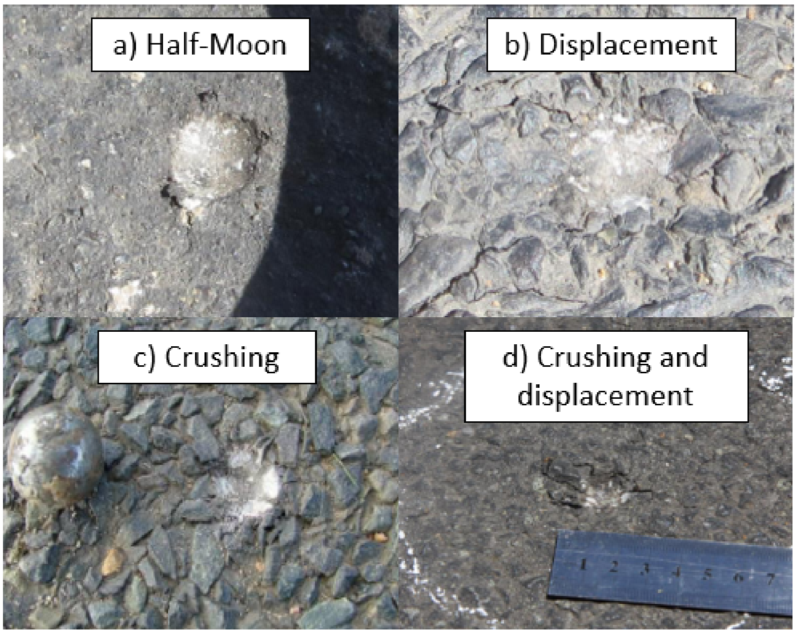

Figure B.1: Where a) Half-Moon, b) displacement, c) crushing and d) crushing and displacement effect

According to the SABITA Manual 40 (2021), when a half-moon is observed in the existing surface, as seen in Figure B.1 a), then embedment could occur and the first penetration value (E1) is used. Potential embedment can be considered as low when only a displacing or crushing effect is observed as per b) and c) in Figure B.1. In this case, only the second penetration value, E2, is used as the first blow is considered a seating hammer blow. Figure B.1 d) shows a crushing and displacement effect together with a half-moon indent after which the SABITA Manual 40 (2021) suggests that the average of the first (E1) and second (E2) blow penetrations be used.

It should be noted that, although the ball penetration test provides an idea as to the hardness of surface upon which the seal is constructed, it does not necessarily predict the embedment of the aggregate. This is mainly due to embedment being affected by various other factors such as the traffic type and intensity, aggregate properties, and the hardness of the existing substrate. According to Neaylon (2012), variation was detected in the test when the surface was non-uniform, COV's were more than 20% and when moisture in the surface was detected. It is also stated that the ball penetration test is dependent on the moisture content of the base material and thus, the test emphasizes that sealing should occur until the base has dried out completely.

All ball penetration tests are done without using the initial seating blow. Abrahams (2015) states that further penetration adjustments could be made when testing pavement surfaces which have been sealed, due to the temperature and binder dependence.

B.2 Texture Depth Test

The texture depth measurement test, as described in SANS 3001-BT11 (2012), is a test involved in the design of surfacing treatments and in particular, it is used to measure the average macro texture depth of a road surface area. The scope of the test procedure involves the measurement of an area that is covered by a known volume of thinly spread sand or glass beads, in a circular manner by making use of a 75 mm disc. The apparatus includes:

- A 50 mL ± 0.5 mL cylinder with a circular shaped base of diameter 75 mm ± 0.5 mm with a rubber membrane, of thickness 6 mm, attached to the bottom of the circular base.
- Rounded or sub-rounded sand or glass bead particles with a minimum specification of 98% passing the 300 µm and a maximum of 2% passing the 75 µm sieve.
- A soft brush with a width of at least 100 mm.
- A 150 mm steel straight edge with one bevelled edge.

To determine the required texture depth, the surface is firstly cleaned from loose particles and dust by making use of the soft brush. Windy conditions should be avoided due to the small sand particles or glass beads used. The cylinder is fully filled with sand and scraped off at the top by making use of the straight edge. To ensure that the sand settles in the cylinder, it is tapped on the base surface and filled again if necessary. The sand is then poured out onto the surface in a cone shaped heap after which the base of the cylinder is placed on top of the cone heap and spread in a circular shape. It is recommended that a continuous spiral movement in an outwards direction be used until the tip of the stones on the surface become visible and the sand layer is even. Five diameter readings are then taken, evenly spaced from one another and the average diameter is calculated to the nearest 0.1 mm. The texture depth is then calculated as per Equation B.5.

$$S_{TD} = 1273 * (\frac{V}{D^2}) \tag{B.5}$$

Where:
S_{TD} = the texture depth (mm),
V = 50 mL of sand and
D = average sand patch diameter (mm).

B.3 MMLS3 - Accelerated Pavement Testing (APT)

B.3.1 Description and Features

The Model Mobile Load Simulator 3 refers to the 1/3 scaled down accelerated pavement tester of the heavy vehicle simulator. According to the MLS Test Systems (2016), the following is a description of the features and attributes of the machine:

- The tester consists of four 300 mm diameter single wheels of a dual axle.
- A maximum of 7200 wheel load applications can be applied per hour which corresponds to a vehicle speed of 9 km/h or 2.5 m/s.
- Tyre pressures could range between 600 kPa and 800 kPa with a normal inflation of 700 kPa.
- The maximum wheel load is 2700 Newton or 2.7 kN.
- The electric motor, which drives the drum, produces 1.5 kW.
- The 80 mm tyre width produces a wheel footprint area of 34cm^2.
- Lateral wander, up to a deviation of 75 mm can be applied.
- The MMLS3 is controlled, in terms of load applications and trafficking speed, by the control box.

Milne (2004) states that in terms of performance testing, APT is able to produce economical (time and resource expenditure) as well as timeous solutions for pavement related problems. Even more so, scaled down pavement testing addresses the economical and timeous factors to an even greater extend to improve accelerated testing. APT methods are required to be completed in a manner such that it can easily be replicated. Subsequently, Milne (2004) reports that the MMLS3 is a technically viable apparatus which is also economically justifiable. The use thereof is sufficient for assessing pavement performance, as well as surfacing performance. The close simulation of APT tests to reality is of major importance in the hierarchy of performance tests. When evaluating the performance of seals where the contact print of the wheel tyre on the stone is to be examined, the contact stress represents similitude and reflects a model of reality. In general, the MMLS3 as a scaled down test, is an economically viable alternative to prioritise certain test variables whilst simulating a smaller, scaled down version of what occurs in practice (Milne, 2004).

Other reasons as to why the MMLS3 is used as a successful accelerated pavement tester includes the successful research record thereof, the testing within a limited budget and the testing within a controlled laboratory and field environment due to its mobility and simplistic operation needs. The MMLS3 has been successfully implemented to measure rutting, moisture variability and susceptibility and aggregate embedment. This provides confidence as to the ability of the MMLS3 to used during this study and for future seal testing. The MLS Test Systems (2016) provides accurate and simplistic guidelines as to the calibration, maintenance and use of the machine. The following aspects are of importance.

B.3.2 Load Application

A wheel load of 2.7 kN is used as a representation of one wheel load of a dual axle system on an E80. This value is derived from the 1/3 scaled factor which relates to 1/3 x 1/3 area of an E80 tyre. Subsequently, the factor translates to a 1:9 scale factor of a contact patch of an E80 tyre while the contact stress is a realistic scale (1:1) of reality (600 - 800 kPa). According to Milne (2004), the 1:9 scale factor of area and loading, while the contact stress has similitude, is consistent with previous research when implementing the MMLS3 on seals.

An important design aspect of the MMLS3 includes the adjustable suspension system which can be used to set the wheel load. The 20 mm displacement travel of the suspension, along with the design geometry thereof ensures that the wheel load is basically independent (±5%) of any displacement within the 20 mm travel. Subsequently, the wheel load can be set beforehand with the requirement that is stays within the specified displacement travel or the machine frame would affect the wheel load (MLS Test Systems, 2016).

B.3.3 Calibrating and setting the wheel load

The wheel load that is applied to the pavement can be calibrated and set by adjusting the suspension springs on the bogies of the system. A calibration unit is provided to aid in setting the correct wheel load.

The calibration unit is mounted, using two bolts, to the top of the machine. To set the wheel load, each wheel is manually moved and positioned directly beneath the calibration unit's flange. With the wheel held in place, the crank on top of the machine is turned to displace the flange vertically downwards as to apply a vertical pressure on the wheel (bogie). The rubber stoppers, or at least one of the two on the wheel trailing arms, should be observed, as they move vertically away from the wheel frame as the wheel is pushed downwards. The gap of the rubber stopper should approximately be 10 mm.

The calibration unit displays the load on the digital screen. The load is adjusted when the desired value is not shown on the screen, when the gap between the wheel frame and rubber stopper is 10 mm. If the load is too low, the springs would need to be compressed by tightening the lock nuts and rotating the spring clockwise. When the load is too high, the spring should be relaxed by loosening the nuts and rotating the spring counter-clockwise. It should be noted that load adjustments, in terms of spring rotations, should be consistent for all of the wheels (bogies). Thus, the number of turns and the compression or relaxation of the springs should be monitored. It is recommended, according to theMLS Test Systems (2016) and Abrahams (2015), that the compression or relaxation of the springs be done in maximum increments of 5 mm in length. Another requirement is that the lengths of the springs should not differ by more than 2 mm. If the load is still not at the desired value, the number of spring rotations and the wheel load increment can be used to calculate the number of turns needed to obtain the desired load. This process is followed until all the bogies have been set correctly.

B.3.4 Setting the machine on the pavement

The machine is firstly moved into an approximate position on the pavement by means of its transport wheels or by crane. After following the correct placement procedure, as stated in the MLS Test Systems (2016), the machine should be levelled. The MMLS3 has four legs that can be adjusted accordingly and individually to obtain the desired level over a test pavement. This allows the machine to stand levelled on an uneven surface or pavement. The bubble level on the machine can be used to ensure that the MMLS3 is level. Once the machine is correctly levelled, all the legs are either cranked upwards or downwards until the 10 mm gap, between the bogie frame and the rubber stopper, is observed when the wheel is on the testing surface. When the machine is lower so that the MMLS3 wheel makes contact with the testing surface, the pavement counteracts the force of the spring by pushing the wheel upwards, causing the stoppers to move away from the frame. The wheel load is now applied to the pavement. The 10 mm gap can be measured at all of the wheels by making use of the supplied tool as seen in Figure B.2.

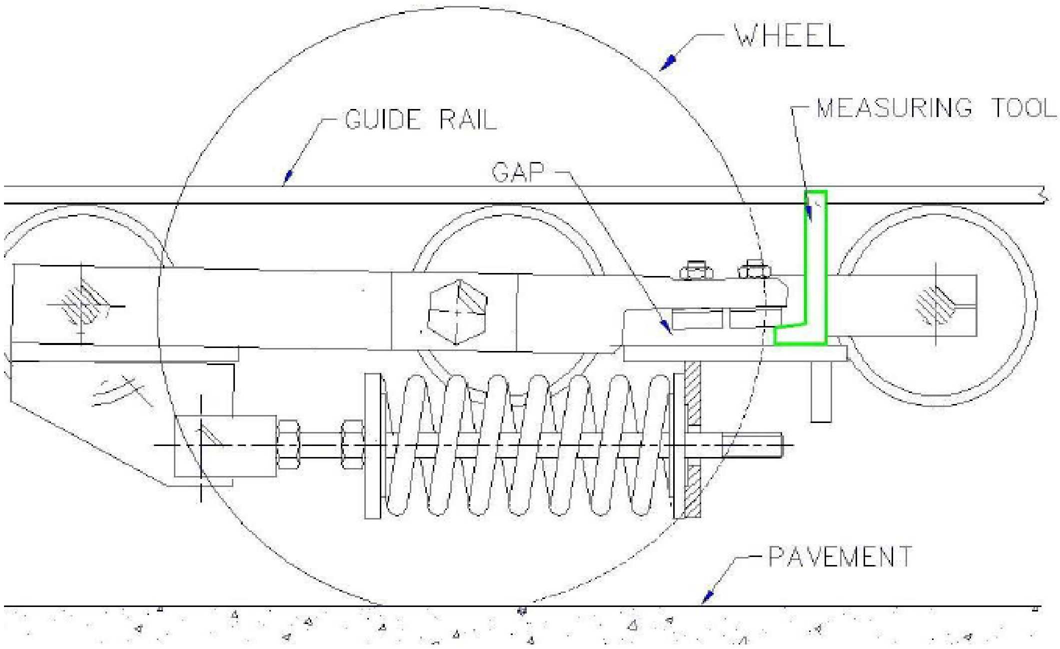

Figure B.2: Measuring the gap of the rubber stopper (MLS Test Systems, 2016)

Once this process is completed, the MMLS3 machine is calibrated accordingly and is ready for testing.

B.3.5 Lateral Displacement System

According to the MLS Test Systems (2016), the purpose of the lateral displacement system is to spread the wheel application loads laterally from the centreline of the track by moving the entire MMLS3 machine. This system consists of the following mechanisms:

- Two base plates that are anchored to the top of the surfacing layer.

- Two roller boards that fit under the adjustable legs of the machine and has four rollers that run on the base plates in the lateral direction. This mechanism allows the machine to move laterally over the pavement from the path's centreline.
- An electric motor with a gearbox to run the system.
- An electronic control system.

The maximum displacement to each side of the path's centreline is 75 mm. This provides a total maximum track of 230 mm as the wheel width is 80 mm. The track, together with the lateral displacement, can be seen in Figure B.3.

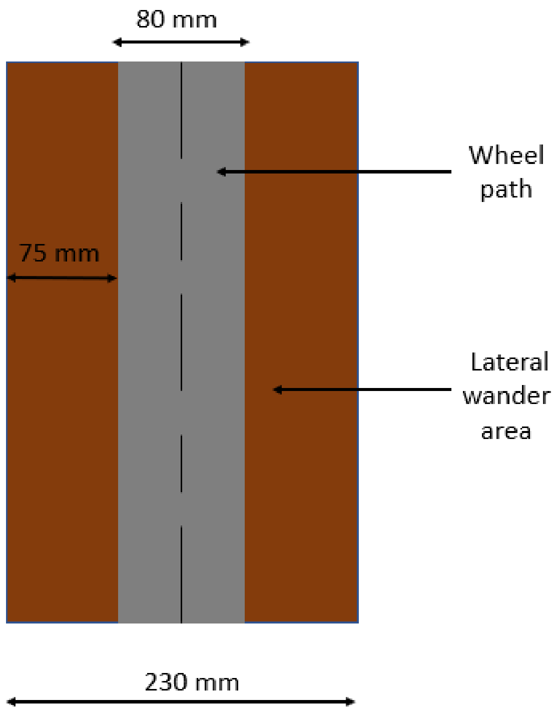

Figure B.3: Lateral wander area

A normal lateral distribution, of the wheel load applications, is achieved by allowing the wheels to spend more time near the centre of the track rather than at the outer edges. The lateral displacements occur at a constant interval of 25 seconds while varying increments are used to achieve the normal load distribution (MLS Test Systems, 2016).

According to Milne (2004), channelised traffic concentrates the applied load applications in the order of 1.5 to 3 times normally distributed traffic. Thus, no lateral wander would be implemented in this study.

Appendix C

Seal Design

C.1 Ball Penetration Tests on the BSM Base

Table C.1 and Table C.2 both present the ball penetration test done to obtain the input ball penetration value for the seal designs.

Table C.1: Ball penetration values for Base 1 containing the S-E1, S-R1 and S-R2 seals

Base 1 (S-E1, S-R1, S-R2)							
Test	**D1 (mm)**	**D2 (mm)**	**D3 (mm)**	**E1 (mm)**	**E2 (mm)**	**BP1 (mm)**	**BP2 (mm)**
				D2 - D1	**D3 - D1**	**E1**	**E2 - E1**
1	47	49.5	50.5	2.5	3.5	2.5	1
2	49	49.5	50.5	0.5	1.5	0.5	1
3	47	48.5	49.5	1.5	2.5	1.5	1
4	47.5	49.5	50	2	2.5	2	0.5
5	47	50	50.5	3	3.5	3	0.5
6	45.5	48.5	49.5	3	4	3	1
7	46	48	49	2	3	2	1
8	46.5	49	49.5	2.5	3	2.5	0.5
9	46.5	48	49	1.5	2.5	1.5	1
10	46	49	50.5	3	4.5	3	1.5
11	46.5	49	50	2.5	3.5	2.5	1
12	48	50	50.5	2	2.5	2	0.5
13	47.5	50.5	52	3	4.5	3	1.5
14	47	48.5	49	1.5	2	1.5	0.5
15	47	49	50	2	3	2	1
Average						2.17	0.90

Table C.2: Ball penetration values for Base 2 containing the S-E2 seals

Base 2 (S-E2)							
Test	**D1 (mm)**	**D2 (mm)**	**D3 (mm)**	**E1 (mm)**	**E2 (mm)**	**BP1 (mm)**	**BP2 (mm)**
				D2 - D1	**D3 - D1**	**E1**	**E2 - E1**
1	47	50	51.5	3	4.5	3	1.5
2	46.5	50	51	3.5	4.5	3.5	1
3	49	52	54	3	5	3	2
4	47	50	52	3	5	3	2
5	47	52	54	5	7	5	2
6	48	53	55	5	7	5	2
7	45.5	48.5	50.5	3	5	3	2
8	46.5	49.5	50.5	3	4	3	1
9	47.5	50.5	51	3	3.5	3	0.5
10	46.5	47.5	49.5	1	3	1	2
Average						3.25	1.60
							2.43

C.2 Binder Application

Table C.3: Seal Design Methodology

SEAL DESIGN				
SEAL	S-E1	S-E2	S-R1	S-R2
CALCULATION				
Equivalent layer thickness (ELT) = 0.85679 *ALD +0.46715 (mm)	7.84	7.84	7.84	7.84
Embedment =((0.1816*LN(CBP)+0.4184)* LN(ELV))- (0.8365*LN(CBP)+2.9284)	0.90	0.97	0.90	0.90
Embedment as fraction of ELT = (Embedment/ELT)	0.11	0.12	0.11	0.11
Fractional void loss due to embedment = 3.0556*(Embedment/ELT)^3- 4.5833* (Embedment/ELT)^2+2.5263* (Embedment/ELT)+0.0002	0.234	0.248	0.234	0.234
Maximum ELV for wear calculation = 5000	3000	3000	3000	3000
Wear (mm) =-0.0011*(10%FACT)+0.2533* (ELV)^0.1747	0.79	0.79	0.79	0.79
Wear as fraction of ELT = (Wear/ELT)	0.10	0.10	0.10	0.10
Fractional void loss due to wear =3.0556* (Wear/ELT)^3- 4.5833*(Wear/ELT)^2+ 2.5263*(Wear/ELT)+0.0002	0.21	0.21	0.21	0.21
Estimated void content for a single seal (%) = 45.3333 - 0.333*ELT	42.72	42.72	42.72	42.72
Fractional Void loss for macro texture = Macro texture requirement/ (Estimated void content%*ELT)	0.30	0.30	0.30	0.30
Total fractional void loss =Fractional void loss due to (Embedment + Wear + Macro texture requirement)	0.75	0.76	0.75	0.75
Available void fraction to be filled with binder = (1 - total fractional void loss)	0.25	0.24	0.25	0.25
% Rolling embedment of total embedment (Assumed 50%)	0.5	0.5	0.5	0.5
Rolling Embed (50% * Total embedment) in mm	0.449	0.485	0.449	0.449
Rolling Embed as fraction of ELT = (Rolling embedment/ELT)	0.06	0.06	0.06	0.06
Fractional void loss due to rolling =3.0556* (Rolling embedment/ELT)^3-4.5833* (Rolling embedment/ELT)^2 +2.5263*(Rolling embedment/ELT)+0.0002	0.13	0.14	0.13	0.13
Minimum voids to be filled with binder =42%	0.42	0.42	0.42	0.42
Filled void fraction to hold stone = Min void fraction to be filled with binder - Fractional void loss due to Rolling Embedment	0.29	0.28	0.29	0.29

SEAL DESIGN (cont.)				
SEAL	**S-E1**	**S-E2**	**S-R1**	**S-R2**
MAX and MIN NCCB				
NCCBmin = (Min void fraction to be filled with binder - Fractional void loss due to Rolling Embedment)*(Estimated void content for a single seal (%)*(ELT)	0.97	0.94	0.97	0.97
Practical Construction Minimum	0.76	0.76	0.76	0.76
NCCBmax = Estimated void content * Available void fraction to be filled with binder * ELT	0.85	0.80	0.85	0.85
Selected practical maximum NCCBmax = 0.1458*ALD+0.1444	1.40	1.40	1.40	1.40
ADJUSTMENTS				
Existing Macro Texture (mm)	0.442	0.950	0.414	0.442
Additional Binder required for existing texture (l/m^2)	0.240	0.300	0.240	0.240
Contractor's tolerance = +5% (l/m^2)	0.048	0.047	0.048	0.048
Heavy Vehicle Speed -10% (10 km/h)	-0.097	-0.094	-0.097	-0.097
Channelisation (Yes) -5%	-0.048	-0.047	-0.048	-0.048
Adjustment (l/m^2)	0.143	0.206	0.143	0.143
CONVERSIONS				
NCCB = NCCBmin	1.11	1.14	1.11	1.11
NCCB = NCCBmax	1.09	1.10	1.09	1.09
Conversion to Hot Modified Factor	1.3	1.4	1.8	1.7
Net Cold to Hot Spray Factor	1.08	1.06	1.07	1.07
Hot Spray Application (l/m^2) **[MIN]**	1.56	1.70	2.14	2.02
Hot Spray Application (l/m^2) **[MAX]**	1.53	1.64	2.10	1.98
Sh - Sh Hot Spray application rate (l/m^2)	**1.56**	**1.70**	**2.14**	**2.02**
Volume Required per 600 x 300 Mould Area (litre) = mass required (kg)	**0.281**	**0.306**	**0.385**	**0.363**

C.3 Dynamic Viscosity

The dynamic viscosity results (Pa.s) for the S-E1, S-E2, S-R1 and S-R2 binders are seen in Table C.4. All viscosity tests were done by means of the Brookefield Viscometer DV-I Prime. The properties of hot polymer modified binders and rubber binders, as per the SABITA TG 1 (2019), is presented in Table C.5 and Table C.6.

Table C.4: Dynamic viscosity results in accordance with the SABITA TG 1 (2019)

Binder	Dynamic Viscosity (Pa.s)	Specification
S-E1	0.25	≤ 0.55 at 165°C
S-E2	0.45	≤ 0.6 at 165°C
S-R1	2.2	2-4 at 190°C
S-R2	2.3	-

Table C.5: Hot applied modified binder properties for surfacing seals as per the SABITA TG 1 (2019)

Property	Unit	Test Method	Class	
Before ageing			**S-E1**	**S-E2**
Softening Point	°C	MB-17	50-70	60-80
Elastic Recovery at 15°C	%	MB-4	> 50	> 60
Dynamic Viscosity at 165°C	Pa.s	MB-18	≤ 0.55	≤ 0.6
Storage stability at 25°C	°C	MB-6	≤ 5	≤ 5
Flash point	°C	ASTM D92	≥ 230	≥ 230
After ageing (RTFOT)				
Mass change	%	MB-3	≤ 1.0	≤ 1.0
Elastic Recovery at 15°C	%	MB-4	> 50	> 60

Table C.6: Bitumen rubber properties for chip seals and asphalt as per the SABITA TG 1 (2019)

Property	**Unit**	**Test Method**	**A-R1**	**S-R1**	**A-R2**	**S-R2**
Softening Point	°C	MB-17	55-65	55-65	65-80	65-80
Dynamic Viscosity at 190°C			20-50	20-40	-	-
Dynamic Viscosity at 170°C	dPa.s	MB-13	-	-	10-40	10-40
Compression Recovery						
5 minutes			> 80	> 70	> 70	> 70
1 hour	%	MB-11	> 70	> 70	> 70	> 70
24 hours			n/a	> 40	n/a	> 25
Resilience at 25°C	%	MB-10	13-40	13-35	10-40	10-40
Flow at 60°C	mm	MB-12	10-50	15-70	0-40	0-40

C.4 Temperature Regulation

Figure C.1 - Figure C.3 show the temperature regulation during MMLS3 trafficking as measured by means of infrared thermometers on the seal surface.

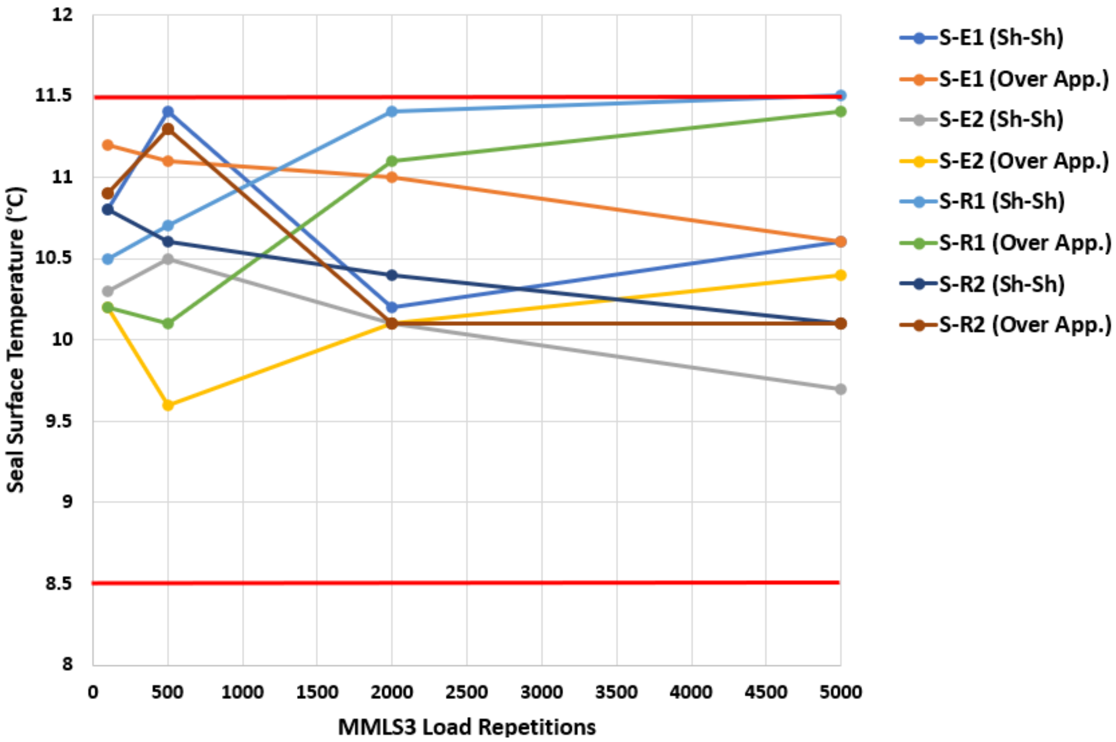

Figure C.1: Seal surface temperature regulation at 10°C trafficking

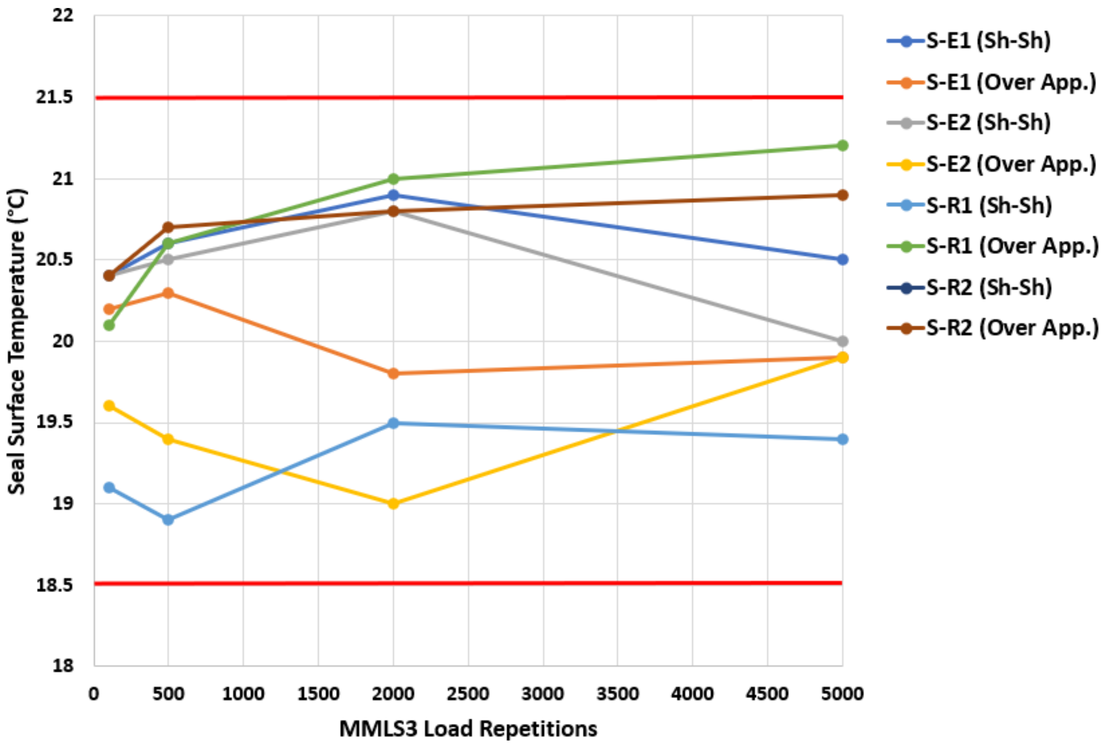

Figure C.2: Seal surface temperature regulation at 20°C trafficking

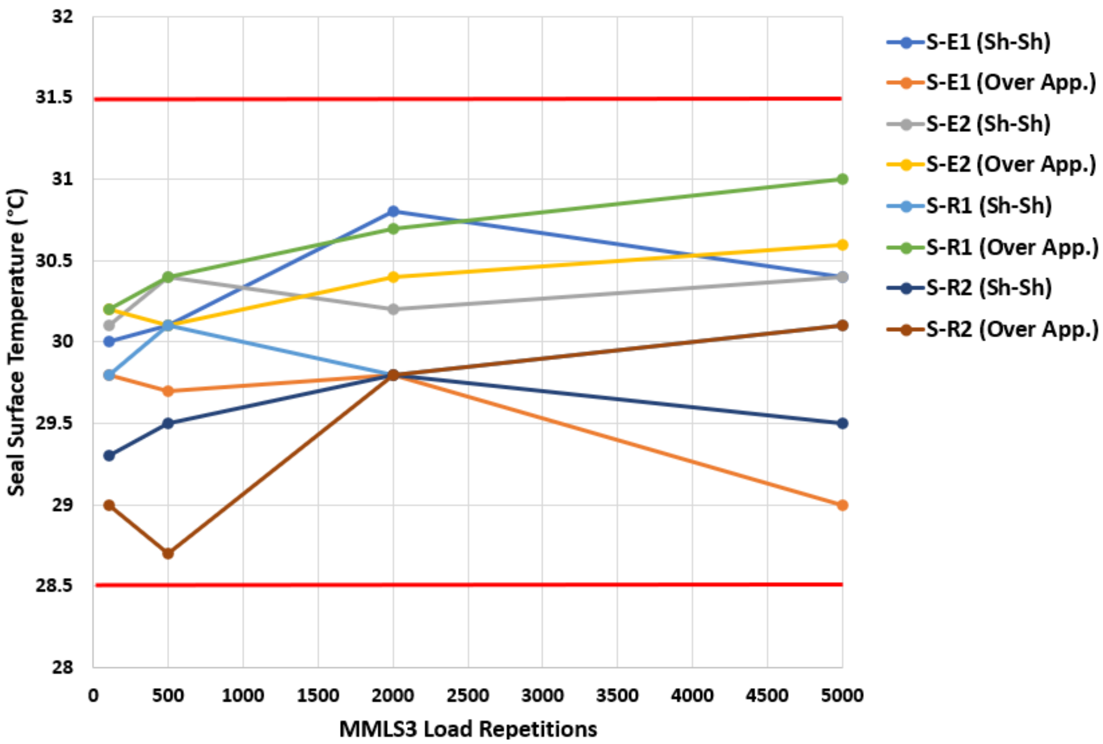

Figure C.3: Seal surface temperature regulation at 30°C trafficking

Appendix D

Texture Results

D.1 Temperature influence on embedment

Table D.1 - Table D.4 show the results obtained after performing various ball penetration tests on the BSM-emulsion test base.

Table D.1: Embedment values at a BSM-emulsion base temperature of 25°C

25°C Base Temperature							
Test	**D1 (mm)**	**D2 (mm)**	**D3 (mm)**	**E1 (mm)**	**E2 (mm)**	**BP1 (mm)**	**BP2 (mm)**
				D2 - D1	**D3 - D1**	**E1**	**E2 - E1**
1	49	50	51	1	2	1	1
2	46	47.5	48.5	1.5	2.5	1.5	1
3	47.5	49	50	1.5	2.5	1.5	1
4	46	48	48.5	2	2.5	2	0.5
5	47	48.5	49.5	1.5	2.5	1.5	1
6	46.5	48	49	1.5	2.5	1.5	1
7	47.5	49	49.5	1.5	2	1.5	0.5
8	47.5	49	50	1.5	2.5	1.5	1
9	48.5	50	51	1.5	2.5	1.5	1
Average						1.50	0.89

Table D.2: Embedment values at a BSM-emulsion base temperature of 30°C

30°C Base Temperature							
Test	**D1 (mm)**	**D2 (mm)**	**D3 (mm)**	**E1 (mm)**	**E2 (mm)**	**BP1 (mm)**	**BP2 (mm)**
				D2 - D1	**D3 - D1**	**E1**	**E2 - E1**
1	47.5	49	50	1.5	2.5	1.5	1
2	47	49	50	2	3	2	1
3	47.5	49	50.5	1.5	3	1.5	1.5
4	47	49	49.5	2	2.5	2	0.5
5	47.5	49	50	1.5	2.5	1.5	1
6	47.5	48.5	49	1	1.5	1	0.5
7	46	47.5	48	1.5	2	1.5	0.5
8	47	48.5	49	1.5	2	1.5	0.5
9	45.5	46.5	48.5	1	3	1	2
Average						1.50	0.94

Table D.3: Embedment values at a BSM-emulsion base temperature of 35°C

35°C Base Temperature							
Test	**D1 (mm)**	**D2 (mm)**	**D3 (mm)**	**E1 (mm)**	**E2 (mm)**	**BP1 (mm)**	**BP2 (mm)**
				D2 - D1	**D3 - D1**	**E1**	**E2 - E1**
1	46	49	50.5	3	4.5	3	1.5
2	47.5	48.5	49	1	1.5	1	0.5
3	47.5	49.5	49.5	2	2	2	0
4	48.5	50	51	1.5	2.5	1.5	1
5	48.5	50	51	1.5	2.5	1.5	1
6	47	48.5	50	1.5	3	1.5	1.5
7	47.5	48.5	50	1	2.5	1	1.5
8	47	48.5	49.5	1.5	2.5	1.5	1
9	48	49	50	1	2	1	1
Average						1.56	1

Table D.4: Embedment values at a BSM-emulsion base temperature of 40°C

40°C Base Temperature							
Test	**D1 (mm)**	**D2 (mm)**	**D3 (mm)**	**E1 (mm)**	**E2 (mm)**	**BP1 (mm)**	**BP2 (mm)**
				D2 - D1	**D3 - D1**	**E1**	**E2 - E1**
1	46.9	48.9	49.9	2	3	2	1
2	46	48	49	2	3	2	1
3	48.5	50.5	51	2	2.5	2	0.5
4	47	49	50	2	3	2	1
5	47.5	50	52.5	2.5	5	2.5	2.5
6	48.5	50.5	51.5	2	3	2	1
7	48	50	51	2	3	2	1
8	46	47.5	48	1.5	2	1.5	0.5
9	46	48	49	2	3	2	1
Average						2	1.06

D.2 Profile Depth and Texture Depth

Table D.5 - Table D.19 shows the mean texture depth calculations as performed with 100 ml glass beads.

Table D.5: MTD values at 10°C and 0 MMLS3 load repetitions

Seal	D1 (mm)	D2 (mm)	D3 (mm)	D4 (mm)	Average D (mm)	Texture Depth (mm)
SE-1, sh-sh	135	130	138	137	135	6.98
SE-1, over app.	142	124	140	121	131.75	7.33
SE-2, sh-sh	138	130	133	127	132	7.31
SE-2, over app.	142	141	133	137	138.25	6.66
SR-1, sh-sh	126	128	134	134	130.5	7.47
SR-1, over app.	129	124	137	137	131.75	7.33
SR-2, sh-sh	142	138	131	115	131.5	7.36
SR-2 over app.	131	128	129	121	127.25	7.86

Table D.6: MTD values at 10°C and 100 MMLS3 load repetitions

Seal	D1 (mm)	D2 (mm)	D3 (mm)	D4 (mm)	Average D (mm)	Texture Depth (mm)
SE-1, sh-sh	136	136	138	131	135.25	6.96
SE-1, over app.	134	141	137	134	136.5	6.83
SE-2, sh-sh	146	146	132	131	138.75	6.61
SE-2, over app.	142	141	130	139	138	6.68
SR-1, sh-sh	131	126	133	132	130.5	7.47
SR-1, over app.	139	141	141	140	140.25	6.47
SR-2, sh-sh	126	148	131	131	134	7.09
SR-2 over app.	138	122	139	129	132	7.31

Table D.7: MTD values at 10°C and 500 MMLS3 load repetitions

Seal	D1 (mm)	D2 (mm)	D3 (mm)	D4 (mm)	Average D (mm)	Texture Depth (mm)
SE-1, sh-sh	139	129	136	134	134.5	7.04
SE-1, over app.	147	129	131	134	135.25	6.96
SE-2, sh-sh	129	140	140	145	138.5	6.64
SE-2, over app.	144	145	141	147	144.25	6.12
SR-1, sh-sh	137	125	127	132	130.25	7.50
SR-1, over app.	141	143	141	143	142	6.31
SR-2, sh-sh	147	141	141	144	143.25	6.20
SR-2 over app.	134	131	149	125	134.75	7.01

Table D.8: MTD values at 10°C and 2000 MMLS3 load repetitions

Seal	D1 (mm)	D2 (mm)	D3 (mm)	D4 (mm)	Average D (mm)	Texture Depth (mm)
SE-1, sh-sh.	141	124	137	135	134.25	7.06
SE-1, over app.	148	125	136	137	136.5	6.83
SE-2, sh-sh	147	125	142	140	138.5	6.64
SE-2, over app.	143	146	141	145	143.75	6.16
SR-1, sh-sh	135	134	131	133	133.25	7.17
SR-1, over app.	142	147	138	139	141.5	6.36
SR-2, sh-sh	144	146	132	141	140.75	6.43
SR-2 over app.	144	131	133	131	134.75	7.01

Table D.9: MTD values at 10°C and 5000 MMLS3 load repetitions

Seal	D1 (mm)	D2 (mm)	D3 (mm)	D4 (mm)	Average D (mm)	Texture Depth (mm)
SE-1, sh-sh	143	139	128	140	137.5	6.73
SE-1, over app.	149	140	138	139	141.5	6.36
SE-2, sh-sh	155	130	138	127	137.5	6.73
SE-2, over app.	149	135	147	139	142.5	6.27
SR-1, sh-sh	139	132	132	134	134.25	7.06
SR-1, over app.	147	142	138	142	142.25	6.29
SR-2, sh-sh.	135	149	137	144	141.25	6.38
SR-2 over app.	135	140	136	140	137.75	6.71

Table D.10: MTD values at 20°C and 0 MMLS3 load repetitions

Seal	D1 (mm)	D2 (mm)	D3 (mm)	D4 (mm)	Average D (mm)	Texture Depth (mm)
SE-1, sh-sh	143	139	128	140	137.5	6.73
SE-1, over app.	149	140	138	139	141.5	6.36
SE-2, sh-sh	155	130	138	127	137.5	6.73
SE-2, over app.	149	135	147	139	142.5	6.27
SR-1, sh-sh	139	132	132	134	134.25	7.06
SR-1, over app.	147	142	138	142	142.25	6.29
SR-2, sh-sh	135	149	137	144	141.25	6.38
SR-2 over app.	135	140	136	140	137.75	6.71

Table D.11: MTD values at 20°C and 100 MMLS3 load repetitions

Seal	D1 (mm)	D2 (mm)	D3 (mm)	D4 (mm)	Average D (mm)	Texture Depth (mm)
SE-1, sh-sh	143	131	135	145	138.5	6.64
SE-1, over app.	141	142	139	147	142.25	6.29
SE-2, sh-sh	140	142	139	146	141.75	6.34
SE-2, over app.	145	150	148	151	148.5	5.77
SR-1, sh-sh	132	137	141	133	135.75	6.91
SR-1, over app.	142	143	145	150	145	6.05
SR-2, sh-sh	148	139	149	144	145	6.05
SR-2 over app.	137	141	139	139	139	6.59

Table D.12: MTD values at 20°C and 500 MMLS3 load repetitions

Seal	D1 (mm)	D2 (mm)	D3 (mm)	D4 (mm)	Average D (mm)	Texture Depth (mm)
SE-1, sh-sh	147	141	140	137	141.25	6.38
SE-1, over app.	142	149	144	146	145.25	6.03
SE-2, sh-sh	148	136	137	145	141.5	6.36
SE-2, over app.	158	143	147	144	148	5.81
SR-1, sh-sh	141	147	142	145	143.75	6.16
SR-1, over app.	147	149	149	147	148	5.81
SR-2, sh-sh	147	140	153	146	146.5	5.93
SR-2 over app.	142	140	139	149	142.5	6.27

Table D.13: MTD values at 20°C and 2000 MMLS3 load repetitions

Seal	D1 (mm)	D2 (mm)	D3 (mm)	D4 (mm)	Average D (mm)	Texture Depth (mm)
SE-1, sh-sh	148	146	137	143	143.5	6.18
SE-1, over app.	160	141	151	148	150	5.66
SE-2, sh-sh	141	143	143	142	142.25	6.29
SE-2, over app.	153	142	152	147	148.5	5.77
SR-1, sh-sh	145	141	146	146	144.5	6.10
SR-1, over app.	146	149	151	148	148.5	5.77
SR-2, sh-sh	160	145	151	151	151.75	5.53
SR-2 over app.	147	136	145	142	142.5	6.27

Table D.14: MTD values at 20°C and 5000 MMLS3 load repetitions

Seal	D1 (mm)	D2 (mm)	D3 (mm)	D4 (mm)	Average D (mm)	Texture Depth (mm)
SE-1, sh-sh	148	133	141	137	139.75	6.52
SE-1, over app.	147	134	158	142	145.25	6.03
SE-2, sh-sh	153	139	150	140	145.5	6.01
SE-2, over app.	162	145	161	148	154	5.37
SR-1, sh-sh	147	142	143	148	145	6.05
SR-1, over app.	156	150	150	156	153	5.44
SR-2, sh-sh	156	145	151	151	150.75	5.60
SR-2 over app.	144	144	147	138	143.25	6.20

Table D.15: MTD values at 30°C and 0 MMLS3 load repetitions

Seal	D1 (mm)	D2 (mm)	D3 (mm)	D4 (mm)	Average D (mm)	Texture Depth (mm)
SE-1, sh-sh	148	133	141	137	139.75	6.52
SE-1, over app.	147	134	158	142	145.25	6.03
SE-2, sh-sh	153	139	150	140	145.5	6.01
SE-2, over app.	162	145	161	148	154	5.37
SR-1, sh-sh	147	142	143	148	145	6.05
SR-1, over app.	156	150	150	156	153	5.44
SR-2, sh-sh	156	145	151	151	150.75	5.60
SR-2 over app.	144	144	147	138	143.25	6.20

Table D.16: MTD values at 30°C and 100 MMLS3 load repetitions

Seal	D1 (mm)	D2 (mm)	D3 (mm)	D4 (mm)	Average D (mm)	Texture Depth (mm)
SE-1, sh-sh	145	140	143	137	141.25	6.38
SE-1, over app.	148	141	147	150	146.5	5.93
SE-2, sh-sh	142	140	149	152	145.75	5.99
SE-2, over app.	155	150	147	154	151.5	5.55
SR-1, sh-sh	145	150	144	146	146.25	5.95
SR-1, over app.	156	153	155	160	156	5.23
SR-2,sh-sh	164	143	138	162	151.75	5.53
SR-2 over app.	150	143	149	145	146.75	5.91

Table D.17: MTD values at 30°C and 500 MMLS3 load repetitions

Seal	D1 (mm)	D2 (mm)	D3 (mm)	D4 (mm)	Average D (mm)	Texture Depth (mm)
SE-1, sh-sh	150	130	149	149	144.5	6.10
SE-1, over app.	150	140	150	155	148.75	5.75
SE-2, sh-sh	159	139	146	149	148.25	5.79
SE-2, over app.	150	145	148	163	151.5	5.55
SR-1, sh-sh	154	141	147	148	147.5	5.85
SR-1, over app.	160	149	149	167	156.25	5.21
SR-2, sh-sh	170	145	147	150	153	5.44
SR-2 over app.	160	140	149	147	149	5.73

Table D.18: MTD values at 30°C and 2000 MMLS3 load repetitions

Seal	D1 (mm)	D2 (mm)	D3 (mm)	D4 (mm)	Average D (mm)	Texture Depth (mm)
SE-1, sh-sh	157	140	160	148	151.25	5.56
SE-1, over app.	165	143	146	165	154.75	5.32
SE-2, sh-sh	162	147	150	152	152.75	5.46
SE-2, over app.	158	148	153	157	154	5.37
SR-1, sh-sh	165	141	160	150	154	5.37
SR-1, over app.	160	155	155	161	157.75	5.12
SR-2, sh-sh	160	164	168	156	162	4.85
SR-2 over app.	166	149	150	157	155.5	5.26

Table D.19: MTD values at 30°C and 5000 MMLS3 load repetitions

Seal	D1 (mm)	D2 (mm)	D3 (mm)	D4 (mm)	Average D (mm)	Texture Depth (mm)
SE-1, sh-sh	152	150	156	148	151.5	5.55
SE-1, over app.	156	150	156	156	154.5	5.33
SE-2, sh-sh	165	145	150	157	154.25	5.35
SE-2, over app.	163	150	148	156	154.25	5.35
SR-1, sh-sh	161	146	158	152	154.25	5.35
SR-1, over app.	156	159	159	158	158	5.10
SR-2, sh-sh	160	155	165	164	161	4.91
SR-2 over app.	160	155	152	157	156	5.23

The wheel path mean profile depth (MPD) values for the 10°C trafficking temperature can be seen in Table D.20 - Table D.23 whilst the values for the 20°C and 30°C temperatures are seen in Table D.24 - Table D.27 and Table D.28 - Table D.31.

Table D.20: Mean profile depth values at 10°C for the S-E1 binder

	S-E1: Sh-Sh at 10°C					S-E1: Over App. at 10°C				
Position	**MMLS3 Applications**					**MMLS3 Applications**				
x-Distance	**0**	**100**	**500**	**2000**	**5000**	**0**	**100**	**500**	**2000**	**5000**
131	4.59	5.45	5.14	4.85	4.63	5.19	6.00	5.28	5.37	5.16
133	5.75	5.08	5.04	4.72	4.98	5.28	5.11	5.43	4.92	4.83
135	5.83	5.35	5.28	4.98	4.98	7.60	5.57	5.55	4.79	4.88
137	5.56	5.17	4.97	5.20	4.89	5.53	5.71	5.79	5.39	5.50
139	6.02	5.28	4.97	4.77	4.89	5.24	5.38	5.16	4.92	4.86
141	5.45	5.22	5.49	4.92	5.07	6.13	5.10	4.92	4.71	4.54
143	5.68	5.32	5.41	5.26	4.68	5.00	4.85	4.56	4.18	4.19
145	5.52	5.35	5.26	4.98	5.08	4.70	4.27	4.26	4.02	3.80
147	5.71	4.90	4.81	4.72	4.55	5.57	4.23	4.31	4.30	4.06
149	5.40	4.99	5.21	4.71	4.52	4.78	4.74	4.71	4.53	4.58
151	6.08	5.64	5.01	4.59	4.78	5.99	5.00	4.81	4.78	4.27
153	5.65	4.88	4.82	4.48	4.41	5.83	4.69	4.74	4.76	4.29
155	4.49	4.66	4.34	3.97	3.80	5.69	4.95	5.11	4.84	4.38
157	4.43	5.06	4.76	4.17	3.93	5.49	4.85	4.84	4.46	4.09
159	5.66	4.53	4.22	4.10	3.70	4.68	4.07	4.28	4.15	3.74
161	5.32	4.52	4.44	4.35	4.07	4.54	3.77	4.02	3.57	3.58
163	5.24	4.84	4.87	4.72	4.28	4.02	3.87	3.85	3.44	3.45
165	5.37	5.23	5.10	5.03	4.84	4.96	4.03	4.37	4.21	3.76
167	5.21	5.30	5.18	4.37	4.67	5.30	4.10	4.36	4.50	4.24
169	5.35	4.14	3.93	3.36	3.91	5.37	4.55	4.77	4.81	4.68
171	4.35	3.94	3.65	3.71	3.36	6.12	4.87	4.74	4.65	4.57
173	5.83	4.22	4.17	4.51	3.56	4.63	4.57	4.33	4.15	4.24
175	6.04	5.22	5.17	4.75	4.77	4.68	4.19	4.14	4.21	3.89
177	5.83	5.15	5.23	4.44	4.47	4.43	4.22	4.24	4.59	4.20
179	5.22	4.45	4.17	3.99	4.32	7.00	4.27	4.20	4.41	4.20
181	5.30	4.49	4.36	3.36	3.81	5.48	4.37	4.50	4.39	4.03
183	4.49	4.12	4.20	3.67	3.37	4.52	3.78	3.66	3.69	3.55
185	4.50	3.87	3.80	3.89	3.54	4.82	3.84	4.36	4.48	4.05
187	4.13	3.84	3.89	4.06	3.97	4.92	4.65	4.25	4.42	4.21
189	4.79	4.13	4.38	4.08	4.02	4.93	4.15	4.07	4.11	3.94
191	4.37	4.12	4.26	4.55	4.06	4.54	4.18	3.98	4.06	3.93
193	5.46	4.89	4.89	4.30	4.55	4.43	3.81	4.08	4.18	4.08
195	6.17	4.51	4.42	4.49	4.36	4.95	4.59	4.58	4.63	4.42
197	5.02	4.73	4.60	4.53	4.62	5.15	4.82	5.16	4.61	4.55
199	4.19	3.87	3.86	3.77	4.14	5.41	4.92	4.99	4.83	4.48
201	4.85	3.74	3.77	3.81	3.82	5.82	5.35	5.27	5.14	5.07
203	4.12	3.86	3.80	4.03	3.86	5.78	5.29	4.80	5.13	4.72
205	4.64	3.82	3.63	4.03	3.57	5.67	5.13	5.13	4.84	4.24
207	4.44	4.48	4.60	4.50	3.92	4.86	5.03	4.55	5.32	4.24
209	5.06	4.68	4.62	4.66	4.39	5.00	4.71	4.27	4.11	3.80
211	5.56	5.45	5.77	5.74	4.79	4.33	3.97	3.69	3.93	3.76
Average	5.19	4.69	4.62	4.42	4.29	5.23	4.62	4.59	4.50	4.27

Table D.21: Mean profile depth values at 10°C for the S-E2 binder

	S-E2: Sh-Sh at 10°C					S-E2: Over App. at 10°C				
Position	**MMLS3 Applications**					**MMLS3 Applications**				
x-Distance	**0**	**100**	**500**	**2000**	**5000**	**0**	**100**	**500**	**2000**	**5000**
95	5.35	5.14	4.79	4.56	5.00	6.12	5.55	5.71	5.64	5.38
97	4.90	4.99	4.86	4.70	4.72	5.75	5.33	5.43	5.67	4.80
99	3.74	4.73	4.62	4.40	4.49	4.99	4.46	4.64	4.69	4.23
101	4.45	3.58	3.77	3.84	3.84	4.69	4.28	4.21	4.05	4.02
103	5.24	3.94	4.15	4.67	4.61	4.32	4.30	4.63	3.82	4.05
105	5.63	5.08	4.77	4.94	4.73	4.32	4.82	4.36	5.04	4.63
107	5.39	5.23	5.29	5.29	4.72	5.60	4.79	4.99	5.22	4.67
109	4.92	4.89	5.10	4.70	4.48	5.26	5.93	5.32	4.77	4.87
111	4.83	4.84	5.25	4.71	4.97	4.41	4.29	4.18	5.26	5.00
113	4.14	4.59	4.40	4.61	4.83	5.37	4.70	4.95	4.72	4.95
115	4.63	4.37	4.14	4.17	4.12	5.04	4.98	5.11	4.49	4.71
117	4.50	4.55	4.31	4.26	3.97	5.89	5.30	5.59	5.13	5.07
119	4.75	4.36	4.25	4.34	4.09	6.21	5.92	5.29	5.41	5.08
121	4.64	4.15	4.19	4.12	4.34	5.72	5.61	5.24	5.38	5.30
123	4.90	4.25	4.65	4.41	4.49	5.46	5.60	5.37	5.31	5.08
125	5.08	4.79	4.89	4.72	4.51	5.79	4.91	4.93	5.08	4.25
127	5.37	4.31	4.46	3.97	4.33	5.44	4.80	4.52	4.75	4.25
129	5.36	5.20	5.45	5.10	4.04	4.81	4.83	4.71	4.61	4.26
131	5.30	5.27	4.95	4.68	4.59	4.72	5.01	4.66	4.61	4.44
133	6.02	4.99	4.99	5.13	4.54	4.56	5.38	4.80	4.85	5.36
135	5.34	4.99	5.12	4.43	4.74	6.11	5.44	5.04	5.12	5.17
137	5.21	5.36	5.32	5.24	4.57	4.89	5.35	5.18	5.06	4.75
139	4.23	4.47	4.49	3.81	4.16	4.49	4.69	4.57	4.37	4.12
141	4.40	4.07	3.96	3.56	3.61	4.23	3.98	3.78	3.61	3.40
143	4.70	4.28	4.12	4.48	3.78	4.51	3.99	3.85	4.33	3.44
145	5.12	4.32	4.37	4.76	4.18	4.36	4.25	4.05	4.28	3.71
147	5.08	4.84	5.00	4.65	4.42	5.01	4.63	4.74	4.33	4.23
149	5.62	4.92	5.23	4.93	4.56	4.87	4.36	4.37	4.33	4.19
151	4.99	4.94	5.23	4.95	4.75	4.57	4.91	4.56	4.25	4.53
153	4.53	4.10	3.97	3.61	4.26	5.83	5.05	4.98	5.36	4.54
155	4.90	3.94	4.05	4.09	3.73	5.25	4.83	4.88	4.93	4.41
157	5.33	4.43	4.26	4.91	4.09	5.24	4.52	4.45	4.99	4.23
159	5.76	5.46	5.10	4.85	4.61	5.31	4.23	4.46	4.39	4.30
161	5.01	5.29	5.16	4.99	4.66	4.95	4.21	4.36	4.41	3.90
163	4.97	4.42	4.61	4.42	4.59	4.99	4.86	4.73	4.80	5.03
165	5.69	4.25	4.40	4.35	4.22	5.49	5.16	5.11	5.01	4.74
167	5.04	4.85	4.84	5.04	4.51	5.01	4.74	4.86	5.11	4.07
169	4.79	4.48	4.99	4.40	5.11	5.65	4.67	4.57	4.81	4.10
171	5.21	4.58	4.78	4.76	4.21	5.21	4.34	4.33	4.71	4.19
173	5.37	5.02	5.12	4.86	4.59	5.24	4.56	4.07	4.59	4.39
175	5.19	5.02	5.15	4.97	5.05	4.24	3.68	3.58	3.82	3.53
Average	5.02	4.66	4.70	4.57	4.43	5.12	4.81	4.71	4.76	4.47

Table D.22: Mean profile depth values at 10°C for the S-R1 binder

	S-R1: Sh-Sh at 10°C					S-R1: Over App. at 10°C				
Position	**MMLS3 Applications**					**MMLS3 Applications**				
x-Distance	**0**	**100**	**500**	**2000**	**5000**	**0**	**100**	**500**	**2000**	**5000**
131	4.65	4.87	4.24	4.29	4.21	4.82	4.59	4.60	4.93	4.19
133	5.19	4.57	4.19	4.41	4.04	4.83	4.30	4.01	5.28	4.02
135	5.06	4.76	4.44	4.23	4.00	4.38	3.76	4.08	4.49	3.51
137	5.30	4.65	4.39	4.63	4.29	4.83	3.96	3.93	4.64	4.08
139	4.49	5.15	4.31	3.93	4.05	5.01	4.26	3.86	4.49	3.77
141	4.58	4.12	4.05	4.39	3.87	6.00	5.37	4.36	5.12	4.41
143	5.11	4.82	4.26	4.37	4.56	5.77	5.59	5.42	5.26	5.24
145	5.56	5.17	5.10	4.60	4.43	6.03	5.57	5.27	5.07	5.16
147	4.97	4.61	4.02	4.44	4.13	6.03	5.71	4.97	4.90	4.73
149	4.41	4.73	4.02	4.12	4.16	5.52	5.29	4.50	4.47	4.18
151	5.03	4.03	4.24	4.22	4.47	4.42	5.18	4.04	4.09	4.01
153	5.09	4.25	4.00	3.78	3.54	5.57	5.04	4.12	4.21	4.10
155	6.32	4.63	4.56	4.49	4.36	5.73	5.10	4.27	4.13	4.08
157	7.19	5.43	4.80	4.24	3.96	5.19	5.00	4.51	4.26	4.26
159	6.40	5.09	4.59	4.84	4.30	5.87	5.03	4.43	4.31	4.16
161	6.11	5.88	4.83	4.53	4.50	5.31	4.61	4.51	4.31	4.38
163	5.95	5.19	4.32	4.28	4.13	5.01	4.25	4.20	4.10	4.02
165	5.02	4.87	4.37	4.18	3.80	5.12	4.65	3.99	4.02	3.94
167	5.03	4.26	4.11	3.78	4.09	6.33	4.64	4.47	4.36	4.39
169	4.88	4.40	3.84	4.05	3.85	5.48	4.49	4.34	4.47	4.33
171	4.77	4.31	3.98	4.04	4.19	5.00	3.87	3.64	3.52	3.45
173	4.07	4.17	3.84	3.75	3.69	5.11	4.01	3.55	4.03	3.59
175	4.49	3.83	3.60	3.83	4.09	4.87	4.21	3.86	3.64	3.74
177	4.97	3.86	4.21	4.24	4.11	5.42	4.67	4.14	4.13	4.19
179	5.52	4.37	4.34	4.65	4.36	5.20	5.04	4.21	4.71	4.15
181	5.74	4.69	5.01	4.50	4.18	4.71	4.47	4.62	4.45	4.31
183	5.78	5.06	4.82	4.41	4.47	4.73	4.23	4.19	4.13	4.25
185	5.89	5.08	4.41	4.19	4.32	5.24	4.55	4.11	3.93	3.77
187	5.80	4.41	4.70	4.48	4.21	5.41	4.79	4.18	4.20	4.07
189	5.35	4.59	4.50	5.29	4.81	5.51	5.21	4.58	4.52	4.40
191	5.66	5.23	5.02	4.75	4.83	5.11	4.52	4.86	4.85	4.51
193	5.06	5.08	4.77	4.40	4.58	5.17	4.60	4.00	4.35	4.17
195	5.09	4.71	4.85	4.93	4.40	5.62	5.20	4.19	4.32	4.24
197	5.71	5.07	4.86	4.39	5.13	5.02	5.38	4.65	5.19	4.74
199	4.99	5.34	4.87	4.88	4.25	5.40	4.86	4.94	4.66	5.23
201	5.60	5.15	4.97	5.23	4.71	4.52	4.49	4.54	4.32	4.38
203	5.65	5.16	5.06	5.13	5.11	4.96	4.58	4.55	4.31	4.33
205	6.31	5.31	5.72	6.07	5.79	4.68	4.84	4.38	4.17	4.15
207	6.40	6.40	5.88	5.42	5.73	5.57	4.39	4.78	4.36	4.39
209	4.68	5.61	5.64	4.26	5.85	5.46	4.75	4.68	4.40	4.44
211	4.74	4.50	4.56	4.50	4.42	5.34	4.50	4.50	4.47	4.63
Average	5.33	4.82	4.54	4.47	4.39	5.25	4.72	4.37	4.43	4.25

Table D.23: Mean profile depth values at 10°C for the S-R2 binder

	S-R2: Sh-Sh at 10°C					S-R2: Over App. at 10°C				
Position	**MMLS3 Applications**					**MMLS3 Applications**				
x-Distance	**0**	**100**	**500**	**2000**	**5000**	**0**	**100**	**500**	**2000**	**5000**
131	4.35	3.87	3.70	4.29	4.43	5.56	4.92	4.64	4.29	4.30
133	5.10	3.97	3.94	4.23	4.09	3.95	4.89	4.20	3.91	3.98
135	4.25	4.09	3.92	3.71	4.00	5.24	4.30	4.58	4.57	4.68
137	4.19	4.06	3.93	4.23	3.59	5.90	5.13	5.05	4.98	5.01
139	5.70	4.34	4.41	4.48	4.06	5.75	5.21	5.32	5.09	4.52
141	4.77	4.53	4.32	3.41	4.11	5.46	4.94	4.71	4.24	4.25
143	4.72	4.18	3.98	4.16	3.63	5.47	4.84	4.66	4.56	4.41
145	5.99	5.40	5.26	5.20	4.46	5.11	4.90	4.69	4.67	4.37
147	5.83	5.36	5.09	4.97	5.21	5.09	4.42	4.32	4.22	4.15
149	5.96	5.30	5.19	4.87	5.08	4.76	4.37	4.06	4.03	3.87
151	6.13	5.23	4.98	4.40	4.77	4.19	4.05	3.73	3.51	3.50
153	5.43	4.79	4.76	4.44	5.08	5.72	3.60	4.17	4.12	4.15
155	5.14	4.40	4.31	4.20	4.45	4.99	4.35	4.73	4.46	4.47
157	4.99	4.51	4.53	4.22	4.12	5.71	4.42	4.27	4.55	4.48
159	5.24	4.66	4.52	4.26	4.20	5.32	5.06	4.74	4.75	4.60
161	6.71	5.42	4.93	4.84	4.65	5.60	4.61	4.17	4.40	4.43
163	6.44	5.78	5.25	4.94	4.93	5.62	4.46	4.48	4.88	4.73
165	5.95	5.44	4.93	4.80	4.88	6.57	5.19	5.02	5.28	5.04
167	6.17	5.38	4.69	4.33	4.45	5.38	5.35	4.86	5.56	4.66
169	5.03	5.16	4.80	4.00	4.23	4.73	4.59	4.41	4.78	4.20
171	6.19	4.35	4.43	4.20	4.24	5.60	4.49	4.59	4.50	4.33
173	5.33	4.99	4.78	4.14	4.08	5.28	4.85	4.89	4.69	4.52
175	5.18	4.60	4.17	3.70	3.90	6.54	4.83	5.15	4.96	4.72
177	4.20	4.21	3.92	4.04	3.72	6.30	5.23	5.19	5.03	4.87
179	5.25	4.78	5.08	5.09	4.20	5.74	5.11	4.74	4.71	4.51
181	5.30	5.51	5.15	5.56	4.93	5.78	5.06	5.04	4.67	4.47
183	6.16	6.08	5.39	4.96	5.14	5.49	5.06	4.90	4.74	4.44
185	6.45	5.39	5.34	4.86	4.64	6.20	5.13	5.15	4.95	4.74
187	6.03	5.08	5.03	4.64	4.53	6.46	5.34	5.23	5.06	4.67
189	5.65	5.34	5.08	4.94	4.55	6.35	5.77	5.13	4.85	4.69
191	5.69	5.42	4.95	4.72	4.57	5.65	4.73	4.59	4.75	4.41
193	4.98	5.18	4.92	5.06	4.71	4.43	4.77	4.30	4.35	4.14
195	6.22	5.71	5.35	5.21	5.25	4.81	4.11	3.83	3.71	3.81
197	5.58	4.57	5.16	4.70	4.92	5.30	4.24	4.33	4.27	4.10
199	4.79	4.61	4.33	4.85	4.54	5.67	4.74	5.02	4.80	4.56
201	4.82	4.89	4.94	4.33	4.41	5.70	5.34	4.91	4.77	4.61
203	4.79	5.13	4.24	4.04	4.35	6.11	5.10	4.87	4.85	4.63
205	4.16	4.17	3.87	4.02	4.17	5.85	5.25	4.91	4.59	4.31
207	4.06	4.25	4.06	4.06	3.99	5.79	4.54	4.63	4.79	4.47
209	4.33	4.07	4.14	4.33	4.30	5.11	5.21	4.78	4.78	4.60
211	3.97	3.65	3.54	4.23	3.57	4.77	4.95	4.80	4.60	4.70
Average	5.30	4.83	4.62	4.48	4.42	5.49	4.82	4.68	4.62	4.44

Table D.24: Mean profile depth values at 20°C for the S-E1 binder

	S-E1: Sh-Sh at 20°C					S-E1: Over App. at 20°C				
Position	**MMLS3 Applications**					**MMLS3 Applications**				
x-Distance	**0**	**100**	**500**	**2000**	**5000**	**0**	**100**	**500**	**2000**	**5000**
131	4.63	5.08	5.25	4.99	5.17	5.16	5.13	5.04	5.12	4.82
133	4.98	4.86	5.02	4.87	4.99	4.83	4.85	4.76	5.05	4.68
135	4.98	4.92	5.04	4.99	4.97	4.88	4.78	4.88	4.64	4.97
137	4.89	4.95	4.96	4.93	5.18	5.50	5.28	5.33	5.28	5.09
139	4.89	4.97	4.77	5.02	4.57	4.86	4.82	4.75	4.92	4.74
141	5.07	5.02	5.34	4.93	4.86	4.54	4.45	4.56	4.44	4.46
143	4.68	4.96	4.88	5.20	5.51	4.19	4.23	4.14	4.20	3.92
145	5.08	5.31	5.01	5.26	5.04	3.80	3.73	3.80	3.87	3.81
147	4.55	4.59	4.64	4.47	4.64	4.06	4.03	4.17	4.01	3.94
149	4.52	4.53	4.40	4.37	4.06	4.58	4.56	4.56	4.52	4.54
151	4.78	4.48	4.60	4.50	4.38	4.27	4.48	4.46	4.33	4.18
153	4.41	4.39	4.40	4.16	4.10	4.29	4.32	4.36	4.32	4.28
155	3.80	4.23	3.91	3.77	3.72	4.38	4.24	4.33	4.40	4.32
157	3.93	3.83	4.04	3.81	3.96	4.09	3.89	3.92	3.94	3.80
159	3.70	4.06	3.86	3.52	3.53	3.74	3.49	3.40	3.46	3.53
161	4.07	3.99	4.07	3.86	3.85	3.58	3.54	3.42	3.29	3.41
163	4.28	4.29	4.33	3.95	4.26	3.45	3.53	3.40	3.48	3.31
165	4.84	4.74	4.72	4.58	4.77	3.76	3.93	3.95	3.78	4.07
167	4.67	5.23	4.58	5.35	4.54	4.24	4.39	4.31	4.34	4.28
169	3.91	4.04	3.88	4.00	3.56	4.68	4.34	4.49	4.48	4.61
171	3.36	3.61	3.33	3.63	3.59	4.57	4.33	4.32	4.32	4.49
173	3.56	3.85	3.62	3.62	3.79	4.24	4.16	4.35	4.27	4.03
175	4.77	4.48	4.85	4.30	4.55	3.89	3.83	3.94	3.89	3.78
177	4.47	4.36	4.30	4.65	4.21	4.20	4.08	4.12	4.05	4.06
179	4.32	4.02	4.40	4.33	4.02	4.20	4.09	4.13	4.09	4.16
181	3.81	3.68	3.68	3.80	3.48	4.03	4.10	4.23	4.15	4.15
183	3.37	3.51	3.29	3.35	3.38	3.55	3.78	3.70	3.58	3.68
185	3.54	3.66	3.59	3.70	3.59	4.05	4.09	3.97	3.88	4.11
187	3.97	3.88	4.02	3.93	3.67	4.21	3.99	4.12	4.07	4.05
189	4.02	3.93	4.23	3.87	3.88	3.94	4.07	4.04	3.77	4.06
191	4.06	4.30	4.50	4.12	4.14	3.93	3.76	3.96	3.68	3.96
193	4.55	4.48	4.86	4.69	4.41	4.08	3.95	3.71	3.66	3.88
195	4.36	4.47	4.34	4.31	4.26	4.42	4.29	4.20	4.20	4.27
197	4.62	4.67	4.61	4.61	4.77	4.55	4.42	4.28	4.16	4.21
199	4.14	4.04	3.89	4.28	4.08	4.48	4.49	4.70	4.27	4.73
201	3.82	4.15	3.64	3.78	3.77	5.07	4.69	4.90	4.59	5.12
203	3.86	3.78	4.09	3.73	3.62	4.72	4.65	4.89	4.81	4.84
205	3.57	3.87	3.73	3.78	3.56	4.24	4.37	4.57	4.36	4.25
207	3.92	3.93	4.01	4.26	4.16	4.24	4.04	4.13	4.13	3.92
209	4.39	4.26	4.41	3.84	4.03	3.80	3.69	3.73	3.70	3.78
211	4.79	4.57	4.79	4.85	5.07	3.76	3.94	3.76	3.80	3.65
Average	4.29	4.34	4.34	4.29	4.24	4.27	4.22	4.24	4.18	4.19

Table D.25: Mean profile depth values at 20°C for the S-E2 binder

	S-E2: Sh-Sh at 20°C					S-E2: Over App. at 20°C				
Position	**MMLS3 Applications**					**MMLS3 Applications**				
x-Distance	**0**	**100**	**500**	**2000**	**5000**	**0**	**100**	**500**	**2000**	**5000**
95	5.00	4.88	4.73	4.63	4.51	5.38	5.37	5.07	5.27	5.99
97	4.72	4.79	4.74	4.46	4.40	4.80	5.46	5.31	4.41	4.90
99	4.49	4.56	4.11	3.76	4.17	4.23	4.38	4.47	4.27	3.87
101	3.84	3.58	3.53	4.58	4.00	4.02	4.10	4.13	3.93	3.75
103	4.61	4.49	4.62	4.31	4.03	4.05	4.10	3.87	4.17	4.54
105	4.73	4.58	4.77	4.62	4.21	4.63	4.44	4.66	4.57	4.80
107	4.72	4.89	5.41	4.75	4.95	4.67	4.72	4.62	4.87	4.85
109	4.48	4.78	4.59	4.69	4.53	4.87	5.06	4.79	4.68	4.40
111	4.97	4.86	4.85	4.75	4.67	5.00	4.30	4.45	4.76	4.82
113	4.83	4.63	4.06	3.94	4.08	4.95	4.75	4.92	5.33	4.44
115	4.12	4.01	3.79	3.91	3.67	4.71	4.96	4.79	4.82	5.20
117	3.97	3.93	4.12	3.96	4.05	5.07	5.10	4.92	4.98	4.72
119	4.09	4.00	4.09	3.67	4.06	5.08	5.19	4.94	5.04	4.66
121	4.34	3.96	4.21	4.40	4.22	5.30	5.19	5.11	4.87	4.64
123	4.49	4.64	4.52	4.56	4.56	5.08	4.99	5.11	4.56	4.30
125	4.51	4.47	4.64	4.12	4.13	4.25	4.55	4.77	4.07	3.79
127	4.33	3.86	4.12	4.17	3.78	4.25	4.12	4.24	3.83	3.99
129	4.04	4.42	4.40	4.49	4.30	4.26	4.36	4.10	4.28	4.32
131	4.59	5.35	4.66	4.64	4.34	4.44	4.33	4.29	4.34	3.83
133	4.54	4.49	4.39	4.42	4.49	5.36	4.91	4.32	4.67	4.48
135	4.74	4.51	4.43	4.41	4.32	5.17	4.82	5.05	4.67	4.71
137	4.57	4.61	4.49	4.33	4.26	4.75	4.79	4.74	4.17	4.06
139	4.16	3.98	3.63	3.56	3.67	4.12	4.06	3.93	3.52	3.35
141	3.61	3.90	4.00	3.68	3.70	3.40	3.19	3.37	3.71	3.48
143	3.78	4.22	4.09	4.25	4.30	3.44	3.47	3.47	3.61	3.30
145	4.18	4.40	4.45	4.32	4.50	3.71	3.75	3.46	4.26	3.95
147	4.42	4.62	4.31	4.50	4.31	4.23	4.05	3.98	4.48	3.88
149	4.56	4.72	4.89	4.87	5.00	4.19	4.58	4.09	4.10	3.81
151	4.75	5.00	4.32	3.78	4.32	4.53	4.42	3.98	4.27	4.24
153	4.26	4.06	3.78	3.53	3.56	4.54	4.57	4.62	4.42	4.22
155	3.73	3.85	3.97	4.24	3.95	4.41	4.35	4.48	4.19	4.09
157	4.09	4.32	4.70	4.61	4.68	4.23	4.25	4.33	4.31	3.90
159	4.61	4.80	4.67	5.06	4.73	4.30	4.34	3.93	3.56	3.57
161	4.66	5.05	4.49	4.45	4.65	3.90	3.96	4.13	4.48	4.07
163	4.59	4.04	4.08	4.05	4.17	5.03	4.85	4.84	4.68	4.76
165	4.22	4.59	4.28	4.69	4.39	4.74	4.71	4.85	4.38	4.57
167	4.51	4.77	4.77	5.01	4.81	4.07	4.38	4.42	3.77	3.71
169	5.11	4.54	4.15	4.33	4.29	4.10	4.06	3.94	4.23	4.09
171	4.21	4.45	4.60	4.67	4.57	4.19	4.24	4.09	4.28	4.08
173	4.59	4.83	4.97	4.85	5.09	4.39	4.38	4.37	3.84	3.75
175	5.05	4.87	5.01	5.05	5.04	3.53	3.58	3.73	3.56	3.54
Average	4.43	4.47	4.40	4.37	4.33	4.47	4.47	4.41	4.35	4.23

Table D.26: Mean profile depth values at 20°C for the S-R1 binder

	S-R1: Sh-Sh at 20°C					S-R1: Over App. at 20°C				
Position	**MMLS3 Applications**					**MMLS3 Applications**				
x-Distance	**0**	**100**	**500**	**2000**	**5000**	**0**	**100**	**500**	**2000**	**5000**
131	4.21	4.16	4.36	4.16	4.06	4.19	4.09	4.04	3.99	3.76
133	4.04	4.16	4.32	4.14	4.05	4.02	4.14	3.57	3.29	3.43
135	4.00	4.00	4.11	4.45	4.08	3.51	3.67	3.32	3.64	4.24
137	4.29	4.32	4.41	4.14	3.88	4.08	4.05	3.98	3.94	3.87
139	4.05	3.86	3.94	4.67	4.23	3.77	3.91	3.73	4.06	4.05
141	3.87	4.08	3.72	3.84	3.77	4.41	4.66	4.47	4.65	4.95
143	4.56	4.40	4.98	4.17	4.07	5.24	5.13	5.28	5.36	5.06
145	4.43	4.52	4.72	4.61	4.68	5.16	4.99	5.16	5.11	5.17
147	4.13	4.07	4.11	4.14	4.05	4.73	4.60	4.70	4.59	4.34
149	4.16	4.14	4.25	4.15	4.13	4.18	4.26	4.14	4.27	3.95
151	4.47	4.28	4.16	4.01	4.21	4.01	3.70	3.91	3.87	3.87
153	3.54	3.65	3.76	3.67	3.70	4.10	4.00	3.98	3.94	4.23
155	4.36	4.11	4.27	4.15	3.87	4.08	3.99	3.99	4.03	4.18
157	3.96	3.80	3.99	3.89	3.65	4.26	4.28	4.31	4.23	4.35
159	4.30	4.41	3.89	3.84	3.87	4.16	4.22	4.14	4.98	4.27
161	4.50	4.41	4.38	4.33	4.40	4.38	4.28	4.54	4.24	4.09
163	4.13	4.14	3.93	4.28	4.06	4.02	3.84	4.04	3.85	3.82
165	3.80	3.73	3.95	4.01	4.11	3.94	3.99	3.99	4.17	3.99
167	4.09	4.14	3.70	3.79	3.57	4.39	4.24	4.35	4.34	3.99
169	3.85	3.94	3.65	3.74	3.61	4.33	4.29	3.84	3.78	3.31
171	4.19	3.89	4.05	3.89	3.86	3.45	3.48	3.19	3.38	3.52
173	3.69	3.63	3.67	3.70	3.60	3.59	3.53	3.57	3.67	3.49
175	4.09	3.93	3.92	4.20	3.84	3.74	3.66	3.69	3.74	3.64
177	4.11	4.15	4.10	3.75	4.07	4.19	4.07	4.23	4.13	3.94
179	4.36	4.41	4.18	4.21	3.97	4.15	4.37	4.21	4.33	3.99
181	4.18	4.40	4.68	4.17	4.33	4.31	4.53	4.37	4.36	4.14
183	4.47	4.33	4.39	4.22	4.22	4.25	4.16	4.06	4.19	4.04
185	4.32	4.53	4.42	4.12	4.24	3.77	4.16	3.72	3.77	4.11
187	4.21	3.98	3.81	4.01	3.83	4.07	4.50	4.25	4.50	4.47
189	4.81	5.03	4.99	4.28	4.16	4.40	4.30	4.57	4.18	3.99
191	4.83	4.69	4.79	4.94	4.52	4.51	4.88	4.20	4.09	3.89
193	4.58	4.53	4.41	4.53	4.52	4.17	4.55	4.08	4.09	4.07
195	4.40	4.71	4.52	4.44	4.27	4.24	4.54	4.69	4.58	4.55
197	5.13	4.46	5.02	4.72	4.79	4.74	4.58	4.89	5.35	5.23
199	4.25	4.72	4.44	4.15	4.08	5.23	4.68	5.01	5.22	4.48
201	4.71	4.91	4.89	4.71	4.77	4.38	4.52	4.58	4.18	4.29
203	5.11	5.35	4.97	4.80	4.73	4.33	4.29	4.55	4.19	4.37
205	5.79	5.84	5.53	5.22	5.56	4.15	4.34	4.27	4.59	4.39
207	5.73	5.42	5.79	5.88	5.74	4.39	4.46	4.36	4.39	4.77
209	5.85	5.49	5.80	6.06	5.91	4.44	4.33	4.34	4.28	4.40
211	4.42	4.32	4.17	3.87	3.85	4.63	4.55	4.64	4.22	4.48
Average	4.39	4.37	4.37	4.29	4.22	4.25	4.26	4.22	4.24	4.17

Table D.27: Mean profile depth values at 20°C for the S-R2 binder

	S-R2: Sh-Sh at 20°C					S-R2: Over App. at 20°C				
Position	MMLS3 Applications					MMLS3 Applications				
x-Distance	0	100	500	2000	5000	0	100	500	2000	5000
131	4.43	4.47	3.64	3.73	3.54	4.30	4.31	4.39	4.78	4.85
133	4.09	3.93	3.54	3.33	3.18	3.98	3.74	3.89	4.17	4.42
135	4.00	3.97	3.28	3.39	3.38	4.68	4.76	4.55	4.72	4.99
137	3.59	3.70	4.10	3.24	3.43	5.01	5.03	5.15	5.10	4.94
139	4.06	4.31	4.00	3.88	3.95	4.52	5.00	4.72	4.64	4.67
141	4.11	3.78	3.49	3.81	3.40	4.25	4.19	4.11	4.22	4.01
143	3.63	3.88	3.76	3.18	3.61	4.41	4.41	4.36	4.30	4.18
145	4.46	4.79	4.57	4.09	4.13	4.37	4.43	4.37	4.33	4.20
147	5.21	5.10	4.85	4.99	4.40	4.15	4.36	4.32	4.30	4.10
149	5.08	4.95	4.52	4.96	4.14	3.87	4.31	4.03	3.94	3.57
151	4.77	4.64	4.38	4.34	4.42	3.50	3.67	3.76	3.69	3.63
153	5.08	4.98	4.41	4.58	4.40	4.15	4.00	4.01	4.02	3.89
155	4.45	4.28	3.94	4.14	3.82	4.47	4.46	4.57	4.67	4.06
157	4.12	4.36	4.19	4.06	4.04	4.48	4.54	4.90	4.60	4.59
159	4.20	4.24	4.08	3.97	4.14	4.60	4.76	4.92	4.69	4.41
161	4.65	4.50	4.61	4.36	4.53	4.43	4.28	4.57	4.32	4.34
163	4.93	4.79	5.00	4.76	4.78	4.73	4.50	4.56	4.59	4.62
165	4.88	4.63	4.77	4.58	4.64	5.04	5.26	5.11	5.18	5.16
167	4.45	4.34	4.40	4.46	4.30	4.66	4.80	4.99	4.79	4.59
169	4.23	4.15	4.14	4.02	3.88	4.20	4.27	4.10	4.19	4.15
171	4.24	4.34	4.13	4.25	4.17	4.33	3.97	4.06	4.05	4.20
173	4.08	4.59	3.92	3.99	4.02	4.52	4.39	4.43	4.36	4.04
175	3.90	3.83	3.57	3.93	3.67	4.72	4.73	4.67	4.57	4.38
177	3.72	3.91	3.82	3.39	3.57	4.87	4.87	4.80	4.80	4.30
179	4.20	4.47	4.76	3.93	4.02	4.51	4.56	4.49	4.41	4.13
181	4.93	4.99	4.92	4.63	5.06	4.47	4.48	4.43	4.18	3.97
183	5.14	5.31	4.80	4.99	4.95	4.44	4.61	4.43	4.56	4.38
185	4.64	4.59	4.77	4.82	4.36	4.74	4.81	4.72	4.73	4.68
187	4.53	4.42	4.16	4.05	3.93	4.67	4.90	4.99	5.01	4.84
189	4.55	4.95	5.02	4.30	4.37	4.69	4.65	4.79	4.55	4.66
191	4.57	4.55	4.31	4.28	4.04	4.41	4.48	4.64	4.35	4.22
193	4.71	5.09	4.95	4.43	4.65	4.14	4.10	4.26	4.17	3.67
195	5.25	4.76	4.77	4.66	4.39	3.81	3.92	3.71	3.64	3.75
197	4.92	4.83	4.71	4.52	4.64	4.10	3.94	3.99	3.93	4.00
199	4.54	4.71	4.72	4.43	4.36	4.56	4.70	4.68	4.36	4.75
201	4.41	4.70	4.31	4.66	4.37	4.61	4.61	4.60	4.54	4.39
203	4.35	4.24	3.87	4.15	4.12	4.63	4.89	4.83	4.65	4.89
205	4.17	3.90	3.95	4.27	4.13	4.31	4.47	4.47	4.51	4.37
207	3.99	4.47	4.01	4.06	4.00	4.47	4.59	4.58	4.46	4.42
209	4.30	4.11	3.95	4.38	4.11	4.60	4.50	4.43	4.51	4.42
211	3.57	3.69	3.93	3.66	3.68	4.70	4.63	4.65	4.44	4.49
Average	4.42	4.45	4.27	4.19	4.11	4.44	4.48	4.49	4.44	4.35

Table D.28: Mean profile depth values at 30°C for the S-E1 binder

	S-E1: Sh-Sh at 30°C					**S-E1: Over App. at 30°C**				
Position	**MMLS3 Applications**					**MMLS3 Applications**				
x-Distance	**0**	**100**	**500**	**2000**	**5000**	**0**	**100**	**500**	**2000**	**5000**
131	5.17	4.95	5.16	4.11	4.03	4.82	4.84	4.91	4.67	4.60
133	4.99	4.83	4.86	4.26	4.26	4.68	4.71	4.55	4.84	4.98
135	4.97	5.09	5.09	4.82	4.57	4.97	4.71	4.62	4.58	4.64
137	5.18	5.13	5.15	4.42	4.40	5.09	5.15	4.90	5.01	4.95
139	4.57	4.55	5.04	4.41	4.57	4.74	4.78	4.93	4.30	4.71
141	4.86	4.83	5.00	4.70	4.65	4.46	4.33	4.33	4.38	4.67
143	5.51	5.43	4.89	4.92	4.78	3.92	4.04	4.26	3.92	3.83
145	5.04	4.73	4.85	4.32	4.08	3.81	3.61	3.90	3.67	3.79
147	4.64	4.32	4.32	4.21	4.00	3.94	3.90	3.94	4.22	4.05
149	4.06	3.92	4.10	3.85	3.86	4.54	4.55	4.34	4.47	4.32
151	4.38	4.22	3.99	3.74	3.81	4.18	4.38	4.37	4.00	4.04
153	4.10	3.69	4.13	3.66	3.65	4.28	3.99	4.14	4.09	4.14
155	3.72	3.62	3.54	3.58	3.59	4.32	4.05	4.08	3.92	3.99
157	3.96	3.69	4.18	3.27	3.25	3.80	3.81	3.73	3.59	3.50
159	3.53	3.43	3.53	3.15	3.03	3.53	3.34	3.36	3.40	3.21
161	3.85	3.58	3.84	3.26	3.09	3.41	3.18	3.27	3.03	3.13
163	4.26	4.15	3.89	4.02	3.67	3.31	3.19	3.30	3.10	3.19
165	4.77	4.49	4.47	4.38	4.16	4.07	3.89	3.30	3.76	3.81
167	4.54	4.07	4.22	4.16	4.00	4.28	3.92	4.04	4.22	4.16
169	3.56	3.45	3.64	3.39	3.35	4.61	4.24	4.21	4.32	4.30
171	3.59	3.33	3.15	3.09	2.82	4.49	4.08	4.08	4.33	4.19
173	3.79	3.69	3.39	3.72	3.43	4.03	4.23	4.29	3.78	3.86
175	4.55	4.27	4.15	4.02	3.98	3.78	3.64	3.67	3.77	3.44
177	4.21	4.16	4.13	3.92	3.65	4.06	3.81	3.72	3.65	4.18
179	4.02	3.92	4.37	3.41	3.46	4.16	4.15	4.02	3.89	4.45
181	3.48	3.28	3.21	3.07	2.87	4.15	3.93	3.75	3.91	3.86
183	3.38	3.46	3.25	3.31	3.18	3.68	3.53	3.42	3.44	3.62
185	3.59	3.71	3.51	3.57	3.53	4.11	3.76	3.60	3.84	3.50
187	3.67	3.66	3.68	3.62	3.39	4.05	3.86	4.02	3.77	3.58
189	3.88	3.92	3.85	3.69	3.39	4.06	3.73	3.63	3.58	3.75
191	4.14	3.98	3.96	4.20	3.86	3.96	3.67	3.88	3.53	3.58
193	4.41	4.30	4.42	4.22	4.40	3.88	3.54	3.51	3.65	3.61
195	4.26	4.10	3.97	4.12	3.76	4.27	4.05	3.96	3.97	3.59
197	4.77	4.46	4.55	4.54	4.03	4.21	4.01	4.07	4.05	3.63
199	4.08	3.98	4.19	4.07	3.69	4.73	4.02	4.16	4.28	4.05
201	3.77	3.19	3.51	3.53	3.24	5.12	4.71	4.38	4.68	4.69
203	3.62	3.59	3.34	3.81	3.42	4.84	4.58	4.74	4.54	4.60
205	3.56	3.63	3.52	3.81	3.58	4.25	4.24	4.31	4.30	4.02
207	4.16	3.98	4.07	4.08	3.85	3.92	4.01	4.07	3.78	3.96
209	4.03	4.09	3.82	3.90	3.85	3.78	3.57	3.49	3.67	3.81
211	5.07	5.23	4.47	4.71	4.51	3.65	3.52	3.43	3.76	3.38
Average	4.24	4.10	4.11	3.93	3.77	4.19	4.03	4.02	3.99	3.98

Table D.29: Mean profile depth values at 30°C for the S-E2 binder

	S-E2: Sh-Sh at 30°C					S-E2: Over App. at 30°C				
Position	**MMLS3 Applications**					**MMLS3 Applications**				
x-Distance	**0**	**100**	**500**	**2000**	**5000**	**0**	**100**	**500**	**2000**	**5000**
95	4.51	3.97	4.28	4.41	3.41	5.99	4.66	4.51	3.96	5.49
97	4.40	4.07	4.03	4.21	3.60	4.90	4.69	4.21	4.08	4.44
99	4.17	3.82	3.92	4.13	3.39	3.87	4.26	4.19	3.93	4.23
101	4.00	3.74	3.77	3.83	3.42	3.75	4.21	3.61	3.45	4.07
103	4.03	3.93	3.84	4.13	3.49	4.54	4.27	4.16	3.74	4.21
105	4.21	4.23	4.04	4.53	3.60	4.80	4.25	4.04	3.99	4.02
107	4.95	4.72	4.01	4.78	4.02	4.85	4.52	4.40	3.95	4.34
109	4.53	4.55	4.59	4.36	4.28	4.40	4.02	4.47	4.59	4.46
111	4.67	4.64	4.50	4.92	4.44	4.82	4.49	4.47	4.43	4.26
113	4.08	4.04	4.62	4.19	4.29	4.44	4.11	4.44	4.53	4.36
115	3.67	3.96	4.12	4.53	3.95	5.20	4.43	4.33	3.99	4.49
117	4.05	3.98	3.74	4.88	3.56	4.72	4.58	3.91	3.73	4.67
119	4.06	4.04	4.13	4.61	3.95	4.66	4.76	4.57	3.88	4.65
121	4.22	4.33	4.05	4.17	3.53	4.64	4.49	4.04	3.92	4.56
123	4.56	4.57	4.22	3.41	4.21	4.30	4.02	4.05	4.14	3.97
125	4.13	3.98	4.51	3.60	4.57	3.79	3.57	4.25	4.43	3.25
127	3.78	3.81	4.00	3.56	3.41	3.99	3.53	3.62	3.98	3.58
129	4.30	4.17	3.77	3.73	3.91	4.32	3.64	3.83	3.88	3.81
131	4.34	4.43	4.18	4.18	3.99	3.83	4.04	4.06	4.13	4.11
133	4.49	4.28	4.17	4.13	3.72	4.48	4.45	4.25	4.19	4.27
135	4.32	4.18	4.10	4.36	3.62	4.71	4.15	4.11	3.94	3.98
137	4.26	4.19	4.13	3.27	3.70	4.06	3.86	3.88	3.89	3.89
139	3.67	3.44	4.06	3.10	3.77	3.35	3.22	3.38	3.97	3.33
141	3.70	3.68	3.42	3.28	2.82	3.48	3.41	3.18	3.12	3.25
143	4.30	3.91	3.36	3.53	3.04	3.30	3.47	3.45	3.40	3.33
145	4.50	4.35	3.83	4.13	3.41	3.95	4.03	3.77	3.71	3.84
147	4.31	4.24	4.22	3.87	3.42	3.88	3.99	3.98	3.95	3.64
149	5.00	4.70	4.18	3.94	3.61	3.81	3.95	3.90	3.88	3.74
151	4.32	4.14	4.69	3.65	4.33	4.24	4.05	4.16	4.58	3.66
153	3.56	3.65	4.08	3.63	3.51	4.22	3.99	4.08	4.10	3.56
155	3.95	4.07	3.59	4.02	3.49	4.09	3.97	3.91	3.66	3.70
157	4.68	4.45	4.01	3.13	3.74	3.90	4.02	3.86	3.81	3.78
159	4.73	4.75	4.19	3.69	3.95	3.57	3.60	3.74	4.26	2.95
161	4.65	4.43	4.68	4.03	4.05	4.07	4.52	4.53	4.54	3.65
163	4.17	4.12	4.59	4.08	4.14	4.76	4.59	4.60	4.65	4.03
165	4.39	4.36	4.11	3.38	3.69	4.57	3.99	3.90	3.88	3.59
167	4.81	4.84	4.26	3.23	4.03	3.71	3.52	3.67	4.24	3.03
169	4.29	4.17	4.66	3.73	4.24	4.09	3.90	4.42	4.56	3.28
171	4.57	4.47	4.13	3.66	4.17	4.08	4.40	4.35	4.16	3.45
173	5.09	4.83	4.35	2.81	4.31	3.75	3.85	4.34	4.47	3.31
175	5.04	4.88	4.84	3.48	4.63	3.54	3.50	3.79	4.86	2.89
Average	4.33	4.22	4.15	3.91	3.81	4.23	4.07	4.06	4.06	3.88

Table D.30: Mean profile depth values at 30°C for the S-R1 binder

	S-R1: Sh-Sh at 30°C					S-R1: Over App. at 30°C				
Position	**MMLS3 Applications**					**MMLS3 Applications**				
x-Distance	**0**	**100**	**500**	**2000**	**5000**	**0**	**100**	**500**	**2000**	**5000**
131	4.06	3.78	3.88	3.84	3.52	3.76	3.60	3.56	3.37	3.41
133	4.05	3.70	3.71	4.24	3.74	3.43	3.31	3.33	3.27	3.72
135	4.08	3.65	3.87	5.25	3.10	4.24	4.04	3.82	3.94	3.64
137	3.88	4.15	4.10	3.45	3.36	3.87	3.82	3.78	3.70	3.64
139	4.23	3.79	3.86	3.65	3.19	4.05	3.92	3.83	3.96	4.13
141	3.77	3.64	3.72	3.60	3.98	4.95	4.89	4.23	4.80	4.87
143	4.07	4.28	4.29	4.43	4.73	5.06	5.09	5.19	5.00	4.56
145	4.68	4.43	4.48	4.57	4.36	5.17	4.81	4.77	4.65	4.45
147	4.05	3.93	4.02	4.13	4.16	4.34	4.34	4.40	4.20	4.02
149	4.13	3.96	3.98	3.82	3.94	3.95	3.94	3.83	3.72	3.42
151	4.21	3.90	4.10	4.03	3.81	3.87	3.71	3.65	3.41	3.50
153	3.70	3.77	3.59	3.72	3.47	4.23	3.84	3.75	3.65	3.69
155	3.87	3.79	3.87	3.52	3.41	4.18	4.15	4.07	3.65	3.81
157	3.65	3.68	3.44	3.23	3.39	4.35	4.19	4.08	3.68	3.51
159	3.87	4.16	3.54	3.51	3.86	4.27	4.12	4.01	3.74	3.59
161	4.40	3.91	4.04	3.99	3.92	4.09	3.96	3.97	3.53	3.57
163	4.06	4.02	3.84	3.70	3.97	3.82	3.65	3.54	3.36	3.41
165	4.11	3.77	3.92	3.66	3.49	3.99	3.80	3.72	3.46	3.43
167	3.57	3.52	3.62	3.51	3.57	3.99	3.80	4.16	3.46	3.12
169	3.61	3.56	3.50	3.43	3.47	3.31	3.38	3.37	3.24	3.29
171	3.86	3.68	3.73	3.61	3.57	3.52	3.39	3.25	3.47	3.50
173	3.60	3.61	3.49	3.45	3.23	3.49	3.44	3.60	3.30	3.18
175	3.84	3.57	3.68	3.73	3.67	3.64	3.51	3.46	3.22	3.17
177	4.07	3.73	3.92	3.76	3.76	3.94	3.70	3.56	3.27	3.22
179	3.97	3.89	3.87	3.52	3.73	3.99	3.88	3.84	3.25	3.34
181	4.33	4.19	4.23	3.69	3.92	4.14	4.01	4.08	3.66	3.68
183	4.22	3.99	3.92	3.83	3.92	4.04	3.64	3.89	3.57	3.65
185	4.24	3.98	4.04	3.62	3.85	4.11	3.97	3.93	3.86	3.80
187	3.83	3.90	3.71	3.72	3.64	4.47	4.39	4.14	3.73	3.82
189	4.16	4.61	4.08	3.51	4.11	3.99	4.12	4.24	3.70	3.61
191	4.52	4.46	4.37	3.95	3.84	3.89	3.73	3.81	3.69	3.60
193	4.52	4.25	4.32	3.97	3.99	4.07	3.89	3.70	3.21	3.40
195	4.27	4.09	4.28	3.81	3.90	4.55	4.41	4.20	3.73	3.67
197	4.79	4.65	4.50	4.23	3.95	5.23	4.88	4.75	4.59	4.74
199	4.08	4.36	4.27	3.80	4.26	4.48	4.53	4.73	4.54	4.35
201	4.77	4.70	4.81	4.34	4.38	4.29	4.15	4.17	4.11	4.11
203	4.73	4.90	4.61	4.43	4.48	4.37	4.21	4.43	3.86	4.24
205	5.56	5.41	5.59	4.98	5.36	4.39	4.40	4.18	4.18	4.57
207	5.74	5.41	5.90	5.43	5.22	4.77	4.27	4.48	3.84	4.46
209	5.91	4.21	4.70	5.43	5.12	4.40	4.22	4.14	3.81	3.94
211	3.85	3.96	3.89	3.81	3.78	4.48	4.53	4.37	3.95	4.26
Average	4.22	4.07	4.08	3.95	3.91	4.17	4.04	4.00	3.76	3.78

Table D.31: Mean profile depth values at 30°C for the S-R2 binder

	S-R2: Sh-Sh at 30°C					S-R2: Over App. at 30°C				
Position	MMLS3 Applications					MMLS3 Applications				
x-Distance	0	100	500	2000	5000	0	100	500	2000	5000
131	3.54	3.26	3.25	2.99	2.99	4.85	4.74	4.35	4.20	4.08
133	3.18	3.27	3.38	3.39	3.44	4.42	4.44	4.72	4.03	4.18
135	3.38	3.15	3.06	3.29	3.17	4.99	5.11	4.88	4.69	4.24
137	3.43	3.69	3.64	3.74	3.42	4.94	4.72	4.81	4.30	4.44
139	3.95	3.77	3.80	3.72	3.80	4.67	4.96	4.83	4.24	4.19
141	3.40	3.14	3.50	3.33	3.27	4.01	4.26	4.07	3.72	3.65
143	3.61	3.56	3.39	3.42	3.44	4.18	3.97	3.82	3.41	3.51
145	4.13	4.29	4.08	3.90	3.82	4.20	4.02	3.87	3.86	4.10
147	4.40	4.25	4.01	3.99	3.98	4.10	3.92	3.73	3.79	3.76
149	4.14	4.09	4.13	3.66	3.54	3.57	3.53	3.47	3.49	3.41
151	4.42	4.22	4.33	4.06	3.77	3.63	3.71	3.78	3.56	3.74
153	4.40	4.24	4.38	4.18	3.86	3.89	3.68	3.84	3.62	3.56
155	3.82	3.90	3.85	3.75	3.80	4.06	3.99	4.05	3.62	3.78
157	4.04	4.07	3.97	3.90	4.06	4.59	4.56	3.95	4.18	3.74
159	4.14	3.91	4.02	3.83	3.87	4.41	4.15	4.16	4.07	3.94
161	4.53	4.39	4.29	4.13	3.85	4.34	4.26	4.22	4.27	4.28
163	4.78	4.48	4.53	4.20	4.17	4.62	4.67	4.68	4.22	4.00
165	4.64	4.49	4.50	4.30	4.32	5.16	4.86	4.71	4.48	4.56
167	4.30	4.39	4.33	4.02	4.61	4.59	4.61	4.32	4.33	4.14
169	3.88	4.09	4.20	4.01	4.09	4.15	3.91	3.67	3.90	3.61
171	4.17	3.90	4.05	3.82	4.08	4.20	3.94	3.92	4.02	3.69
173	4.02	3.79	3.75	3.68	3.36	4.04	4.01	3.94	4.37	3.62
175	3.67	3.41	3.62	3.34	3.51	4.38	4.27	4.21	3.69	3.40
177	3.57	3.67	3.26	3.40	3.19	4.30	4.23	4.08	3.83	3.68
179	4.02	4.16	4.00	4.04	3.46	4.13	4.08	3.81	3.68	3.43
181	5.06	5.03	5.02	4.93	4.66	3.97	3.90	3.83	3.54	3.12
183	4.95	4.71	4.61	4.55	4.98	4.38	4.21	4.19	3.68	3.49
185	4.36	4.24	4.06	4.04	4.04	4.68	4.48	4.64	4.00	3.69
187	3.93	3.73	3.66	3.74	3.83	4.84	4.57	4.55	4.35	4.06
189	4.37	4.34	4.09	3.78	3.75	4.66	4.31	4.34	4.13	4.28
191	4.04	3.99	3.72	3.55	3.46	4.22	4.25	4.31	4.01	3.90
193	4.65	4.67	4.27	4.35	3.90	3.67	3.78	3.61	3.84	3.58
195	4.39	4.39	4.34	4.40	4.53	3.75	3.64	3.63	3.66	3.35
197	4.64	4.32	4.38	4.24	4.14	4.00	3.77	3.82	3.51	3.35
199	4.36	4.60	4.35	4.32	4.31	4.75	4.53	4.51	3.97	3.78
201	4.37	4.32	4.46	4.56	4.58	4.39	4.26	4.48	3.97	3.99
203	4.12	4.10	4.19	4.21	4.26	4.89	4.52	4.20	4.22	4.08
205	4.13	4.20	4.28	4.20	4.24	4.37	4.32	4.47	4.20	4.52
207	4.00	4.09	4.28	4.16	4.41	4.42	4.34	4.28	4.34	4.28
209	4.11	4.34	4.13	3.93	4.11	4.42	4.35	4.16	4.33	4.21
211	3.68	3.74	3.76	3.64	3.55	4.49	4.34	4.42	4.05	4.03
Average	4.11	4.06	4.02	3.92	3.89	4.35	4.25	4.18	3.99	3.86

Table D.32 - Table D.34 shows the average MPD values as calculated in the wheel path together with the MTD values as obtained by performing Sand Patch Tests (100 ml).

Table D.32: MPD and MTD values at 10°C

Average MPD in Wheel Path at 10°C						
Seal Information		**MMLS3 Trafficking Interval**				
Binder	**Configuration**	**0**	**100**	**500**	**2000**	**5000**
S-E1	**Sh-Sh**	5.19	4.69	4.62	4.42	4.29
S-E1	**Over app.**	5.23	4.62	4.59	4.50	4.27
S-E2	**Sh-Sh**	5.02	4.66	4.66	4.57	4.43
S-E2	**Over app.**	5.12	4.81	4.71	4.71	4.47
S-R1	**Sh-Sh**	5.33	4.82	4.54	4.47	4.39
S-R1	**Over app.**	5.25	4.72	4.37	4.32	4.25
S-R2	**Sh-Sh**	5.30	4.83	4.62	4.48	4.42
S-R2	**Over app.**	5.49	4.82	4.68	4.62	4.44
Average MTD (100 ml) at 10°C						
Seal Information		**MMLS3 Trafficking Interval**				
Binder	**Configuration**	**0**	**100**	**500**	**2000**	**5000**
S-E1	**Sh-Sh**	6.98	6.96	7.04	7.06	6.73
S-E1	**Over app.**	7.33	6.83	6.96	6.83	6.36
S-E2	**Sh-Sh**	7.31	6.61	6.64	6.64	6.73
S-E2	**Over app.**	6.66	6.68	6.12	6.16	6.27
S-R1	**Sh-Sh**	7.47	7.47	7.50	7.17	7.06
S-R1	**Over app.**	7.33	6.47	6.31	6.36	6.29
S-R2	**Sh-Sh**	7.36	7.09	6.20	6.43	6.38
S-R2	**Over app.**	7.86	7.31	7.01	7.01	6.71

Table D.33: MPD and MTD values at 20°C

Average MPD in Wheel Path at 20°C						
Seal Information		**MMLS3 Trafficking Interval**				
Binder	**Configuration**	**0**	**100**	**500**	**2000**	**5000**
S-E1	**Sh-Sh**	4.29	4.20	4.20	4.20	4.15
S-E1	**Over app.**	4.27	4.22	4.20	4.18	4.18
S-E2	**Sh-Sh**	4.43	4.47	4.40	4.37	4.33
S-E2	**Over app.**	4.47	4.47	4.41	4.35	4.23
S-R1	**Sh-Sh**	4.39	4.37	4.37	4.29	4.22
S-R1	**Over app.**	4.25	4.25	4.22	4.22	4.17
S-R2	**Sh-Sh**	4.42	4.45	4.27	4.19	4.11
S-R2	**Over app.**	4.44	4.44	4.44	4.40	4.35
Average MTD (100 ml) at 20°C						
Seal Information		**MMLS3 Trafficking Interval**				
Binder	**Configuration**	**0**	**100**	**500**	**2000**	**5000**
S-E1	**Sh-Sh**	6.73	6.64	6.38	6.18	6.52
S-E1	**Over app.**	6.36	6.29	6.03	5.66	6.03
S-E2	**Sh-Sh**	6.73	6.34	6.36	6.29	6.01
S-E2	**Over app.**	6.27	5.77	5.81	5.77	5.37
S-R1	**Sh-Sh**	7.06	6.91	6.16	6.10	6.05
S-R1	**Over app.**	6.29	6.05	5.81	5.77	5.44
S-R2	**Sh-Sh**	6.38	6.05	5.93	5.53	5.60
S-R2	**Over app.**	6.71	6.59	6.27	6.27	6.20

Table D.34: MPD and MTD values at 30°C

Average MPD in Wheel Path at 20°C						
Seal Information		**MMLS3 Trafficking Interval**				
Binder	**Configuration**	**0**	**100**	**500**	**2000**	**5000**
S-E1	**Sh-Sh**	4.15	4.10	4.10	3.93	3.77
S-E1	**Over app.**	4.18	4.03	4.02	3.99	3.98
S-E2	**Sh-Sh**	4.33	4.22	4.15	3.91	3.81
S-E2	**Over app.**	4.23	4.07	4.06	4.06	3.88
S-R1	**Sh-Sh**	4.22	4.07	4.07	3.95	3.91
S-R1	**Over app.**	4.17	4.04	4.00	3.76	3.76
S-R2	**Sh-Sh**	4.11	4.06	4.02	3.92	3.89
S-R2	**Over app.**	4.35	4.25	4.18	3.99	3.86
Average MTD (100 ml) at 20°C						
Seal Information		**MMLS3 Trafficking Interval**				
Binder	**Configuration**	**0**	**100**	**500**	**2000**	**5000**
S-E1	**Sh-Sh**	6.52	6.38	6.10	5.56	5.55
S-E1	**Over app.**	6.03	5.93	5.75	5.32	5.33
S-E2	**Sh-Sh**	6.01	5.99	5.79	5.46	5.35
S-E2	**Over app.**	5.37	5.55	5.55	5.37	5.35
S-R1	**Sh-Sh**	6.05	5.95	5.85	5.37	5.35
S-R1	**Over app.**	5.44	5.23	5.21	5.12	5.10
S-R2	**Sh-Sh**	5.60	5.53	5.44	4.85	4.91
S-R2	**Over app.**	6.20	5.91	5.73	5.26	5.23

D.3 Trafficking History

Figure D.1 - Figure D.3 show the total depth comparison, over all trafficking temperatures and MMLS3 load repetitions.

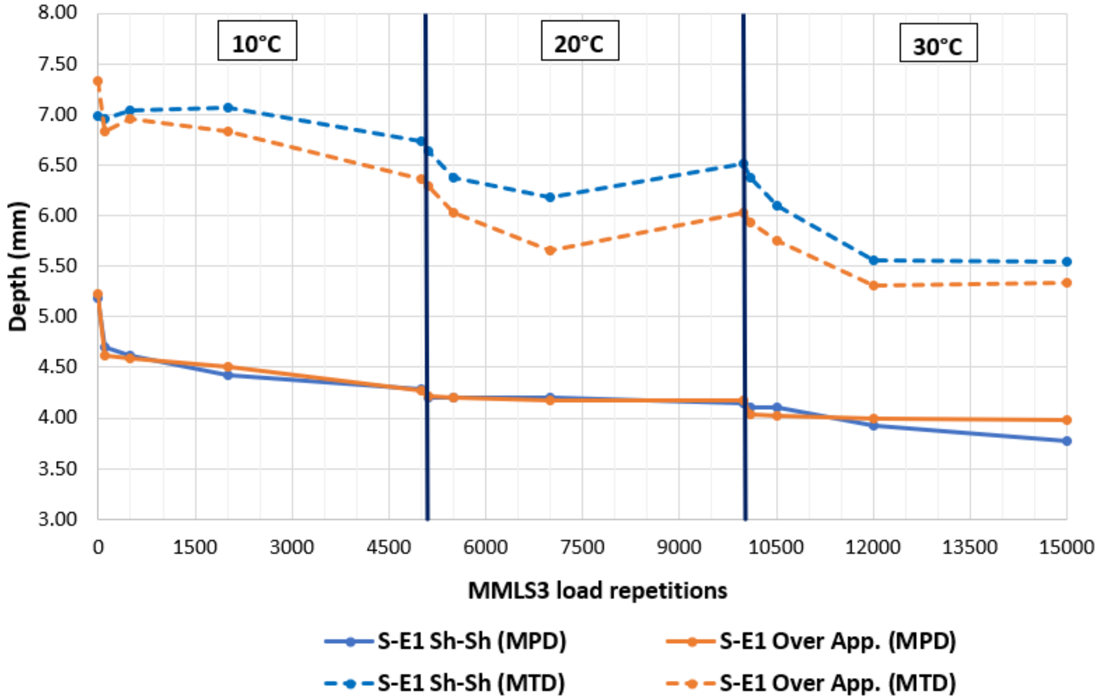

Figure D.1: MPD and MTD decrease for S-E1

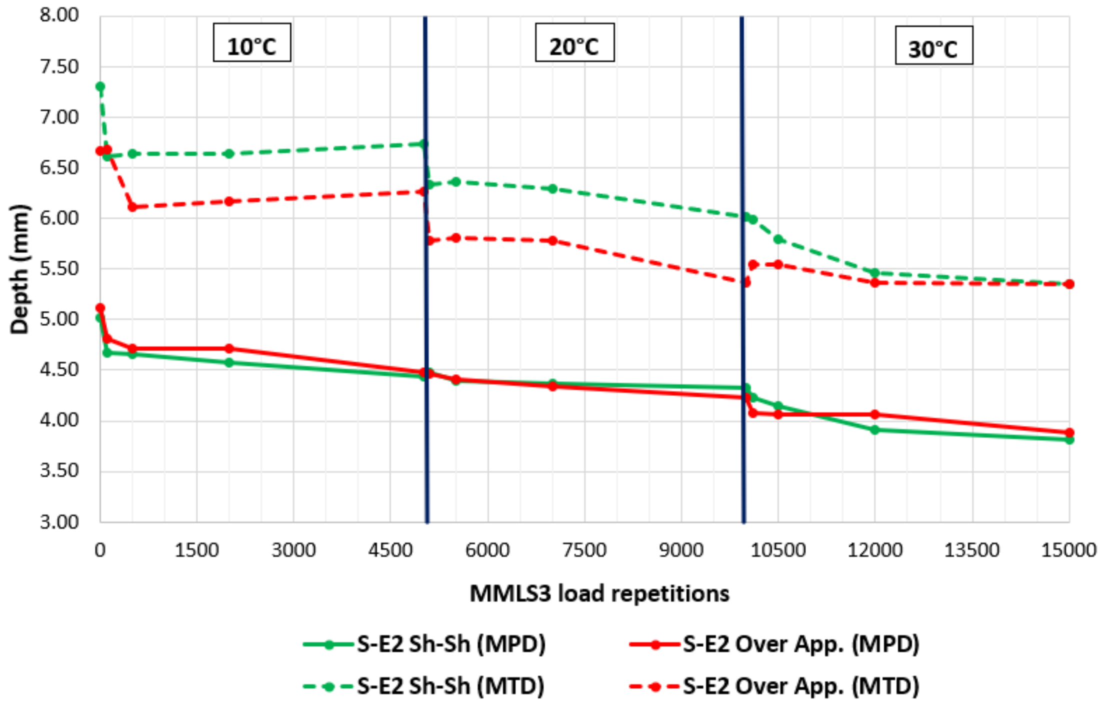

Figure D.2: MPD and MTD decrease for S-E2

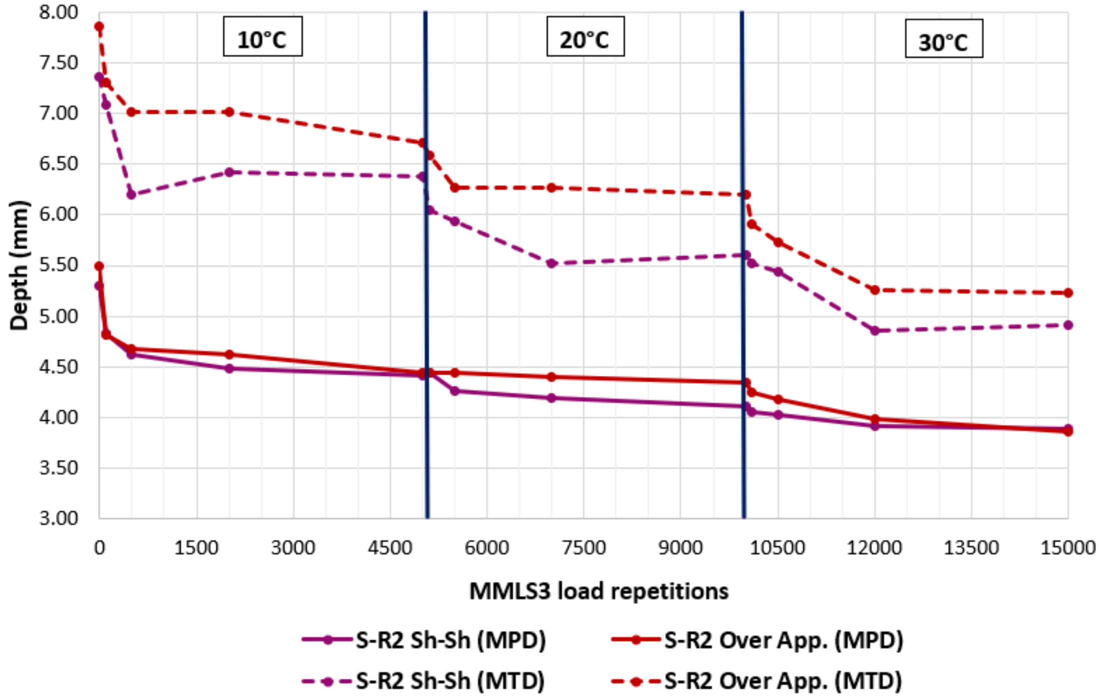

Figure D.3: MPD and MTD decrease for S-R2

D.4 Reduction in MPD

A summary of the reduction in MPD (mm) for each binder type, aggregate matrix and trafficking temperature can be seen in Table D.35.

Table D.35: Summary of the reduction in MPD (mm) for each binder, trafficking temperature and aggregate matrix at the trafficking intervals

Binder	Trafficking Temperature	Aggregate Configuration	100	500	2000	5000
S-E1	10°C	Sh-Sh	0.49	0.57	0.77	0.90
		Over App.	0.56	0.60	0.69	0.92
	20°C	Sh-Sh	0.58	0.66	0.86	1.04
		Over App.	0.62	0.67	0.78	1.01
	30°C	Sh-Sh	0.63	0.71	1.08	1.41
		Over App.	0.77	0.83	0.97	1.20
S-E2	10°C	Sh-Sh	0.35	0.36	0.45	0.58
		Over App.	0.21	0.30	0.31	0.54
	20°C	Sh-Sh	0.31	0.39	0.51	0.69
		Over App.	0.21	0.37	0.43	0.79
	30°C	Sh-Sh	0.42	0.57	0.93	1.20
		Over App.	0.37	0.54	0.60	1.13
S-R1	10°C	Sh-Sh	0.52	0.79	0.87	0.94
		Over App.	0.61	0.97	1.02	1.08
	20°C	Sh-Sh	0.54	0.81	0.96	1.11
		Over App.	0.61	1.00	1.05	1.16
	30°C	Sh-Sh	0.69	0.96	1.23	1.43
		Over App.	0.75	1.17	1.46	1.57
S-R2	10°C	Sh-Sh	0.47	0.68	0.82	0.88
		Over App.	0.48	0.62	0.68	0.86
	20°C	Sh-Sh	0.44	0.83	1.05	1.18
		Over App.	0.48	0.62	0.72	0.95
	30°C	Sh-Sh	0.50	0.92	1.24	1.41
		Over App.	0.58	0.79	1.09	1.43

D.5 Rate of Change in MPD

A summary of the rate of change (mm/MMLS3 load rep.) for each binder type, aggregate matrix and trafficking temperature can be seen in Table D.36.

Table D.36: Summary of the rate of change in MPD (mm/MMLS3 load rep.) for each binder, trafficking temperature and aggregate matrix during Phase 2 and Phase 3 of MMLS3 load reps

Binder	Trafficking Temperature	Aggregate Configuration	Phase 2 500 - 2000	Phase 3 2000 - 5000
S-E1	10°C	Sh-Sh	1.4E-04	4.2E-05
		Over App.	5.8E-05	7.7E-05
	20°C	Sh-Sh	1.4E-04	5.9E-05
		Over App.	7.3E-05	7.6E-05
	30°C	Sh-Sh	2.5E-04	1.1E-04
		Over App.	8.9E-05	7.9E-05
S-E2	10°C	Sh-Sh	6.0E-05	4.5E-05
		Over App.	8.0E-07	7.9E-05
	20°C	Sh-Sh	8.2E-05	5.9E-05
		Over App.	4.1E-05	1.2E-04
	30°C	Sh-Sh	2.4E-04	9.0E-05
		Over App.	3.9E-05	1.8E-04
S-R1	10°C	Sh-Sh	5.1E-05	2.6E-05
		Over App.	3.5E-05	2.2E-05
	20°C	Sh-Sh	9.9E-05	5.2E-05
		Over App.	3.5E-05	3.6E-05
	30°C	Sh-Sh	1.8E-04	6.6E-05
		Over App.	1.9E-04	3.6E-05
S-R2	10°C	Sh-Sh	9.2E-05	2.1E-05
		Over App.	4.1E-05	5.8E-05
	20°C	Sh-Sh	1.5E-04	4.5E-05
		Over App.	6.8E-05	7.5E-05
	30°C	Sh-Sh	2.2E-04	5.4E-05
		Over App.	2.0E-04	1.2E-04

Appendix E

Results Interpretation

E.1 Master Curves

The master curves for the different binders, at reference temperatures of 10°C, 20°C and 30°C, can be seen in Figure E.1 - Figure E.12.

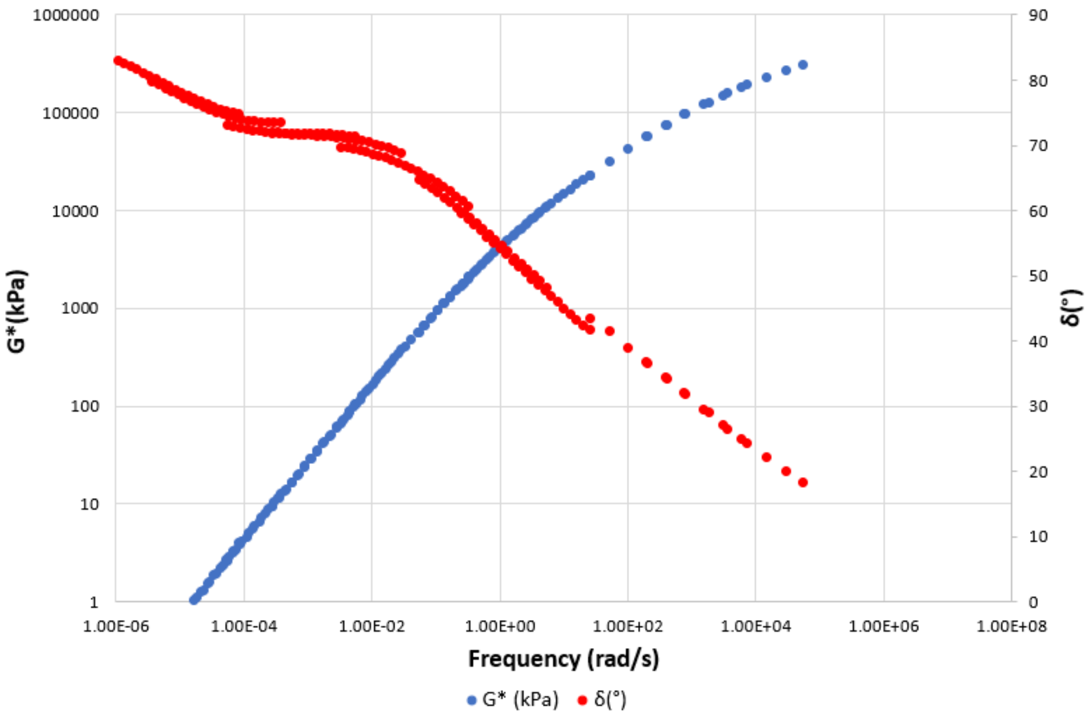

Figure E.1: Mastercurve for S-E1 at 10°C reference temperature

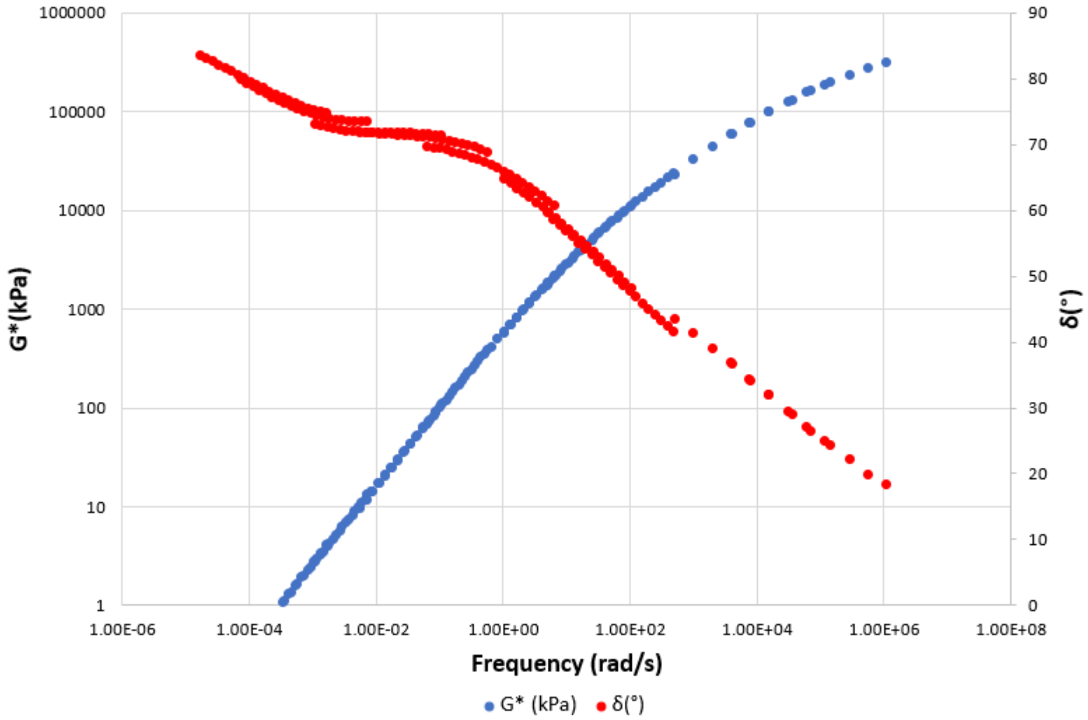

Figure E.2: Mastercurve for S-E1 at 20°C reference temperature

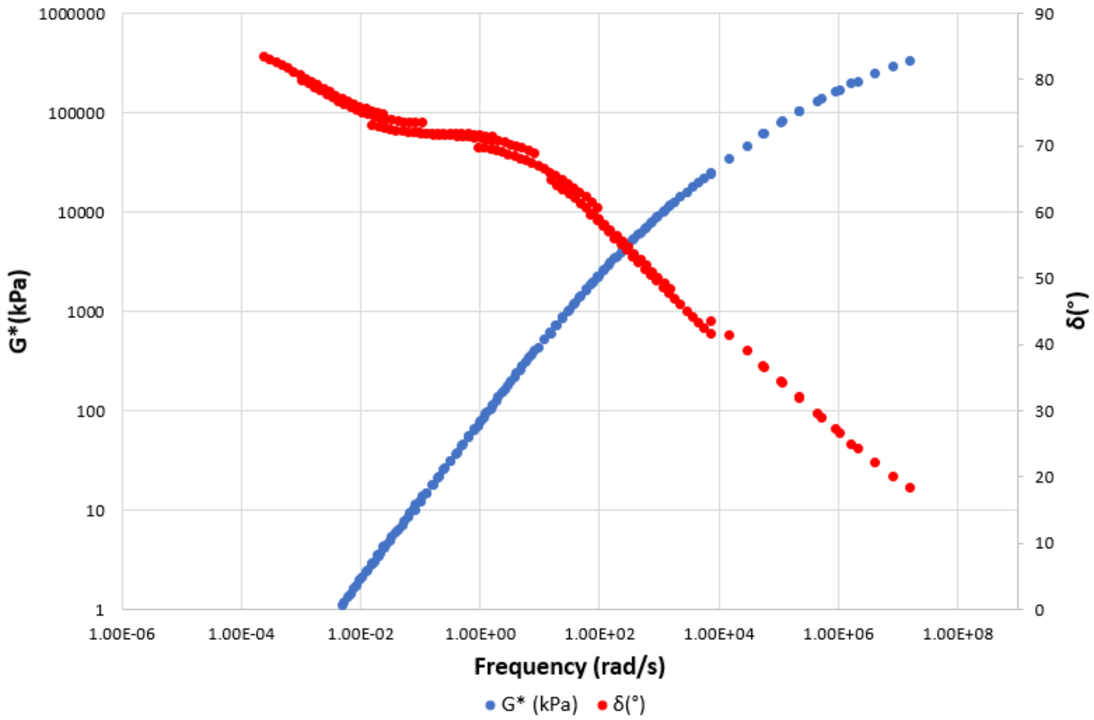

Figure E.3: Mastercurve for S-E1 at 30°C reference temperature

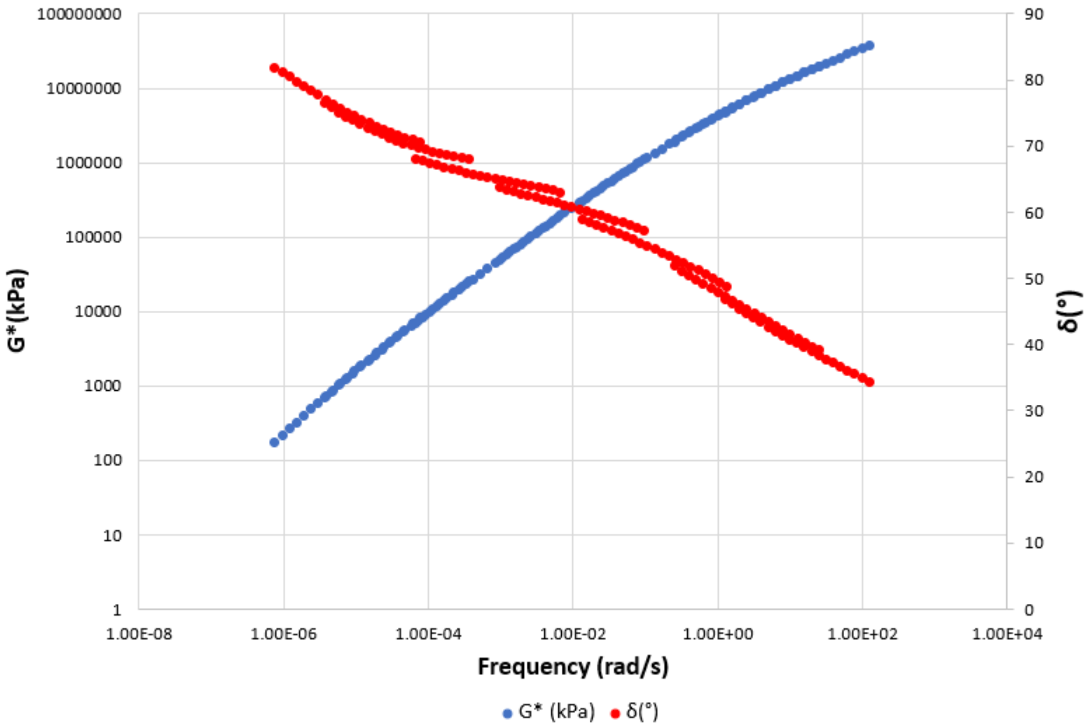

Figure E.4: Mastercurve for S-E2 at 10°C reference temperature

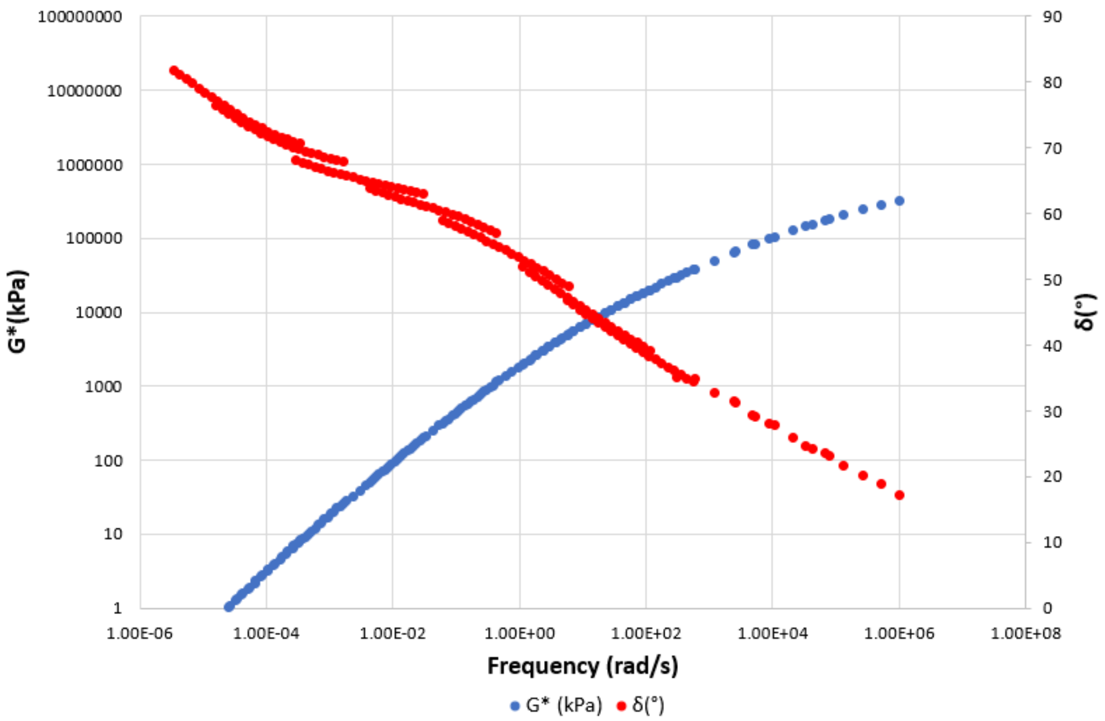

Figure E.5: Mastercurve for S-E2 at 20°C reference temperature

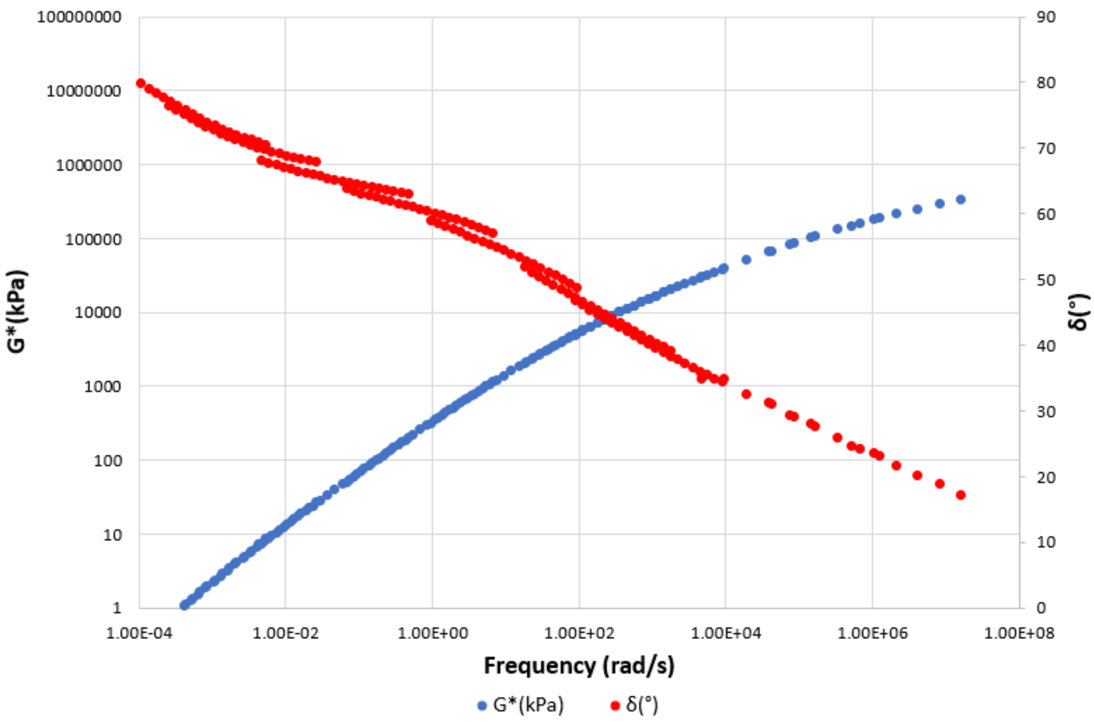

Figure E.6: Mastercurve for S-E2 at 30°C reference temperature

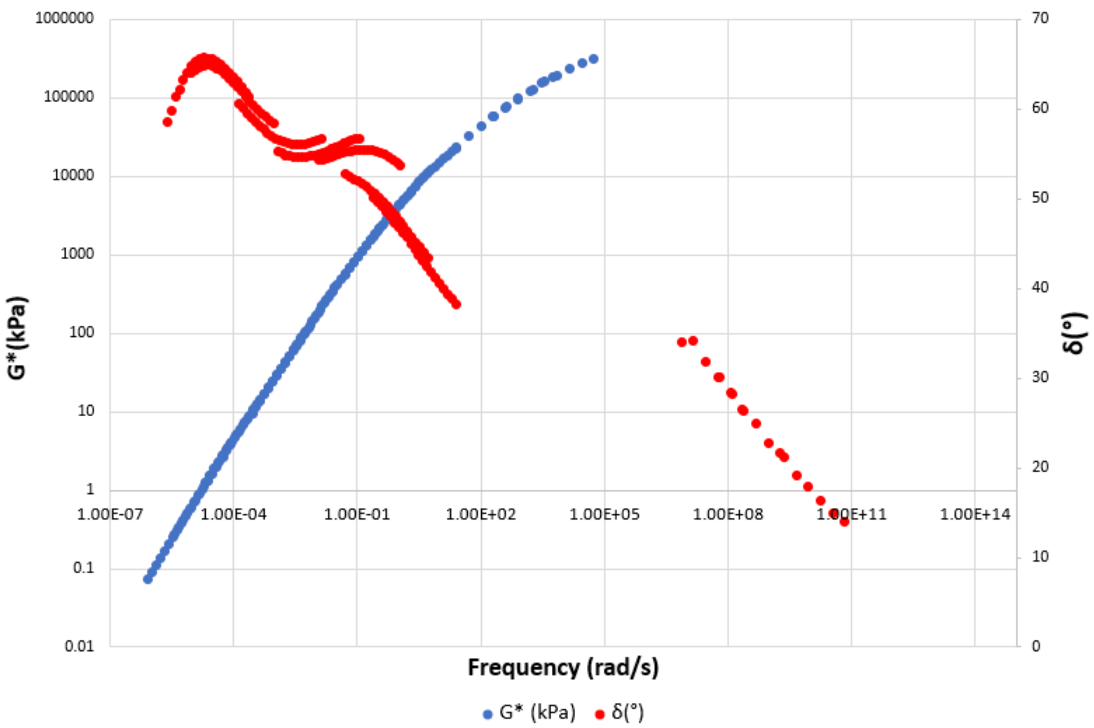

Figure E.7: Mastercurve for S-R1 at 10°C reference temperature

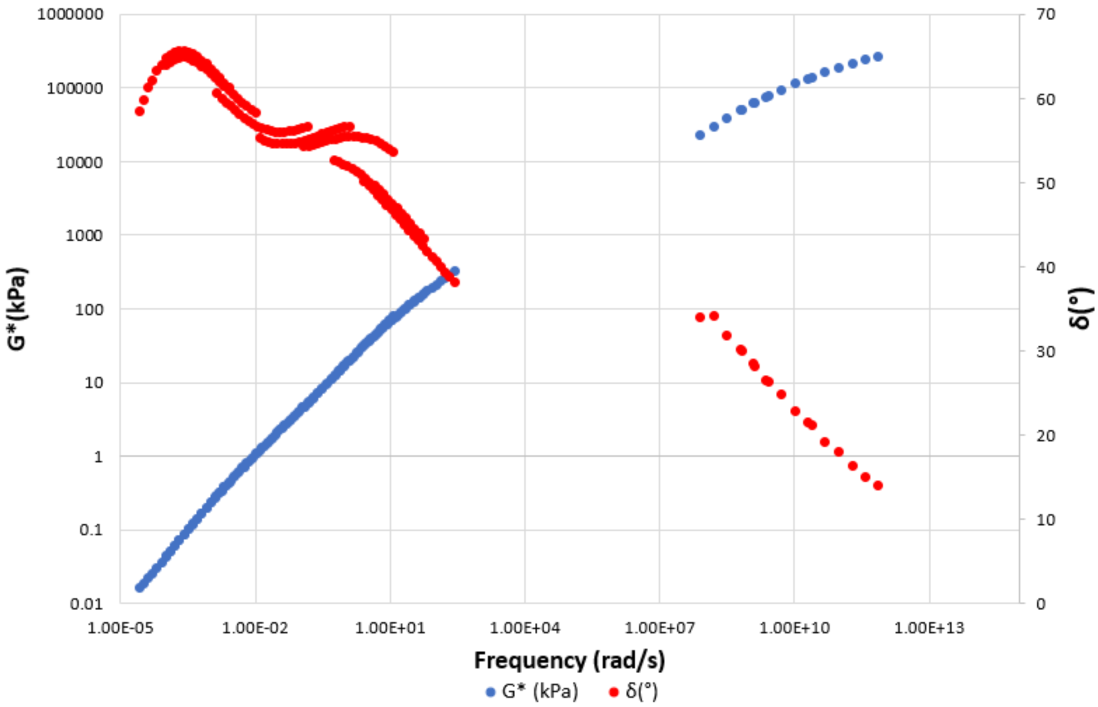

Figure E.8: Mastercurve for S-R1 at 20°C reference temperature

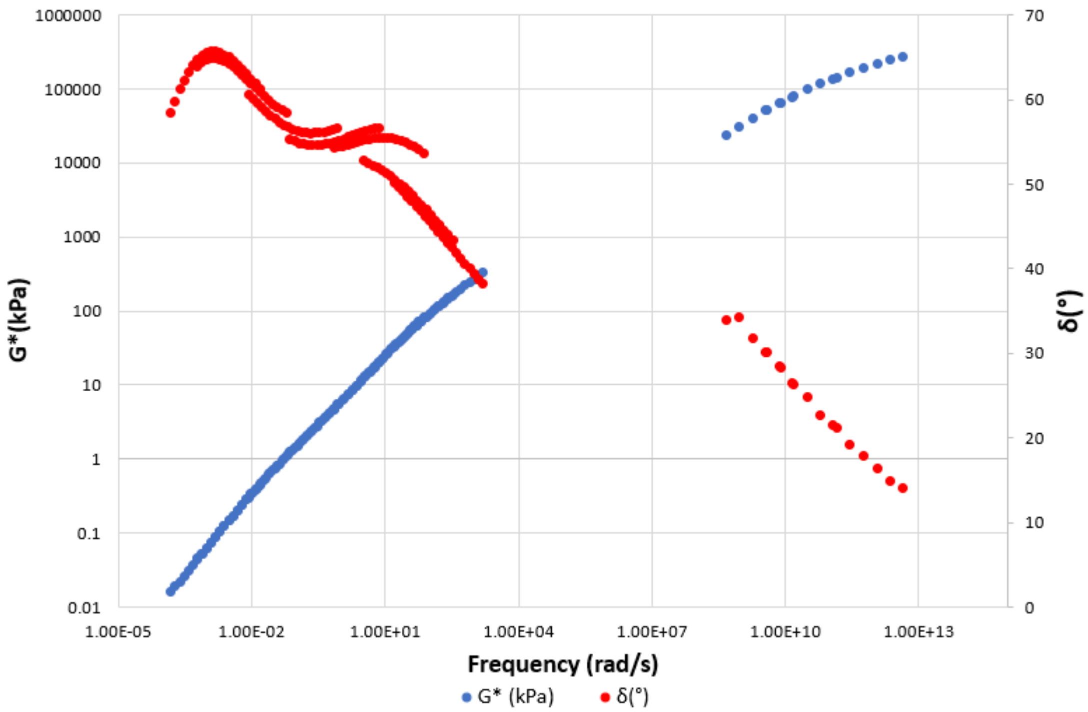

Figure E.9: Mastercurve for S-R1 at 30°C reference temperature

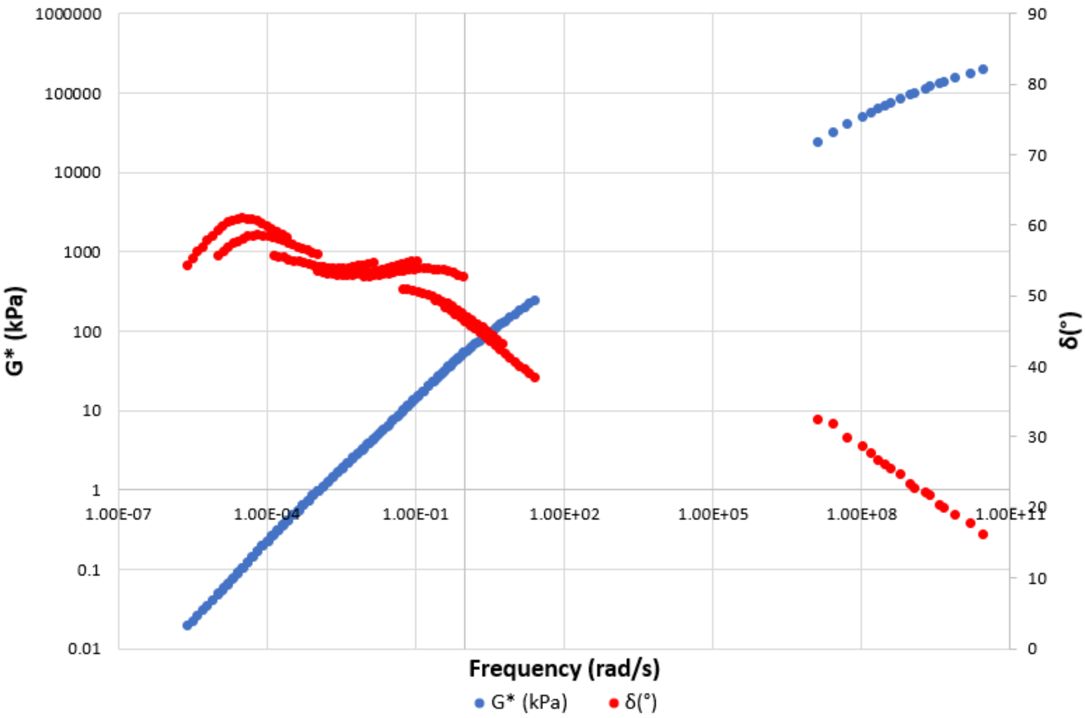

Figure E.10: Mastercurve for S-R2 at 10°C reference temperature

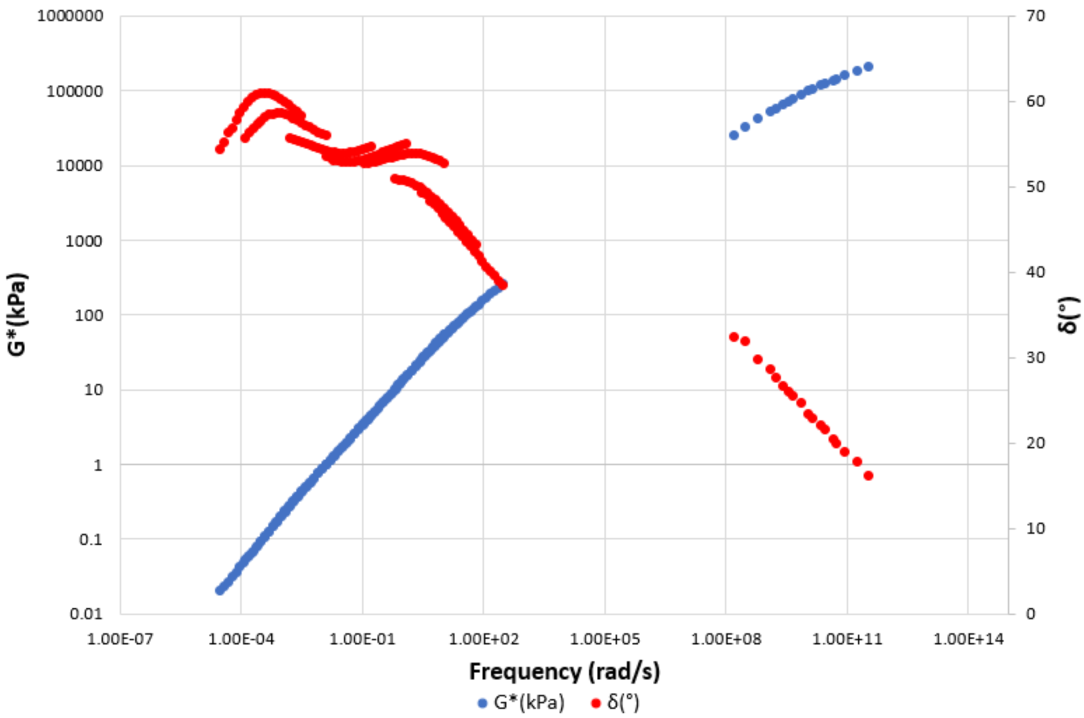

Figure E.11: Mastercurve for S-R2 at 20°C reference temperature

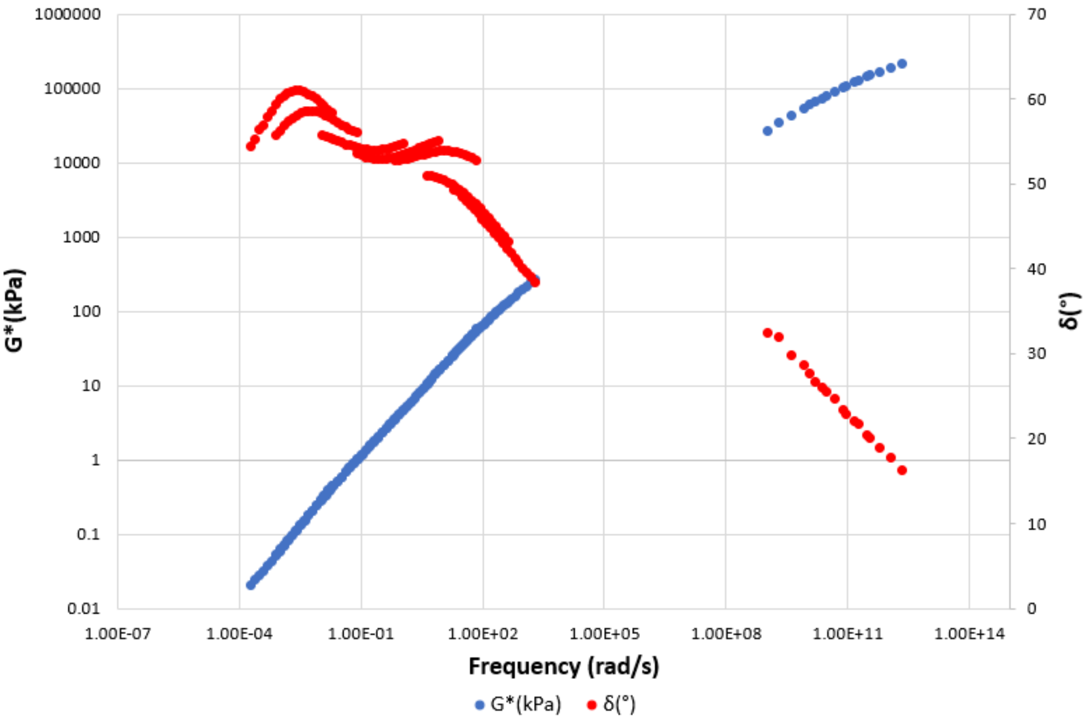

Figure E.12: Mastercurve for S-R2 at 30°C reference temperature